Mục lục

KHOA HỌC XÃ HỘI VÀ NHÂN VĂN

On the applicability of the energy balancing passivity-based control approach

Ứng dụng của phương pháp điều khiển dựa trên thụ động cân bằng năng lượng

Hoang Ngoc Ha[a,*], Nguyen Huu Hiep[a], Le Phuong Quyen[b]
Hoàng Ngọc Hà, Nguyễn Hữu Hiệp, Lê Phượng Quyên

[a]Center for Information Technology & Communication, Institute of Research and Development,
Duy Tan University, Danang, Vietnam
Trung tâm Công nghệ Thông tin và Truyền thông, Viện Nghiên cứu và Phát triển Công nghệ cao,
Đại học Duy Tân, Đà Nẵng, Việt Nam
[b]Faculty of Electrical & Electronics Engineering, Duy Tan University, Danang, Vietnam
Khoa Điện - Điện tử, Đại học Duy Tân, Đà Nẵng, Việt Nam

Abstract

This paper addresses the energy balancing passivity-based control design approach for the purpose of stabilizing dynamical systems at a desired set-point. A simple electrical network is used to illustrate and discuss the applicability of the proposed approach. Besides, closed-loop simulations are included.

Keywords: Passivity-based control, energy balancing controller, dissipation obstacle, electrical network.

Tóm tắt

Bài báo này giới thiệu phương pháp thiết kế điều khiển dựa trên thụ động cân bằng năng lượng để ổn định hóa hệ động lực tại điểm cài đặt mong muốn. Một mạng điện đơn giản được sử dụng để minh họa và chỉ ra khả năng ứng dụng của phương pháp. Bên cạnh đó, mô phỏng vòng kín cũng được thực hiện.

Từ khóa: Điều khiển dựa trên thụ động, bộ điều khiển cân bằng năng lượng, trở ngại phân tán, mạng điện.

1. Introduction

This paper deals with the control design of general nonlinear dynamical systems [1–3] whose dynamics are described by a set of Ordinary Differential Equations (ODEs) and affine in the input u as follows:

$$\begin{cases} \dfrac{dx}{dt} = f(x) + g(x)u; \ x(t=0) = x_{init} \\ y = h(x) \end{cases} \quad (1)$$

where $x = x(t)$ is the state vector in the operating region $D \subset \mathbb{R}^n$, $f(x) \in \mathbb{R}^n$ and $h(x) \in \mathbb{R}^m$ express the smooth (nonlinear) functions with respect to the vector field x x. The input-state map, the control input and the output are represented by $g(x) \in \mathbb{R}^{n \times m}$, $u \in \mathbb{R}^m$ and $y \in \mathbb{R}^m$, respectively. It is worth noting that many industrial applications of electrical, mechanical or biochemical engineering belong to this kind of systems [4–9].

Email: ngocha.h@gmail.com

Many control methodologies have been developed for the stabilization of the system (1) at a desired set-point x^*. This is for instance the case for sliding mode control, adaptive control, model predictive control and machine learning control etc. to cite a few. Recently, passivity-based control methodology which is recognized as an extension of the Lyapunov approach has attracted much attention from researchers and practitioners (see e.g. [4, 5] for the control design of electromechanical systems and [7–9] for open thermodynamic systems and nonlinear systems). In addition, the authors in [6] proposed an interconnection and damping assignment passivity-based control framework. Those results were of great interest, yet for instance limited to a particular structure of the system dynamics called the port-Hamiltonian representation. In this work, the applicability of energy balancing passivity-based control is discussed without the port-Hamiltonian formulation, with a particular emphasis on the electrical network in order to further explore the network topology. The control design and simulation scenario are main contributions of this work.

This paper is organized as follows. Section 2 gives a brief overview of the energy balancing passivity-based control design approach. Section 3 is devoted to the case study of a simple electrical network. The energy balancing controller design, discussions on the applicability and numerical simulation are included. Section 4 ends the paper with some concluding remarks.

Notations. The following notations are considered throughout the paper:

- $\mathbb{R}$ is the set of real number;
- T is the matrix transpose operator;
- m and n ($m \le n$) are the positive integers;
- x^* is the set-point;
- x_{init} is the initial value of the state vector.

2. The energy balancing passivity-based control design approach

2.1. Some basic concepts

Definition 1 [2, 3, 8]. The nonlinear dynamical system defined by (1) is said to be *dissipative* regarding to the supply rate $s(u(t), y(t))$ if there exists a storage function $H : D \to \mathbb{R}^+$ so that the inequality below holds for all $x \in D$ and $t > 0$,

$$H(x(t)) - H(x(0)) \le \int_0^t s(u(\tau), y(\tau)) d\tau \quad (2)$$

The above inequality shows a physical meaning that the increase in the energy of the system from 0 to t is always smaller than the total amount of energy supplied by an external source at the same time. The value of storage function $H(x(t))$ expresses the total energy of the system at any time. As a consequence, if the storage function $H(x(t))$ is differentiable for all $x \in D$, the inequality given by (2) is equivalent to $\dot{H}(x(t)) \le s(u(t), y(t))$.

Definition 2 [2, 3, 8]. The nonlinear dynamical system (1) is said to be *passive* if it is dissipative with respect to the supply rate given by $s(u(t), y(t)) = u(t)^T y(t)$, i.e.:

$$\dot{H}(x(t)) \le u(t)^T y(t) \quad (3)$$

2.2 The energy balancing passivity-based control design approach

The key idea of energy balancing passivity-based control is to find a static state feedback [3, 5]

$$u(t) = \beta(x(t)) + \upsilon(t) \quad (4)$$

so that the closed-loop system is again a passive system with storage function H_d, with respect to $\upsilon \mapsto y$ where υ is the novel input. Indeed, we derive from equations (3) and (4):

$$\dot{H}_d(x(t)) \le \upsilon(t)^T y(t) \quad (5)$$

where

$$\dot{H}_a(x(t)) \triangleq -\beta(x(t))^T y(t) \quad (6)$$

and

$$H_d(x(t)) = H(x(t)) + H_a(x(t)) \quad (7)$$

Eq. (7) is called the Energy Balance Equation (EBE). Moreover, the storage function H_d has the global minimum at the desired set-point x^* for the purpose of stabilization when settling $v = 0$. For the dynamic system (1), the EBE is equivalent to the following partial differential equation (PDE)

$$-\beta(x)^{\mathrm{T}} h(x) = \left(\frac{\partial H_a}{\partial x}\right)^{\mathrm{T}} \left(f(x) + g(x)\beta(x)\right) \quad (8)$$

A necessary condition for the solvability of the PDE (8) is [5]:

$$\beta(x^*)^{\mathrm{T}} h(x^*) = 0 \qquad (9)$$

In physical systems, this necessary condition may be related to the so-called dissipation obstacle. In such a situation, the system is said to be *pervasive* or power is not equal to zero at equilibrium.

3. The case study

3.1. A simple electrical network

To illustrate the concepts introduced in Section 2, we consider next a simple electrical system, which is the *RLC* series circuit as sketched in Figure 1.
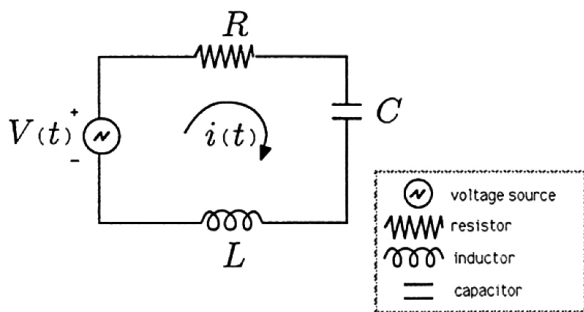
Figure 1: A series circuit.

By considering Kirchhoff's voltage law together with constitutive equations considered for three passive elements R, L and C, a second order ordinary differential equation of the circuit can be derived below

$$L\frac{d^2 q_C(t)}{dt^2} + R\frac{dq_C(t)}{dt} + \frac{1}{C} q_C(t) = V(t) \,(10)$$

where $\dfrac{dq_C(t)}{dt}$ is the electric current with $q_C(t)$

the charge stored in the capacitor. The electric current is assumed to be the controlled variable (i.e. the output) of the electrical network.

Let $x := \left(q_C(t), \phi_L(t)\right)^{\mathrm{T}}$ be the vector consisting of the charge $q_C(t)$ and the magnetic flux through the conductor, that is, $\phi_L(t) = L\dfrac{dq_C(t)}{dt}$, Eq. (10) can be rewritten as follows [5]:

$$\frac{dq_C(t)}{dt} = \frac{1}{L}\phi_L(t) \qquad (11a)$$

$$\frac{d\phi_L(t)}{dt} = -\frac{1}{C} q_C(t) - \frac{R}{L}\phi_L(t) + V(t) \qquad (11b)$$

The system dynamics (11a)(11b) lead to the state-space representation given by (1) with:

$$f(x) = \begin{pmatrix} \dfrac{1}{L}\phi_L(t) \\[2mm] -\dfrac{1}{C} q_C(t) - \dfrac{R}{L}\phi_L(t) \end{pmatrix}, \qquad (12)$$

$$g(x) = \begin{pmatrix} 0 \\ 1 \end{pmatrix}, u = V \qquad (13)$$

$$y = \frac{1}{L}\phi_L(t) \equiv i(t) \text{ (the electric current). (14)}$$

It is shown that the system is passive with the storage function defined by [5]

$$H\left(q_C(t), \phi_L(t)\right) = \frac{1}{2C} q_C^2 + \frac{1}{2L}\varphi_L^2 \qquad (15)$$

This storage function is equal to the total energy of the system (i.e., it characterizes the amount of energy stored in capacitor and inductor). Hence it has the unit of energy.

Remark 1. The states $q_C(t)$ and $\phi_L(t)$ converge to the nonzero values at steady state, that is, $q_C^* = CV^*$ and $\varphi_L^* = 0$, if the constant voltage source V^* is different from 0.

3.2 The control design

Proposition 1. A state feedback law given by

$$u(t) = -\frac{1}{K} q_C(t) + \left(\frac{1}{C} + \frac{1}{K}\right) q_C^* \qquad (16)$$

with $\left(\dfrac{1}{C} + \dfrac{1}{K}\right) > 0$ [1] globally asymptotically

---

[1] This implies that either $K > 0$ or $K < -C$.

stabilizes the system (1)(12)–(14) at the equilibrium $x^* = (x_1^*, 0)^T$.

Proof. (see also [5] for a different version of the stability proof) First of all, we can check easily that the power of any equilibrium is equal to zero, i.e. $u^* y^* = 0$. Hence, the condition (9) is met and the energy balancing passivity-based control design is therefore applicable. In fact, as the natural energy $H(q_C(t), \phi_L(t))$ (15) already has a minimum at the desired equilibrium $\varphi_L^* = 0$, we only need to shape the total energy $H_d(x(t)) = H(x(t)) + H_a(x(t))$ with respect to q_C in such a way that $H_d(x(t))$ reaches a global minimum at $x^* = (x_1^*, 0)^T$. Consequently, we can take H_a as a function of q_C only. We derive from (8)

$$\beta(q_C) = -\frac{dH_a(q_C)}{dq_C} \qquad (17)$$

Using (16), Eq. (17) leads to $H_a(q_C) = \frac{1}{2K} q_C^2 - \left(\frac{1}{C} + \frac{1}{K}\right) q_C^* q_C$. From this, it follows that the total energy function $H_d(x)$ admits a global minimum at $x^* = (x_1^*, 0)^T$ since its

Hessian matrix $\begin{pmatrix} \left(\frac{1}{C} + \frac{1}{K}\right) & 0 \\ 0 & \frac{1}{L} \end{pmatrix}$ is positive definite

and the time derivative $\frac{dH_d(x)}{dt} = -R\left(\frac{\phi_L}{L}\right)^2$ is negative. As a consequence, $H_d(x)$ plays the role of a global Lyapunov function for the purpose of the stabilization [1]. The latter completes the proof.

Remark 2. If the structure of the circuit is changed to a parallel RLC circuit (i.e. L in series with R in parallel C circuit), the dynamic equations of the circuit are described by the state-space representation (1) with [5]:

$$f(x) = \begin{pmatrix} -\frac{1}{RC} q_C(t) + \frac{1}{L} \phi_L(t) \\ -\frac{1}{C} q_C(t) \end{pmatrix}, \qquad (18)$$

$$g(x) = \begin{pmatrix} 0 \\ 1 \end{pmatrix}, u = V \qquad (19)$$

$$y = \frac{1}{L} \phi_L(t) \equiv i(t) \text{ (the electric current).} \qquad (20)$$

The admissible equilibria are now of the form $x^* = \left(CV^*, \frac{L}{R} V^*\right)^T$ for any V^*. We can check easily that the power of any equilibrium except the trivial one is nonzero, i.e. $u \, y \neq$. Hence, the condition (9) is not fulfilled and the energy balancing passivity-based control design is therefore not applicable to this case.

3.3 Numerical simulation

The simulations are implemented using *Matlab & Simulink*. The model parameters are given with $C = 4$ (F), $R = \frac{1}{2}$ (Ω) and $L = 6.25$ (H)[2]. The open loop input voltage is a unit step, that is, $u(t) = S(t)$ where $S(t)$ is the unit step function. The initial conditions are chosen to be $x_1(t = 0) = x_{1,init} = 3$ and $x_2(t = 0) = x_{2,init} = 0$.
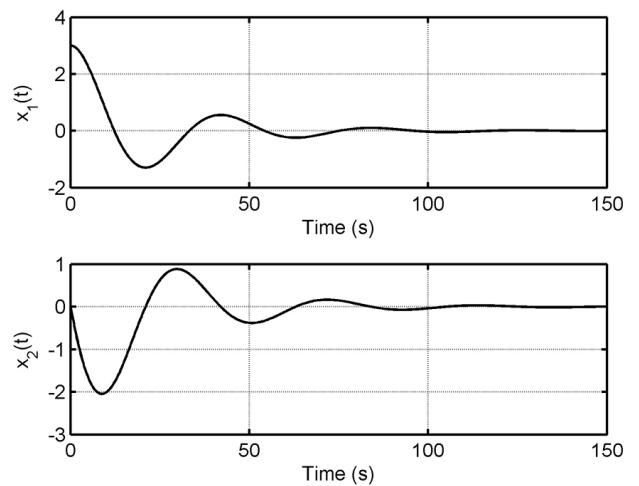
Figure 2: The convergence of the states *w.r.t.* time.

For the control objective, we propose to stabilize the system at the natural equilibrium $x^* = (0,0)^{T}$ [3]

using the energy balancing controller (16) with $K = -10$. Figure 2 shows that the system (1) (12)–(14) is globally stabilized as expected. In addition, the manipulated input u (16) is physically admissible in terms of amplitude and dynamics as seen in Figure 3.
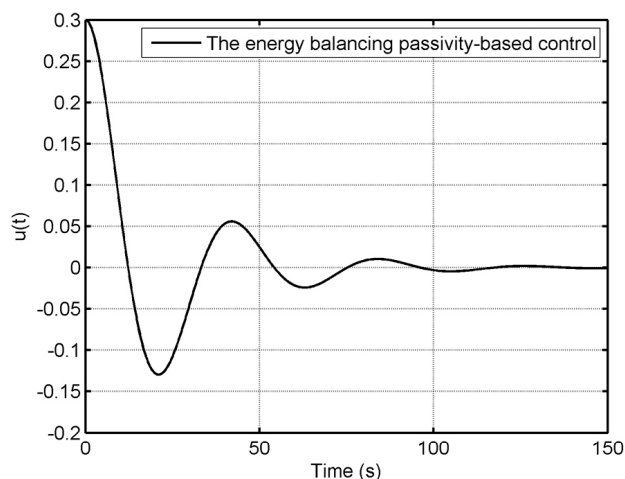
Figure 3: The manipulated input *w.r.t.* time.

4. Conclusion

In this paper, an unstable series *RLC* circuit is used to illustrate the energy balancing passivity-based control and its applicability. It remains now (i) to adapt the proposed results to nonlinear systems with dissipation obstacle and (ii) to compare the performance of the control approach with other control methodologies such as tracking error-based control [8] and/or power-shaping control [9].

References

[1] H.K. Khalil, *Nonlinear systems*. Prentice Hall, Upper Saddle River, 3rd edition, 2002.

[2] R. Ortega, A. Loría, P.J. Nicklasson, and H. Sira-Ramírez, *Passivity-based control of Euler-Lagrange systems: Mechanical, electrical and electromechanical applications.* Springer London, 1st edition, 1998.

[3] A. Van der Schaft, *L₂-gain and passivity techniques in nonlinear control*. Springer, 3rd edition, 2017.

[4] B. Maschke, R. Ortega, and A. Van der Schaft, "Energy-based Lyapunov functions for forced Hamiltonian systems with dissipation," *IEEE Transactions on Automatic Control*, 45(8), pp. 1498-1502, 2000.

[5] R. Ortega, A. Van der Schaft, I. Mareels, and B. Maschke, "Putting energy back in control," *IEEE Control Syst.Mag.*, 21(2), pp. 18-33, 2001.

[6] R. Ortega, A. Van der Schaft, B. Maschke, and G. Escobar, "Interconnection and damping assignment passivity-based control of port-controlled Hamiltonian systems," *Automatica*, 38(4), pp. 585-596, 2002.

[7] M. Guay, and N. Hudon, "Stabilization of nonlinear systems via potential-based realization," *IEEE Transactions on Automatic Control*, 61(4), pp. 1075-1080, 2016.

[8] T.S. Nguyen, N.H. Hoang, and M.A. Hussain. "Feedback passivation plus tracking error-based multivariable control for a class of free-radical polymerization reactors," *Int. J. of Control*, 2018. https://doi.org/10.1080/00207179.2017.1423393

[9] H. Hoang, D. Dochain, F. Couenne, and Y. Le Gorrec, "Dissipative pseudo-Hamiltonian realization of chemical systems using irreversible thermodynamics*,"* *Mathematical and Computer Modelling of Dynamical Systems*, 23(2), pp. 135-155, 2017.

Sequential Piecewise Linear Regression software program for nonlinear regression analysis in structural engineering

Sử dụng phần mềm SPLR cho các bài toán phân tích hồi quy phi tuyến trong ngành xây dựng

Nhat Duc Hoang[a,*], Cong Hai Le[b]
Hoàng Nhật Đức, Lê Công Hải

[a]*Institute of Research and Development, Duy Tan University, Danang, Vietnam*
Viện Nghiên cứu và Phát triển Công nghệ cao, Đại học Duy Tân, Đà Nẵng, Việt Nam
[b]*Hai Nam Construction and Investment LLC, Quangbinh, Vietnam*
Công ty TNHH Xây dựng và Đầu tư Hải Nam, Quảng Bình, Việt Nam

Abstract

This study aims at establishing machine learning models based on Sequential Piecewise Linear Regression (SPLR) for regression analysis in structural engineering. SPLR is a powerful machine learning approach which can deliver good predictive accuracy. In this paper, we develop a software program of SPLR in MATLAB.

Keywords: Regression Analysis, Structural Engineering, MATLAB, SPLR.

Tóm tắt

Nghiên cứu này xây dựng mô hình học máy dựa trên thuật toán Sequential Piecewise Linear Regression (SPLR) dùng cho phân tích hồi quy trong lĩnh vực kết cấu xây dựng. SPLR là một phương pháp học máy có thể đưa ra các mô hình có độ chính xác cao dựa trên phân tích các tập dữ liệu thí nghiệm. Trong bài báo này, chúng tôi phát triển một chương trình phần mềm để dự báo khả năng chịu lực của kết cấu trên nền tảng MATLAB.

Từ khóa: Phân tích hồi quy, Kết cấu xây dựng, Ngôn ngữ MATLAB, SPLR.

1. Introduction

Regression analysis is widely encountered problems in structural engineering [1-3]. These problems typically involve the construction of the mathematical relationship between a set of influencing factors and a modeled variable. This mathematical relationship is then used for supporting decision making processes in structural design phases [4-7]. Recent works in machine learning have created effective data analysis tools for regression analysis that are demonstrated to be more capable than conventional statistical approaches [8]. Accordingly, these advanced data analysis tools such as neural network [9] and support vector machine [10], and many others have drawn attention of structural engineers.

Particularly, in structural engineering, empirical data modeling is very important because phenomena in this field are inherently complex and heavily relied on experimental

Email: hoangnhatduc@dtu.edu.vn

results. Therefore, machine learning has been widely utilized to generate data-driven models that can be used to predict behavior of real-world structural systems [11]. Hence, the investigation of new machine learning based regression methods is necessary for both practical uses and educational purposes.

Since machine learning has been increasingly popular in the community of structural engineering [12-14], this study constructs a software program based on Sequential Piecewise Linear Regression (SPMR) used for nonlinear function approximation with applications in structural engineering. The SPMR model has been proposed and described in the previous work of Hoang [5]. The main advantages of the SPMR model are that its structure can be explicitly described, visualized, and interpreted. These advantages make this tool suitable for structural engineers in modeling various complex phenomena.

The rest of the paper is organized as follows: the second section briefly mentions the formulation of SPMR; two application cases of the newly developed program are demonstrated in the third section; concluding remarks of this paper are stated in the final section.

2. Sequential Piecewise Linear Regression (SPLR)

In statistical field, multiple linear regression (MLR) is a widely used method for data modeling [15]. Given a set of data, MLR can be used to express a relationship between a set of explanatory variable X and a response variable Y in form of a meaningful predictive equation. Nevertheless, MLR cannot cope with nonlinear data due to its respected assumption on linear relationships among variables [16]. To employ the advantage of the conventional MLR and extend its modeling capability, researchers and practitioners have resorted to piecewise variants of MLR [17].

A piecewise MLR employs an individual linear model to fit a subset of the input data X. The transition location from a predictor domain to another predictor domain is often called as a breakpoint or a knot. A knot is defined as the value of a predictor variable where the linear functions intersect [16]. The break point locations permit the overall learning space to be separated into subspaces within which multiple linear models can be employed to fit the collected data. Generally, appropriate values of knots are unknown and must be identified in a data-driven manner.

The mathematical formula of piecewise MLR with one knot is shown as follows [18]:

$$Y(X_i) = \begin{cases} \sum_{d=1}^{D+1} \beta_d X_{i,d} \ \ if \ \ X_{i,d} \leq b \\ \sum_{d=1}^{D+1} \beta_d X_{i,d} \ \ if \ \ X_{i,d} > b \end{cases} \quad (1)$$

where X_i denotes the vector of the ith explanatory variable consisting of D elements. b denotes the breaking point value. Y denotes the response variable.

3. SPLR Program Applications

Notably, a sequential algorithm described in [5] relied on the concept of a hinge function [19], to automatically construct the piecewise MLR based on the collected data set. The Graphical user interface (GUI) of SPLR program is shown in **Fig. 1**. The SPMLR program supports both single run of model training and testing and multiple runs for model evaluation purpose. The model parameters include the maximum number of iterations, the number of knot candidates, and the regularization parameter. Notably, to run the program, the user needs to download and install MATLAB Runtime version R2017b (9.3) at:

https://www.mathworks.com/products/compiler/matlab-runtime.html
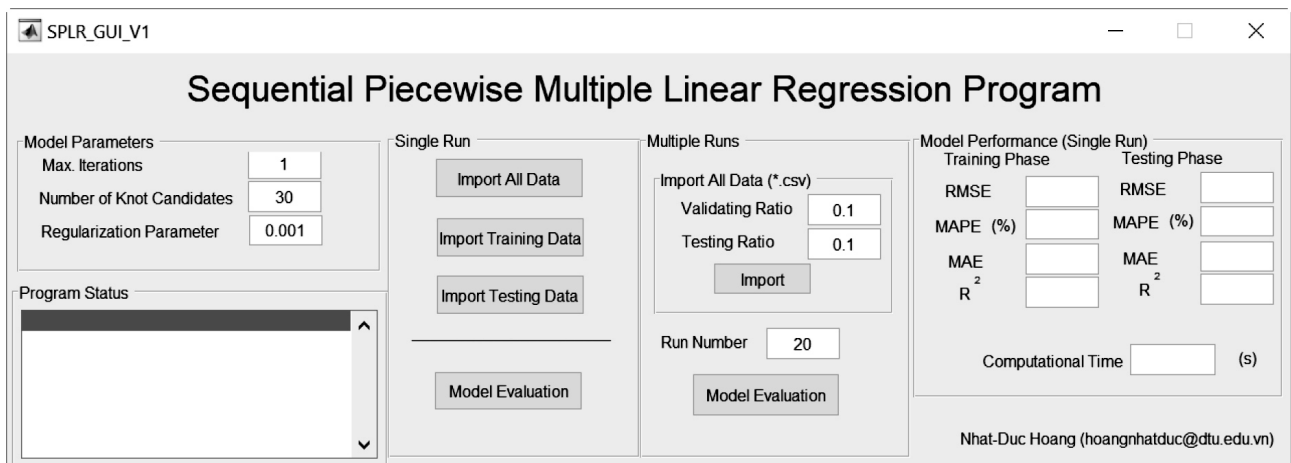
Fig. 1 Graphical user interface (GUI) of SPLR program

Moreover, to appraise the performance of the model, Root Mean Square Error (RMSE), the mean absolute percentage error (MAPE), the mean absolute error (MAE), and the coefficient of determination (R^2) are utilized. These indices are automatically computed by the SPRL program. For a single run, the user needs to provide the whole data set, the divided training set, and the divided testing set. The format of the dataset is .csv. The program will automatically normalize the dataset using Zscore normalization, perform model training, and perform prediction with data converted to the original range. The separated data sets are stored in the folder "**DividedDataSets**". The model results are provided in the folder "**ModelPredictionResult**".

In addition, the file of *ModelTestPerformance.csv* stores the model performance of the testing phase. For multiple runs, the model performance is stored in the files of **MeanModelTestPerformance, MeanModelTrainPerformance, stdModelTestPerformance, stdModelTrainPerformance** which show the average and the standard deviation of the outcomes (RMSE, MAPE, MAE, and R^2). The model structure is provided in the folder **ModelPredictionResult/ ModelStructure**. The file of Knots_X_i stores the knot values of the ith variable. The file of

ReshapedLinearModelParameters.csv stores the parameters of the linear model as described in [5]. Each column of the file includes 5 elements which are the parameters of the linear model (See **Fig. 2**).

Fig. 2 File that store the parameters of the linear models

For instance, if each variable has 1 knot, then the first column is the parameters of the linear model of the 1st variable; the second column is the parameters of the linear model of the 2nd variable and so on. However, if the variable X1 has 2 knots, then the first column is the parameters of the linear model of the 1st knot of X1. The second column is the parameters of the linear model of the 2nd knot of X1. Hence, the third column is the parameters of the linear model of the 1st knot of X2, and so on.

In the first application, the software program is used to estimate the punching shear capacity of steel fibre reinforced concrete (SFRC) flat slabs. The machine learning based model is used to construct a prediction model that can approximate the mapping function between the

punching shear capacity of SFRC flat slabs and its influencing factors. A data set consisting 140 samples with six influencing factors of slab depth, effective depth of the slab, length or radius of the loading pad or column, compressive strength of concrete, the reinforcement ratio, and the fibre volume has been collected from the literature [5]. This data set is then used to train and verify the SPLR program. The prediction performance of SPLR (RMSE = 28.27, MAPE = 12.96%, and R^2 = 0.90) for the first application case is shown in **Fig. 3**.
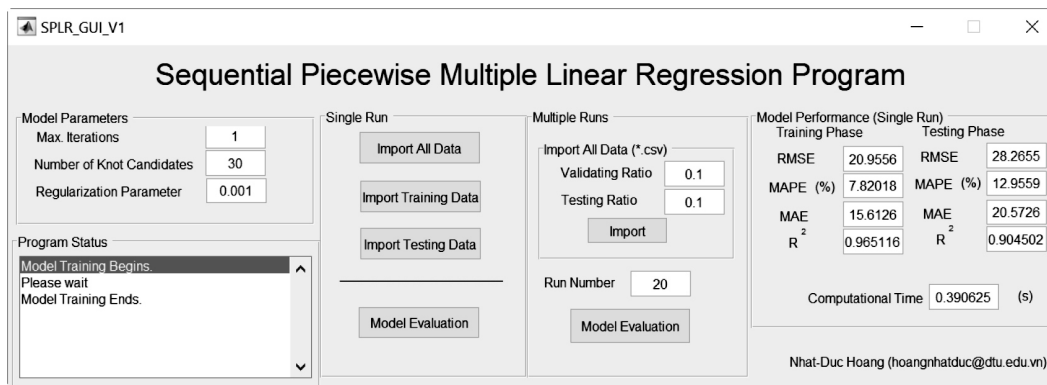
Fig. 3 Prediction performance of SPLR for the first application case

In the second application, the software program is employed to predict the shear strength of fiber reinforced concrete corbels. A dataset including 10 predictors and 108 samples has been collected and documented by Fleming [20]. The employed predictors are the shear span for corbels divided by the effective depth of the corbel, the width of the corbel, the height of the corbel, the steel reinforcement ratio, the tensile strength of fiber, the yield strength of steel reinforcement, the compressive strength of the concrete for cube specimens, the compressive strength of the concrete for cylinder specimens, the splitting tensile strength of fiber reinforced concrete, and the volumetric fiber ratio. The targeted output is the load carrying capacity of fiber reinforced corbels. The prediction performance of SPLR (RMSE = 110.09, MAPE = 12.14%, and R^2 = 0.92) for the second application case is shown in **Fig. 4**.
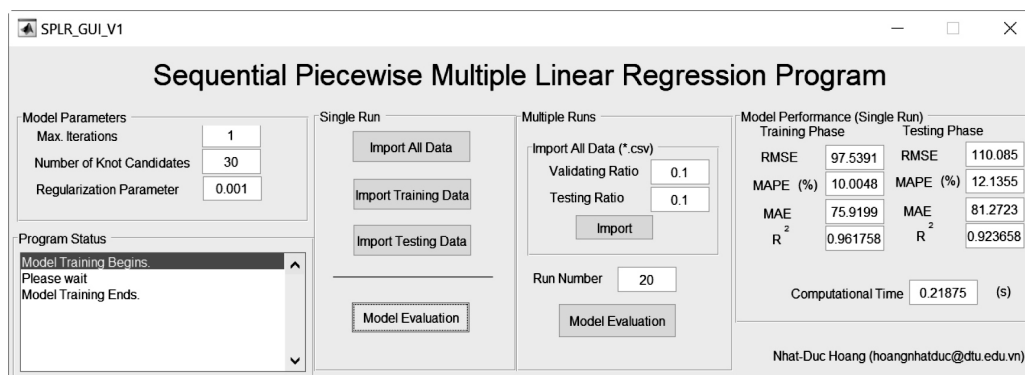
Fig. 4 Prediction performance of SPLR for the second application case

4. Conclusion

Regression analysis is a crucial task in structural engineering. To assist structural engineers in this task, this study develops a software program based on SPLR algorithm. The applicability of the software program has been demonstrated via two case studies using collected data sets of the punching shear capacity of SFRC flat slabs and the shear strength of fiber reinforced concrete corbels. Good predictive results demonstrate that the SPLR

program can be a useful tool for researchers and engineers for modeling other processes in the field of structural engineering.

Supplementary materials

The compiled SPLR program and the experimental datasets can be assessed via:

https://github.com/NhatDucHoang/SPLR_ML

References

[1] N.-D. Hoang, D.-T. Vu, X.-L. Tran, and V.-D. Tran, "Modeling Punching Shear Capacity of Fiber-Reinforced Polymer Concrete Slabs: A Comparative Study of Instance-Based and Neural Network Learning," *Applied Computational Intelligence and Soft Computing,* vol. 2017, p. 11, 2017.

[2] D.-T. Vu and N.-D. Hoang, "Punching shear capacity estimation of FRP-reinforced concrete slabs using a hybrid machine learning approach," *Structure and Infrastructure Engineering,* vol. 12, pp. 1153-1161, 2016/09/01 2016.

[3] P. Chetchotisak, P. Ruengpim, D. Chetchotsak, and S. Yindeesuk, "Punching Shear Strengths of RC Slab-Column Connections: Prediction and Reliability," *KSCE J Civ Eng,* vol. 22, p. 3066, 2018.

[4] H. Naderpour, O. Poursaeidi, and M. Ahmadi, "Shear resistance prediction of concrete beams reinforced by FRP bars using artificial neural networks," *Measurement,* vol. 126, pp. 299-308, 2018/10/01 2018.

[5] N.-D. Hoang, "Estimating Punching Shear Capacity of Steel Fibre Reinforced Concrete Slabs Using Sequential Piecewise Multiple Linear Regression and Artificial Neural Network," *Measurement,* vol. 137, pp. 58-70, 2019/01/18/ 2019.

[6] V.-H. Nhu, N.-D. Hoang, V.-B. Duong, H.-D. Vu, and D. Tien Bui, "A hybrid computational intelligence approach for predicting soil shear strength for urban housing construction: a case study at Vinhomes Imperia project, Hai Phong city (Vietnam)," *Engineering with Computers,* February 06 2019.

[7] K.-W. Liao, N.-D. Hoang, and J. Gitomarsono, "A Probabilistic Safety Evaluation Framework for Multi-Hazard Assessment in a Bridge using SO-MARS Learning Model," *KSCE Journal of Civil Engineering,* vol. 22, pp. 903-915, March 01 2018.

[8] T.-H. Tran and N.-D. Hoang, "Predicting Colonization Growth of Algae on Mortar Surface with Artificial Neural Network," *Journal of Computing in Civil Engineering,* vol. 30, p. 04016030, 2016.

[9] H. Allahyari, I. M. Nikbin, S. Rahimi R, and A. Heidarpour, "A new approach to determine strength of Perfobond rib shear connector in steel-concrete composite structures by employing neural network," *Engineering Structures,* vol. 157, pp. 235-249, 2018/02/15/ 2018.

[10] Y. Zhou, W. Su, L. Ding, H. Luo, and P. E. D. Love, "Predicting Safety Risks in Deep Foundation Pits in Subway Infrastructure Projects: Support Vector Machine Approach," *Journal of Computing in Civil Engineering,* vol. 31, p. 04017052, 2017.

[11] A. Çevik, A. E. Kurtoğlu, M. Bilgehan, M. E. Gülşan, and H. M. Albegmprli, "Support vector machines in structural engineering: a review," *Journal of Civil Engineering and Management,* vol. 21, pp. 261-281, 2015/04/03 2015.

[12] M. H. Rafiei and H. Adeli, "A novel machine learning-based algorithm to detect damage in high-rise building structures," *The Structural Design of Tall and Special Buildings,* vol. 26, pp. 1-11, 2017.

[13] H. Salehi and R. Burgueño, "Emerging artificial intelligence methods in structural engineering," *Engineering Structures,* vol. 171, pp. 170-189, 2018/09/15/ 2018.

[14] Ł. Sadowski, J. Hoła, S. Czarnecki, and D. Wang, "Pull-off adhesion prediction of variable thick overlay to the substrate," *Automation in Construction,* vol. 85, pp. 10-23, 2018/01/01/ 2018.

[15] S. Weisberg, *Applied Linear Regression, Third Edition*: John Wiley & Sons, Printed in the United States of America, 2005.

[16] S. E. Ryan and L. S. Porth, "A tutorial on the piecewise regression approach applied to bedload transport data," *Gen. Tech. Rep. RMRS-GTR-189. Fort Collins, CO: U.S. Department of Agriculture, Forest Service, Rocky Mountain Research Station. 41 p.,* 2007.

[17] E. Papadimitriou, V. Mylona, and J. Golias, "Perceived Level of Service, Driver, and Traffic Characteristics: Piecewise Linear Model," *Journal of Transportation Engineering,* vol. 136, pp. 887-894, 2010.

[18] M. E. Greene, O. Rolfson, G. Garellick, M. Gordon, and S. Nemes, "Improved statistical analysis of pre- and post-treatment patient-reported outcome measures (PROMs): the applicability of piecewise linear regression splines," *Quality of Life Research,* vol. 24, pp. 567-573, March 01 2015.

[19] L. Breiman, "Hinging hyperplanes for regression, classification, and function approximation," *IEEE Transactions on Information Theory,* vol. 39, pp. 999-1013, 1993.

[20] E. Fleming, *Construction Technology: an illustrated introduction*: Blackwell Publishing Ltd, 2005.

An improved space vector modulation method for matrix converters under unbalanced input voltage condition

Phương pháp điều chế vector không gian cho bộ biến tần ma trận trong điều kiện nguồn mất cân bằng

Huu Nhan Nguyen

Nguyễn Hữu Nhân

Institute of Research and Development, Duy Tan University, 03 Quang Trung, Danang, Vietnam
Viện Nghiên cứu và Phát triển Công nghệ cao, Đại học Duy Tân, 03 Quang Trung, Đà Nẵng, Việt Nam

Abstract

This paper presents a space vector modulation (SVM) method for matrix converters under unbalanced input voltage condition. By considering the proper voltages to calculate new duty cycles, the proposed method can achieve a balanced sinusoidal output-current waveform. Under balanced and sinusoidal input voltages, the proposed SVM method provides the same results as the conventional SVM method. The simulation results are shown to confirm the correctness of the proposed method.

Keywords: Matrix converter, ac-ac power converter, space vector modulation method, unbalanced input voltages.

Tóm tắt

Bài báo này trình bày phương pháp điều chế vector không gian cho bộ biến tần ma trận trong điều kiện nguồn mất cân bằng. Bằng cách xem xét các điện áp thích hợp để tính tỉ số đóng cắt trong từng sector, phương pháp đề xuất có thể đạt được dòng đầu ra dạng sin cân bằng. Trong điều kiện nguồn sin cân bằng, phương pháp điều chế vector không gian đề xuất cho kết quả giống với phương pháp truyền thống. Kết quả mô phỏng đã kiểm chứng tính chính xác của phương pháp đề xuất.

Từ khóa: Bộ biến tần ma trận, bộ biến tần ac-ac, phương pháp điều chế vector không gian, nguồn mất cân bằng.

I. Introduction

In the last two decades, matrix converters (MCs) have been received increasing attention since they may become a suitable alternative to the traditional inverters in industrial applications [1]. Indeed, the absence of bulky electrolytic capacitors for energy storage is one of the salient advantages of the MC which leads to the MC being more compact, robust, and reliable [2]. However, due to the lack of dc-link capacitors for energy storage, the MC becomes more sensitive to any disturbance in the supply voltages, because it will be immediately transmitted to the output voltages [3]. Therefore, the MC should be considered under the abnormal input voltage conditions.

Nowadays, there are several modulation strategies that can be applied to the MC. In 1980, the first modulation strategy was proposed by Venturini in [4]. In 1987, the scalar control algorithm was proposed by Roy and April in [5]. In 1987, the

Email: huunhan.vn@gmail.com

first idea of carrier-based modulation method was presented in [6]. In 1989, Huber and Borojevic proposed in [7] the indirect space vector modulation (SVM) method which considers MC as a two-stage converter: a rectifier stage provides a constant imaginary DC-link voltage and a conventional inverter generates the three-phase output voltage. In 1993, Casadei, Grandi, Serra and Tani proposed in [8] the direct SVM method. Compared to other methods, the direct SVM method provides a more flexible technique and easy understanding of the direct power conversion. This paper focuses on the direct SVM method for three-phase MCs.
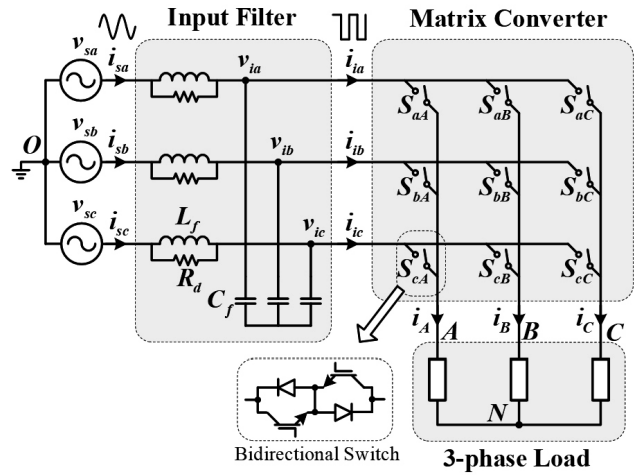
Fig. 1. A common three-phase to three-phase MC configuration.

Table 1. Possible switching configurations in the MC

	Switching configurations			Output Voltage		Input Current	
	No	A	B	C	V_o	α_o	I_i	β_i
Group I	+1	a	b	b	$2v_{ab}/3$	0	$2i_A/\sqrt{3}$	$-\pi/6$
	-1	b	a	a	$-2v_{ab}/3$	0	$-2i_A/\sqrt{3}$	$-\pi/6$
	+2	b	c	c	$2v_{bc}/3$	0	$2i_A/\sqrt{3}$	$\pi/2$
	-2	c	b	b	$-2v_{bc}/3$	0	$-2i_A/\sqrt{3}$	$\pi/2$
	+3	c	a	a	$2v_{ca}/3$	0	$2i_A/\sqrt{3}$	$7\pi/6$
	-3	a	c	c	$-2v_{ca}/3$	0	$-2i_A/\sqrt{3}$	$7\pi/6$
	+4	b	a	b	$2v_{ab}/3$	$2\pi/3$	$2i_B/\sqrt{3}$	$-\pi/6$
	-4	a	b	a	$-2v_{ab}/3$	$2\pi/3$	$-2i_B/\sqrt{3}$	$-\pi/6$
	+5	c	b	c	$2v_{bc}/3$	$2\pi/3$	$2i_B/\sqrt{3}$	$\pi/2$
	-5	b	c	b	$-2v_{bc}/3$	$2\pi/3$	$-2i_B/\sqrt{3}$	$\pi/2$
	+6	a	c	a	$2v_{ca}/3$	$2\pi/3$	$2i_B/\sqrt{3}$	$7\pi/6$
	-6	c	a	c	$-2v_{ca}/3$	$2\pi/3$	$-2i_B/\sqrt{3}$	$7\pi/6$
	+7	b	b	a	$2v_{ab}/3$	$4\pi/3$	$2i_C/\sqrt{3}$	$-\pi/6$
	-7	a	a	b	$-2v_{ab}/3$	$4\pi/3$	$-2i_C/\sqrt{3}$	$-\pi/6$
	+8	c	c	b	$2v_{bc}/3$	$4\pi/3$	$2i_C/\sqrt{3}$	$\pi/2$
	-8	b	b	c	$-2v_{bc}/3$	$4\pi/3$	$-2i_C/\sqrt{3}$	$\pi/2$
	+9	a	a	c	$2v_{ca}/3$	$4\pi/3$	$2i_C/\sqrt{3}$	$7\pi/6$
	-9	c	c	a	$-2v_{ca}/3$	$4\pi/3$	$-2i_C/\sqrt{3}$	$7\pi/6$
Group II	0_a	a	a	a	0	x	0	x
	0_b	b	b	b	0	x	0	x
	0_c	c	c	c	0	x	0	x
Group III	r_1	a	b	c	x	x	x	x
	r_2	a	c	b	x	x	x	x
	r_3	b	c	a	x	x	x	x
	r_4	b	a	c	x	x	x	x
	r_5	c	a	b	x	x	x	x
	r_6	c	b	a	x	x	x	x

Currently, there are some research papers that have been published on reducing the effects of unbalanced input voltages. However, these researches are based on the indirect SVM method

[9], [10] or need complex equations [11], [12]. This paper presents a modified direct SVM that can reduce the undesirable effects of unbalanced input voltages with simple duty cycles. Therefore,

the proposed method can replace the conventional SVM method in most of the cases. Simulation results verify the correctness and effectiveness of the proposed SVM method.

II. Conventional SVM method

Fig. 1 shows a common 3x3 MC configuration which consists of 9 bidirectional switches. In a balanced operation, the instantaneous input voltages are as follows:

$$\mathbf{v_i} = \begin{bmatrix} v_{ia} \\ v_{ib} \\ v_{ic} \end{bmatrix} = V_i \begin{bmatrix} \cos(\omega_i t) \\ \cos(\omega_i t - 2\pi/3) \\ \cos(\omega_i t + 2\pi/3) \end{bmatrix} \quad (1)$$

where V_i and ω_i are the amplitude and the angular frequency of the input voltage, respectively.

With the relevant symbols shown in Fig. 1, the space vectors of input/output voltages and currents are defined, respectively, by the following equations:

$$\vec{v}_i = 2(v_{ia} + v_{ib}e^{j2\pi/3} + v_{ic}e^{j4\pi/3})/3 = V_i e^{j\alpha_i} \quad (2)$$

$$\vec{v}_o = 2(v_A + v_B e^{j2\pi/3} + v_C e^{j4\pi/3})/3 = V_o e^{j\alpha_o} \quad (3)$$

$$\vec{i}_i = 2(i_{ia} + i_{ib}e^{j2\pi/3} + i_{ic}e^{j4\pi/3})/3 = I_i e^{j\beta_i} \quad (4)$$

$$\vec{i}_o = 2(i_A + i_B e^{j2\pi/3} + i_C e^{j4\pi/3})/3 = I_o e^{j\beta_o}. \quad (5)$$

Fig. 2. (a) The location of output voltage vector. (b) The location of input current vector.

Hereafter, any space vector will be referred to simply as a vector.

There are 27 possible switching configurations (SCs) to satisfy 2 main rules in an MC: i) input phases should never be short-circuited, and ii) the output currents should not be interrupted. These 27 SCs are listed in Table I and categorized into three groups:

1) Group I consists of active vectors.

2) Group II consists of zero vectors.

3) Group III consists of synchronous vectors. Normally, the space vectors in group III are not used because the output-voltage and input-current vectors have time-varying directions.

The first 18 SCs determine the location of output voltage vector $\vec{v}_o$ and input current vector $\vec{i}_i$ in (α, β) plane as shown in the (a) and (b). The conventional SVM method is based on the selection of 4 suitable active vectors and zero vectors to control $\vec{v}_o$ and $\vec{i}_i$. The zero SCs are applied to complete the sampling period T_s.

For example, both $\vec{v}_o$ and $\vec{i}_i$ are lying in sector 1 ($k_v = 1$, $k_i = 1$, where k_v and k_i are the output voltage vector sector and the input voltage vector sector, respectively) as shown in Fig. 2. The desired output voltage vector $\vec{v}_o$ can be synthesized from two vectors $\vec{v}_o'$ and $\vec{v}_o''$. The $\vec{v}_o'$ component can be synthesized using two of six possible SCs $\pm 1, \pm 2, \pm 3$. Only two SCs giving higher voltage magnitude vectors are considered to generate $\vec{v}_o'$. In the case $k_i = 1$, two higher voltage values are v_{ab} and v_{ac}, so SCs +1 and -3 should be selected. Likewise, SCs −7 and +9 are selected to generate $\vec{v}_o''$.

Table 2. Selected SCs for each combination of output voltage and input current sectors in the conventional SVM method

		Input Current Vector Sector																							
		1				2				3				4				5				6			
Output Voltage Vector Sector	1	−7	+9	+1	−3	+9	−8	−3	+2	−8	+7	+2	−1	+7	−9	−1	+3	−9	+8	+3	−2	+8	−7	−2	+1
	2	+4	−6	−7	+9	−6	+5	+9	−8	+5	−4	−8	+7	−4	+6	+7	−9	+6	−5	−9	+8	−5	+4	+8	−7
	3	−1	+3	+4	−6	+3	−2	−6	+5	−2	+1	+5	−4	+1	−3	−4	+6	−3	+2	+6	−5	+2	−1	−5	+4
	4	+7	−9	−1	+3	−9	+8	+3	−2	+8	−7	−2	+1	−7	+9	+1	−3	+9	−8	−3	+2	−8	+7	+2	−1
	5	−4	+6	+7	−9	+6	−5	−9	+8	−5	+4	+8	−7	+4	−6	−7	+9	−6	+5	+9	−8	+5	−4	−8	+7
	6	+1	−3	−4	+6	−3	+2	+6	−5	+2	−1	−5	+4	−1	+3	+4	−6	+3	−2	−6	+5	−2	+1	+5	−4
Duty cycles		d_1	d_2	d_3	d_4	d_1	d_2	d_3	d_4	d_1	d_2	d_3	d_4	d_1	d_2	d_3	d_4	d_1	d_2	d_3	d_4	d_1	d_2	d_3	d_4

With a similar procedure, the selected SCs for all combinations of the output voltage and the input current sectors are summarized in Table II.

The general expressions of duty cycles are as follows:

$$d_1 = \frac{2q}{\sqrt{3}} \frac{\sin\alpha_o \sin(\pi/6-\beta_i)}{\cos\delta_i} \qquad (6)$$

$$d_2 = \frac{2q}{\sqrt{3}} \frac{\sin\alpha_o \sin(\pi/6+\beta_i)}{\cos\delta_i} \qquad (7)$$

$$d_3 = \frac{2q}{\sqrt{3}} \frac{\sin(\pi/3-\alpha_o)\sin(\pi/6-\beta_i)}{\cos\delta_i} \qquad (8)$$

$$d_4 = \frac{2q}{\sqrt{3}} \frac{\sin(\pi/3-\alpha_o)\sin(\pi/6+\beta_i)}{\cos\delta_i} . \qquad (9)$$

where $q = V_o/V_i$ is the voltage transfer ratio, $\delta_i = \alpha_i - \beta_i$ is the input current displacement angle.

Zero SCs are required to complete the sampling period with the duty cycle:

$$d_0 = 1 - \frac{2q}{\sqrt{3}} \frac{\cos(\alpha_o - \pi/6)\cos\beta_i}{\cos\delta_i} . \qquad (10)$$
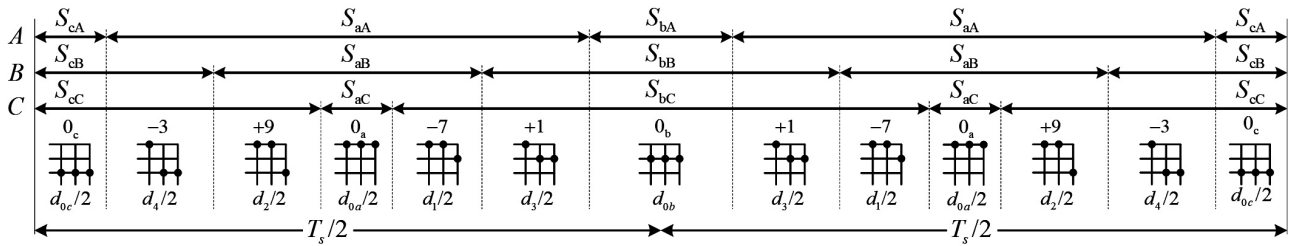

Fig. 3. Switching pattern for output voltage sector 1 and input current sector 1 of the conventional SVM method.

Fig. 3 shows the switching pattern corresponding to the case of $k_v = 1$, $k_i = 1$.

All duty cycles in the conventional SVM method must satisfy the following constraints:

$$0 \leq d_n \leq 1; \quad n = 0,..,4 . \qquad (11)$$

This leads to the well-known restriction of the voltage transfer ratio in the MC:

$$q \leq \frac{\sqrt{3}}{2}\cos\delta_i . \qquad (14)$$

III. Proposed SVM method

Without any assumption, equation (2) can be rewritten as follows:

$$\vec{v}_i = \left(\frac{2}{3}v_{ab} + \frac{1}{3}v_{bc}\right) + j\frac{\sqrt{3}}{3}v_{bc} \qquad (12)$$

From (12), it is worth noting that the input voltage space vector does depend only on the input line-to-line voltages in any condition. Likewise, the output voltage space vector only depends on the input line-to-line voltages.

In principle, the proposed SVM method is based on the selection of four suitable active vectors to synthesize the reference output voltage vector under the unity input power factor constraint. The zero SCs are applied to complete the sampling period T_s. For example, both the out voltage space vector and input current space vector are lying in sector 1. Like in the conventional SVM method, four SCs +1, –3, –7, +9 are selected in this case.

The duty cycles of SCs −7 (d_1) and +9 (d_2) in this case should satisfy the following relationship:

$$\frac{2}{3}v_{ab}d_1 + \frac{2}{3}v_{ac}d_2 = \frac{2}{\sqrt{3}}V_o\sin\alpha_o \qquad (13)$$

Since magnitude of input current is independent of the phase angle of output current, the relationship between d_1 and d_2 is given by:

$$d_1\sin(\pi/6+\beta_i) = d_2\sin(\pi/6-\beta_i) \qquad (14)$$

By solving equations (13) and (14), the duty cycles for SCs −7 and +9 become as follows:

$$d_1 = \frac{V_o}{V_i} \frac{\sin\alpha_o.\sin(\pi/6-\beta_i)}{\text{DEN}} \qquad (15)$$

$$d_2 = \frac{V_o}{V_i} \frac{\sin\alpha_o.\sin(\pi/6+\beta_i)}{\text{DEN}} \qquad (16)$$

where

$$\text{DEN} = \cos(\pi/6+\alpha_i)\sin(\pi/6-\beta_i) + \cos(\pi/6-\alpha_i)\sin(\pi/6+\beta_i)$$

$$(17)$$

Table 3. Simulation parameters

Power supply	Input filter	Output load
$V_s = 220\text{V}$ $f_i = 60\text{Hz}$	$L_f = 2\text{mH}$ $C_f = 22\mu\text{F}$ $R_d = 30\Omega$	$R = 10\Omega$ $L = 15\text{mH}$ $f_o = 50\text{Hz}$ $V_o = 150\text{V}$

Similarly, the duty cycles for SCs +1 (d_3) and −3 (d_4) are as follows:

$$d_3 = \frac{V_o}{V_i}\frac{\sin(\pi/3-\alpha_o).\sin(\pi/6-\beta_i)}{\text{DEN}} \quad (18)$$

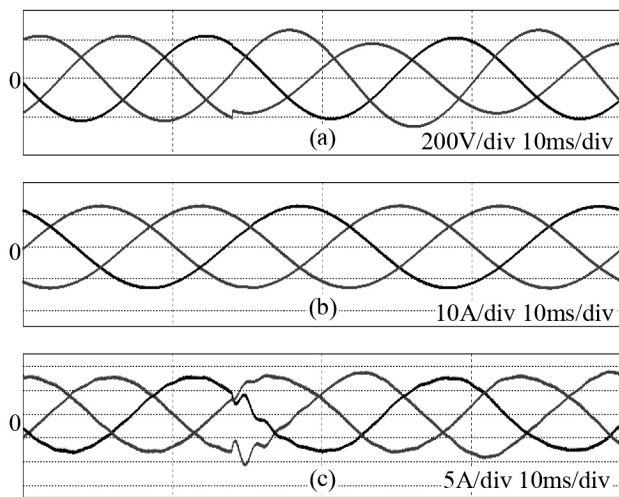$$d_4 = \frac{V_o}{V_i}\frac{\sin(\pi/3-\alpha_o).\sin(\pi/6+\beta_i)}{\text{DEN}} \quad (19)$$

Fig. 4. (a) Three-phase input voltage. (b) Three-phase output current. (c) Three-phase input current.

IV. Simulation results

Simulations are carried out for a three-phase symmetrical *RL* load by using PSIM 9.0 software. The simulation parameters are shown in Table 3. The switching frequency of the SVM methods is 10 kHz, corresponding to the switching period of 100 μs.

Figures 4(a), (b), and (c) show the power supply phase voltage, three-phase output current, and three-phase input current, respectively. At $t = 14\text{ ms}$, the power supply voltage is subjected to an imbalance. As can be seen in Fig. 4(b), the three-phase output current is sinusoidal and balanced. Obviously, the input currents are unbalanced to ensure the conservation of energy law.

V. Conclusion

This paper has presented an improved SVM method that drives MC under the unbalanced input voltage condition. The proposed SVM method requires information about input line-to-line voltage, which is the same as in the conventional SVM method, to calculate the duty cycles. Therefore, the proposed method can replace the conventional SVM method in most of the cases due to the simplicity and generalization. The simulation results are provided to validate the correctness and effectiveness of the proposed method.

References

[1] D. Casadei, G. Serra, and A. Tani, "Reduction of the Input Current Harmonic Content in Matrix Converters Under Input/Output Unbalance," *IEEE Trans. Ind. Electron.,* vol. 45, no. 3, pp. 401–411, Jun. 1998.

[2] R. K. Gupta, K. K. Mohapatra, A. Somani, and N. Mohan, "Direct-Matrix-Converter-Based Drive for a Three-Phase Open-End-Winding AC Machine With Advanced Features," *IEEE Trans. Ind. Electron.,* vol. 57, no. 12, pp. 4032–4042, Dec. 2010.

[3] K. Sun, D. Zhou, L. Huang, and K. Matsuse, "Compensation Control of Matrix Converter Fed Induction Motor Drive Under Abnormal Input Voltage Conditions," in *Proc. IAS,* 2004, pp. 623–630.

[4] M. Venturini, "A new sine wave in, sine wave out, conversion technique eliminates reactive elements," in *Proceedings of Powercon 7, San Diego, CA,* 1980, pp. E3-1-E3-15.

[5] G. Roy and G.-E. April, "Cycloconverter operation under a new scalar control algorithm," *in Proc. 20th Annu. IEEE Power Electron. Spec. Conf.,* Jun. 1989, vol. 1, pp. 368–375.

[6] Jose Rodriguez, "High performance dc motor drive using a PWM rectifier with power transistors," *Proc. Inst. Elect. Eng. B—Elect. Power Appl.,* vol. 134, no. 1, p. 9, Jan. 1987.

[7] L. Huber, D. Borojevic, "Space Vector Modulator for Forced Commutated Cycloconverters," *Proceedings of IEEE/PESC'89,* pp. 871-876, 1989.

[8]   D. Casadei, G. Grandi, G. Serra, A. Tani, "Space vector control of matrix converters with unity input power factor and sinusoidal input/output waveforms," *Proceedings of IEE-EPE'93,* vol. 7, pp. 170-175, 1993.

[9]   N. K. T. Tam, N. V. Nho, and H. T. Hoang, "Indirect space vector modulated three phase ac-ac matrix converter under abnormal input conditions," *in Proc. PEDS,* 2011, pp. 379–384.

[10] M. Hamouda, H. F. Blanchette, and K. Al-Haddad, "Unity power factor operation of indirect matrix converter tied to unbalanced grid," *IEEE Trans. Power*

Electron., vol. 31, no. 2, pp. 1095–1107, Feb. 2016.

[11] X. Li, M. Su, Y. Sun, H. Dan, and W. Xiong, "Modulation strategies based on mathematical construction method for matrix converter under unbalanced input voltages," *IET Trans. Power Electron.,* vol. 6, no. 3, pp. 434–445, Mar. 2013.

[12] J. Lei, B. Zhou, J. Bian, J. Wei, Y. Zhu, J. Yu, and Y. Yang, "Feedback control strategy to eliminate the input current harmonics of matrix converter under unbalanced input voltages," *IEEE Trans. Power Electron.,* vol. 32, no. 1, pp. 878–888, Jan. 2017.

A technique to boost frequent pattern mining algorithms

Một kỹ thuật tăng tốc các thuật toán khai thác mẫu phổ biến

Huu Hiep Nguyen

Nguyễn Hữu Hiệp

Institute of Research and Development, Duy Tan University, 03 Quang Trung, Da Nang, Vietnam
Viện Nghiên cứu và Phát triển Công nghệ cao, Đại học Duy Tân, 03 Quang Trung, Đà Nẵng, Việt Nam

Abstract

Mining frequent itemsets from a transaction database has emerged as a fundamental problem in data mining and been considered as a building block for many mining tasks. In this paper, we present a simple technique to reduce the intersection cost in the existing PrePost scheme. Our technique is based on an early-stopping criterion and general enough to be applicable in many frequent itemset mining algorithms. We have evaluated our technique over several datasets and proved its effectiveness in runtime reduction.

Keywords: Frequent itemset mining, PrePost, N-list, earlystopping criterion.

Tóm tắt

Khai thác các tập phổ biến từ một cơ sở dữ liệu giao dịch đã trở thành một bài toán cơ bản trong khai mỏ dữ liệu và có thể được dùng như một khối cơ sở cho các tác vụ khai thác. Trong bài báo này, chúng tôi trình bày một kỹ thuật đơn giản để giảm chi phí tính phần giao trong thuật toán PrePost đã có. Kỹ thuật của chúng tôi dựa trên một tiêu chuẩn kết thúc sớm và nó khá tổng quát, có thể áp dụng trong nhiều thuật toán khai thác mẫu khác. Chúng tôi đã đánh giá kỹ thuật này trên một số tập dữ liệu và chứng tỏ được khả năng rút ngắn thời gian chạy.

Từ khóa: Khai thác tập phổ biến, PrePost, N-list, tiêu chuẩn dừng sớm.

I. Introduction

Frequent itemset mining, first proposed by Agrawal et al. [1], has become a popular data mining technique and plays a fundamental role in many important data mining tasks such as mining association rules, correlations, episodes and so on. There have been thousands of research publications following this initial idea. Although lots of algorithms have been proposed, how to improve the efficiency of mining algorithms is still one of several key research problems to be solved.

Recently, Deng et al. [2], [4] proposed PrePost and its enhanced version PrePost+ for mining frequent itemsets. Both of them employ a novel data structure named N-list to represent itemsets and adopt single path property of N-list to directly discover frequent itemsets without generating candidate itemsets in some cases. The experiments in [2], [4] show that PrePost/PrePost+ runs faster than some state-of-the-art mining algorithms including FP-growth [7] and FP-growth*[6].

Email: nguyenhuuhiep2@dtu.edu.vn

In this work, we further improve PrePost by proposing a simple yet effective technique to stop early the check of *infrequent* candidate itemsets. Given an infrequent candidate itemset, the technique accumulates that evidence of infrequency and decides it early, so further redundant processing steps are dropped. The runtime reduction is always guaranteed, especially on datasets with complex structures.

We review the related work in the next subsection. The existing PrePost is described in Section II. Our proposed technique will be presented in Section III followed by the evaluation (Section IV). Finally, we conclude the paper and propose future work in Section V.

Related work

Itemset mining is an important problem of data mining. Currently, there are many variations of itemset mining such as frequent itemset mining [1, 7, 12], frequent closed itemset mining [10, 11], frequent weighted itemset mining [9], erasable itemset mining [3] and so on. However, frequent itemset mining is the most popular as it plays an important role in association rule mining [1], sequential mining [5], classification [8]. There have been a large number of algorithms which effectively mine frequent itemsets. They may be divided into three main categories:

- **Methods that use a candidate generate-and-test strategy**: These methods use a level-wise approach for mining frequent itemsets. First, they generate frequent 1-itemsets which are then used to generate candidate 2-itemsets, and so on until no more candidates can be generated. Apriori [1] is a seminal work in this category.

- **Methods that adopt a divide-and-conquer strategy**: Methods that compress the dataset into a tree structure and mine frequent itemsets from this tree by using a divide-and-conquer strategy. FP-Growth [7] and FPGrowth* [6] are exemplar algorithms.

- **Methods that use a hybrid approach**: These methods use vertical data formats to compress the database and mine frequent itemsets by using a divide-and-conquer strategy. Eclat [12], dEclat [11], and Node-list-based method [2], [4], are some examples.

II. PrePost

In this section, we review basic concepts of frequent pattern mining and PrePost before describing the improvement technique in the next section.

A. Frequent itemsets

We assume a dataset *DB* consists of *n* transactions such that each transaction contains a number of items belonging to *I* where $I = \{i_1, i_2, ..., i_m\}$ is the set of all items in *DB*.

The support of an itemset *X*, denoted by $\rho(X)$ where $X \subset I$, is the number of transactions in *DB* which contain all the items in *X*. An itemset *X* is a "frequent itemset" if $\rho(X) \geq [minSup \times n]$, where *minSup* is a given threshold. Note that a frequent itemset with *k* elements is called a frequent k-itemset, and F_1 is the set of frequent 1-itemsets sorted in frequency descending order.

Table I shows a *DB* of 10 transactions with *I*={a,b,c,d,e}. The *minSup* is fixed to 0.3, i.e., itemsets with frequency at least 3 will be output, e.g., {a, c} with frequency 4 as it appears in the transactions 3, 4, 6 and 8. The items are sorted in frequency descending order as {a, c, e, d, b} because their frequencies are 7, 7, 7, 6, and 3 respectively. The third column of Table 1 displays the transactions in *DB* with reordered items.

Table 1. An example of transaction dataset

Transaction	Items	Transaction with reordered items
1	a, d, e	a, e, d
2	b, c, d	c, d, b
3	a, c, e	a, c, e
4	a, c, d, e	a, c, e, d
5	a, e	a, e
6	a, c, d	a, c, d

7	b, c	c, b
8	a, c, d, e	a, c, e, d
9	b, c, e	c, e, b
10	a, d, e	a, e, d

B. PPC-tree and N-list

Given a reordered *DB*, PPC-Tree [2] is a tree structure defined as follows

- It consists of one root labeled as null ({}), and a set of item prefix subtrees as the children of the root.

- Each node in the item prefix subtree contains five fields: *name, frequency, childnodes, pre,* and *post*. The field name registers which item this node represents. The field frequency registers the number of transactions containing a path reaching this node. The field *childnodes* registers all children of the node. The field pre is the pre-order rank of the node. The field post is the post-order rank of the node. For a node, its pre-order is the sequence number of the node when scanning the tree by pre-order traversal and its post-order is the sequence number of the node when scanning the tree by post-order traversal.

Fig. 1 demonstrates how the PPC-Tree is built from the reordered transactions in Table I. We start with a null root. Then the first transaction {*a, e, d*} is inserted in the PPC-Tree by creating nodes named *a, e* and *d* with frequency 1. Similarly, for the second transaction {*c, d, b*}, a new child node of the root and two descendent nodes are added. The third and fourth subfigures show the tree after the insertion of {*a, c, e*} and {*a,c,e,d*}. The full PPC-Tree is shown in Fig. 2.
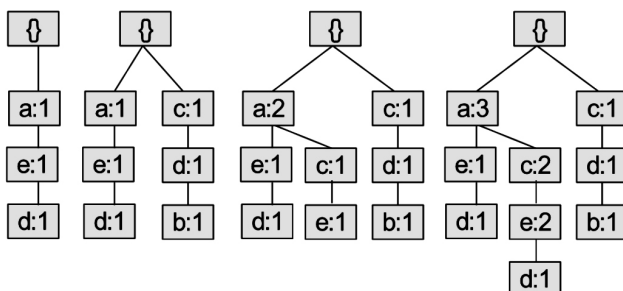

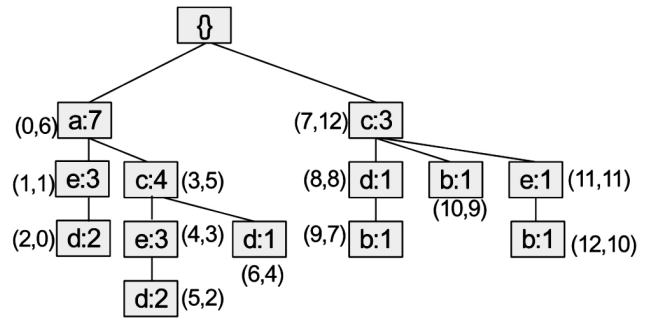Figure 1. Ppc-tree after inserting first four transactions

Figure 2: Full PPC-Tree

The pre-order and post-order ranks are tagged in a pair of numbers next to each node in Fig. 2. *PP-code* [2] of each node *N* in PPC-Tree is a triple $< N.pre, N.post, N.frequency >$.

N-list [2] of a frequent item *x*, denoted as $NL(x)$ is a sequence of all the PP-codes of nodes *N* with *N.name* = *x* in the PPC-Tree. The PP-codes are arranged in an ascending order of their pre-order ranks. Fig. 3 lists the N-list of all 1- itemsets.

Clearly, the support of 1-itemset *x* is the sum of frequencies of PP-codes in $NL(x)$. For example, $\rho(c) = 4 + 3 = 7, \rho(d) = 2 + 2 + 1 + 1 = 6$.

N-list of k-itemset [2] is defined as follows. Let *XA* and *XB* be two (k-1)-itemsets with the same prefix *X* such that *A* is before *B* according to the frequency ordering. $NL(XA)$ and $NL(XB)$ are two N-lists associated with XA and XB, respectively. The N-list associated with XAB is determined as follows (this is performed in *NL intersect* function in Algorithm 2):

1) For each PP-code $P_A \in NL(XA)$ and $P_B \in NL(XB)$, if P_A is an ancestor of P_B in PPC-Tree, the algorithm will add $< P_A.pre, P_A.post, P_B.frequency >$

$a \rightarrow < 0, 6, 7 > \quad c \rightarrow < 3, 5, 4 >, < 7, 12, 3 > \quad e \rightarrow < 1, 1, 3 >, < 4, 3, 3 >, < 11, 11, 1 > \quad d \rightarrow < 2, 0, 2 > < 5, 2, 2 > < 6, 4, 1 > < 8, 8, 1 > \quad b \rightarrow < 9, 7, 1 > < 10, 9, 1 > < 12, 10, 1 >$

Figure 3: N-list of 1- itemsets to $NL(XAB)$.

2) Traversing $NL(XAB)$ to combine the PP-codes which has the same pre and post values.

Example 2.1: $NL(c) = \{< 3, 5, 4 >, < 7, 12, 3 >\}$ and $NL(e) = \{< 1, 1, 3 >, < 4, 3, 3 >, < 11, 11, 1 >\}$, therefore $NL(ce) = \{< 3, 5, 3 >, < 7, 12, 1 >\}$ and

the support of ce is $\rho(ce) = 3 + 1 = 4$.

C. PrePost Algorithm

In this section, we briefly describe the PrePost algorithm [2] (see Algorithm 1). PrePost starts with the construction of PPC-Tree (Line 1) and computation of NL-list of frequent 1-itemsets (Line 2). At each level k (Lines 4-13), we try to test every pair of k-itemsets XA and XB having the same (k-1)-prefix X by computing the intersection $XAB = NL\ intersect(NL(XA),NL(XB))$ (Line 8). If XAB is frequent (Line 9) then it is inserted in F_{k+1} and its N-list is appended to NL_{k+1}.

Algorithm 1 PrePost [2]

Input: DB: database with n transactions. $minSup$: minimum support.

Output: F, the set of all frequent itemsets

1: Scan DB to obtain F_1, the set of all frequent 1- itemset, and build the PPC-Tree

2: Scan the PPC-tree to generate the N-lists of frequent 1itemset NL_1

3: $F = F \cup F_1, k = 1$

4: **while** $F_k! = \emptyset$ **do**

5:     $F_{k+1} = \emptyset$

6:     $NL_{k+1} = \emptyset$

7:     **for** $XA,XB \in F_k$ with the same (k-1)-prefix X **do**

8:         $XAB = $ NL intersect$(NL(XA),NL(XB))$

9:         **if** $XAB.frequency \geq \lceil minSup \times n \rceil$ **then**

10:            $F_{k+1} = F_{k+1} \cup XAB$

11:                        $NL_{k+1} = NL_{k+1} \cup NL(XAB)$

12:        $F = F \cup F_{k+1}$

13:        $k = k + 1$

14: **return** F.

Algorithm 1 is presented as a Breadth-First-Search (BFS), similar to Apriori [1]. In practice, however, we usually run it in Depth-First-Search (DFS) to reduce the memory usage.

The main steps of *NL intersect* are depicted in Algorithm 2. Similar to the well-known technique to merge two sorted lists, we maintain two indexes i and j and check for the intersection from left-to-right. The criteria for the merge (Lines 5-6) is stated in Section II-B, i.e., the i-th triple in $NL(XA)$ is mergeable to the j-th triple in $NL(XB)$ if and only if the former is the ancestor of the latter in the PPC-Tree.

Again with Example 2.1, the step-by-step merge between $NL(c)$ and $NL(e)$ is as follows. $< 3,5,4 >$ is non-mergeable to $< 1,1,3 >$ so it is tested against the next j, i.e., $< 4,3,3 >$ where it is mergeable and returns $< 3,5,3 >$. Then $< 3,5,4 >$, when compared to $< 11,11,1 >$, fails at Line 6, so we consider the next i, i.e., $< 7,12,3 >$.

Clearly, $< 7,12,3 >$ is mergeable to $< 11,11,1 >$, returning $< 7,12,1 >$. The intersection stops and we get $NL(ce) = \{< 3,5,3 >,< 7,12,1 >\}$.

Algorithm 2 NL intersect [2]

Input: $NL(XA) = \{< x_{1i}, y_{1i}, z_{1i} >\}$, $NL(XB) = \{< x_{2j}, y_{2j}, z_{2j} >\}$: N-lists of k-itemsets XA and XB.

Output: $NL(XAB)$, N-list of (k+1)-itemset XAB

1: $i = 1, j = 1$

2: $n_1 = |NL(XA)|$, $n_2 = |NL(XB)|$

3: $NL(XAB) = \emptyset$

4: **while** $i \leq n_1$ AND $j \leq n_2$ **do**

5: **if** $x_{1i} < x_{2j}$ **then** 6: **if** $y_{1i} > y_{2j}$ **then**

7:     $NL(XAB) = NL(XAB) \cup < x_{1i}, y_{1i}, z_{2j} >$

8:     $j = j + 1$

9:     **else**

10:    $i = i + 1$

11:    **else**

12:    $j = j + 1$

13: merge elements with same *(pre,post)* pair in $NL(XAB)$ 14: **return** $NL(XAB)$.

III. PrePost-ES: An early stopping criterion

In PrePost, calls to *NL intersect* (Algorithm 2, Line 8) contribute to the main runtime cost. We observe that the intersection set *XAB* needs to go through the size test in Line 9 before it is used to update F_{k+1} and NL_{k+1} (Lines 10 and 11).

Our main idea is to integrate the size test into function *NL intersect* in order that if the test fails early, we can stop the computation in *NL intersect* and return an empty *XAB*. As we will see, this simple technique is quite general and reduces the runtime effectively.

We present this idea in Algorithm 3. Compared to *NL intersect*, the new points in *NL intersect ES* includes the new input *minS* and Lines 3,4,12-14. Line 4 sets the upper limit for *skip*. At any triple *i* of *NL(XA)*, if it is non-mergeable, we increase *skip* (Line 12). If *skip* exceeds Δ, we stop and return an empty set (Lines 13-14). We demonstrate the effectiveness of *NL intersect ES* in the next example.

Example 3.1: Given $NL(d) = \{< 2,0,2 >< 5,2,2 >< 6,4,1 >< 8,8,1 >\}$ and $NL(b) = \{< 9,7,1 >< 10,9,1 >< 12,10,1 >\}$, if we call

NL intersect(NL(d),NL(b)), we need to run 5 checks for

$(i,j) = (0,0),(1,0),(2,0),(3,0),(3,1)$ in which only pair $(3,0)$ matches, so we get$NL(db) = \{< 8,8,1 >\}$. With support 1 (less than *minS* = 3), *db* is not frequent.

In calling *NL intersect ES(NL(d),NL(b))*, we know that *minS* = $0.3 \times 10 = 3$ and $\Delta = \rho(d) - minS = 6 - 3 = 3$.

After the two (failed) checks $(i,j) = (0,0),(1,0)$, we increase *skip* to $2 + 2 = 4$, exceeding Δ, so we safely conclude that *db* is not frequent, omitting the three remaining checks.

Algorithm 3 NL intersect ES

Input: $NL(XA) = \{< x_{1i},y_{1i},z_{1i} >\}$, $NL(XB) = \{< x_{2j},y_{2j},z_{2j} >\}$: N-lists of k-itemsets *XA* and *XB*.

Absolute minimum support $minS = \lceil minSup \times n \rceil$

Output: $NL(XAB)$, N-list of (k+1)-itemset *XAB*

1: $i = 1, j = 1$

2: $n_1 = |NL(XA)|$, $n_2 = |NL(XB)|$

3: $skip = 0$

4: $\Delta = \rho(XA) - minS$

5: $NL(XAB) = \emptyset$

6: **while** $i \leq n_1$ AND $j \leq n_2$ **do**

7:      **if** $x_{1i} < x_{2j}$ **then**

8:      **if** $y_{1i} > y_{2j}$ **then**

9:      $NL(XAB) = NL(XAB) \cup < x_{1i},y_{1i},z_{2j} >$

10:      $j = j + 1$

11:      **else**

12:      $skip = skip + z_{1i}$

13:      **if** $skip > \Delta$ **then**

14:      **return** $\emptyset$

15:      $i = i + 1$

16:      **else**

17:      $j = j + 1$

18: merge elements with same *(pre,post)* pair in $NL(XAB)$ 19: **return** $NL(XAB)$.

Table 2: Dataset properties

Dataset	#Items	#Trans
Accidents	468	340,183
Chess	76	3,196
T10I4D100K	870	100,000
T40I10D100K	942	100,000

IV. Experiments

In this section, we compare the performance of the proposed technique PrePost-ES and the baseline PrePost only in terms of running time. Both of them return correct results and consume the same amount of memory, so the memory comparison is omitted. The datasets are described in Sections IV-A. We show the comparison of runtime in Section IV-B. The algorithms are

implemented in C++ and run on a desktop PC with *Intel* Core i7-6700@ 3.4Ghz, 16GB memory.

A. Experiment Setup

We use four datasets as shown in Table II. The *chess* dataset is from different game steps. The *accidents* dataset contains traffic accident data. The *T10I4D100K* and *T40I10D100K* datasets are synthetic datasets from [1].

We compare our technique *PrePost-ES* (Early Stopping) against the original PrePost [2]. Recall that the technique is easily plugged to any frequent pattern mining schemes that require the intersection operation for support counting.

B. Comparison of Runtime

In this section, we evaluate the runtime improvement of our proposed scheme PrePost-ES. Table 3 compares the

Table 3: PrePost-ES vs. PrePost in number of checks and runtime (in seconds)

Dataset	minSup	PrePost		PrePost-ES	
		#Checks	Runtime	#Checks	Runtime
Accidents	0.1	1.117e9	18.335	1.011e9	18.323
	0.2	2.059e8	5.886	1.743e8	5.672
	0.3	5.356e7	4.716	4.459e7	4.466
	0.4	1.674e7	4.447	1.496e7	4.295
Chess	0.2	1.474e9	278.292	1.440e9	267.839
	0.3	2.581e8	32.863	2.491e8	32.669
	0.4	5.630e7	5.697	5.355e7	5.697
	0.5	1.374e7	1.134	1.297e7	1.133
T10I4D100K	0.0002	1.195e9	3.354	8.764e8	2.812
	0.0005	2.717e8	1.483	2.177e8	1.391
	0.001	9.266e7	1.334	8.153e7	1.310
	0.002	3.888e7	1.092	3.487e7	1.058
T40I10D100K	0.002	4.792e10	104.234	3.509e10	78.116
	0.005	1.338e10	29.262	8.908e9	20.021
	0.01	2.206e9	7.074	1.292e9	5.274
	0.02	8.316e7	2.937	5.984e7	2.862

performance of PrePost and PrePost-ES over four datasets and different values of *minSup*. We report the number of checks (refer to Example 3.1) and runtime (in second).

Clearly, PrePost-ES reduces the number of checks thanks to the early-stopping criterion. The runtime, therefore, decreases considerably, especially on T10I4D100K and T40I10D100K.

V. Conclusion

We have presented a simple yet effective technique to accelerate the existing PrePost algorithm. Our technique is based on an early-stopping criterion for N-list intersection. We have evaluated our proposed scheme PrePost-ES over four datasets and different minimum supports. The results confirm the effectiveness of our method. For future work, we plan to apply this technique to other frequent pattern mining problems that rely on list intersections.

References

[1] R. Agrawal, R. Srikant, et al. Fast algorithms for mining association rules. In *Proc. 20th int. conf. very large data bases, VLDB*, volume 1215, pages 487–499, 1994.

[2] Z. Deng, Z. Wang, and J. Jiang. A new algorithm for fast mining frequent itemsets using n-lists. *Science China Information Sciences*, 55(9):2008–2030, 2012.

[3] Z.-H. Deng, G.-D. Fang, Z.-H. Wang, and X.-R. Xu. Mining erasable itemsets. In *Machine Learning and Cybernetics, 2009 International Conference on*, volume 1, pages 67–73. IEEE, 2009.

[4] Z.-H. Deng and S.-L. Lv. Prepost+: An efficient n-lists-based algorithm for mining frequent itemsets via children–parent equivalence pruning. *Expert Systems with Applications*, 42(13):5424–5432, 2015.

[5] P. Fournier-Viger, J. C.-W. Lin, R. U. Kiran, Y. S. Koh, and R. Thomas. A survey of sequential pattern mining. *Data Science and Pattern Recognition*, 1(1):54–77, 2017.

[6] G. Grahne and J. Zhu. Fast algorithms for frequent itemset mining using fp-trees. *IEEE transactions on knowledge and data engineering*, 17(10):1347–1362, 2005.

[7] J. Han, J. Pei, and Y. Yin. Mining frequent patterns without candidate generation. In *ACM sigmod record*, volume 29, pages 1–12. ACM, 2000.

[8] L. T. Nguyen, B. Vo, T.-P. Hong, and H. C. Thanh. Classification based on association rules: A lattice-based approach. *Expert Systems with Applications*, 39(13):11357–11366, 2012.

[9] B. Vo, F. Coenen, and B. Le. A new method for mining frequent weighted itemsets based on wit-trees. *Expert Systems with Applications*, 40(4):1256–1264, 2013.

[10] M. J. Zaki and C.-J. Hsiao. Charm: An efficient algorithm for closed itemset mining. In *Proceedings of the 2002 SIAM international conference on data mining*, pages 457–473. SIAM, 2002.

[11] M. J. Zaki and C.-J. Hsiao. Efficient algorithms for mining closed itemsets and their lattice structure. *IEEE Transactions on Knowledge & Data Engineering*, (4):462–478, 2005.

[12] M. J. Zaki, S. Parthasarathy, M. Ogihara, W. Li, et al. New algorithms for fast discovery of association rules. In *KDD*, volume 97, pages 283 – 286, 1997.

Proposing a method to improve the effectiveness of Vietnam traffic Sign recognition based on PCA-LDA with navigation system

Đề xuất phương pháp nâng cao hiệu quả của ứng dụng Nhận dạng biển báo giao thông dùng thuật toán PCA-LDA kết hợp hệ thống dẫn đường

Truong Van Truong[a,*], Pham Phu Khuong[b], Dac Binh Ha[a]
Trương Văn Trương, Phạm Phú Khương, Hà Đắc Bình

[a]*Faculty of Electrical and Electronic Engineering, Duy Tan University, Danang, Vietnam*
Khoa Điện - Điện tử, Đại học Duy Tân, Đà Nẵng, Việt Nam
[b]*Inspection Office, Duy Tan University, Danang, Vietnam*
Phòng Thanh tra, Đại học Duy Tân, Đà Nẵng, Việt Nam

Abstract

Traffic sign recognition is one of the most challenging issues in traffic monitoring systems, driver assistance systems, or unmanned vehicles. In this paper, we present a combinational method of Principal Component Analysis (PCA), Linear Discriminant Analysis (LDA) and smart navigation system for Vietnam traffic sign recognition in unmanned vehicles. This proposed method employs the information of navigation system to reduce the capacity of trained database, while it still promotes the advantages of PCA and LDA combination to recognize Vietnam traffic signs. The effectiveness of this proposed method is verified by simulation in Matlab. The simulation results have shown that the proposed system has attained an accurate rate of 98.88%.

Keywords: Vietnam traffic sign, recognition, PCA, LDA, smart navigation system, unmanned vehicle.

Tóm tắt

Nhận dạng biển báo giao thông là một trong những vấn đề thách thức nhất trong hệ thống giám sát giao thông, hệ thống hỗ trợ người lái hoặc phương tiện không người lái. Trong bài viết này, chúng tôi trình bày một phương pháp kết hợp Phân tích thành phần chính (PCA), Phân tích phân biệt đối xử tuyến tính (LDA) và hệ thống điều hướng thông minh để nhận dạng biển báo giao thông Việt Nam trên xe không người lái. Phương pháp đề xuất này sử dụng thông tin của hệ thống định vị để giảm dung lượng của cơ sở dữ liệu được đào tạo, trong khi vẫn phát huy những lợi thế của kết hợp PCA - LDA để nhận biết biển báo giao thông Việt Nam. Hiệu quả của phương pháp đề xuất này được xác minh bằng mô phỏng trong Matlab. Kết quả mô phỏng đã chỉ ra rằng hệ thống được đề xuất đã đạt được tỷ lệ chính xác là 98,88%.

Từ khóa: Biển báo giao thông Việt Nam, nhận dạng, PCA, LDA, hệ thống dẫn đường thông minh, xe không người lái.

1. Introduction

Transportation system plays a very important role in developing the economy and society of a nation. It consists of traffic roads, vehicles, and equipment, such as traffic signs, lights and traffic information. Traffic signs are signs located at the side of or above roads to give instructions or provide information to road users via graphics or symbols.

Email: vantruong57@gmail.com

Each nation has own traffic sign system based on international criteria. However, the differences of them are the language and culture, and Vietnam is not an exception. Traffic sign recognition system is regarded as a vital component of Intelligent Transportation System (ITS), driver assistance systems and autonomous vehicles [1-3]. In this traffic sign recognition (TSR) system, there are two major parameters: Running Time per sample (RT) and Correct Rate Recognition (CRR) [4-6]. However, it is very difficult to ensure that both parameters are improved. The reason is the correct recognition rate of the system depends upon the training database. The larger the database, the higher the reliability, but the running time gets higher. To solve this problem, H. Fleyeh and E. Davami [7] proposed a method using Eigen-based for traffic sign recognition. This method was based on invoking the principal component analysis (PCA) algorithm [6]. An algorithm has attained the performance rate of 96.8% in traffic sign recognition. Hagar et al. [8] proposed using PCA and Linear Discriminant Analysis (LDA) as the pre-classification steps before passing to the K-Nearest Neighbor (KNN) for identification. Zenghao Shi et al. [10] proposed a method for traffic sign recognition based on a combination of PCA and LDA. The combination of PCA and LDA created a better class of space than previous studies, namely higher recognition rates than traditional PCA. Especially, when the number of training samples is greater than 6, the efficiency reached up to 99.37% in TSR. Johannes Stallkamp [11] proposed an improvised German traffic sign recognition system. A dataset of more than 43 classes of 50,000 traffic sign images has been collected with the strong variations in visual appearance of signs due to distance, illumination, weather conditions, partial occlusions, and rotations. One of the practical ideas is based on the Histograms of Oriented Gradients (HOG), LDA, and Vector Quantization (VQ). A recognition rate of 96.87 % was obtained in the technique proposed. Yi Lei et al. [12] proposed a sparse representation method with

add-on advantages in terms of good expression, cognitive and compression. An algorithm proposed was highly effective over German traffic signs database (GTSDB) with a staggering performance of 96%. The technique was used in five different KNN parameters for evaluation of system data and the performance rate in some cases touched even 100%.

Although the above-mentioned studies were very promising in the traffic sign recognition, this problem still continue to impact ITS because of massive database. Because of massive database, the precise system identification can increase but the speed of processing reduces the real time response. However if the database size is small and simple, the reliability of the system can decrease. The objective of this paper is to address this problem by adding a subsystem to the traditional traffic sign recognition system. The proposed system is capable of compacting the traffic sign database for each route and re-training the database, reducing the complexity of the database as well as reducing the calculation time for each identification sample. The algorithm used in the proposed technique is the combination of PCA and LCA and makes use of existing navigation system in Vietnam to support the reduction of database.

The rest of this paper is organized as follows: Section II presents our proposed traffic sign recognition system model in detail. Section III discuss about the experimental results. Finally, Section IV is our conclusions and future works.

2. Proposed traffic sign recognition system

2.1. Traditional traffic sign recognition systems

An ordinary traffic sign recognition system works in two modes: Training Mode and Prediction Mode. In Training mode, the database is built via collecting a set of traffic signs for training and validation. In Prediction mode, the system can recognize a traffic sign which has not been seen before. Figure 1 gives the overview of Traditional Traffic Sign recognition system.
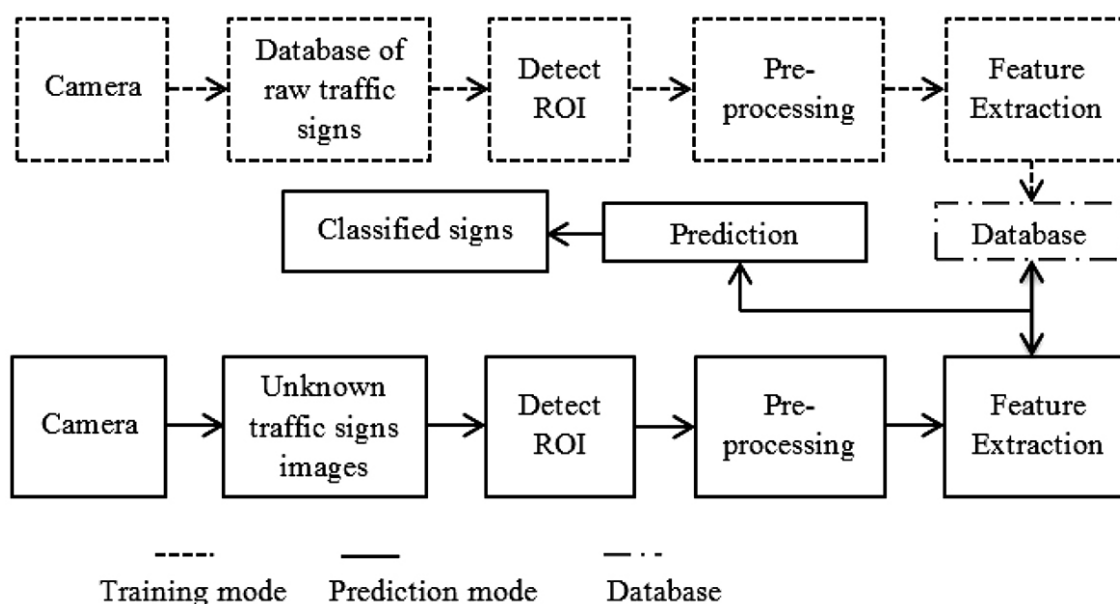
Fig. 1. Traditional Traffic Sign Recognition System- Phases

In the Training mode, the camera module performs the task of collecting image data of traffic signs. These images contain the useful information about the traffic signs and may also contain other information such as trees, houses, signage, and transportation. These images are called "Raw Traffic Sign Images". These photos are taken via traffic sign detection algorithms to determine the Region of Interest (ROI). After acquiring the images, the ROI images are normalized in size, adjusted with brightness cum contrast and converted into gray-scale image in pre-processing process. After pre-processing, the feature extraction process gets the significant information of the traffic signs for training. These images form the database of the system.

In Prediction mode, the camera collects images containing unknown signs. These images are processed in the same manner like Training mode. Data extracted is matched with the database, from which the system can determine what type of traffic sign it is. In particular, the database is created once during Training mode and used throughout the Prediction mode. In order to apply the model in real-time especially in country like Vietnam, the database has to be very large, covering 233 types of traffic signs in Vietnam.

The main drawback observed from Training and Prediction modes is that it is too complex to understand and difficult to predict the images in real-time, which automatically affects the real-time performance. In order to overcome this limitation, the novel method for Traffic Sign recognition is proposed in this paper.

2.2. Terminologies

Principal Component Analysis (PCA)

Feature vectors in traffic sign recognition problems have very large dimensions, up to thousands. In addition, the number of data points is also very large. The system will have difficulty with both storage and calculation speed when executing on the original database. Therefore, reducing the number of dimensional data is an important step. Dimensionality Reduction, simply stated, is a function of finding a function, which takes the input as a primitive data point $x \in R^D$ with very large D, and produces a new data point $z \in R^K$ with K <D. The simplest method in Dimensionality Reduction algorithms is based on a linear model, called Principal Component Analysis. This method is based on the observation that data are often not randomly distributed in space that is usually distributed near

particular planes. The PCA considers a special case where those particular aspects are linearly represented as subspaces. The simplest way to reduce the dimension from D to K < D is to retain only the most important K elements. However, this is certainly not the best way since we do not know which component is more important. Or in the worst case, the amount of information that each component carries is the same, leaving out any component that leads to the loss of a large amount of information. However, if we could represent the initial data vectors in a new base system, the importance of the components is distinct; we can ignore the least important components. PCA method enables finding a new base system so that the information of the data is concentrated in a few coordinates, while the rest is carried only by small amounts of information.

The following steps highlight the working of PCA:

Step 1. Take the whole dataset consisting of n-dimensional samples ignoring the class labels. All images in the database are converted into column vectors $I_1, I_2, \ldots, I_n$. These images are converted to gray-scale images and calibrated to the same size.

Step 2. Compute the d-dimensional mean vector.

Step 3. Standardize the database.

Step 4. Compute the covariance matrix of the whole data set.

$$S = \frac{1}{N}\hat{X}\hat{X}^T$$

Step 5. Compute eigenvectors ($u_1, u_2, \ldots, u_n$) and corresponding eigenvalues ($\lambda_1, \lambda_2, \ldots, \lambda_n$).

Step 6: Sort the eigenvectors by decreasing eigenvalues and choose k eigenvectors with the largest eigenvalues.

Step 7: Project data to selected eigenvectors.

Step 8: Obtain projected points in low dimension.

PCA is an unsupervised method. The implementation of the PCA over all data does not depend on the class (if any) of each data. This sometimes causes PCA not to work for classification problems. Indeed, suppose in two-dimensional space, two classes are distributed along two sides of a straight line. As such, the PCA will most likely allow us to retain the main component of that line. When projecting data onto this line, both classes are mixed, resulting in poor classification. There is a method similar to PCA to take advantage of information about classes to determine which projection direction, the method called Linear Discriminant Analysis.

Linear Discriminant Analysis (LDA)

The idea of an LDA was created to address the problem of PCA survival. Consider the following example in Fig 2.
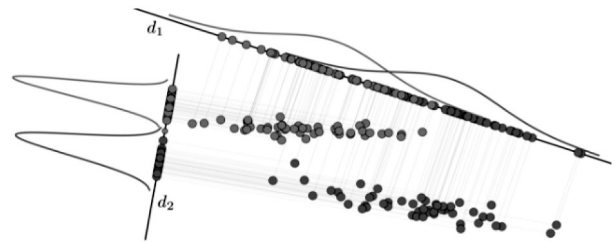

Fig. 2. Example of classification problem with 2 classes

There are two data layers illustrated by blue and red dots. Data dimension is reduced by projecting them to different lines d1 and d2. In these two dimensions, the direction of d1 is similar to the direction of the first major component of the data, and the direction of d2 is closer to the subset of the data if PCA is used. Although it is the main component, when projected onto d1, red and green dots overlap, making classification of data impossible on this line. But when we view on d2, the data of the two classes are separated into corresponding clusters, which makes classification easier and more efficient. The bell curve represents the approximate distribution of the projection data in each class.

Small standard deviations indicate less scattered data. This means that the data in each class tends to be the same. The gap between

the expectations is great, demonstrating that the classes are far apart, meaning that the data between the classes is very different. The distance between expectations is also called between-class variance. Classes are called discriminative if the between-class variance is large and within-class variance is small. Linear Discriminant Analysis is an algorithm for finding a projection so that the ratio between between-class variance and within-class variance is the greatest possible.

The following steps highlight the working of LDA:

Step 1. Compute the d−dimensional mean vectors for the different classes from the dataset Y.

Step 2. Compute the scatter matrices (in-between-class and within-class scatter matrix).

Step 3. Compute the eigenvectors $(e_1, e_2,...,e_d)$ and corresponding eigenvalues $(\lambda_1, \lambda_2,...\lambda_d)$ for the scatter matrices.

Step 4. Sort the eigenvectors by decreasing eigenvalues and choose k eigenvectors with the largest eigenvalues to form a d×k dimensional matrix W (where every column represents an eigenvector).

Step 5. Use this d×k eigenvector matrix to transform the samples onto the new subspace. This can be summarized by the matrix multiplication: Y=X×W, where X is a n×d−dimensional matrix representing the n samples, and y are the transformed n×k−dimensional samples in the new subspace.

2.3. Proposed traffic sign recognition system

The main task of the proposed method is to compact the database via case-by-case approach, which ensures speedy identification, and overall increases the efficiency of the system during real time operations.

The proposed system consists of two sub-systems.

The first sub-system is termed as "Navigation System" (the blue border block in Figure 3) which is updated regularly with transport infrastructure information of Vietnam. The information that can be acquired via proposed system is: Physical coordinates, traffic sign information on a specific route. The second subsystem termed as "Recognition System" (The red border in Figure 3) performs the task of collecting sign information from Navigation system, re-training the database for each route, and implementing traffic sign recognition algorithms on a simple database. Figure 3 gives detailed overview of Novel Traffic Sign Proposed System.

The proposed model combines two subsystems. The first is the "Navigation system" available in Vietnam, which provides information on the transport system in Vietnam, including information of traffic signs. This sub-system lists all traffic signs on a route and their actual status. This information is used for the upgrading and repair of annual traffic infrastructure in Vietnam. We will use this information to improve system performance. The second sub-system, termed as "Recognition system", which is responsible for gathering and extracting information about traffic signs using combination of PCA and LDA. The information of traffic signs from navigation system is employed by recognition system to reduce the capacity of database. In other words, the navigation system limits the number of traffic signs on the road and at the same time recognition system will rebuild a simpler set of database based on this information. A feasibility and effectiveness for the proposed model is conducted using an experimental Vietnamese traffic sign database which contains 3000 images of 18 sign types.

Case Study: Suppose we are traveling on a self-drive car fitted with the traffic sign recognition system proposed by authors. As the car enters the road, the traffic sign database is immediately updated to a much smaller number than the original database. For example, in the

suburbs of the city, signs such as parking signs, residential areal signs, and bans for the use of horns signs will not appear. On the other hand, in a crowded urban area, signs such as falling rocks signs, slippery road signs, and area signs

of cattle or wildlife will not appear. With the proposed system, the traffic signs database in each area is reduced to a different level which in turn minimizes the complexity of the recognition system.
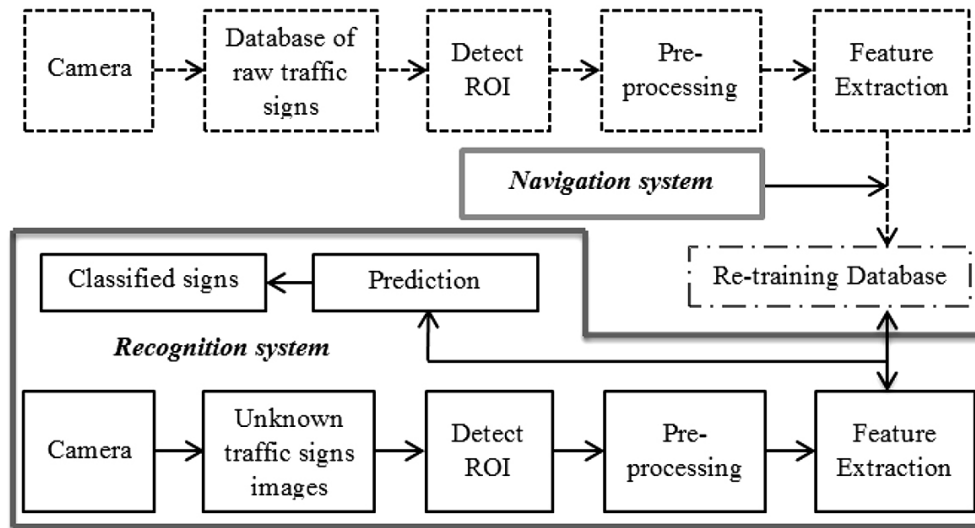

Fig. 3. Overview of Novel Traffic Sign Proposed System- Phases

In the proposed system, the training database is not only created once, but continuously updated on each route which can be termed as "online training". The re-training of this database can be a burden on system performance, because

the system needs resources and time to perform this operation. However, with simple databases set, the system can support prediction module to respond efficiently and quickly.
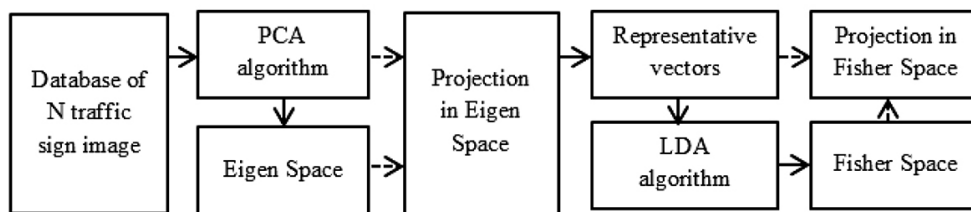
Fig. 4. PCA and LDA combination

In order to perform traffic sign recognition, two algorithms are used: PCA and LDA. The primary purpose of PCA algorithm is to reduce the complexity of the original database. The task of LDA algorithm is to classify objects into one of two or more groups based on a set of features that describe the objects.

The combination of two algorithms is executed when the LDA input is the Projected in Eigen Space dataset extracted from the original database by the PCA algorithm.

For testing the proposed system, there are two parameters selected for investigation: Running time (RT) and Correct Recognition Rate (CRR). These parameters when compared to each other along with the results drawn state that proposed system is highly efficient as compared to other conventional systems.

3. Simulation & result analysis

3.1 Simulation

In this section, the proposed traffic sign recognition system is tested on the traffic database collected in Vietnam. The testing of the proposed

system is performed on certain scenarios and comparison is done with traditional traffic sign recognition systems.

The testing of the complete proposed system is done on MATLAB 2017b. Figure 5 states the simulation model of proposed system.
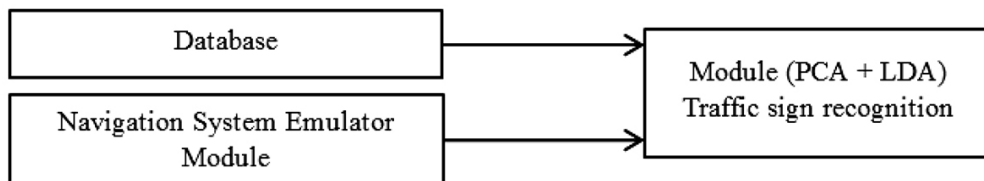

Fig. 5. Proposed Traffic Sign Recognition Systems- MATLAB Model

3.2 Database

The Navigation System Emulator Module provides the following information:

- Random information on the number of signs in the database

- Random information type in the database

The above information is used for database update and is also utilized by recognition module on different routes. The identification module will train the small database and classify the data using PCA and LDA combination algorithm.

Fig. 6. Images for Testing the Proposed System

To test the proposed system's efficiency, the traffic data database was collected between September 2017 and February 2018 in Da Nang City, Vietnam. The database includes 2880 images of 18 types of traffic signs in Vietnam, each sign has 160 different images. We use 2340 pictures for

training set and 540 pictures for testing set. This database ensures the following criteria:

The first criterion is that the database must contain all major types of traffic signs in Vietnam. We have tried to select the typical traffic signs, shown in the following statistics of Table 1.

Table 1. Statistics table of traffic signs in the database

Sign type	The name of the sign	Total number of sign type
Warning Signs	- Dangerous bend to left and right sign - Intersection ahead where vehicles on the right must give way sign, 90° left and right sign - High voltage hazard sign; Narrow road on the left side sign	6
Prohibitory Signs	Various maximum speed sign: 30, 40, 50, 60, 80, 100 km/h	6

Informative Signs	- Priority road for cars sign - End of Road for cars sign - Bus stop sign - Priority line sign - End of priority road sign - Turn Around Ahead Sign	6

The second criterion of database is the types of signs have to cover all the cases as shown in the Figure 6: a.) Signs contain only signs, b.) Signs that contain information which are numbers, c.) Signs that contain Vietnamese characters.

And the final criterion is that signs are collected under different weather conditions: a.) Bad light geometry, b.) Blurred images, c.) Noisy images.

3.3 Results and Analysis

We evaluated the proposed system on various Test Case Scenarios to determine the efficiency in real-time operational scenarios. The following are various Testing Scenarios developed by us for testing Novel Traffic Sign Recognition System:

3.3.1 Testing Scenarios

To test the proposed system, we categorized the testing in four test cases as follows: a.) Normal conditions, b.) Signs are taken at various angles, c.) Different environmental conditions, d.) Specific signs in Vietnam.

In each scenario, we run the test and compared the results between the traditional recognition model and the proposed recognition model. Each case performs 100 tests and implements two parameters: Correct Recognition Rate (CRR) and Running Time (RT).

- Case 1: The recognition program uses only one large database of 18 types of signs. This case uses ordinary traffic sign recognition system.

- Case 2: The recognition program uses a large database of 18 types of signage (18 signage). This case and subsequent cases will use the proposed model, which is to receive information about the number of traffic sign layers issued by the navigation system for re-training the dataset and identifying images containing unknown signs.

- Case 3: The recognition program using the database has 9 types of „random" signs (equal to half the total number of signs in the large database)

- Case 4: The recognition program using database has 6 types of „random" signs (equal 1/3 of the total number of signboards included in the large database)

- Case 5: The recognition program using database has 3 types of „random" signs (equal 1/ of the total number of signboards included in the large database)

3.3.2 Data Results

Scenario 1: Signs are taken under normal circumstances

The simulation results are as Table 2.

Table 2. Performance rating of images taken under normal circumstances

Sign name	Sign	Case 1		Case 2		Case 3		Case 4		Case 5	
		CRR (%)	RT (ms)	CRR (%)	RT (ms)	CRR (%)	RT (ms)	CRR (%)	RT (ms)	CRR (%)	RT (ms)
Warning Signs		93.75	326.4	93.75	327.1	95	328.7	96.25	326.3	98.75	325.8

Prohibitory Signs		92.94	326.9	92.94	328.3	94.11	328.4	95.29	325.7	98.82	324.6
Informative Signs		93.33	325.9	93.33	326.3	95.29	328.5	95.29	326.1	98.88	325.5

Scenario 2: Signs are taken at various angles

The simulation results are as Table 3.

Table 3. Performance rate of the images was taken at the left or right offset, ranging from 30° to 45°

Sign name	Sign	Case 1		Case 2		Case 3		Case 4		Case 5	
		CRR (%)	RT (ms)	CRR (%)	RT (ms)	CRR (%)	RT (ms)	CRR (%)	RT (ms)	CRR (%)	RT (ms)
Warning Signs		58.33	0.3274	58.33	328.9	61.53	328.4	61.53	326.9	63.33	325.5
Prohibitory Signs		58.46	327.8	58.46	328.5	63.07	327.9	63.07	328	64.61	327.6
Informative Signs		58.57	330.1	58.57	331.4	60	330.3	61.42	330.5	62.85	329.4

Scenario 3: Signs are taken in low light conditions such as at night, it rains so the picture is disturbed, partially masked

The simulation results are as Table 4.

Table 4. Performance rate of of images taken in low light, noise, partially obscured

Sign name	Sign	Case 1		Case 2		Case 3		Case 4		Case 5	
		CRR (%)	RT (ms)	CRR (%)	RT (ms)	CRR (%)	RT (ms)	CRR (%)	RT (ms)	CRR (%)	RT (ms)
Warning Signs		70	330.7	70	331.9	72.5	331.1	75	331.0	77.5	330.8
Prohibitory Signs		64	329.9	64	330.3	66	330.4	68	330.3	72	329.9
Informative Signs		71.42	329.7	71.42	330.6	74.28	331.3	77.14	330.4	82.85	329.5

Scenario 4: Specific sign in Vietnam

Table 5. Performance rate of Typical signs in Vietnam

Sign	Case 1		Case 2		Case 3		Case 4		Case 5	
	CRR (%)	RT (ms)	CRR (%)	RT (ms)	CRR (%)	RT (ms)	CRR (%)	RT (ms)	CRR (%)	RT (ms)

	92.5	331.7	92.5	332.3	92.5	332.5	95	331.5	95	331.4
	92	329.7	92	330.2	94	330.4	94	329.9	96	329.7
	93.33	330.1	93.33	330.5	96.66	330.8	96.66	330.4	100	329.4

3.3.3 Data Analysis

Figure 6 interprets Table 1 to 4 with respect to Average Correct Rate Recognition for the large database (18 classes) in the ordinary model compared with the proposal model and the results state that model proposed is completely at par as compared to existing systems but the rate increases if the database gets shrunk. The reason behind this is as the number of traffic sign types in the database decreases, the corresponding to the number of images that have been reduced in the large database; and when matching data, the system will significantly eliminate those instances, retaining only the signs provided by the navigation system. The more the layers are eliminated, the simpler the data, the more accurate the data.
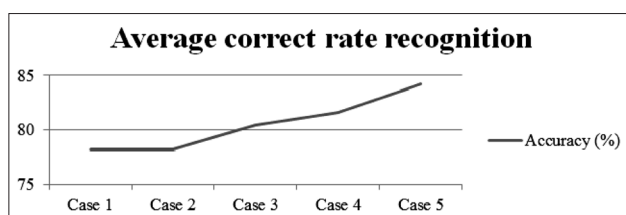
Figure 7 . The Average correct rate recognition of 5 cases

Figure 7 interprets Table 1 to 4 with respect to Average Running Time for large database (18 types). The results state that Average Running Time of proposed model is higher as compared to existing ones. The reason for this is in the new model, more complex algorithms are used to collapse the original database. However, when collapsing the database, the recognition time tends to decrease when the number of sign types is reduced more than a half. The more the layers are eliminated, the simpler the data, the faster the calculation of a sample
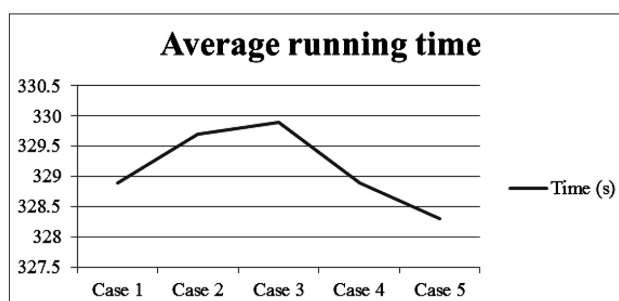
Figure 8. The Average running time of 5 cases

4. Conclusion & future research

In this research paper, an Intelligent Traffic Sign Recognition system by combination of PCA, LDA and Smart Navigation System for evaluating Traffic in Vietnam is proposed. The system is tested on dataset of 2880 images consisting of 18 regulatory signs. Experimental results state that the proposed system performs best as compared to existing systems in terms of Traffic Sign Recognition under both parameters of time and accuracy. Under normal conditions, the system performance reaches 98.88% while the running time decreases to 325.5 mili second per sample.

In the near future, research would be directed to test the proposed system in more complex scenarios and also the integrating of some Machine

learning technique to make the real-time traffic sign recognition more powerful and fast.

References

[1] Amiri, A., Ebrahimpour, R., & Amiri, M., Shape-Based Traffic Sign Recognition Using Biologically Motivated Features, International Journal of Computer Information Systems and Industrial Management Applications, ISSN 2150-7988, Volume 9 (2017), pp. 71-79.

[2] Bengler, K., Dietmayer, K., Farber, B., Maurer, M., Stiller, C., & Winner, H., *Three decades of driver assistance systems: Review and future perspectives*, IEEE Intelligent Transportation Systems Magazine, 6(4), 2014, pp. 6-22.

[3] Brookhuis, K. A., De Waard, D., & Janssen, W. H., *Behavioural impacts of advanced driver assistance systems–an overview*, European Journal of Transport and Infrastructure Research, 1(3), 2001, pp. 245-253.

[4] Cho, H., Han, S., & Hwang, S. Y., *Design of an Efficient Real-Time Algorithm Using Reduced Feature Dimension for Recognition of Speed Limit Signs*. The Scientific World Journal, Volume 2013, pp. 1-6.

[5] Christopher, M. B., *Pattern Recognition and Machine Learning*, Springer-Verlag New York, 2016.

[6] De la Escalera, A., Armingol, J. M., & Mata, M., *Traffic sign recognition and analysis for intelligent vehicles*, Image and vision computing, 21(3), 2003, pp. 247-258

[7] Fleyeh, H., & Davami, E., *Eigen-based traffic sign recognition*, IET intelligent transport systems, 5(3), 2011, pp. 190-196.

[8] Hagar, A. A., Alshewimy, M. A., & Saidahmed, M. T. F., *A new object recognition framework based on PCA, LDA, and K-NN*, 11th International Conference on Computer Engineering & Systems (ICCES), December 2016, pp. 141-146).

[9] Mogelmose, A., Trivedi, M. M., & Moeslund, T. B., *Vision-based traffic sign detection and analysis for intelligent driver assistance systems: Perspectives and survey*, IEEE Transactions on Intelligent Transportation Systems, 13(4), 2012, pp. 1484-1497.

[10] Shi, Z., Wang, H., Wang, F., Zhao, M., Wang, Y., & Yao, Q., A method for traffic signs recognition using PCA and LDA, Journal of Information & Computational Science, 8(8), 2011, pp. 1365-1372.

[11] Stallkamp, J., Schlipsing, M., Salmen, J., & Igel, C., The German traffic sign recognition benchmark: a multi-class classification competition, The 2011 International Joint Conference on Neural Networks (IJCNN), July 2011, pp. 1453-1460.

[12] Yi, L., & Zhang, C. Y., A sparse representation method for traffic sign recognition based on similar class, IEEE International Conference on Signal Processing, Communications and Computing (ICSPCC), August 2014, pp. 262-266.

Estimation of scour depth around bridge piers using a Least Squares Support Vector Machine program developed in Visual C# .NET

Dự báo độ sâu xói mòn tại chân cầu sử dụng chương trình LSSVM phát triển trên nền tảng Visual C#. NET

Nhat Duc Hoang

Hoàng Nhật Đức

Institute of Research and Development, Duy Tan University, Danang, Vietnam
Viện Nghiên cứu và Phát triển Công nghệ cao, Đại học Duy Tân, Đà Nẵng, Việt Nam

Abstract

This study aims at establishing machine learning models based on Least Squares Support Vector Machine (LSSVM) for estimating local scour around complex piers under steady clear-water condition and streambed scour at bridges. LSSVM is a powerful machine learning approach for solving regression analysis problems. In this paper, we develop a software program for scour depth estimation based on LSSVM in Visual C#. NET framework 4.6.1.

Keywords: Regression analysis, Visual C#. NET, Civil engineering, C# programming, Scour at bridge.

Tóm tắt

Nghiên cứu này xây dựng các mô hình học máy dựa trên Least Squares Support Vector Machine (LSSVM) để ước tính xói mòn xung quanh các trụ cầu. LSSVM là một phương pháp học máy có hiệu quả cao trong phân tích hồi quy. Trong bài báo này, chúng tôi phát triển một chương trình phần mềm để ước tính độ sâu xói mòn xung quanh các trụ cầu dựa trên LSSVM trên nền tảng Visual C #. NET.

Từ khóa: Phân tích hồi quy, Kỹ thuật xây dựng, Ngôn ngữ C #, Xói mòn chân cầu.

1. Introduction

Bridge scour is generally known as the removal of sediment (e.g. sand and gravel) from around bridge abutments or piers [1, 2]. Scour caused by swiftly moving water is able to scoop out scour holes; which causes the deterioration of the integrity of a bridge structure [3, 4]. It is estimated that about 60% of bridge failures in the United States were caused by scour [5]. Additionally, scour failures of bridges may happen abruptly and it is very difficult to monitor

them during events of flood [5, 6]. Therefore, it is necessary to develop advanced tools for predicting the level of scouring at bridge piers.

Regression analysis (or function approximation) involves the identification of a functional relationship between a set of predictors and a variable of interest. This mathematical relationship is then used for modeling complex phenomena in civil engineering [7]. Recent advancements in machine learning (ML) have established intelligent data analysis approaches

Email: hoangnhatduc@dtu.edu.vn

effectively used for regression analysis including neural networks [8], multivariate adaptive regression splines [9], support vector machine [10], and LSSVM [11]. These advanced ML tools have been confirmed to have excellent capability for modeling complex and multivariate data [12].

LSSVM [13] is a powerful machine learning technique which has many advanced features reflected in its strong learning capability and low computational expense. Notably, in the training process of LS-SVM, a least squares cost function is employed to obtain a linear set of equations in the dual space [11]. Thus, the model training phases boil down to solving a set of linear equations that can be efficiently solved by conjugate gradient algorithm [13]. Similar to the standard Support Vector Machine, LSSVM relies on the inductive principle of Structural risk minimization; hence, a LSSVM model has a trade-off between hypothesis space complexity and the quality of fitting the training data [14]. Due to such reasons, LSSVM can be a very effective tool for solving regression analysis problems.

Accordingly, this paper focuses on LSSVM based regression analysis model for estimating scour depth. Although there is existing toolbox for implementing LSSVM [15], open software for LSSVM implementation has not yet been developed for academic purposes. This current work aims at contributing a software program based on LSSVM to solving regression analysis problems in civil engineering. The rest of the paper is organized as follows: the second section describes the formulation of LSSVM; several applications of the newly developed program are demonstrated in the third section; concluding remarks of this study are stated in the final section.

2. Least Squares Support Vector Machine (LSSVM)

Consider the following model of interest, which infers the mapping between the scour depth and its predicting variables:

$$y(x) = w^T \phi(x) + b, \qquad (1)$$

where $x \in R^n$, $y \in R$, and $\phi(x):R^n \rightarrow R^{nh}$ is the mapping to the high dimensional feature space.

In LSSVM for regression analysis, given a training dataset $\{x_k, y_k\}_{k=1}^N$, the model training phase is converted to the following optimization problem [11, 13]:

$$\text{Minimize } J_p(w,e) = \frac{1}{2} w^T w + \gamma \frac{1}{2} \sum_{k=1}^N e_k^2 , \quad (2)$$

subjected to $y_k = w^T \phi(x_k) + b + e_k$, $k = 1,...,N$

where $e_k \in R$ are error variables; $\gamma > 0$ denotes a regularization constant.

It is necessary to establish the Lagrangian and derive the corresponding dual problem. The Lagrangian is given as follows:

$$L(w,b,e;\alpha) = J_p(w,e) - \sum_{k=1}^N \alpha_k \{w^T \phi(x_k) + b + e_k - y_k\}, (3)$$

where α_k are Lagrange multipliers.

After using the conditions for optimality, the following linear system is obtained:

$$\begin{bmatrix} 0 & 1_v^T \\ 1_v & \omega + I/\gamma \end{bmatrix} \begin{bmatrix} b \\ \alpha \end{bmatrix} = \begin{bmatrix} 0 \\ y \end{bmatrix}, \qquad (4)$$

where $y = y_1;...;y_N$, $1_v=[1;...;1]$ and $\alpha=[\alpha_1;...; \alpha_N]$.

In addition, the kernel function is applied as follows:

$$\omega = \phi(x_k)^T \phi(x_l) = K(x_k, x_l). \qquad (5)$$

The LSSVM model for scour depth estimation is given as follows:

$$y(x) = \sum_{k=1}^N \alpha_k K(x_k, x_l) + b , \qquad (6)$$

where α_k and b are the solution to the linear system shown in **Eq. (5)**. The kernel function that is often utilized is Radial Basis Function (RBF) kernel described as follows:

$$K(x_k, x_l) = \exp(-\frac{\|x_k - x_l\|^2}{2\sigma^2}), \qquad (7)$$

where σ is the kernel function parameter.

3. The LSSVM based scour depth estimation software program

The Graphical user interface (GUI) of LSSVM program is provided in **Fig. 1**.To run the

program, it is required that the .NET framework 4.6.1 must be installed via the following link: https://www.microsoft.com/en-us/download/details.aspx?id=49981. Before running the model evaluation, the hyper-parameters of LSSVM including the regularization parameter (e.g. 100) and the RBF kernel function parameter (e.g. 1)

must be specified. These two parameters can be identified via a grid search [16]. After the training and testing phases are finished, the model results are stored in the two files of TrainResult.csv and TestResult.csv. These two files store the actual (the first column) and the predicted output (the second column).
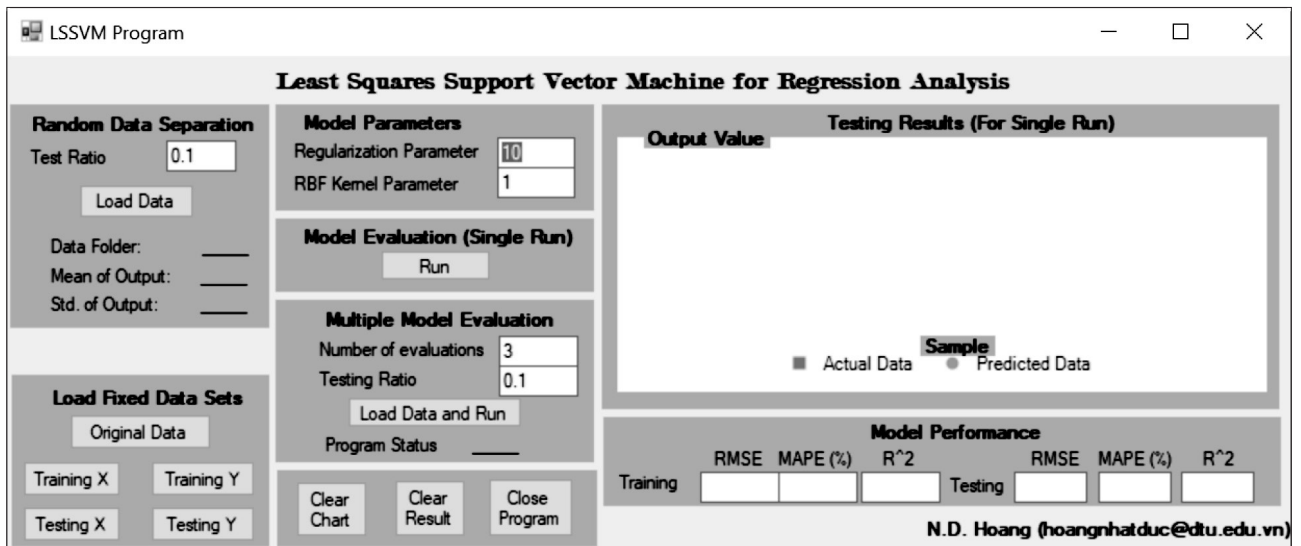
Fig. 1 Graphical user interface (GUI) of LSSVM program

The program supports various running scenarios:

1) Model evaluation (Single Run)

    1.1 Random Data Separation: One .csv file which stores the whole data set is needed. The last column is the output variables. The Z score normalization is automatically performed. The model also converts the output variable to its original range. The parameter of Test Ratio needs to be specified. If Test Ratio is 0.1, 10% of the data will be randomly drawn to form a testing dataset; the rest of the dataset is used for model training.

    1.2 Load Fixed Data Sets: The users need to prepare a .csv file which stores the whole dataset, and 4 other .csv files to store a training input X, a testing input X, a training output Y, and a testing output Y.

2) Multiple Model Evaluation

The user needs to prepare a .csv file which stores the whole data. The parameters of evaluations (number of runs) and the Testing Ratio must be prepared.

4. Program application

The first application is a machine learning based model using LSSVM for estimating local scour around complex piers under steady clear-water condition. A data set consisting of scour depth measurement cases has been collected to construct the prediction models [2, 17]. The dataset has 8 influencing factors that consider aspects of pier geometry, flow property, and river bed material. In total, 174 data instances are collected. The 8 influencing factors (the flow depth y, the pier width perpendicular to the flow direction b_c, the pile-cap width b_{pc}, the longitudinal extension of pile cap face out from pier face L_u, the soil covering height Y, the ratio

of the mean velocity to the critical velocity of sediment movement V/V_c, the median grain size d_{50}, and the river bed material geometric standard deviation σ_g) are used to predict the scour depth d_s of complex pier foundations. The LSSVM

prediction result for this application case is shown in **Fig. 2**. As can be seen from the figure, the program has obtained a good prediction result with the coefficient of determination R^2 = 0.86.

Fig. 2 Result of prediction of local scour around complex piers under steady clear-water condition

In the second application, data collected from real-time field measurements of bridge scour done by Mueller and Wagner [18] is used to construct a model for evaluations of streambed scour. The dataset includes 314 instances collected during 6 years of dedicated effort by the U.S. Geological Survey researchers to collect scour data during flood events in the United States. The variables

of Upstream/downstream, Pier Type, Pier Shape, Pier Width (m), Pier Length (m), Skew (deg), Velocity (m/s), Depth (m), D50 (mm), and Gradation are used to predict the Scour Depth (m). The LSSVM prediction result is reported in **Fig. 3**. For this data set, the LSSVM program has obtained a relatively good prediction result with the coefficient of determination R^2 = 0.81.

Fig. 3 Result of prediction of streambed scour at bridges

5. Conclusion

Scour depth estimation is an important task in bridge health assessment. To assist civil engineers in this task, this study develops a LSSVM program in Visual C#. The effectiveness of the program has been demonstrated via two case studies using two historical datasets. Good predictive results show that the LSSVM program can be a useful tool for researchers and engineers for modeling other complex processes in civil engineering field.

References

[1] D. S. Mueller and C. R. Wagner, "Field Observations and Evaluations of Streambed Scour at Bridges," *Office of Engineering Research and Development Federal Highway Administration, McLean, VA,* 2005.

[2] N.-D. Hoang, K.-W. Liao, and X.-L. Tran, "Estimation of scour depth at bridges with complex pier foundations using support vector regression integrated with feature selection," *Journal of Civil Structural Health Monitoring,* June 02 2018.

[3] L. P. Warren, "Scour at Bridges: Stream Stability and Scour Assessment at Bridges in Massachusetts," *U.S. Geological Survey,* 2011.

[4] A. N. Kallias and B. Imam, "Probabilistic assessment of local scour in bridge piers under changing environmental conditions," *Structure and Infrastructure Engineering,* vol. 12, pp. 1228-1241, 2016/09/01 2016.

[5] L. Deng and C. S. Cai, "Bridge Scour: Prediction, Modeling, Monitoring, and Countermeasures - Review," *Practice Periodical on Structural Design and Construction,* vol. 15, pp. 125-134, 2010.

[6] M. N. Landers, "Bridge Scour Sata Management. Published in Hydraulic Engineering: Saving a Threatened Resource—In Search of Solutions," *In Proceedings of the Hydraulic Engineering sessions at Water Forum '92. Baltimore, Maryland, August 2–6, 1992. Published by American Society of Civil Engineers,* 1992.

[7] D. Tien Bui, V.-H. Nhu, and N.-D. Hoang, "Prediction of soil compression coefficient for urban housing project using novel integration machine learning approach of swarm intelligence and Multi-layer Perceptron Neural Network," *Advanced Engineering Informatics,* vol. 38, pp. 593-604, 2018/10/01/ 2018.

[8] H. Tanyildizi, "Prediction of the Strength Properties of Carbon Fiber-Reinforced Lightweight Concrete Exposed to the High Temperature Using Artificial Neural Network and Support Vector Machine," *Advances in Civil Engineering,* vol. 2018, p. 10, 2018.

[9] N.-D. Hoang, C.-T. Chen, and K.-W. Liao, "Prediction of chloride diffusion in cement mortar using Multi-Gene Genetic Programming and Multivariate Adaptive Regression Splines," *Measurement,* vol. 112, pp. 141-149, 2017/12/01/ 2017.

[10] S. Ghosh, A. Roy, and S. Chakraborty, "Support vector regression based metamodeling for seismic reliability analysis of structures," *Applied Mathematical Modelling,* vol. 64, pp. 584-602, 2018/12/01/ 2018.

[11] M.-Y. Cheng and N.-D. Hoang, "Estimating construction duration of diaphragm wall using firefly-tuned least squares support vector machine," *Neural Computing and Applications,* vol. 30, pp. 2489–2497, January 10 2018.

[12] A. Çevik, A. E. Kurtoğlu, M. Bilgehan, M. E. Gülşan, and H. M. Albegmprli, "Support vector machines in structural engineering: a review," *Journal of Civil Engineering and Management,* vol. 21, pp. 261-281, 2015/04/03 2015.

[13] J. Suykens, J. V. Gestel, J. D. Brabanter, B. D. Moor, and J. Vandewalle, "Least Square Support Vector Machines," *World Scientific Publishing Co. Pte. Ltd., Singapore,* 2002.

[14] M. Sewell, "Structural Risk Minimization " *Technical Report, Department of Computer Science University College London,* 2008.

[15] K. De Brabanter, P. Karsmakers, F. Ojeda, C. Alzate, J. De Brabanter, K. Pelckmans, *et al.*, "LS-SVMlab Toolbox User's Guide version 1.8," 2010.

[16] N.-D. Hoang and D. T. Bui, "Predicting earthquake-induced soil liquefaction based on a hybridization of kernel Fisher discriminant analysis and a least squares support vector machine: a multi-dataset study," *Bulletin of Engineering Geology and the Environment,* vol. 77, pp. 191-204, February 01 2018.

[17] K.-W. Liao, Y. Muto, and J.-Y. Lin, "Scour Depth Evaluation of a Bridge with a Complex Pier Foundation," *KSCE Journal of Civil Engineering,* vol. 22, pp. 2241-2255, July 01 2018.

[18] D. S. Mueller and C. R. Wagner, "Field Observations and Evaluations of Streambed Scour at Bridges," *Technical Report, FHWA-RD-03-052, U.S. Geological Survey, Water Resources Division,* 2005.

Silk fibroin-based materials for biomedical application: A brief review

Tổng quan về vật liệu từ tơ fibroin cho ứng dụng y sinh

Vu Quynh Nga Huynh[a], Quang Vinh Nguyen[b,*]
Huỳnh Vũ Quỳnh Nga, Nguyễn Quang Vĩnh

[a]The Faculty of Pharmacy, Duy Tan University, Danang, Vietnam
Khoa Dược, Đại học Duy Tân, Đà Nẵng, Việt Nam
[b]Center for Advanced Chemistry, Institute of Research & Development, Duy Tan University, Danang, Vietnam
Trung tâm Hóa học tiên tiến, Viện Nghiên cứu và Phát triển Công nghệ cao, Đại học Duy Tân, Đà Nẵng, Việt Nam

Abstract

Since the first appearance from thousand years ago, silkworm silk has been known as an abundant biopolymer with a vast range of attractive properties. The utilization of silk fibroin (SF), main protein of silk, is not only limited in textile industry but has been broadened into more high-tech application areas, including biomaterials. This article addresses fundamental structure, general properties and structure/properties relationship of silk and SF. Besides, a brief introduction of material fabrication methods as well as examples of biomedical application are also provided.

Keywords: Silk, fibroin, biomedical application, biopolymer.

Tóm tắt

 Kể từ khi được phát hiện từ hàng nghìn năm trước, tơ tằm đã được biết đến như một loại polymer sinh học có trữ lượng lớn với nhiều tính năng hấp dẫn. Ứng dụng của fibroin, thành phần protein chính của tơ tằm, không chỉ giới hạn ở công nghiệp dệt may mà hiện đang được mở rộng ra nhiều lĩnh vực công nghệ cao, chẳng hạn như vật liệu y sinh. Bài viết này sẽ đề cập đến cấu trúc, các tính chất cơ bản và mối tương quan giữa cấu trúc/tính chất của tơ tằm và fibroin. Bên cạnh đó, những phương pháp tổng hợp, gia công vật liệu và các ứng dụng y sinh tiêu tiểu của fibroin cũng sẽ được giới thiệu.

Từ khóa: Tơ tằm, fibroin, ứng dụng y sinh, polymer sinh học.

I. Introduction of silk

Silk, one of the most abundant biopolymers from nature, has been renowned as a luxury raw material in textile industry for thousands of years from its first appearance back to between 4000 and 3000 BC. The unique luster, tactile properties, durability and dyeability make silks queen of textiles. Moreover, fabrics from silk fibers also exhibit extraordinary mechanical strength, flexibility, comfort in warm or cold weather. With these exceptional properties as well as the mild processing condition, silk can rival a lot of synthetic polymers. It has been estimated that more than 120000 tons of silks are produced globally with the main markets are located in China, India and Japan [1]. However, it is only rather recent, we are beginning to see the real potential of this sophisticated material. Advanced technologies and modern tools in chemistry, material engineering, chemical engineering,

Email: nguyenquangvinh10@duytan.edu.vn

conceptual modeling have contributed much in realizing remarkable structure and extraordinary properties of silk. Owning to its hierarchical structure and versatility, silk has been investigated as an inspiration source for designing novel materials with tailored properties, high performance, added value to a diverse range of target applications such as wearable electronic devices, water ultrafiltration, biosensors, drug delivery and tissue engineering. To realize full potential of silks in those advanced applications, fundamental material knowledge as well as physical, chemical and biological understanding are highly required. Besides, nanoscience and nanotechnologies would play a significant role in applying this ancient material to modern areas of technological fields [1].

Silks are defined as a unique class of biopolymer that are products of secretion 'spinning' from a number of arthropod lineages to build their cocoons and webs. There have been more than 30000 known species of spiders and most of 113000 species of insect order *Lepidoptera* can produce silks [2]. Besides, there are several silk sources such as crickets, bees, wasps, fleas, lacewings, caddisfly larvae, aquatic midge larvae, glowworm and fungus gnats [1]. However, the most production of silks are limited to *Nephila clavipes* and *Araneus diadematus* spiders, *Bombyx Mori* domestic silkworms, *Antheraea pernyi* and *Samia Cynthia Ricini* wild silkworms. Although spider silks are superior in mechanical strength in comparison with silkworm silk, nevertheless, due to the limited availability, only filament generated by *Bombyx mori* (*B. Mori*) is dominant in commercial silk industry [3]. *B. Mori* silks are normally produced through a cycle of different stages [1]. Firstly, silkworm eggs are laid in a controlled environment. Secondly, the eggs are incubated for 10 days in prior to larvae hatching. Thereafter, larvae are fed with mulberry leaves for 6 weeks. Then, the larvae spin fibers to form a cocoon that protect

them against microbial, moisture and predators during metamorphosis period. In the middle of metamorphosis period, *B. Mori* silkworms are killed before forming pupae and the cocoon fibers are unraveled into commercial silk fibers. In our article, we just focus on various aspects of *B. Mori* silkworm silks, which are simply termed as "silk" from now on.
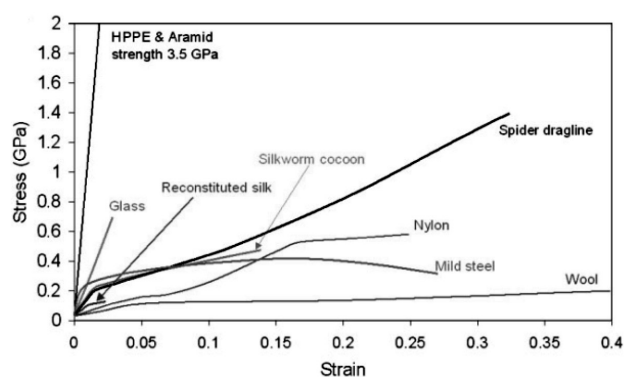
Figure 1. Representative experimental stress-strain plots for a range of different materials compared with silk (reproduced from [6])

Owing to its hierarchical protein structure, silk possesses many desirable properties, which make it a promising material for future application in a diverse range of areas. In general, silks achieve impressive mechanical properties and perfect balance between strength, modulus, toughness, extensibility, light weight and flexibility [4]. The tensile strength of silk is comparable to nylon and mild steel while still appears to be light weight (**Figure 1**). Thus, strength-to-density ratio of silk is very high, which is suitable for applications which require the combination of strength and low density. Thanks to protein nature, mechanical strength, cytocompatibility and slow degradation, silk is an excellent candidate for biomaterials. After implanting into body, silk causes less immunogenicity response than other common biomaterials such as synthetic polymer(lactic-co-glycolic acid) (PLGA) and even collagen [5]. Otherwise, degradation of silk is enzymatically driven and can be precisely controlled by the change of processing parameters as well as crystallinity [5]. This is a clear win for silk over

other biopolymers such as chitosan, gelatin, collagen for such application.

Although possessing superior biocompatibility and excellent mechanical strength, native silk materials still do not meet demands for specific applications. With advancements in physical, chemical and genetic engineering, silks can be functionalized and modified at multi-levels to achieve desired properties. Firstly, chemical modification via reactive amino acid groups on silk polymer chain would be a promising solution to yield silk-derivatives as well as conjugation products with photo-sensitivity, cell attachment ability and anti-adhesion ability [7]. Secondly, genetic engineering is a strategy to modify structure of silk protein to customize properties at gene level. Transgenic silkworms can produce silk with enhanced fluorescence or even recombinant spider silk fibers at large-scale [4]. Thirdly, feeding method can be potential for large-scale production of silk with enhanced properties. Using this approach, a variety of fluorescent dyes or functional nanomaterials such as graphene, carbon nanotubes, gold nanoparticles, silver nanoparticles can be in incorporated intrinsically into silk fibers, just only by feeding silkworms with special diet containing those materials. Besides, functional molecules can also be incorporated into silk by doping technique. Hence, silk with functions such as mechanical sensitive color-changing, NIR-sensitive for phototherapy can be produced by doping with stimuli-sensitive molecules such as polydiacetylene, gold nanoparticles, quantum dots and enzymes. Lastly, macroscopic mixing would be a simple yet powerful method to manufacture silk-based composite with tailored characteristics by combining with other materials such as collagen, chitosan and gelatin.

II. Silk protein structure

Generally, natural silkworm silk thread composes of two structural proteins which are fibroin and sericin, with schematic structure described in **Figure 2**. Fibroin is the dominant component of silk, acts as inner core that provides mechanical strength while sericin is the outer glue coating. Particularly, each single fiber of silk contains two fibroin filaments with outer sericin coating [8]. It also has been proposed that fibroin is assembled from nanofibrils with diameter of 3-5 nm, which are fundamental units of silk. Otherwise, those nanofibrils interlock, strongly interact with each other and assemble into bigger fibril units with diameter of 20-200 nm, which are called microfibrils. Microfibrils and nanofibrils arrange in a parallel axis along the silk fibers. Strong friction between those twisted bundles of nanofibrils is the main reason accounts for strong domain interaction, results in superior mechanical strength of silk fibers.
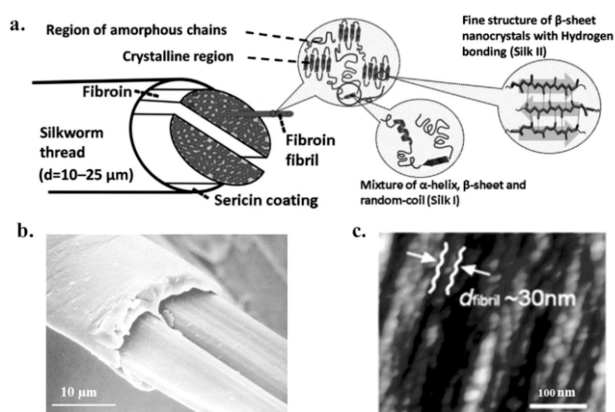
Figure 2. Hierarchical structure of B. mori silk: a) schematic structure of silk fiber b) scanning electron microscopy image of silk fiber c) atomic force microscopy shows the fibroin fibrils (reproduced from [9])

Silk fibroin (SF), the dominant structural protein of silk, contains polypeptide chains with molecular weight in range of $200-350$ kDa. These amino acid chains comprise of repetitive blocks of hydrophobic heavy chain (H-fibroin) and hydrophilic light chain (L-chain) with terminal C and N groups. Disulfide bonds are the linkers between those chains. Besides, a glycoprotein (P25) is also found in fibroin structure, which is non-covalently linked to abovementioned chains and provides the integrity to the whole structure.

In *B. Mori* silk, H-fibroin, L-fibroin and P25 are assembled in ratio of 6:6:1 [1].

The hydrophilic L-fibroin is formed by a fewer numbers of amino acid sequences, mostly contains alanine (14%) serine (10%), glycine (9%) and N-acetylated terminal serine residues. Whereas, the hydrophobic H-fibroin possesses 45.9% of glycine, 30.3% alanine, 12.1% of serine, 5.3% of tyrosine and 1.8% of valine [9]. Hence, the amino acid sequence of H-fibroin can be described as (-Gly-Ser-Gly-Ala-Gly-Ala-)$_n$. Indeed, the hydrophobic H-fibroin chains consist of hydrophobic repetitive domains interspersed in between hydrophilic non-repetitive domains [8,10]. Through hydrogen bonding, van der Waals forces and hydrophobic interaction, those hydrophobic repetitive amino acid domains of H-fibroin fold and bond together to form anti-parallel β-sheet crystalline structures. Those crystalline domains act as the crosslinking points in a less ordered, poorly oriented amorphous matrix, which is formed by non-repetitive domains, to finally form a molecular fishnet structure [11,12]. The strong β-sheet interaction, high degree of ordering and high density of β-crystallites are believed to absorb impact pressure and distribute to the whole fibroin network, thus bring superior mechanical strength to silk network (**Figure 3**). Secondary structures of silk can be classified into three types: silk I, silk II and silk III [12–14]. Among them, silk I is the liquid, metastable form of fibroin that stores in the silk gland and has been described as partially ordered structure that could contain α-helix and even random coil structures. On the other hands, silk II is the solid fibroin formed after spinning process, which is termed for β-sheet crystalline structure. Lastly, silk III is a solid form of fibroin mostly formed by trifold helical chain conformation and is found in the interface of air-water [14]. In the spinning process of silkworm, the conformation change from dissolved, less-ordered silk I into solidified, highly ordered silk

II occurs and results in formation of silk fibers [1]. The control over internal secondary structure of silk is a powerful tool to sophistically adjust external properties such as mechanical strength, solubility and biodegradation.
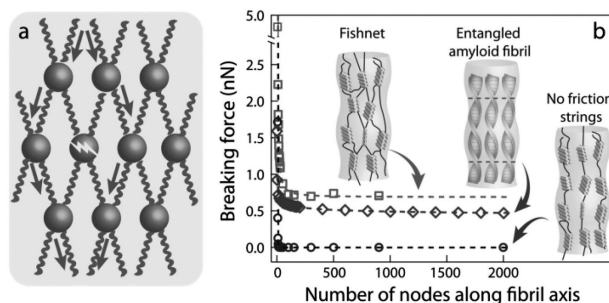
Figure 3. Modeling of mechanical strength of the fishnet structure of silk fiber; a) stress can be absorb and bypass the broken β-sheet; b) mechanical strength of fishnet model in comparison with non- friction strings and entangled amyloid fibril models. (reproduced from [11])

III. Silk materials preparation

Silk-fibroin based materials could be prepared by a variety of techniques, depending on the desired material formats [15] (**Figure 4**). However, for all preparation methods, the raw silk cocoon first must undergo a degumming process to eliminate sericin. In this process, silk is boiled in diluted solution of sodium bicarbonate (Na_2CO_3), rinsed and washed with pure water in prior to drying overnight. By boiling for a sufficient time in Na_2CO_3 solution, sericin could be removed from silk fibers and fibroin fibers can be obtained. The boiling time and salt concentration in this process should be well controlled in order to prevent any negative effect towards resulting fibroin [16]. High salt concentration and prolonged boiling time could lead to protein degradation and lowering down the molecular weight of resulting fibroin. Subsequently, SF-based materials could be either prepared from pure fibroin solution/powder or nanofibril contained solution/lyophilized nanofibril. The latter approach is employed whenever properties originate from nanosize effect are demanded. The exfoliation of silk into microfibril/nanofibrils could be performed by ultrasonication; dissolving in $CaCl_2$-Formic

acid, LiBr-Formic acid, Hexafluoroisopropanol (HFIP), sodium hypochloride; or combination of them [17]. However, the most commonly utilized strategy for preparation of silk-based materials is dissolution of SF threads into pure fibroin solution and regeneration into various material formats, which is covered in our review. The resulting fibroin is termed regenerated SF.

In this approach, an appropriate solvent system, for instance, concentrated solution of chaotropic salts such as lithium bromide, calcium/ethanol/water, lithium thiocyanate, calcium nitrate, eco-friendly solvent such as N-methyl morpholine-N oxide, organic solvent HFIP or ionic liquids, are used to dissolve SF. Each solvent system exhibits different solubility power, thus requires different operating time and temperature [18]. Thereafter, electrolytes are normally removed through dialysis process against pure water, yielding aqueous solution of fibroin. In this step, aqueous solution of polyethylene glycol (PEG) 20 wt% could be utilized instead of pure water to obtain more concentrated fibroin solution. Fibroin solution obtained after dialysis can be stored at 4°C for 1-2 months or lyophilized into powder state for further use.
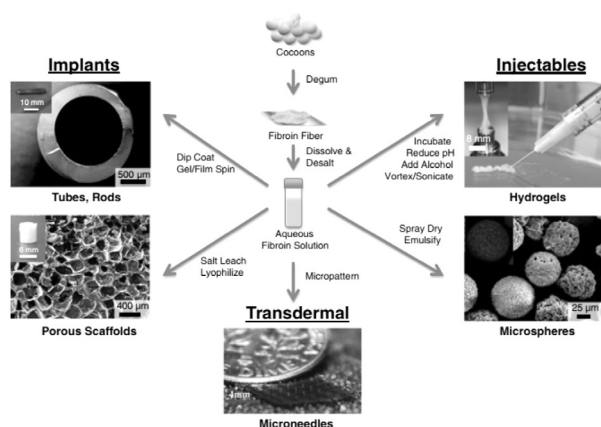
Figure 4. Aqueous SF extraction and biomaterial processing options (reproduced from [19]).

Depending on the end-use material formats such as film, hydrogel, microsphere, powder, fiber or scaffold, regeneration of fibroin can be carried out by different processes as follows:

1. SF film can be generated simply by casting, spin-coating, layer-by-layer methods. Generally, non-patterned SF film can be obtained by depositing a SF solution onto a collecting plate and drying overnight. Subsequently, β-sheet crystalline transformation can be improved by immersing in alcohol (methanol/ethanol) solution or water annealing using a vacuum desiccator. Otherwise, patterned SF film can be achieved by placing a pre-formed polydimethylsiloxane (PDMS) mold into a Petri dish before fibroin depositing, drying and β-sheet inducing. Tweezers are used to peel SF film from PDMS mold.

2. SF hydrogel is termed for water-containing three dimensional network of SF [20]. Physically crosslinked SF hydrogel can be produced by transition process from liquid-like sol-state into solid-like gel-state, in which protein self-assembly by enhanced hydrophobic interaction is the underlying mechanism. The self-assembly gelation process can occur naturally but usually takes long time (3 months at 37°C). To accelerate gelation process, various stimulating tools can be employed such as low pH condition, enhanced temperature, vortexing, ultrasonication, electrical current, lyophilization, ion concentration and dehydrating agents [21]. Besides, chemically crosslinked SF hydrogel can be generated by various chemical reaction of functionalized silk-based and other precursors, depending on specific design. Indeed, the most commonly deployed crosslinking approach is the enzymatic catalyzed reaction of tyrosine groups on fibroin chain using hydrogen peroxide and horseradish peroxidase [22]

3. SF fibers are usually prepared by wet-spinning, dry jet spinning and electro-spinning processes [23]. While wet and dry spinning methods yield micro-diameter fibers, electrospinning technology can generate submicron to nano-diameter fibers with significantly large surface areas and ability to incorporate nano-sized molecules onto spun

fibers. Generally, spinning dope is prepared with highly concentrated solution (25%), silk proteins thus can self-assemble into micelles via hydrophobic interaction and hydrogen bonding. Thereafter, those resultant micelles can align and form a fiber via shear stress and dehydration. The electrospun SF can be produced by applying a positive voltage to the SF solution-loaded syringe to initiate a jet towards a grounded collector plate. Then, resultant SF fibers/mats are treated with methanol first and washed with water to trigger the β-sheet transformation.

4. SF can form a porous 3D structure, namely sponge, foam or scaffold, which could be used for biomedical applications such as tissue engineering, implantable devices and disease models. There are aqueous-based and HFIP-based SF sponges, which present different mechanical strength, surface smoothness, interconnectivity and degradation rate [15]. The general process for fabrication of aqueous-based silk foam involves these key steps: pouring and evenly distributing salt into SF solution, allowing mixture silk solution to form gel, removing salt by immersing in water to obtain salt-free 3D porous scaffold. On the other hands, HFIP-based SF sponge can be prepared by dissolving silk in HIFP, dropping silk/HIFP over salt-contained glass, evaporating of HFIP, treating using methanol and eliminating methanol and salt in last step.

5. SF microspheres/particles, which are useful for drug/protein/gene intravenous delivery systems, can be generated using an unsaturated fatty acid lipid or a polymer as temporary emulsifier and co-carrier of SF/payloads. In the lipid-based silk microspheres fabrication procedure, a lipid (e.g. 1,2-dioleoyl-sn-glycero-3-phosphocholine (DOPC)) film is prepared in a tube and used to emulsify dropped silk/payload solution [24]. After removing of water by freezing/thawing cycles and lyophilizing, the lipid-coated silk vesicles are suspended in methanol, centrifuged to remove lipid and obtain SF microspheres. Otherwise, for more simple and aqueous based approach, SF microspheres can be prepared by phase separation technique with other polymer such as polyvinyl alcohol (PVA) [25]. In this process, the silk-PVA mixture solution obtained by mixing SF and PVA solutions are targeted to ultrasonication to induce phase separation. Thereafter, silk/PVA film are prepared and dissolved before centrifuging to remove PVA and obtain SF microspheres.

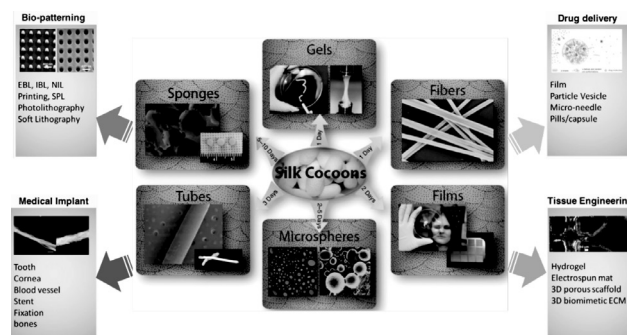## IV. Biomedical applications of SF-based materials

Thanks to sophisticated hierarchical structure and a diverse range of attractive properties, SF-based materials are paving a new path for more advanced applications other than the use in traditional textile industry, including electronic and optoelectronics, optics and photonics, water/oil filtration and biomaterials [1,4,8,9]. Several biomedical applications of SF are schematically depicted in **Figure 5**. In this review, we would like to cover several important biomedical applications of SF-based materials: small molecule drug delivery, biological drug delivery, wound healing and bone regeneration.

SF-based materials are excellent choice for delivery of bioactive molecules due to its outstanding mechanical properties, controllable biodegradability and drug stabilization effect. In a general process, after incorporating into fibroin network, therapeutic agents are maintained, transported into targeted sites and released in a controlled manner [8]. In detail, the first step is loading bioactive agents by bulk mixing, surface coating or even chemical conjugating. Then, the payloads are stabilized within fibroin network mostly by hydrophobic interaction and/or hydrogen bonding. Subsequently, the whole system is transported to targeted operating site by localized, systemic or even intra-cellular delivery routes. β-sheet crystalline domains act as mechanical barrier, the bioactive agents thus

are diffused out through the semi-amorphous regions, resulting in a sustained release profile with reduced initial burst. The release behavior can be precisely controlled by crystalline phase content or the breaking rate of labile bonds in case of conjugation fibroin system. Some examples of fibroin-based biomaterials for delivery of therapeutic drugs, biological protein or gene are given as follows.

One of the most extensively studied topics in drug delivery system is cancer therapy, fibroin thus is also investigated for this application, thanks to its drug stabilization ability. Indeed, via hydrophobic interaction with β-sheet crystallites in fibroin network, the loaded anticancer drug, such as doxorubicin (DOX), can be stabilized and maintain its bioactivity after releasing. In a report of Seib *et. al.*, a fibroin-based hydrogel is employed to deliver DOX for the localized treatment of primary breast cancer [26]. The aqueous solution of fibroin is mixed with DOX before self-assembling into a thixotropic hydrogel (a type of hydrogel appears as solid-like gel-state in prior to injection, flows under shear force and completely recovers gel-state at the target site). After locally injected into breast cancer bearing rats, loaded DOX can be released from fibroin hydrogel in a controllable manner, exhibited excellent tumor regression response and reduced metastatic spread. Another progress was made by Wu *et. al.*, in which DOX-loaded fibroin hydrogel was prepared and undergone a concentrating/ diluting process to induce nanofibers formation [27]. This system exhibited a pH-responsive and concentration-depending release of DOX, thus might provide a promising tool to control antitumor activity. Beside chemotherapy with anticancer drug, phototherapy is considered as an effective treatment method to get rid of tumor [28]. In this approach, SF-based hydrogels were loaded with complex of nano graphene oxide with lanthanide-doped rare earth nanoparticles for combination of photothermal effect and upconversion luminescence imaging ability. Under exposure to near infrared radiation laser, the fibroin-based theranostic hydrogels induced great size reduction of treated tumor.

Figure 5. SF material formats and biomedical applications (reproduced from [4,15])

Besides small molecule drug, the delivery of biological drug (protein, growth factor, peptide) and gene is also an important part of biomedical applications. For instance, a semi-interpenetrating network hydrogel of fibroin/polyacrylamide (PAAm) was developed by Mandal *et. al.* for the delivery of FITC-inulin [29]. By incorporating and crosslinking PAAm simultaneously with fibroin, the swelling and mechanical properties of this IPN hydrogel was enhanced. The SF / PAAm ratio can be used to control degradation, swelling and payload release behavior. In another report by Guziewicz *et. al.*, therapeutic monoclonal antibodies can be maintained and released from a lyogel of SF over long-term period [30]. High density of β-sheet network achieved in lyophilized gel allowed the prolonged release of loaded antibody. Besides aqueous solution form, SF can be used in electrospun mats form in preparation of silk-hyaluronic acid composite hydrogels for controlled release of a cytokine model, vascular endothelial growth factor [31]. For gene therapeutic delivery, silk-elastin-like polymers have been extensively deployed as a gene carrier for delivery of plasmid DNA or adenoviral vectors [32–35]. The control of monomer structure at genetic level and adenoviral viability are the special benefits endowed by this material.

Due to its intrinsic biocompatibility, material versatility, mechanical robustness and signaling molecules stabilization ability, silk-based material systems have been increasingly studied as potential wound healing agents. In a report of Gil *et. al.*, silk-based film, lamellar porous film and electrospun mat were loaded or coated with endothelial growth factor (EGF)/silver sulfadiazine and applied as wound dressing on BALB/C mice. Wound healing effects from these systems were comparable and even better than positive control dressing, Hydrocolloid® [36]. Also, a composite hydrogel of SF, calcium alginate and carboxymethyl cellulose has been reported by Ju *et. al.* for treatment of burn induced wound [37]. After 21 days of treatment, the SF composite hydrogel provided better cytotoxicity and comparable wound healing effect to Purilon Gel®, as a positive control. Moreover, a blending hydrogel system that combined the flexibility, elasticity and swelling ability of elastin with tunable biodegradation and high mechanical strength of silk was developed by Vasconcelos *et. al.* as wound dressing material [38]. Genipin crosslinked elastin/silk almost healed the burnt wound after 6 days of treatment, which was better than commercial collagen dressing.

In the demand for bone tissue regeneration, a potential material system is usually manufactured from bioceramic, synthetic/natural polymer or combination of them. Hence, with superior mechanical strength, impressive biocompatibility and non-immunogenicity, silk has entered this emerging application with its functionalized variants, hybrid systems and blending systems. The first example is the dual crosslinked, self-healing hydrogel prepared from calcium phosphate (CaP) modified SF microfibers (mSF) and hyaluronic-based binder [39]. In this system, dynamic metal-biphosphonate coordination (BP) between CaP-mSF and BP-polymeric binder responded for self-healing property. Additionally, the presented system can be UV-induced photocrosslinked by the presence of unsaturated double bonds in the polymeric binder chain. The hydrogel implanted group on rat cranial critical defect model exhibited much better bone regeneration response after 8 weeks in comparison with untreated group. In another attempt, Bhunia *et. al.* introduced a blending system from SF of *Bombyx mori* and *Antheraea assamensis* for disc regeneration. Interestingly, gelation time can be tuned by changing combination ratio [40]. The silk hydrogel treated regenerated disc in *ex vivo* biomechanical study showed maintained compressive properties in comparison with PBS filled degenerated disc. Lastly, an important, dominant silk-based platform for bone tissue engineering is SF/hydroxyapatite composite material, which is reviewed by Farokhi *et. al.* [41]. In those systems, hydroxyapatite, a biodegradable bioceramic with osteogenicity but brittle, is combined with extraordinary elasticity, flexibility from silk to generate a ceramic/polymer hybrid system that is very similar to natural bone structure, thus can be applied as bone constituent. The combination with silk can improve the crystal formation of hydroxyapatite and provide coordinative effect between structure and properties of silk and hydroxyapatite. Silk/hydroxyapatite can induce osteogenesis and angiogenesis by stimulating the proliferation, adhesion and differentiation of osteoblasts, thus resulting in effective bone regeneration. Those systems can be prepared as direct-written 3D scaffold [42], injectable hydrogel [43], film [44] and nanoparticle reinforced scaffold [45].

V. Conclusion

Over this brief review, we have discussed and given an insight of an ancient yet attractive material, silk, for emerging biomedical application. The abundant availability, unique hierarchical structure, outstanding mechanical strength, excellent biocompatibility, tunable biodegradation, versatility in material format design are some of the key advantageous

characteristics of SF. Current advancement in nanofabrication technologies is promising for more sophistically designed SF-based materials. However, in order to translate from academic research achievement into industrial settings, a lot of attempts should be made in development of eco-friendly, easy scale-up, less batch-to-batch variation, simple and lesser time-taking processes. Another intrinsic limitation of natural polymers which is the difficulty to control polymer structure and molecular weight should be seriously considered. Hopefully, this ancient, luxury textile material can find its own way into future applications to bring extra values not only to sericulture but also to other modern industries.

References

[1] R. F. P. Pereira, M. M. Silva, and V. De Zea Bermudez, *Macromol. Mater. Eng.* 2015, **300**, 1171–1198.

[2] D. Kaplan, W. W. Adams, B. Farmer, and C. Viney, "Chapter 1 Silk : Biology , Structure , Properties , and Genetics," 1994,2–16.

[3] K. Murugesh Babu, *Silk from silkworms and spiders as high-performance fibers*. Elsevier Ltd, 2016.

[4] Y. Cao, B. Marelli, T. H. Tao, Z. Zhou, S. Zhang, and X. Xia, *Adv. Mater.* 2018, **30**, 1706983.

[5] B. Kundu, R. Rajkhowa, S. C. Kundu, and X. Wang, *Adv. Drug Deliv. Rev.* 2013, **65**, 457–470.

[6] D. Porter and F. Vollrath, *Adv. Mater.* 2009, **21**, 487–492.

[7] A. R. Murphy and D. L. Kaplan, *J. Mater. Chem.* 2009, **19**, 6443–6450.

[8] L.D. Koh, Y. Cheng, C. P. Teng, Y. W. Khin, X. J. Loh, S. Y. Tee, M. Low, E. Ye, H. D. Yu, Y. W. Zhang, M. Y. Han, *Prog. Polym. Sci.* 2015, **46**, 86–110.

[9] W. Huang, S. Ling, C. Li, F. G. Omenetto, and D. L. Kaplan, *Chem. Soc. Rev. 2018*, **47**, 6486–6504.

[10] K. Numata, N. Ifuku, H. Masunaga, T. Hikima, and T. Sakai, *Biomacromolecules* 2017 , **18**, 1937–1946.

[11] R. Liu, Q. Deng, Z. Yang, D. Yang, M. Y. Han, and X. Y. Liu, *Adv. Funct. Mater.* 2016, **26**, 5534–5541.

[12] A. T. Nguyen, Q. L. Huang, Z. Yang, N. Lin, G. Xu, and X. Y. Liu, *Small* 2015, **11**, 1039–1054.

[13] T. Asakura, K. Okushita, and M. P. Williamson, *Macromolecules* 2015, **48**, 2345–2357.

[14] R. Valluzzi, S. P. Gido, W. Muller, and D. L. Kaplan, *Int. J. Biol. Macromol.* 1999, **24**, 237–242.

[15] X. Wang, D. N. Rockwood, D. L. Kaplan, T. Yücel, M. L. Lovett, and R. C. Preda, *Nat. Protoc.* 2011, **6**,

[16] M. K. Sah, A. Kumar, and P. K, *Int. J. Bioinforma.* 2010, **2**, 33–41.

[17] S. Ling, W. Chen, Y. Fan, K. Zheng, K. Jin, H. Yu, M. J. Buehler, D. L. Kaplan, *Prog. Polym. Sci.* 2018, **85**, 1–56.

[18] E. S. Sashina, A. M. Bochek, N. P. Novoselov, and D. A. Kirichenko, *Russ. J. Appl. Chem.* 2006, **79**, 869–876.

[19] T. Yucel, M. L. Lovett, and D. L. Kaplan, *J. Control. Release*, 2014, **190**, 381–397.

[20] S. Kapoor and S. C. Kundu, *Acta Biomater.* 2016, **31**, 17–32.

[21] B. Galateanu, A. Hudita, C. Zaharia, M.C. Bunea, E. Vasile, M.R. Buga and M. Costache, 2019,1791–1817.

[22] T. V. Chirila, S. Suzuki, and C. Papolla, *Biotechnol. Appl. Biochem.* 2017, **64**, 771–781.

[23] S. Chandra Mohan and P. Roli, *Int. J. Res. Advent Technol.* 2014, **2**, 267–277.

[24] X. Wang, E. Wenk, A. Matsumoto, L. Meinel, C. Li, and D. L. Kaplan, *J. Control. Release*,2007, **117**, 360–370.

[25] X. Wang, T. Yucel, Q. Lu, X. Hu, and D. L. Kaplan, *Biomaterials*, 2010, **31**, 1025–1035.

[26] F. P. Seib, E. M. Pritchard, and D. L. Kaplan, *Adv. Funct. Mater.* 2013, **23**, 58–65.

[27] H. Wu, S. Liu, L. Xiao, X. Dong, Q. Lu, and D. L. Kaplan, *ACS Appl. Mater. Interfaces*, 2016, **8**, 17118–17126.

[28] W. He, X. Huang, M. Liu, P. Li, H. Qi, and Y. Zhu, *New J. Chem.* 2018, **43**, 2213–2219.

[29] B. B. Mandal, S. Kapoor, and S. C. Kundu, *Biomaterials*, 2009, **30**, 2826–2836.

[30] N. Guziewicz, A. Best, B. Perez-Ramirez, and D. L. Kaplan, *Biomaterials* 2011, **32**, 2642–2650.

[31] R. Elia, D. R. Newhide, P. D. Pedevillano, G. R. Reiss, M. A. Firpo, E. W. Hsu, D. L. Kalplan, G. D. Prestwich and R. A. Peattie *et al.*, *J. Biomater. Appl.* 2011, **27**, 749–762.

[32] A. Hatefi, J. Cappello, and H. Ghandehari, *Pharm. Res.* 2007, **24**, 773–779.

[33] K. Greish, K. Araki, D. Li, B. W. O'Malley Jr, R. Dandu, J. Frandsen, J. Cappello and H. Ghandehari, *Biomacromolecules*, 2009, **10**, 2183–2188.

[34] D. Li, H. Ghandehari, B. W. O'Malley, M. Haider, Z. Megeed, and J. Cappello, *J. Control. Release*, 2004, **94**, 433–445.

[35] H. Ghandehari, J. Cappello, K. Greish, J. Frandsen, and J. Gustafson, *J. Control. Release*, 2009, **140**, 256–261.

[36] E. S. Gil, B. Panilaitis, E. Bellas, and D. L. Kaplan,

Adv. Healthc. Mater. 2013, **2**, 206–217.

[37] H. W. Ju, O. J. Lee, B. M. Moon, F. A. Sheikh, J. M. Lee, J. H. Kim, H. J. Park, D. W. Kim, M. C. Lee, S. H. Kim, C. H. Park, H. R. Lee, *Tissue Eng. Regen. Med.* 2014, **11**, 203–210.

[38] A. Vasconcelos, A. C. Gomes, and A. Cavaco-Paulo, *Acta Biomater.* 2012, **8**, 3049–3060.

[39] L. Shi, F. Wang, W. Zhu, Z. Xu, S. Fuchs, J. Hilborn, L. Zhu, Q. Ma, Y. Wang, X. Weng, D. A. Ossipov, *Adv. Funct. Mater.* 2017, **27**, 1–14.

[40] B. K. Bhunia and B. B. Mandal, *ACS Biomater. Sci. Eng.* 2019, **5**, 870–886.

[41] M. Farokhi, F. Mottaghitalab, S. Samani, M. A. Shokrgozar, S. C. Kundu, R. L. Reis, Y. Fatahi, D. L. Kaplan, *Biotechnol. Adv.* 2018, **36**, 68–91.

[42] L. Sun, S. T. Parker, D. Syoji, X. Wang, J. A. Lewis, and D. L. Kaplan, *Adv. Healthc. Mater.* 2012, **1**, 729–735.

[43] Z. Ding, H. Han, Z. Fan, H. Lu, Y. Sang, Y. Yao, Q. Cheng, Q. Lu, D. L. Kaplan, *ACS Appl. Mater. Interfaces*, 2017, **9**, 16913–16921.

[44] R. Mi, Y. Liu, X. Chen, and Z. Shao, *Nanoscale*, 2016, **8**, 20096–20102.

[45] S. Behera, D. Naskar, S. Sapru, P. Bhattacharjee, T. Dey, A. K. Ghosh, M. Mandal, S. C. Kundu, *Nanomedicine Nanotechnology, Biol. Med.* 2017, **13**, 1745–1759.

Quantum dynamics and nonclassicalities in three-mode Kerr-like nonlinear coupler

Động lực học lượng tử và các tính chất phi cổ điển trong mô hình bộ ghép ba mode phi tuyến kiểu Kerr

Nguyen Thi Dung[a,*], Doan Quoc Khoa[b], Le Van Hieu[a], Ho Khac Hieu[c]
Nguyễn Thị Dung, Đoàn Quốc Khoa, Lê Văn Hiếu, Hồ Khắc Hiếu

[a]*Hong Duc University, 565 Quang Trung, Dong Ve, Thanh Hoa, Vietnam*
Trường Đại học Hồng Đức, 565 Quang Trung, Đông Vệ, Thanh Hóa, Việt Nam
[b]*Quang Tri Teacher Training College, Dong Ha, Quang Tri, Vietnam*
Trường Cao đẳng Sư phạm Quảng Trị, Đông Hà, Quảng Trị, Việt Nam
[c]*Duy Tan University, 03 Quang Trung, Da Nang, Vietnam*
Trường Đại học Duy Tân, 03 Quang Trung, Đà Nẵng, Việt Nam

Abstract

In this article, we present the techniques of simulation, modeling quantum dynamics of a Kerr-like nonlinear coupler system which consists of three nonlinear quantum oscillators mutually coupled by continuous nonlinear interaction. We prove that by using evolution operator formalism and the common inequalities expressed in terms of various moments defined by products of creation and annihilation operators, we can model the quantum system and derive the "exact" solutions to finding the quantum properties. We show and discuss the parameters considered to be the indicators of generating nonclassicalities such as squeezing, antibunching, intermodal entanglement and their higher order counter parts, and quantumness of the system.

Keywords: squeezing, antibunching, intermodal entanglement, nonclassicality.

Tóm tắt

Trong bài báo này, chúng tôi trình bày công nghệ mô phỏng động lực học lượng tử của hệ phi tuyến kiểu Kerr bao gồm ba dao động tử phi tuyến tương tác với nhau bằng kiểu tương tác tuyến tính. Chúng tôi chứng minh rằng bằng việc sử dụng các công thức biến đổi theo thời gian của các toán tử và các bất đẳng thức diễn đạt dưới dạng các tích của toán tử sinh và hủy, chúng tôi có thể mô hình hóa hệ lượng tử và đưa ra các nghiệm "chính xác" để tìm các tính chất phi cổ điển. Chúng tôi đưa ra và thảo luận các tham số được xem xét có thể xem như là các chỉ số trong việc tạo thành các tính chất phi cổ điển như nén, phản kết chùm, rối lượng tử đa phương và hiệu ứng bậc cao tương ứng, cũng như tính lượng tử của hệ.

Từ khóa: hiệu ứng nén, phản kết chùm, rối lượng tử đa phương, tính chất phi cổ điển.

1. Introduction

Over the past few decades, there exists a speedy development of a particular attention to research of nonclassical properties in multi-party systems.

Such properties are the significant problems from both the physical viewpoints and applications in quantum communication, quantum information processing and quantum computation [1 - 3].

Email: nguyenthidungvatly@hdu.edu.vn

These signatures of nonclassicalities are related to different quantum features such as squeezing, higher order squeezing, antibunching, higher order antibunching, intermodal entanglement, and higher order entanglement [4, 5]. Generation of those interesting properties in physical systems became one of the most important points. Therefore, seeking physical models allowing for the generating such correlations seems to be especially substantial. This paper aims to show how it is possible to generate nonclassicalities by using techniques of simulation modeling for quantum dynamics of Kerr-like nonlinear coupler system. Quantum Kerr-like nonlinearity models are widely discussed in numerous applications. For instance, they were considered as a source of non-Gaussian motional states of trapped ions [6], and were discussed in a context of the Bell's

inequality violations [6]. Such models can also be applied in description of nanomechanical resonators and various optomechanical systems [7], Bose-Einstein condensates [8]. Thus, the models of nonlinear directional coupler proved to be promising devices, easy treatment for finding numerical solutions and for producing nonclassicalities and hence its quantumness.

2. The model description and simulation method

To begin with, let us consider system which consists of three nonlinear Kerr-like oscillators mutually coupled by linear interaction where each oscillator corresponds to a single mode of the field labeled *a*, *b* and *c* [9]. The Hamiltonian comprising all above − terms which describes the dynamics of the system can be written as (assuming $\hbar = 1$):

$$\hat{H} = \frac{\chi_a}{2}\hat{a}^{\dagger 2}\hat{a}^2 + \frac{\chi_b}{2}\hat{b}^{\dagger 2}\hat{b}^2 + \frac{\chi_c}{2}\hat{c}^{\dagger 2}\hat{c}^2 + \varepsilon_{ab}\hat{a}^{\dagger}\hat{b} + \varepsilon_{ab}{}^*\hat{b}^{\dagger}\hat{a} + \varepsilon_{bc}\hat{b}^{\dagger}\hat{c} + \varepsilon_{bc}{}^*\hat{c}^{\dagger}\hat{b}. \qquad (1)$$

The parameters $\chi_a\left(\chi_b, \chi_c\right)$ are proportional to the third-order susceptibilities, whereas ε_{ab} and ε_{bc} describe the strength of the linear interaction between mode *a-b* and *b-c*, respectively. Since Hamiltonian of system is expressed in terms of bosonic creation and annihilation operators, the quantum problem can be solved in Schrödinger picture. The time evolution of the system can be figured out as progression of the vector in Hilbert space. For solution $\left|\psi\left(t\right)\right\rangle$ of Schrodinger equation takes the form:

$$\left|\psi\left(t\right)\right\rangle = \exp\left(-i\hat{H}t\right)\left|\psi\left(0\right)\right\rangle. \qquad (2)$$

Using Fock basis, we can construct annihilation and creation operators of each mode sparse matrices in the Hilbert space $\mathsf{H} = \mathsf{H}_a \otimes \mathsf{H}_b \otimes \mathsf{H}_c$ as:

$$\breve{a} = \hat{a} \otimes \hat{I}_m \otimes \hat{I}_m \text{ and } \breve{a}^{\dagger} = \hat{a}^{\dagger} \otimes \hat{I}_m \otimes \hat{I}_m, \quad (3)$$

$$\breve{b} = \hat{I}_n \otimes \hat{b} \otimes \hat{I}_n \text{ and } \breve{b}^{\dagger} = \hat{I}_n \otimes \hat{b}^{\dagger} \otimes \hat{I}_n, \quad (4)$$

$$\breve{c} = \hat{I}_l \otimes \hat{I}_l \otimes \hat{c} \text{ and } \breve{c}^{\dagger} = \hat{I}_l \otimes \hat{I}_l \otimes \hat{c}^{\dagger}, \quad (5)$$

for the mode *a*, *b* and *c*, respectively. The operators $\hat{I}_{m,n,l}$ are in form of identity matrix with *m, n, l*

dimension. Assuming that the field was initially in the Glauber coherent states as:

$$\left|\psi\left(0\right)\right\rangle = \left|\alpha\right\rangle \otimes \left|\beta\right\rangle \otimes \left|\gamma\right\rangle. \qquad (6)$$

Where α, β and γ are related to the mean number of photon by the following relation $\left\langle \hat{n}_a \right\rangle = \left\langle \hat{a}^{\dagger}\hat{a} \right\rangle = \left|\alpha\right|^2$, $\left\langle \hat{n}_b \right\rangle = \left\langle \hat{b}^{\dagger}\hat{b} \right\rangle = \left|\beta\right|^2$ and $\left\langle \hat{n}_c \right\rangle = \left\langle \hat{c}^{\dagger}\hat{c} \right\rangle = \left|\gamma\right|^2$.

Using this *quantum mapping procedure*, it is possible to perform and manipulate evolution of the wave functions and then compute the indicators of interesting properties of our quantum system. Matlab computing language [10] is an appropriate *software* for performing our purposes due to their simplicity and ease of use even for computer users who are not very experienced in numerical calculations.

3. Witness of nonclassical properties

3.1. Squeezing and higher-order squeezing

In general, we study the single mode squeezing in terms of quadrature variances [11, 12] as:

$$\begin{Bmatrix} S_a \\ S'_a \end{Bmatrix} = \frac{1}{2}\Big[\big\langle \Delta\hat{a}^\dagger \Delta\hat{a} \big\rangle \pm \mathrm{Re}\big\langle \big(\Delta\hat{a}^2\big)\big\rangle \Big] < 0, \qquad (7)$$

where the fluctuation of operators characterized as $\big\langle \Delta\hat{X}\Delta\hat{Y} \big\rangle = \big\langle \hat{X}\hat{Y} \big\rangle - \big\langle \hat{X} \big\rangle\big\langle \hat{Y} \big\rangle$.
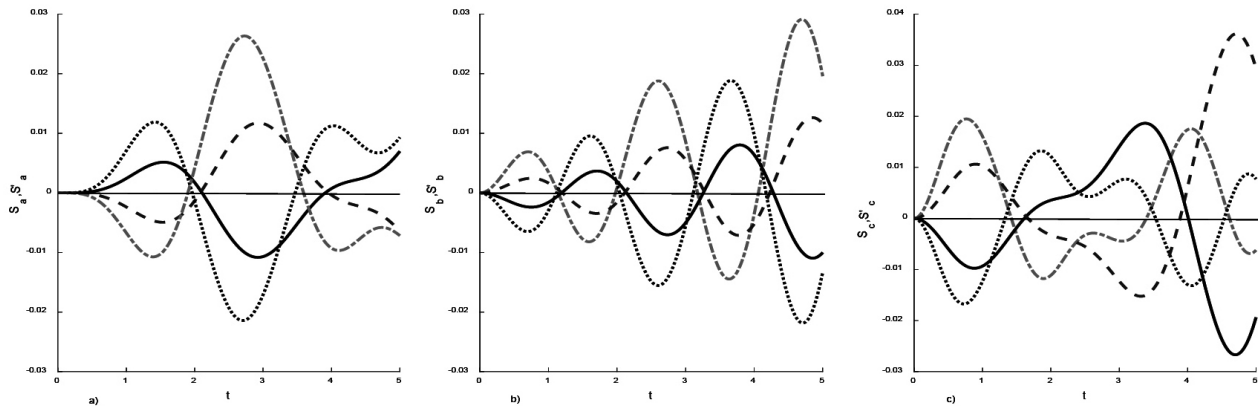

Figure 1. Evolution of one mode squeezing factors for $\alpha = 0$, $\beta = \gamma = 0.2$, $\varepsilon_{ab} = \varepsilon_{bc} = 1$; (a), (b) $\chi_a = \chi_b = \chi_c = \chi = 0.2$ for S_a, S_b (solid line), S'_a, S'_b (dashed line) and $\chi = 0.2$ for S_a, S_b (dotted line), S'_a, S'_b line (dashed dotted line); (c) $\chi = 0.5$ and for S_c (solid line), S'_c (dashed line) and $\chi = 1$ for S_c (dotted line), S'_c (dashed dotted line).

Figure 1 describes the single mode squeezing at different chosen parameters. Assuming that the initial states α is in vacuum state, and $\beta = \gamma = 0.2$. We show evolution of the squeezing parameters in Figure 1 (a), (b) and (c) corresponding to modes *a, b, c*. The behavior of squeezing factors shows that our system can give single mode squeezing with two types of criteria (7) in all three modes. To discuss the effect of interacting terms between modes, we can compare solid line ($\chi = 0.2$) with

dotted line ($\chi = 0.5$) corresponding to S_a in Figure 1 (a). The intensity squeezing (mode *a* and *b*) is increased when the nonlinearity constants are reduced (on contrary with the growth of interaction strength ε_{ab}, ε_{bc}). Particularly, single mode squeezing with rapid oscillations occurs if linear interaction terms are greater.

Two mode squeezing can be defined from two mode quadrature variances (for example, with mode *a* and *b* as [13]:

$$\begin{Bmatrix} S_{ab} \\ S'_{ab} \end{Bmatrix} = 2\Big[1 + \big\langle \Delta\hat{a}^\dagger \Delta\hat{a} \big\rangle + \big\langle \Delta\hat{b}^\dagger \Delta\hat{b} \big\rangle + 2\,\mathrm{Re}\big\langle \Delta\hat{a}^\dagger \Delta\hat{b} \big\rangle \pm \mathrm{Re}\Big(\big\langle \big(\Delta\hat{a}^2\big)\big\rangle + \big\langle \big(\Delta\hat{b}^2\big)\big\rangle + 2\big\langle \Delta\hat{a}^\dagger \Delta\hat{b} \big\rangle \Big) \Big] < 2. \qquad (8)$$

In Figure 2, we show the coupled mode quadrature variances S_{ab}, S'_{ab} and S_{bc}, S'_{bc} for $\alpha=0, \beta=0.2, \gamma=0.2$, $\varepsilon_{ab} = \varepsilon_{bc} = 1$ and different values of Kerr-like nonlinearities. The signature of two mode squeezing can be realized in two quadratures for particular values of interaction time. When the nonlinearities are decreasing (the linear coupling constants are increasing), the period of effectively squeezing is reducing and the intensity is higher. Two mode squeezing between the first and second modes in two quadratures S_{ab} and S'_{ab} seem to be

opposite (Fig. 2 (a) and Fig. 2 (b)). If squeezing occupies in S_{ab}, immediately it disappears in S'_{ab} and conversely. Also this interesting phenomenon happens similarly for squeezing between the second and third oscillators. This means that the linear interaction terms in the system can play an important role in magnifying nonclassicalities.

Single and two - mode squeezing can be regarded as the lowest order nonclassicalities, whereas it appears that there are other criteria which can be applied to test *higher - order*

squeezing effect. For the convenience we use the definition given by Hillery [14], which provides witness for the existence of higher - order nonclassicality through the two amplitude powered quadrature variables defined with use of higher power of creation and annihilation operators as (for example of mode *a*):

$$\hat{X}_{1,a} = \frac{\hat{a}^l + \hat{a}^{\dagger l}}{2}, \quad \hat{X}_{2,a} = i\frac{\hat{a}^{\dagger l} - \hat{a}^l}{2}, \quad (9)$$

where *l* is a positive integer. Because two operator $\hat{X}$ and $\hat{Y}$ do not commute, from uncertain relation, we can obtain the conditions of higher - order squeezing [14]:

$$H_{j,a}^l = \left\langle \left(\Delta \hat{X}_{j,a}\right)^2 \right\rangle - \frac{1}{2}\left|\left\langle \left[\hat{X}_{1,a}, \hat{X}_{2,a}\right]\right\rangle\right| < 0, \quad (10)$$
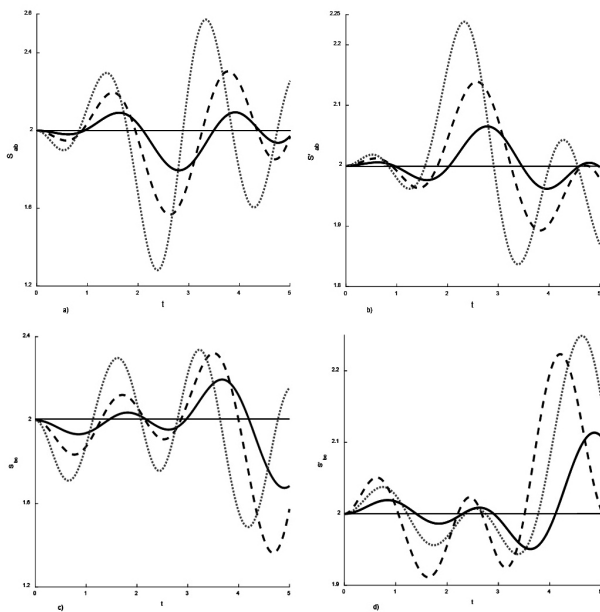
where $j = \{1, 2\}$.

Figure 2. Evolution of couple mode squeezing factors for $\alpha = 0$, $\beta = \gamma = 0.2$, $\varepsilon_{ab} = \varepsilon_{bc} = 1$, and $\chi = 0.2$ for the solid line, $\chi = 0.5$ for dashed-line; $\chi = 1$ for dashed-dotted line.

Variation of $H_{1,a}^4$ $\left(H_{1,b}^4, H_{1,c}^4\right)$ and $H_{2,a}^4$ $\left(H_{2,b}^4, H_{2,c}^4\right)$ are illustrated in Fig. 3, where negative parts of the plots depict signature of higher-order squeezing (chosen *l=4*). We can recognize that considered nonclassical properties are periodically present in all three modes. Two types of criteria to obtain this effect seem to be opposite. If squeezing disappears

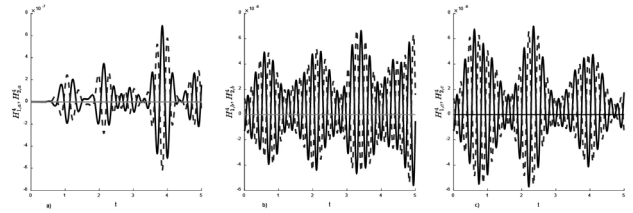in $H_{2,a}^4$ $\left(H_{2,b}^4, H_{2,c}^4\right)$, it happens in $H_{1,a}^4$ $\left(H_{1,b}^4, H_{1,c}^4\right)$ immediately.

Figure 3. The time-evolution of $H_{1,a}^4$ $\left(H_{1,b}^4, H_{1,c}^4\right)$ (solid line), and $H_{2,a}^4$ $\left(H_{2,b}^4, H_{2,c}^4\right)$ (dashed line) for $\alpha = 0$, $\beta = \gamma = 0.2$, $\varepsilon_{ab} = \varepsilon_{bc} = 1$, and $\chi = 1$.

3.2. Antibunching and higher - order antibunching

The general criteria for finding the higher - order antibunching of the pure mode was first given by C.T.Lee [15], and afterwards was simply expressed by Pathak and Garcia [16] as

$$D_a^k = \left\langle \hat{a}^{\dagger k}\hat{a}^k \right\rangle - \left\langle \hat{a}^{\dagger}\hat{a} \right\rangle^k < 0, \quad (11)$$

for mode *a*. When *k=2* we return to the normal antibunching [17].

The existences of the normal and higher order antibunching in three modes of our system are shown in Fig. 4 with quite weak signals. It is easy to recognize that for our system, these nonclassical properties are less evident when the levels of power are set up with greater values. In addition, the linear interaction terms in the system can effect on magnifying this nonclassicality when we compare three lines in each picture of Fig. 4.
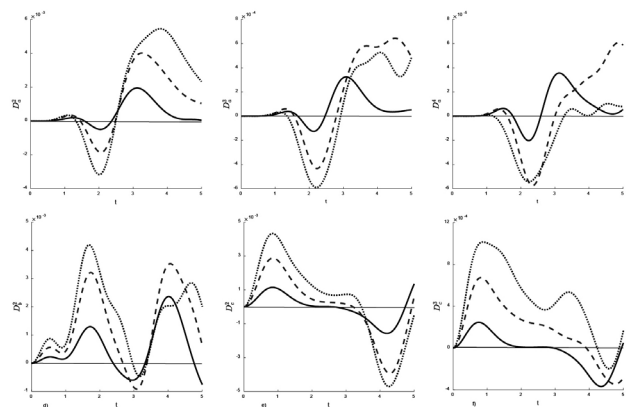
Figure 4. The time-evolution of normal and higher-order antibunching for $\alpha = 0$, $\beta = 0.2$, $\gamma = 0.3$, $\varepsilon_{ab} = \varepsilon_{bc} = 1$, and $\chi = 0.2$ for the solid line, $\chi = 0.5$ for dashed-line; $\chi_a = 1$ and for dashed-dotted line.

3.3. Two mode intermodal entanglement

Entanglement is confirmed to be the central source in quantum information processing. Several entanglement criteria which would be directly applicable for multimode problems exist. Hillery-Zubairy (HZ) inseparable criterion I and criterion II [18, 19] have obtained more attention due to simple computation, experimental practicability and their recent success in observing entanglement in various physical systems. The HZ-I criterion can be generally expressed in terms of the creation and annihilation operators in the following way [19]:

$$E_{ab}^{kl} = \left\langle \hat{a}^{\dagger k} \hat{a}^k \hat{b}^{\dagger l} \hat{b}^l \right\rangle - \left| \left\langle \hat{a}^k \hat{b}^{\dagger l} \right\rangle \right|^2 < 0. \quad (12)$$

The HZ-II criterion can be generalized for higher-order moments as [19]:

$$E_{ab}^{'kl} = \left\langle \hat{a}^{\dagger k} \hat{a}^k \right\rangle \left\langle \hat{b}^{\dagger l} \hat{b}^l \right\rangle - \left| \left\langle \hat{a}^k \hat{b}^l \right\rangle \right|^2 < 0. \quad (13)$$

When one of these inequalities is fulfilled, the multimode system is entangled.

Our numerical simulation shows the existence of two-mode intermodal entanglement between mode $a - b$ and mode $b - c$ in Fig. 5 and Fig. 6. The negative regions of the plots E_{ab}^{11}, E_{bc}^{11}, $E_{ab}^{'12}$ and $E_{bc}^{'12}$ indicate that intermodal entanglement and higher-order one are clearly presented. We also observe that for some time intervals, their depths are proportional to the values of the parameters Kerr-like nonlinearities (greater values of linear interaction strength). Thus, the linear interactions in mode $a - b$ and mode $b - c$ also contribute to intensity of this type of interesting effect. Hence, our results indicate that our three Kerr-like nonlinear coupler system can be seen as a source of intermodal entanglement and its higher orders.
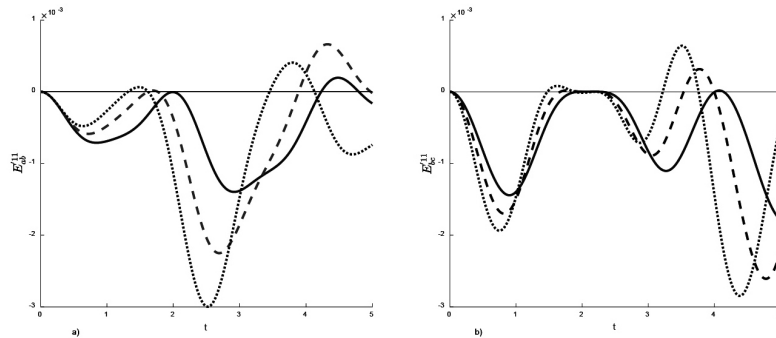

Figure 5. The time evolution of $E_{ab}^{'11}$ (a) and $E_{bc}^{'11}$ (b) where $\alpha = 0$, $\beta = 0.2$, $\gamma = 0.3$, $\varepsilon_{ab} = \varepsilon_{bc} = 1$, and $\chi = 0.2$ for the solid line, $\chi = 0.5$ for dashed-line; $\chi_a = 1$ and for dashed-dotted line.

Figure 6. The time evolution of $E_{ab}^{'12}$ (a) and $E_{bc}^{'12}$ (b) where $\alpha = 0$, $\beta = 0.2$, $\gamma = 0.3$, $\varepsilon_{ab} = \varepsilon_{bc} = 1$, and $\chi = 0.2$ for the solid line, $\chi = 0.5$ for dashed-line; $\chi_a = 1$ and for dashed-dotted line.
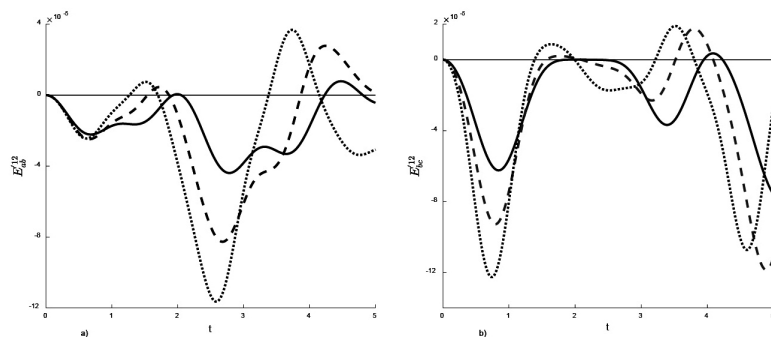
4. Conclusions

Various types of nonclassical effects have been observed in the model of three nonlinear

Kerr-like oscillators mutually coupled by linear interaction, such as squeezing, antibunching, intermodal entanglement and their higher order

counterparts. Using unitary evolution operator formalism we simulated quantum dynamics of system and found numerically the "exact" solutions to these factors under damping effect. We showed that the parameters considered here can be indicators of the generation such as nonclassical effects and hence quantumness of the system. Additionally, it was easy to recognize that the linear interaction terms strongly impact on the strength of creation of those properties.

Acknowledgements

References

[1] Duan L M, Giedke G, Cirac J I and Zoller P 2000 *Phys. Rev. Lett.* **84,** 2722

[2] Ekert A 1991 *Phys. Rev. Lett.* **67,** 661

[3] Hillery M 2000 *Phys. Rev. A* **61,** 022309

[4] Das M, Sen B, Ray A, Pathak A 2018 Annalen der Physik **530**, 1700160

[5] Giri SK, Thapliyal K, B Sen, A Pathak 2017 *Physica A: Statistical Mechanics and its Applications* **466**, 140

[6] Stobinska M, Jeong H, and Ralph T C 2007 *Phys. Rev. A*, **75,** 052105

[7] Stobinska M, Milburn G J, and Wodkiewicz K 2008 *Phys. Rev. A*, **78,** 013810

[8] Perinova V, Luks A, and Krapelka J 2013 *J. Phys. B:At. Mol. Opt. Phys.*, **46,** 195301

[9] Korolkova N, Perina J 1997 Opt. Commun. **136**, 135

[10] Matlab documentation, available at: http://www.mathworks.com/help/matlab/index.html

[11] Tanas R, Miranowicz A and Kielich S 1991 *Phys. Rev. A* **43,** 4014

[12] Luks A, Perinova V and Perina J 1988 *Opt. Commun.* **67,** 149

[13] Karska M and Perina J 1990 *J. Mod. Opt.* **37,** 195

[14] Hillery M 1987 *Phys. Rev. A* **36,** 37968

[15] Lee C T 1990 *Phys. Rev. A.* **41,** 1569; Lee C 1990 *Phys. Rev. A* **41,** 1721

[16] Pathak A and Garcia M 2006 *Applied Physics B* **84**, 484

[17] Mandel L and Wolf E 1995 Optical Coherence and Quantum Optics. *Cambridge, New York*

[18] Hillery M and Zubairy M S 2006 *Phys. Rev. A* **74,** 032333

[19] Hillery M and Zubairy M S 2006 *Phys. Rev. Lett.* **96,** 050503

Applying MCNP6 code for the modeling and optimization of the Compton suppression gamma-ray spectroscopy

Ứng dụng chương trình MCNP6 cho việc mô hình hóa và tối ưu hóa hệ phổ kế gamma nén Compton

Sy Minh Tuan Hoang

Hoàng Sỹ Minh Tuấn

Institute of Fundamental and Applied Sciences, Duy Tan University, Ho Chi Minh City, Vietnam
Viện Nghiên cứu Khoa học Cơ bản và Ứng dụng, Đại học Duy Tân, Thành phố Hồ Chí Minh, Việt Nam

Abstract

The HPGe spectroscopy system integrated with a BGO detector that operated in the anti-coincidence mode is well suited to analyze the low-radioactivity of samples to unmask the buried peaks under Compton continuum background. In the present study, the performance of Compton suppression system (CSS) at the NAA's lab (KAERI) was optimized using MCNP6 code through the evaluation of the Compton Suppression factor (CSF). After validating the CSS model by comparing the calculated efficiencies with the experimental ones, the optimal values have been obtained as 10 cm and 1.8 cm in the relative position of two detectors and a thickness of the BGO detector, respectively. The lowest threshold energy (from 30 to 100 keV) of the BGO detector was suitable in operating the CSS that has been confirmed based on the simulation. As the optimal performance of the CSS, the CSF was enhanced to 8 when the CSS reinstalled at the optimal parameters.

Keywords: Compton Suppression System, MCNP, Detector Response Function, HPGe detector, Gamma-ray spectroscopy.

Tóm tắt

Hệ phổ kế HPGe tích hợp với đầu dò nhấp nháy BGO vận hành ở chế độ phản trùng phùng thích hợp cho việc phân tích các mẫu hoạt độ thấp với các đỉnh bị che khuất bởi phông nền Compton. Trong nghiên cứu này, hệ nén Compton tại phòng thí nghiệm NAA (KAERI) đã được tối ưu bằng chương trình MCNP6 dựa vào việc đánh giá hệ số nén Compton. Dựa vào mô hình hệ CSS sau khi đã được phê chuẩn thông qua việc so sánh giữa hiệu suất tính toán và thực nghiệm, giá trị tối ưu đối với khoảng cách tương đối của hai đầu dò và độ dày của đầu dò nhấp nháy thu được là 10 cm và 1.8 cm. Ngưỡng năng lượng từ 30 keV đến 100 keV của đầu dò BGO tương thích cho việc vận hành hệ nén Compton đã được xác nhận lại bằng thực nghiệm. Hệ số nén Compton của hệ đã được nâng lên giá trị 8 sau khi cài đặt lại hệ nén Compton tại các giá trị thông số tối ưu.

Từ khóa: Hệ nén Compton, MCNP, hàm đáp ứng phổ, đầu dò HPGe, hệ phổ kế gamma.

1. Introduction

Gamma-ray spectroscopy system based on high-purity germanium (HPGe) detectors has a competent capacity that utilized for non-destructive assay of radioactive materials in a variety of applications, including neutron activation analysis (NAA), environmental radioactivity, and fundamental physics research [1-3]. Due to having the excellent

Email: hsmtuan@gmail.com

energy resolution and high efficiency, the analyses of various radionuclides in composite samples can be analyzed by the HPGe detectors. From several hundreds of keV to several MeV of energy range, the interaction between γ-rays and detector takes place mainly through Compton scattering. Thus, detection of the low intensity of γ-rays is always complicated because the Compton continuum arises from partial energy depositions of incident γ-ray radiation scattering out from the principal detector and consequently raises the lower detection limits for gamma-ray energies in that region [4, 5]. The Compton continuum also obscures lower energy decays, reducing the observed Peak-to-Count (P/C) ratio for these transitions. The reduction of the component scattered in the detector can be obtained by active Compton suppression techniques [6]. There are different principles that have been proposed for the reduction of the Compton continuum exist [7, 8]. An anti-coincidence Compton suppression is one such technique, which uses a secondary detector to capture escaping γ-ray radiation. If the detectors are time-synchronized, it is possible to identify coincident events which can then be vetoed the registration of Compton events occurring in the central detector, and the Compton continuum can be therefore suppressed by this way. The CSS to improve the P/C ratio of HPGe detectors have been successfully used for several decades in the areas of the NAA, low-level radioactive waste, environmental naturally occurring radioactivity measurements and basic nuclear physics research [9, 10]. The essential advantages of CSS which are the substantial decrease of background activity, will also help to resolve peaks buried under the background and peaks in close vicinity of others leading to improve the Minimum Detectable Activity and overall spectrum quality. The NAA's lab at the Korea Atomic Energy Research Institute (Republic of Korea) has recently installed a new CSS to measure the radioactivity of the low

activity material accurately. The CSS at NAA's lab is composed of a primary HPGe detector and a cylindrical annular BGO guard detector to detect scattered gamma-rays.

Monte Carlo (MC) techniques have been used to simulate the response of CSS, mainly for utilization to design and optimize the geometrical configuration in the last few years [11, 12]. This study's purpose was to determine the optimal parameters of the CSS by MC simulating the anti-coincidence effect. The correlation between experiments and simulations was verified and therefore applied it for finding the optimal configuration for practical. The experimental suppression performance of the CSS has been verified in comparison with the results of the simulation by checking the Compton Suppression Factors (CSF). Through careful optimization of the geometrical and electronic configuration, the CSS has achieved high performance.

2. Experimental

The CSS at the NAA's lab is a typical CSS involving the use of an annular detector surrounding the principal detector. Some auxiliary components were installed additionally for supporting the operation of the CSS such as a lead shield, a liquid nitrogen dewar, electronic modules, and an emulator software (MAESTRO-32). The electronic modules of the CSS are comprised of a timing filter amplifier (TFA), constant fraction discriminator (CFD), gate and delay generator (GDG), high voltage power supply (HV), single channel analyzer (SCA), time-to-amplitude converter (TAC) and DSPECPLUS. The working principle of the system's anti-coincidence measurement process is shown in Fig. 1.
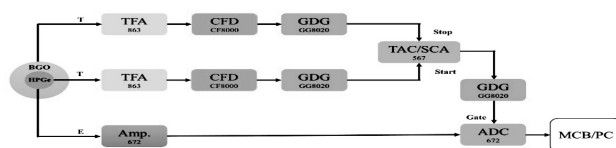
Figure 1. (top) the schematic diagram of Compton suppression system. (bottom) the photograph of the CSS at NAA's lab.

In this CSS, an ORTEC GEM detector is used as a central detector, which is a p-type coaxial HPGe detector having an ultra-thin entrance window thickness of 0.3 μm. The HPGe detector was supported vertically by a J-type cryostat. The HPGe detector capsule having an end cap diameter of 7.6 cm was mounted on the cryostat with a right-angle bend at 40.6 cm from the side of the dewar. The Ge crystal is 6.07 cm in outer diameter and 6.19 cm in length. Inside the Ge crystal, there was a hole with a diameter of 10.3 cm and a depth of 5.52 cm. The Ge crystal had a nominal rounded corner as 0.8 cm in radius and was held in an aluminum cylinder with a thickness of 0.8 cm. The resolution of this HPGe detector obtained as 1.95 and 5.9 keV at 1.33 MeV (^{60}Co) and 5.9 keV (^{55}Fe), whereas the relative efficiency was 40% with the P/C ratio of 59:1. Guard detector efficiency depends on the density and thickness of the material. The high-density of bismuth (7.13 g cc^{-1}) leads to a linear attenuation coefficient at 500 keV of 0.95 cm^{-1} thus much small BGO ($Bi_4Ge_3O_{12}$) guard detector can be employed popularly as a suppressor where a high photoelectric fraction is required. A SAINT-GOBAIN BGO detector (A/C 127 YPE 152/BGO model) is used as the annular guard detector in this CSS. The BGO crystal is a hollow cylinder with a beveled top having an outer diameter of 12.1 cm, an inner diameter of 9.1 cm, and a height of 1.52 cm. An aluminum shell enclosed this annulus with an outer diameter of 15.2 cm, an inner diameter of 8.6 cm, and a height of 16.85 cm. The ORTEC lead shield (HPLBS2F model) is employed to reduce the counts of unexpected sources from outside that interfere to the spectral counts. This shield with a 28 cm in inner diameter and 40 cm in height is designed to accommodate a J-type cryostat which provides a complete 360° shielding for the central and guard detectors. The wall of lead shield consists of a low-carbon steel casing, and a certified Doe Run lead with the thicknesses of 0.95 and 10.1 cm, respectively. To prevent X-ray interferences, 0.1 cm of tin and 0.16 cm of copper line inside the shield.

Monte Carlo (MC) method is a powerful modeling tool, which can be of great aid in the analysis of complex systems, due to its inherent capability of achieving a closer adherence to reality. It may be generally defined as a methodology for obtaining estimates of the solution of mathematical problems by means of random numbers. In particle transport, the Monte Carlo technique is pre-eminently realistic (a theoretical experiment). It consists of actually following each of many particles from a source throughout its life to its death in some terminal category (absorption, escape, etc.). Probability distributions are randomly sampled using transport data to determine the outcome at each step of its life. In the last few years, MC methods have been used to simulate the response of CSS, mainly for the evaluation and optimization of the multiple components of such systems. MCNP is a coupled neutron/photon/electron Monte Carlo transport code for modeling the interaction of radiation with matter, and its quality has been guaranteed with some advanced features as a general-purpose, continuous-energy, generalized-geometry, and time-dependent. In this study, the MCNP (version 6.1) was adopted to optimize this

CSS due to the available anti-coincidence feature of the pulse high tally function that can run in the parallel mode in comparison with other codes [13].

3. Modeling

The geometrical dimensions of the detectors and lead shield provided by the manufacturer were used as an initial guess in the simulations. However, it was necessary to fine-tune several parameters, including dead-layer thicknesses, to get a closer agreement with the measurements. According to the studies [14, 15], the best solution to achieve the closest match between simulation and experiment is a comparison with its efficiency curves because the efficiency is strongly sensitive with the change of experimental geometry. For p-type detectors, the thick dead layer is at the inside core, and the outer contact is thin. Therefore, their effect on the efficiency tends to grow towards higher energies. The MCNP calculation of efficiencies was carried out on the condition that a multi-nuclide standard point source was located at 12.5 cm from the center of the HPGe detector window so the true coincident-summing effect can be negligible. The multi-nuclide standard source (consisting of ^{113}Sn, ^{57}Co, ^{60}Co, ^{123m}Te, ^{51}Cr, ^{85}Sr, ^{109}Cd, ^{137}Cs, ^{88}Y and ^{241}Am) which covers the energy range of 60-1836 keV for satisfying the interested energy range in NAA method. The efficiencies were calculated with the same experimental condition in the normal mode. Because the calculated efficiencies are typically higher than the experiment about 10-20%, and in particular, the calculated efficiency is very sensitive to the HPGe detector parameters in the low energy range such as a dead layer thickness, a detector cap face to crystal distance, a depth of crystal hole, etc. [16, 17]. The strong discrepancies arise between the calculated and experimental efficiencies when referencing the technical data of the manufacturer describes. Therefore, the CSS geometry used in MCNP simulation should be slightly tuned from the nominal dimension of Ge crystal in order to reproduce the measured

efficiency values in the best consistency. In this study, the dead layer thickness was tuned by considering the discrepancy in the energy region below 100 keV strictly. The efficiency was calculated by increasing the outer and inner dead layer thickness from a nominal value of 0.3 to 21 μm, and from 700 to 1260 μm, respectively. In addition, the rounded corner of the Ge crystal was also created in the model with 8 mm radius. Figure 2 presents the result of calculating efficiencies based on the MCNP model (Fig. 3) that were in agreement within 4% of the experimental efficiencies over the interested energy range.
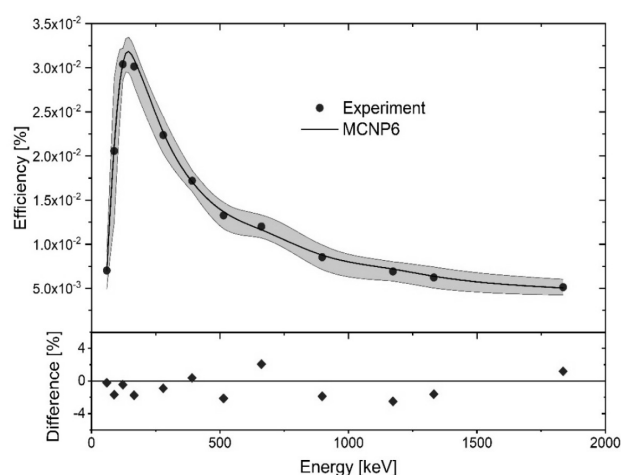

Fig. 2 Calculated and experimental efficiencies of the CSS for the multi-nuclide source in the upper part and the percentage difference between the calculation and experiment in the lower part.

Fig. 3 The MCNP model of the CSS in 3D construction. (a) radioactive source, (b) sample mount, (c) annular BGO crystal, (d) aluminum cover of BGO detector, (e) germanium crystal, (f) aluminum cover of HPGe detector.

In the MCNP simulations, the calculation of deposited energy, which is a measure of a pulse-height spectrum, in both main HPGe detector and suppression scintillators can be undertaken in two different approaches by analyzing PTRAC

card and using pulse-height (F8) tally [18]. All the necessary information for anti-coincidence consideration required by the CSS can be generated using PTRAC card. The PTRAC output is usually a large data file of positions, direction cosines, energies and interaction times; this approach was therefore not adopted in this study because the extraction of precise deposition energies is very complex. In another approach, the F8 tally with Gaussian energy broadening (GEB) option was used to generate gamma spectra of the HPGe detector. To remove coincidence particles, the F8 incorporates with the FT PHL option, which causes the omission of the pulse heights corresponding to those gamma rays escaped from the main detector and detected in the suppression detector. The Bremsstrahlung option of the phys:p card with mode n p was turned on the simulation, and the couple parameters (a, b, and c) were passed to the GEB option in the FT card for the HPGe (1.05×10^{-3} MeV, 1.35×10^{-4} MeV$^{1/2}$, and 33.47 MeV^{-1}) and BGO (1.47×10^{-2} MeV, 1.06×10^{-1} MeV$^{1/2}$, and 0.0 MeV^{-1}) detectors. These parameters were obtained from Levenberg-Marquardt fitting results of Eq. 1 based on the measured FWHM with the previous multi-nuclide standard source.

$$FWHM = a + b(E + cE^2)^{1/2} \qquad (1)$$

Where, E is the gamma-ray energy measured in MeV; and a, b, and c are parameters obtained from the fit which can be passed to the special GEB treatment in the FT card of the MNCP input.

To reduce computing time when simulated in this study, the source biasing represents the only feasible method to improve computational efficiency. Therefore, the isotropic source irradiating in 4π solid angles was replaced by the source emitting particles only in the semi-sphere oriented toward the CSS. This semi-sphere had no effect on the results since the photons emitted from opposite semi-sphere did not hit to the CSS. Furthermore, to decrease computing time the cutoff energies were set to 1 keV for both

photons and secondary electrons and the setting of minimum deposited energy in the BGO detector as 10 keV. The simulations were run in 10^9 histories for ensuring a statistical uncertainty below 3%.

Several methods are available for quantifying the levels of suppression achieved as the Peak-to-Total ratio (P/T), P/C, and the CSF [19]. However, the main one used in this study will be the CSF that is the ratio of P/C for unsuppressed and suppressed spectra, which also takes into account the reduction in photopeak efficiency as well as the suppression of the continuum. The CSF_{cal} for the simulation is defined as (Eq. 2):

$$CSF_{cal} = \frac{P_{NS\_cal}}{P_{S\_cal}} \qquad (2)$$

Where, P_{NS_cal} and P_{S_cal} are the probability of an event in the Compton continuum without and with suppression, respectively. According to the ASTM [20], the energy ranges were defined from 358 to 382 keV with the ^{137}Cs photopeak at 662 keV and 1040 to 1096 keV with the ^{60}Co photopeak at 1332 keV. Equation 3 returns back the CSF_{exp} in the experimental.

$$CSF_{exp} = \frac{P_{NS\_exp}}{P_{S\_exp}} \qquad (3)$$

Where, P_{NS_exp} and P_{S_exp} are the ratios of the net photopeak area to the average count in the associated Compton continuum that is defined above with compatible sources.
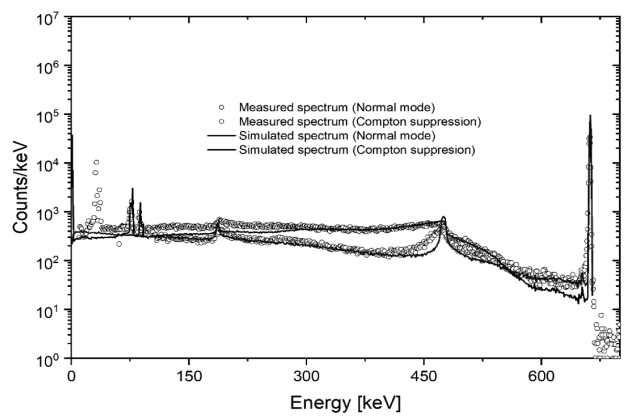

Fig. 4 The comparision between the simulated and experimental spectra of ^{137}Cs in normal and anti-coincidence modes.

As shown in Fig. 4, the measurement results for the gamma-ray energies under the Compton-

edge region were in a good agreement with the simulation results of the standard ^{137}Cs radioactive source. However, in the energy range from 450 to 480 keV, the suppressed spectrum of the simulation forms a small peak. With the ideal or a well-defined CSS with an optimized entrance hole of the collimator, the Compton edge shows a very narrow and sharp shape like a peak [21] in the pulse height spectrum. The Compton edge peak was confirmed in the simulation result due to the MCNP simulations in an ideal calculation. In addition, some difference between the simulation and the measurement results were shown in the energy region around 80 keV. In an effort to comprehend the reasons for the discrepancy in the 80 keV energy region, more simulations and experiments were performed under various conditions. These results showed the same phenomenon that seemed to be due to some physical modeling such as the efficiency of light collection in PMT, signal processing, and so on. Because the MCNP simulation code cannot simulate such parameters as the efficiency of light collection in the PMT, optimized physical modeling will be performed in future studies by using different simulation codes.

4. Optimizations

This study aims to optimize the geometry of this geometric CSS layout, and survey parameters affecting the value of the CSF. Previous studies indicate that CSF depends strongly on the position of the primary detector on the annular detector as well as the thickness of the BGO detector [22, 23]. To estimate the performance of the CSS, the optimal position of the HPGe detector inside the BGO detector and the optimal thickness of the BGO detector were investigated in this study. The input of MCNP was written in the format of WORM code [24] for changing easily the geometry during the optimized process.

4.1 Optimal position between the HPGe and BGO detectors

Finding the optimal position of the HPGe detector inside the annular BGO detector was carried out using the simulation in both normal and anti-coincidence modes with the use of ^{137}Cs and ^{60}Co sources located at 12.5 cm from the HPGe detector window. The HPGe detector was aligned inside the BGO detector so that the axes of both detectors were identical. The relative position between two detectors is determined from the top surface of the HPGe detector to the top of the BGO detector. The series of the CSF calculation has been started at the position of 0 cm, where two top surfaces of detector matched together and continued until the relative position between two detectors reaching 24 cm with an increment of 2 cm for each step. Figure 5 presents the dependence of the CSF ratio on the relative position between two detectors, and the CSF ratio reaches a maximal value at the relative position between two detectors within 10–12.5 cm.
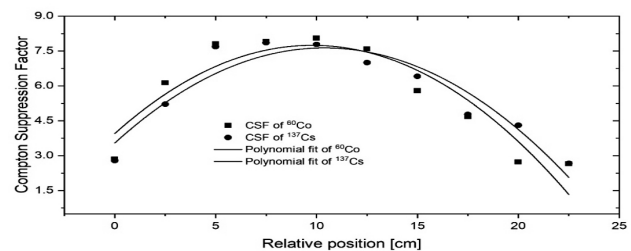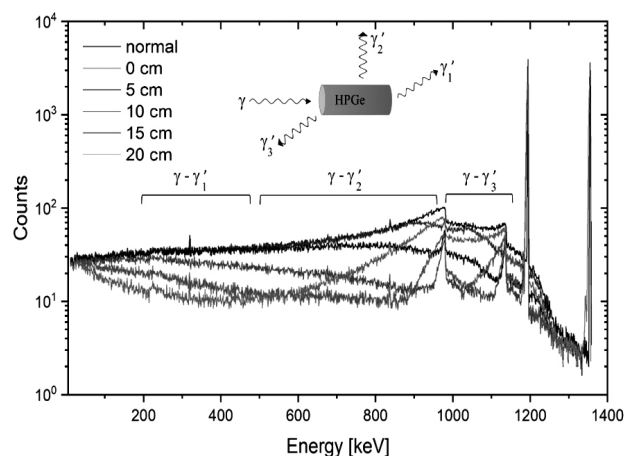

Fig. 5 CSF ratio as a function of the relative position between the central HPGe and annular BGO detectors.
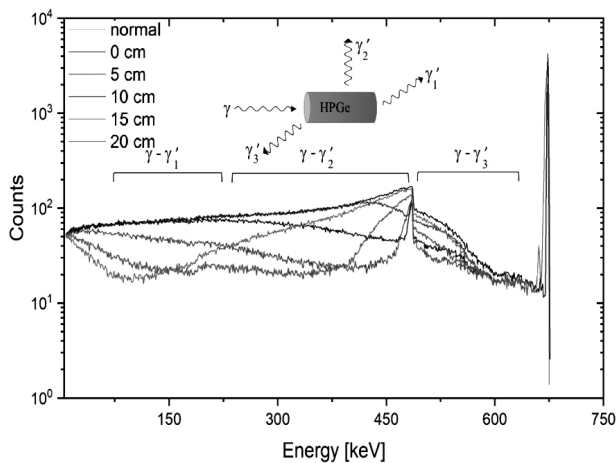
Fig. 6 The relationship between the scattering angle
and resultant Compton continuum contributing
in a simulated spectrum of ^{60}Co (top) and ^{137}Cs (bottom)
in normal and anti-coincidence modes
with several relative positions.

Based on the simulated spectra, the relationship between the scattering angle and resultant Compton continuum contributing in a spectrum of a central detector can be explained in Fig. 6. Failure to detect photons scattered in a given direction will detrimentally influence the suppression ratio in a particular Compton region. Note that the γ_1' photon has lost an little energy in the HPGe detector and is traveling forward with high residual energy, whereas the γ_3' photon has lost most of its energy in the HPGe detector and scattered backward. It dictates the need for high guard detector efficiency in the forward direction and much less in the backward direction with intermediate efficiency in between. With a moving range from 0 to 24 cm, the BGO detector has been moved from the maximum to the minimum of the scattered energies. Each gamma-ray spectrum in Fig. 6 has a different shape depending on the location of the BGO detector during the optimization process. To compare with the experiment, the experimental CSF was measured as 3.5 at 10 cm of the relative position between two detectors and its value in agreement with the calculated values.

4.2 Changing the thickness of the BGO detector

Because the detection efficiency of the BGO detector is sensitive to its size, the assessment of the BGO thickness has been carried out at the relative position of 10 cm. In the first simulation, the BGO thickness of the annular detector was kept at its initial value of 1 cm to observe its effect on the anti-coincidence of the system. The increment of these continued simulations was 0.1 cm until reaching 3.4 cm of the BGO thickness. As can be seen from Fig. 7, as the thickness of the BGO detector increased, the anti-coincidence effect of the system showed a significant upward trend. The CSF of the system increased to 8 in increments of 1.8 cm. However, when the thickness reached 2 cm, the CSF trend flattened, with slow growth and stagnation at a value around 8. Considering the above results, material cost and geometric space of the system, a 2 cm wall thickness of BGO detector was deemed optimal in compared with 1.8 cm of the actual thickness of the BGO detector. Figure 8 shows several gamma-ray spectra corresponding to the different thickness of the BGO detector.
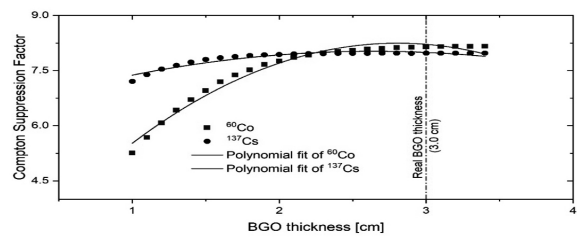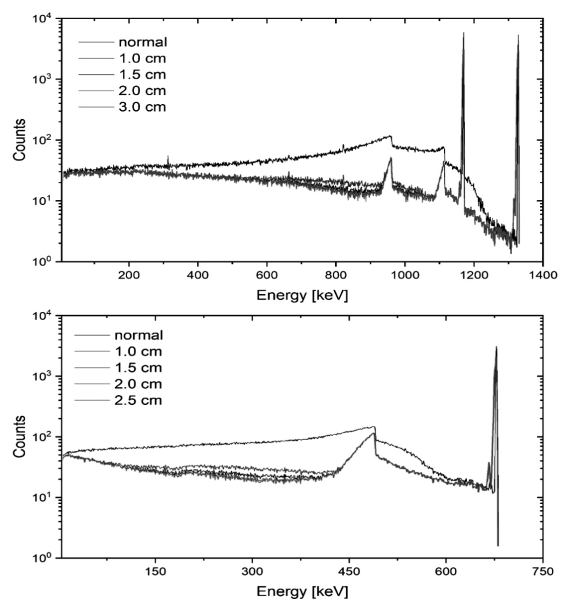

Fig. 7 CSF trend with increasing BGO wall thickness

Fig. 8 The gamma-ray spectra of 60Co (top)
and ^{137}Cs (bottom) corresponding to the different
thickness of the BGO detector.

4.3 Confirm the effect of the threshold level on the BGO detector

The effect of threshold level on the BGO detector was confirmed based on the simulation and experiment. The simulations have been carried out with the variation of energies ranging from 30 to 500 keV with a ^{137}Cs radioactive source based on the optimal values, which have been obtained in the above simulations. Because the threshold energies of BGO detector were adjusted using a fast-filter amplifier (FFA) trigger level, the unit of threshold energy was the DC voltage used in the experiments. In the results (Fig. 9), as the threshold energy was increased from 30 keV to 100 keV, the suppression ratio was reduced slightly. However, as the threshold energy was increased from 100 keV to 500 keV, the suppression ratio was reduced significantly. According to this simulation, and as expected, the lowest threshold energy (from 30 to 100 keV) of the guard detector turned out to be the most suitable.
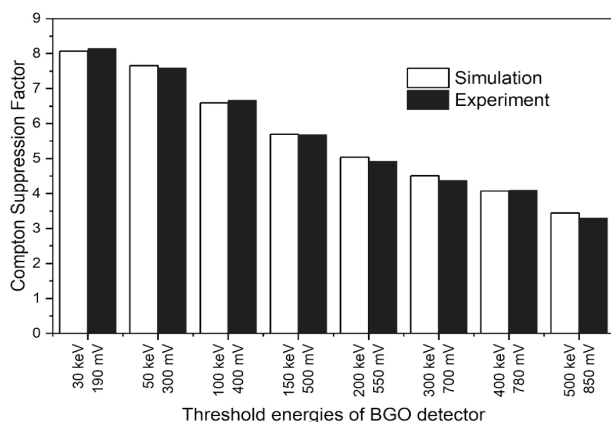

Fig. 9 The effect of the threshold level on the BGO detector in simulation and experiment.

5. Conclusions

In the present study, it has been demonstrated that the MCNP code provides an adequate tool for designing and optimizing the CSS. It is also useful to generate realistic detector response functions and predict the gamma-ray spectra of the CSS modeling in the normal and anti-coincidence modes. Consequently, MCNP code has been used to calculate the gamma-ray spectra and optimize the CSS geometry for NAA application. The agreement between simulation and experimental efficiencies within 4% of each other further supports the use of the MCNP model to predict optimum CSS parameters. Based on the MCNP simulation, the optimization process of the CSS at the NAA's lab has been performed and gave a comprehensive insight of it. The CSS model based on MCNP code has been validated by comparing the calculated efficiencies with the experimental ones. With this model, we have obtained the optimal position between two detectors as well as the assessment of the real thickness of the BGO detector, and its values have been applied to the experiments. From the simulation results, the relative position of 10 cm and 1.8 cm in a thickness has returned back the best CSF values. In addition, the threshold level of the BGO detector has been reconfirmed by the simulation.

References

[1] Mauerhofer, E., U. Tharun, H. O. Denschlag, R. Schmidt, and J. V. Kratz. "A Compton suppression spectrometer for neutron activation analysis." Nucl. Instr. Meth. Phys. Res. A 371, no. 3 (1996): 465-471.

[2] Landsberger, S., S. R. Biegalski, D. J. O'kelly, and M. S. Basunia. "Use of coincident and non-coincident gamma-rays in Compton suppression neutron activation analysis." J. Radioanal. Nucl. Chem. 263, no. 3 (2005): 817-821.

[3] Alharbi, T., P. H. Regan, P. J. R. Mason, N. Mărginean, Zs Podolyák, A. M. Bruce, E. C. Simpson et al. "Electromagnetic transition rates in the N= 80 nucleus Ce-138(58)." Phys. Rev. C 87, no. 1 (2013): 014323.

[4] Mason, P. J. R., Zs Podolyák, N. Mărginean, P. H. Regan, P. D. Stevenson, V. Werner, T. Alexander et al. "Half-life of the yrast 2+ state in ^{188}W: Evolution of deformation and collectivity in neutron-rich tungsten isotopes." Phys. Rev. C 88, no. 4 (2013): 044301.

[5] Kapsimalis, R., S. Landsberger, and N. Reguigui. "Measurement of uranium in small quantities in phosphates by use of γ-ray spectrometry and the 1001 keV peak of [234m]Pa." J. Radioanal. Nucl. Chem.280, no. 2 (2009): 293-298.

[6] Knoll, Glenn F. Radiation detection and measurement. John Wiley & Sons, 2010.

[7] Britton, R., J. Burnett, A. Davies, and P. H. Regan. "Preliminary simulations of NaI (Tl) detectors, and coincidence analysis using event stamping." J. Radioanal. Nucl. Chem. 295, no. 1 (2013): 573-577.

[8] Kapsimalis, R., S. Landsberger, and Y. A. Ahmed. "The determination of uranium in food samples by Compton suppression epithermal neutron activation analysis." Appl. Radiat. Isot. 67, no. 12 (2009): 2097-2099.

[9] Landsberger, S., and R. Kapsimalis. "An evaluation of Compton suppression neutron activation analysis for determination of trace elements in some geological samples." Appl. Radiat. Isot. 67, no. 12 (2009): 2104-2109.

[10] Stover, Tracy, and George Lamaze. "Compton suppression for neutron activation analysis applications at the National Institute of Standards and Technology (NIST)." Nucl. Instr. Meth. Phys. Res. B 241, no. 1-4 (2005): 223-227.

[11] Kiang, L. L., R. H. Tsou, J. H. Li, S. C. Lin, C-Y. Lo, G. C. Kiang, and P. K. Teng. "A study of an asymmetric Compton suppression spectrometer by Monte Carlo simulation." Nucl. Instr. Meth. Phys. Res. A 355, no. 2-3 (1995): 434-438.

[12] McNamara, A. L., H. Heijnis, D. Fierro, and M. I. Reinhard. "The determination of the efficiency of a Compton suppressed HPGe detector using Monte Carlo simulations." J. Radioanal. Nucl. Chem. 106 (2012): 1-7.

[13] Goorley, John T., M. R. James, T. E. Booth, F. B. Brown, J. S. Bull, L. J. Cox, J. W. Durkee et al. "MCNP6 User's Manual, Version 1.0." Los Alamos National Laboratory, Los Alamos (2013).

[14] Challan, Mohsen B. "Gamma-ray efficiency of a HPGe detector as a function of energy and geometry." Appl. Radiat. Isot. 82 (2013): 166-169.

[15] Ewa, I. O. B., D. Bodizs, Sz Czifrus, and Zs Molnar. "Monte Carlo determination of full energy peak efficiency for a HPGe detector." Appl. Radiat. Isot. 55, no. 1 (2001): 103-108.

[16] Boson, Jonas, Göran Ågren, and Lennart Johansson. "A detailed investigation of HPGe detector response for improved Monte Carlo efficiency calculations." Nucl. Instr. Meth. Phys. Res. A 587, no. 2-3 (2008): 304-314.

[17] Dryak, Pavel, and Petr Kovar. "Experimental and MC determination of HPGe detector efficiency in the 40–2754 keV energy range for measuring point source geometry with the source-to-detector distance of 25 cm." Appl. Radiat. Isot. 64, no. 10-11 (2006): 1346-1349.

[18] Ghal-Eh, Nima, H. Doostizadeh, Z. Hazami, and V. Doust-Mohammadi. "A Compton-suppression detection system for use in manganese bath measurements." Radiat. Phys. Chem. 112 (2015): 34-39.

[19] Britton, R., J. L. Burnett, A. V. Davies, and P. H. Regan. "Improving the effectiveness of a low-energy Compton suppression system." Nucl. Instr. Meth. Phys. Res. A 729 (2013): 64-68.

[20] Scates, Wade, John K. Hartwell, Rahmat Aryaeinejad, and Michael E. McIlwain. "Optimization studies of a Compton suppression spectrometer using experimentally validated Monte Carlo simulations." Nucl. Instr. Meth. Phys. Res. A 556, no. 2 (2006): 498-504.

[21] Moszyński, M., J. H. Bjerregard, Jens Jørgen Gaardhøje, B. Herskind, P. Knudsen, and G. Sletten. "Limitation of the Compton suppression in Ge-BGO Compton suppression spectrometers." Nucl. Instr. Meth. Phys. Res. A 280, no. 1 (1989): 73-82.

[22] Kiang, L. L., R. H. Tsou, W. J. Lin, Simon C. Lin, G. C. Kiang, P. K. Teng, and S. D. Li. "A study on T-shape Compton suppression spectrometer by Monte Carlo simulation." Nucl. Instr. Meth. Phys. Res. A 327, no. 2-3 (1993): 427-432.

[23] Badran, H. M., and T. Sharshar. "An experimental method for the optimization of anti-Compton spectrometer." Nucl. Instr. Meth. Phys. Res. A 435, no. 3 (1999): 423-432.

[24] Glazener, Natasha, and Ryan James Kamm. MCNP Parametric Studies of Plutonium Metal and Various Interstitial Moderating Materials. No. LA-UR-17-22614. Los Alamos National Lab. (LANL), Los Alamos, NM (United States), 2017.

A simple proof of the comparison property of a parabolic system

Một chứng minh đơn giản về tính chất so sánh đối với hệ parabolic

Nguyen Thai An, Nguyen Trung Hieu, Phan Quoc Hung[*]
Nguyễn Thái An, Nguyễn Trung Hiếu, Phan Quốc Hưng

Institute of Research and Development, Duy Tan University, 03 Quang Trung, Da Nang, Vietnam
Viện Nghiên cứu và Phát triển Công nghệ cao, Đại học Duy Tân, 03 Quang Trung, Đà Nẵng, Việt Nam

Abstract

We put forward a simple proof of the comparison property of the parabolic system of Lane-Emden type $u_t - \Delta u = v^p$, $v_t - \Delta v = u^q$ in $\mathbb{R}^n$, where $p, q > 0$ and $pq > 1$. Our proof is based on a new argument of maximum principle.

Keywords: Comparison property, Parabolic system, Lane-Emden.

Tóm tắt

Chúng tôi đưa ra một chứng minh đơn giản về tính chất so sánh đối với hệ parabolic dạng Lane-Emden $u_t - \Delta u = v^p$, $v_t - \Delta v = u^q$ trong $\mathbb{R}^n$, với $p, q > 0$ và $pq > 1$. Chứng minh của chúng tôi dựa trên một lí luận mới về nguyên lý cực đại.

Từ khóa: Tính chất so sánh, Hệ parabolic, Lane-Emden.

1. Introduction

The motivation of this research paper stems from the work of Bidaut-Véron [1] and Souplet [5] in which an important pointwise differential inequality for positive solutions of the famous Lane–Emden system was shown as follows:

$$\begin{cases} -\Delta u &= v^p, \\ -\Delta v &= u^q \end{cases} \quad \text{in } \mathbb{R}^n, \qquad (1)$$

where $p \geqslant q > 0$. A very interesting question concerning the system (1) is the Lane-Emden conjecture, which states that system (1) has no entire positive solution if and only if

$$\frac{1}{p+1} + \frac{1}{q+1} > 1 - \frac{2}{n}. \qquad (2)$$

Toward tackling the Lane–Emden conjecture, a pointwise differential inequality for positive solutions of (1) was found by Souplet. To be more precise, it was proved in [5, Lemma 2.7] that

$$\frac{v^{p+1}}{p+1} \leqslant \frac{u^{q+1}}{q+1}. \qquad (3)$$

This inequality was then extended to positive solutions of Hénon-Lane-Emden system in [4].

Email: phanquochung@dtu.edu.vn

Such a comparison as in (3) is highly important as it allows us to obtain various Liouville-type results for stable solutions, see e.g., [7, 6, 2]. This kind of comparison property was proved for Dirichlet problem in bounded domain by Bidaut-Véron [1, Remark 3.2].

The inequality (3) in particular case $q = 1$ provide a pointwise inequality for solutions of equation

$$\Delta^2 v = v^p$$

as

$$-\Delta v \geqslant \sqrt{\frac{2}{p+1}} v^{\frac{p+1}{2}} \quad \text{in } \mathbb{R}^n. \quad (4)$$

In this paper, we use a powerful argument of maximum principle to derive a poinwise inequality of parabolic system of Lane-Emden type

$$\begin{cases} u_t - \Delta u = v^p, \\ v_t - \Delta v = u^q \end{cases} \quad \text{in } \mathbb{R}^n, \quad (5)$$

where $p, q > 0$. Our result is as follows:

Theorem 1. *Let (u, v) be a positive solution of system (5). Assume that $p \geq q > 0$ and $pq > 1$, then we have the following pointwise inequality*

$$\frac{v^{p+1}}{p+1} \leqslant \frac{u^{q+1}}{q+1} \quad in \ \mathbb{R}^n. \quad (6)$$

We note that the Liouville-type theorem for system (5) is conjectured to hold in the range (2). However, it is still an open question, even in dimension $n = 1$ or in the class of radial solutions, we refer to papers [3, 8] for some partial results. It is expected that the pointwise inequality is an important step to tackle the Liouville-type for system (5).

The rest of this paper is devoted to the proof of Theorem 1.

2. Proof of Theorem 1

Denote

$$w = v - lu^\sigma,$$

where $\sigma := (q + 1)/(p + 1)$ and $l := \sigma^{-1/(p+1)}$. By a direct computation and taking into account

$\sigma \in (0, 1]$, we have

$$\begin{aligned} \Delta w &\geq \Delta v - l\sigma u^{\sigma-1}\Delta u \\ &= v_t - u^q + l\sigma u^{\sigma-1}(v^p - u_t) \\ &= l\sigma u^{\sigma-1}(v^p - l^p u^{\sigma p}) + w_t. \end{aligned} \quad (7)$$

We prove $w \leqslant 0$ by way of contradiction. Suppose that $M = \sup_{\mathbb{R}^n \times \mathbb{R}} w(x, t) > 0$ ($M \leqslant +\infty$). There are two possible cases:

Case 1. If (x_0, t_0) is a global maximum point of w in $\mathbb{R}^n \times \mathbb{R}$, that is

$$w(x_0, t_0) = \sup_{(x,t)\in\mathbb{R}^n\times\mathbb{R}} w(x) = M > 0$$

with $\Delta w(x_0, t_0) \leqslant 0$ and $w_t(x_0, t_0) = 0$. We have a contradiction with (7) at (x_0, t_0).

Case 2. The supremum of w is attained as $|x| + |t|^{1/2} \to \infty$. Let ψ be a smooth cuff-off function in $\mathbb{R}^N$, $0 \leq \psi \leqslant 1$, $\psi = 1$ if $|x| + |t|^{1/2} \leq 1/2$ and $\psi = 0$ if $|x|+|t|^{1/2} > 1$. Let $\varphi = \psi^m$ with $m > 0$ being chosen later. Then we have the upper bound

$$|\varphi_t| + |\Delta\varphi| + \varphi^{-1}|\nabla\varphi|^2 \leqslant C\varphi^{1-2/m}. \quad (8)$$

For each $R > 0$ we set

$$\varphi_R(x, t) = \varphi(x/R, t/R^2), \quad w_R = \varphi_R w.$$

Since w_R is zero if $|x|+|t|^{1/2} > R$, then there exists (x_R, t_R) such that

$$M_R := \max_{\mathbb{R}^n\times\mathbb{R}} w_R = w_R(x_R, t_R).$$

The choice of φ implies that $M_R \to M$ as $R \to \infty$. The property of local maximum gives

$$\begin{cases} w_t = -\dfrac{(\varphi_R)_t}{\varphi_R} w, \\ \nabla w = -\dfrac{\nabla\varphi_R}{\varphi_R} w, \\ 0 \geqslant \Delta w_R \qquad \text{at } (x_R, t_R). \end{cases}$$

Combining this with (7), at (x_R, t_R), we have

$$\begin{aligned} 0 \geqslant &\varphi_R \Delta w + 2\nabla\varphi_R \cdot \nabla w + \Delta\varphi_R w \\ \geqslant &\varphi_R\big(l\sigma u^{\sigma-1}(v^p - l^p u^{\sigma p}) + w_t\big) \\ &+ 2\nabla\varphi_R \cdot \nabla w + \Delta\varphi_R w \\ = &\varphi_R l\sigma u^{\sigma-1}(v^p - l^p u^{\sigma p}) - (\varphi_R)_t w \\ &- 2\varphi_R^{-1}|\nabla\varphi_R|^2 w + \Delta\varphi_R w \end{aligned}$$

This combined with (8) yields

$$CR^{-2}\varphi_R^{1-2/m}w \geqslant \varphi_R\, l\sigma u^{\sigma-1}(v^p - l^p u^{\sigma p}) \qquad (9)$$

at (x_R, t_R). We now consider the following two subcases.

Case 2.1: If the sequence $u(x_R, t_R)$ is bounded, then $u^{\sigma-1}(x_R, t_R)$ is bounded below away from zero. Recalling $p > 1$, then using the inequality

$$(a+b)^p - a^p \geqslant b^p, \quad a, b \geqslant 0, \qquad (10)$$

it follows from (9) that, at (x_R, t_R)

$$CR^{-2}\varphi_R^{1-2/m}w \geqslant C\varphi_R\, w^p$$

Hence,

$$CR^{-2} \geqslant \varphi_R^{2/m}(x_R, t_R)\, w^{p-1}(x_R, t_R).$$

Choosing $m > 0$ such that $2/m = p-1$, we arrive at

$$CR^{-2} \geqslant \varphi_R^{p-1}(x_R, t_R)\, w^{p-1}(x_R, t_R) = M_R^{p-1},$$

which is impossible when R is large.

Case 2.2: If the sequence $u(x_R, t_R)$ is unbounded, up to a subsequence, we may assume that

$$\lim_{R\to\infty} u(x_R, t_R) = \infty.$$

Since $pq > 1$ and $p > 1$, there exists $\varepsilon > 0$ small enough such that $pq - 1 - \varepsilon(q+1) > 0$ and $p > 1 + \varepsilon$. For $0 < b < a$, using the convexity of function $f(s) = s^{p/(1+\varepsilon)}$ in $(0, \infty)$ and (10), we have

$$\begin{aligned}
a^p - b^p &= (a^{1+\varepsilon})^{\frac{p}{1+\varepsilon}} - (b^{1+\varepsilon})^{\frac{p}{1+\varepsilon}} \\
&\geqslant \frac{p}{1+\varepsilon}(b^{1+\varepsilon})^{\frac{p}{1+\varepsilon}-1}(a^{1+\varepsilon} - b^{1+\varepsilon}) \\
&= \frac{p}{1+\varepsilon}(b^{p-\varepsilon-1})(a^{1+\varepsilon} - b^{1+\varepsilon}) \\
&\geqslant \frac{p}{1+\varepsilon}(b^{p-\varepsilon-1})(a - b)^{1+\varepsilon}.
\end{aligned}$$

Taking $a = v(x_R, t_R)$, $b = lu^\sigma(x_R, t_R)$, we deduce from (9) that, at (x_R, t_R),

$$\begin{aligned}
CR^{-2}\varphi_R^{1-2/m}w &\geqslant \varphi_R\, u^{\sigma-1}u^{\sigma(p-\varepsilon-1)}w^{1+\varepsilon} \\
&= \varphi_R u^{\frac{pr-1-\varepsilon(r+1)}{p+1}}w^{1+\varepsilon} \\
&\geqslant C\varphi_R w^{1+\varepsilon}.
\end{aligned}$$

where $C > 0$ independent of R, and in the last inequality we used the unboundedness of the sequence $u(x_R, t_R)$. Hence,

$$CR^{-2} \geqslant \varphi_R^{2/m}(x_R, t_R)\, w^\varepsilon(x_R, t_R).$$

Again, choosing $m > 0$ such that $2/m = \varepsilon$, we arrive at

$$CR^{-2} \geqslant \varphi_R^\varepsilon(x_R, t_R)\, w^\varepsilon(x_R, t_R) = M_R^\varepsilon,$$

which is impossible when R is large. Theorem is proved.

References

[1] Marie-Francoise Bidaut-Veron. Local behaviour of the solutions of a class of nonlinear elliptic systems. *Adv. Differential Equations*, 5(1-3):147–192, 2000.

[2] Craig Cowan. Liouville theorems for stable Lane-Emden systems with biharmonic problems. *Nonlinearity*, 26(8):2357–2371, 2013.

[3] M. Escobedo and M. A. Herrero. Boundedness and blow up for a semilinear reaction-diffusion system. *J. Differential Equations*, 89(1):176–202, 1991.

[4] Quoc Hung Phan. Liouville-type theorems and bounds of solutions of Hardy-Hénon systems. *Adv. Differential Equations*, 17(7-8):605–634, 2012.

[5] Philippe Souplet. The proof of the Lane-Emden conjecture in four space dimensions. *Adv. Math.*, 221(5):1409–1427, 2009.

[6] Juncheng Wei, Xingwang Xu, and Wen Yang. On the classification of stable solutions to biharmonic problems in large dimensions. *Pacific J. Math.*, 263(2):495–512, 2013.

[7] Juncheng Wei and Dong Ye. Liouville theorems for stable solutions of biharmonic problem. *Math. Ann.*, 356(4):1599–1612, 2013.

[8] Hatem Zaag. A Liouville theorem and blowup behavior for a vector-valued nonlinear heat equation with no gradient structure. *Comm. Pure Appl. Math.*, 54(1):107–133, 2001.

Expression pattern of ANAC053, a transcription factor in *Arabidopsis thaliana*

Cấu trúc biểu hiện của ANAC053, một nhân tố phiên mã ở *Arabidopsis thaliana*

Hung Nguyen Minh

Nguyễn Minh Hùng

Center for Molecular Biology, Institute of Research and Development, Duy Tan University,
03 Quang Trung, Danang, Vietnam
Trung tâm Sinh học phân tử, Viện Nghiên cứu và Phát triển Công nghệ cao, Đại học Duy Tân,
03 Quang Trung, Đà Nẵng, Việt Nam

Abstract

Leaf development is a progressive process with several different stages, in which leaf senescence is often considered as the final phase from maturation to attrition. Leaf senescence is a fateful phenomenon in leaf development and usually started from cells distant from the main vascular tissue and continues to move to the center. We show that in pANAC053::GUS reporter lines starts at the tip of the leaf, followed by the leaf margin and progression to the base. The pattern of this expression is consistent with the enhanced expression of *ANAC053* during leaf senescence as reported by several expression studies.

Keywords: Arabidopsis thaliana, senescence, ANAC053, transcription factor, expression pattern.

Tóm tắt

Phát triển lá là một quá trình gồm nhiều giai đoạn phát triển liên tục, trong đó quá trình lão hóa được xem như pha cuối cùng tính từ giai đoạn trưởng thành cho đến lúc lá rụng. Lão hóa lá là một hiện tượng không thể tránh khỏi trong tiến trình phát triển lá và thường khởi đầu từ các tế bào ở xa gân lá nhất và dần dần tiến vào phần trung tâm. Trong nghiên cứu này, chúng tôi đã xây dựng cấu trúc pANAC053::GUS và chuyển vào cây *Arabidopsis*, kết quả cho thấy cấu trúc biểu hiện tập trung chủ yếu ở các tế bào xa gân lá nhất. Một số nghiên cứu khác về điều khiển biểu hiện gene cũng cho thấy nhân tố phiên mã *ANAC053* liên quan đến việc điều khiển một số gen kiểm soát quá trình lão hóa của lá.

Từ khóa: Arabidopsis thaliana, lão hóa, *ANAC053*, nhân tố phiên mã, cấu trúc biểu hiện.

1. Introduction

Leaf development includes many different phases, from leaf primodium formation to proliferation, expansion, maturation and attrition. The final phase, from maturation to attrition, is referred to as leaf senescence [1]. Leaf senescence is a fateful phenomenon in progression of leaf development and occurs in an age-dependent manner. It involves many metabolic processes in the cell at different levels. During progression of leaf senescence, the cells in a given leaf are at different stages since senescence progresses from the tip to the base. Normally, cells distant from the main vascular tissue initiate the leaf

Email: hungmolbio@gmail.com

senescence, followed by cells around margins; then senescence moves gradually into the center of the leaf. In contrast, cells in the vascular tissues are still active to salvage and transport the breakdown product to other growing parts of the plant or the reproductive organs. Thus, leaf senescence must be tightly controlled by a genetic program, but it is strongly dependent on external environmental factors. Recently, a series of factors controlling leaf senescence have been identified such as WRKY, WRKY22, WRKY6, WRKY53, WRKY70... [2-4]. Especially, many recent studies have shown that some *NAC* transcription factors regulate leaf senescence such as *ORE1* (ANAC092) *ORS1* (ANAC059), *AtNAP* (ANAC029) [5-6].

The study of the expression patterns of transcription factors plays an important role in determining and predicting their function. In this study, we report the expression pattern of NAC053, a transcription factor in *Arabidopsis thaliana* with a potential role in leaf senescence.

2. Methods

2.1. Promoter-reporter construct

To study the tissue-specific expression pattern of ANAC053, the ANAC053 promoter (1701-bp upstream of the transcription start site, including 228 bp of the 5'-UTR) was amplified using PCR with pANAC053-F primer: 5'- CACC CCA ACA GAA TCA TCA TGA GAA TGA CC -3' and pANAC053-R primer: 5'- ATA CTC GAT GGA CCA AAA CTC AAA CAC A -3' and cloned into the pENTR/D-TOPO vector. The ANAC053 promoter was then fused to the β-glucuronidase (GUS) reporter gene in the pKGWFS7.0 gateway vector (http://gateway.psb.ugent.be) by LR recombination (Invitrogen). The ANAC053 promoter regulates the transcription of the β-glucuronidase (GUS) reporter gene.

2.2. Subcellular localization construct

The 1647-bp long coding sequence of ANAC053 (without stop codon) was cloned into the pENTR/D-TOPO vector using RT-PCR with ANAC053-CDS-F primer: 5'- CACC ATG GGT CGT GGC TCA GTA ACA TCG CT -3' and ANAC053-CDS-R primer: 5'- CCT GGA AGA GAC CAA AAT GCT CAC -3'. The ANAC053 gene in the pENTR/D-ANAC053 vector was then fused to the enhanced green fluorescent protein (eGFP) gene at the N-terminus in the pK7FWG2 gateway vector (pK7FWG2/ p35S::ANAC053::eGFP) (http://gateway.psb. ugent.be) by LR recombination (Invitrogen).

2.3. Plant transformation and identification of transgenic plants

A binary vector carrying the appropriate construct was introduced into Agrobacterium tumefaciens strain GV3101 by electroporation, and the Agrobacterium carrying the recombinant vector was infiltrated into Arabidopsis thaliana Col-0 by the floral dip method [7]). For overexpression and inducible overexpression transgenic plants, T3 generation progeny were screened to obtain homozygous lines by genetic analysis and their expression levels of the ANAC053 gene were determined by quantitative RT-PCR. Some representative transgenic lines of ANAC053 were used for further analyses.

2.4. Histochemical GUS staining

Transgenic plants of the full-length sequence of the ANAC053 promoter fused to the GUS gene were incubated with a X-GLUC staining solution [50 mM Na-phosphate buffer (pH 7.2), 10 mM EDTA, 3 mM K-Hexacyanoferrat (III), 0.1% Triton X-100, 0.1% Tween 20 and 0.5 mg/ ml 5-bromo-4-chloro-3-indolyl-β-glucuronic acid (Duchefa)] for overnight at 37°C. Samples were then washed with 70% ethanol for at least 4 hours to fix the tissues and to remove chlorophyll. Then cleared tissues were observed and imaged under the stereo microscopy (Olympus, Germany).

3. Results and Discussion

3.1. Subcellular localization of ANAC053

To determine the subcellular localization of ANAC053, its coding sequence (without stop codon) was fused to the green fluorescent protein (eGFP) gene at its N-terminus (Fig. 1a). Initial investigations of transgenic plants expressing the GFP fusion-protein indicated the presence of ANAC053 both, in the nucleus and the cytoplasm or roots (Fig. 1b). A similar pattern of localization was observed in leaves. Moreover, a recent publication of ANAC053::GFP in tobacco leaves revealed a similar distribution of the protein [8]. Interestingly, we did not observe any insertion of the ANAC053 protein into the plasma membrane, suggesting the C-terminal hydrophobic domain might not represent a true transmembrane domain.
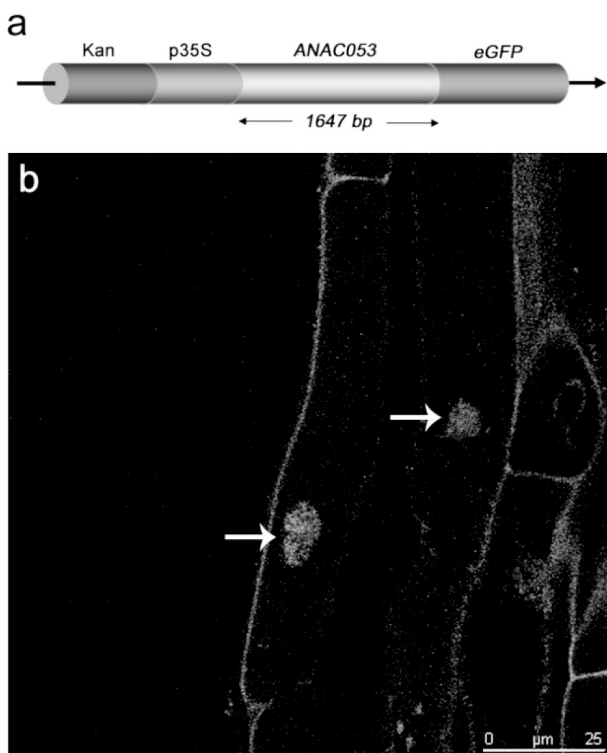

Fig. 1. **Subcellular localization of ANAC053**. (a) ANAC053-eGFP fusion construct. (b) GFP signal of ANAC053-GFP fusion-protein in the nucleus (arrows) and the cytosol of an *Arabidopsis* root.

3.2. Expression pattern of ANAC053

To determine the expression domain of ANAC053 in leaves, a histochemical analysis of the GUS activity in transgenic plants, containing a construct of the ANAC053 promoter (covering 1473 bp of the promoter and 228 bp of the 5'-UTR) fused to the GUS gene (Fig. 2e), was performed. GUS activity was first detected in the tip of the growing leaf which spread around the leaf margin in a mature leaf (Fig. 2a,b). In older leaves before visual onset of senescence ANAC053 started to be expressed in the whole lamina (Fig. 2c). In contrast to RPX, ANAC053 is not expressed in the vascular tissue indicating that the homologous NAC proteins act in different tissues of the leaf. The expression of ANAC053 is probably related to ageing of the leaf as also demonstrated by the reported pattern of ANAC053 in the eFP browser (Fig. 2d).
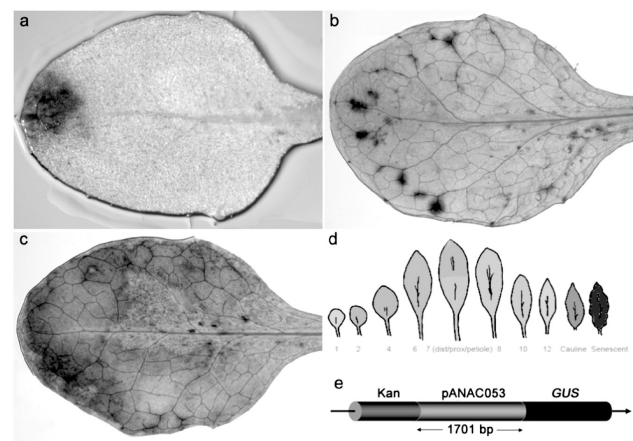
Fig. 2. **ANAC053 expression pattern**. (a) A young leaf with GUS signal at the tip. (b) GUS signal around the leaf margin. (c) GUS signal is spread from the leaf margin to the center of the leaf. (d) Expression pattern of the ANAC053 gene as presented in the eFP browser. (e) ANAC053 promoter::GUS fusion construct.

Conclusion: Using a *pANAC053::GUS* reporter we found that expression starts at the leaf tip, followed by expression in the leaf margin and later in the leaf center. ANAC053, a NAC-domain transcription factor, probably regulates leaf senescence.

References

[1] Guo, Y., Cai, Z., and Gan, S., (2004) Transcriptome of Arabidopsis leaf senescence. Plant Cell Environ, 2004.. 27: p. 521–549.

[2] Miao, Y., Smykowski, A., and Zentgraf, U., (2008) A novel upstream regulator of WRKY53 transcription during leaf senescence in Arabidopsis thaliana. Plant Biol, 2008. 1: p. 110-120.

[3] Uelker, B., Mukhtar, M.S., and Somssich, I.E., (2007) The WRKY70 transcription factor of Arabidopsis influences both the plant senescence and defense signaling pathways. Planta, 2007. 226: p. 125-137.

[4] Zhou, X., Jiang, Y., and Yu, D., (2011) WRKY22 transcription factor mediates dark-induced leaf senescence in Arabidopsis. Mol. Cells, 2011.. 31: p. 303-313.

[5] Kim, J.H., et al., Woo HR, Kim J, Lim PO, Lee IC, Choi SH, Hwang D, Nam HG (2009) Trifurcate feed-forward regulation of age-dependent cell death involving miR164 in Arabidopsis. Science,. 2009. 323: p. 1053-1057.

[6] Balazadeh, S., et al., Siddiqui H, Allu AD, Matallana-Ramirez LP, Caldana C, Mehrnia M, Zanor MI, Köhler B, Mueller-Roeber B (2010) A gene regulatory network controlled by the NAC transcription factor ANAC092/AtNAC2/ORE1 during salt-promoted senescence. . Plant,. 2010. 62: p. 250-264.

[7] Logemann, E., et al., Birkenbihl RP, Ülker B, Somssich IE (2006) An improved method for preparing Agrobacterium cells that simplifies the Arabidopsis transformation protocol. Plant Methods,. 2006. 2:16. doi:10.1186/1746-4811-2-16.

[8] Inzé, A., et al., Vanderauwera S, Hoeberichts FA, Vandorpe M, Gaever TV, Breusegem FV (2011) A subcellular localization compendium of hydrogen peroxide-induced proteins. Plant Cell Environ, 2011. doi: 10.1111/j.1365-3040.2011.02323.x.

Developing a simulated workplace neutron field by moderating Am-Be source

Phát triển trường chuẩn liều neutron mô phỏng thực tế bằng cách nhiệt hóa nguồn Am-Be

Thiem Ngoc Le[a], Quynh Ngoc Nguyen[a], Dang Thi My Linh[a], Hong Thi Bui[b], Hoai Nam Tran[c,*]
Lê Ngọc Thiệm, Nguyễn Ngọc Quỳnh, Đặng Thị Mỹ Linh, Bùi Thị Hồng, Trần Hoài Nam

[a]*Institute for Nuclear Science and Technology, VINATOM, 179 Hoang Quoc Viet, Hanoi, Vietnam*
Viện Khoa học và Kỹ thuật Hạt nhân, VINATOM, 179 Hoàng Quốc Việt, Hà Nội, Việt Nam
[b]*Faculty of Physics, VNU university of Science, 334 Nguyen Trai, Hanoi, Vietnam*
Khoa Vật lý, Đại học Khoa học Tự nhiên, 334 Nguyễn Trãi, Hà Nội, Việt Nam
[c]*Institute of Fundamental and Applied Sciences, Duy Tan University, Ho Chi Minh City, Vietnam*
Viện Nghiên cứu Khoa học Cơ bản và Ứng dụng, Đại học Duy Tân, Thành phố Hồ Chí Minh, Việt Nam

Abstract

This paper presents the development of a simulated workplace neutron field at the Institute for Nuclear Science and Technology (a branch of the Vietnam Atomic Energy Institute) by moderating the Am-Be source. Methylmethacrylate sphere with the diameter of 15 cm was used to moderate the Am-Be neutron source. Characterization of the simulated neutron field was then performed using a Bonner sphere spectrometer in combination with MAXED and FRUIT unfolding codes. The discrepancies of the field related quantities such as neuron fluence rates and the neutron ambient dose equivalent rate, $H^*(10)$, satisfy the standard uncertainty criteria as recommended by ISO 12789 series. Further development and characterization of the various simulated neutron fields are being conducted for supporting research and application activities.

Keywords: neutron fluence rate, Am-Be source, simulated workplace neutron field.

Tóm tắt

Bài báo mô tả việc nghiên cứu, phát triển trường chuẩn liều neutron mô phỏng thực tế bằng cách nhiệt hóa nguồn Am-Be tại Viện Khoa học và Kỹ thuật Hạt nhân, Viện Năng lượng Nguyên tử Việt Nam. Quả cầu Methylmethacrylate với đường kính 15 cm được sử dụng để nhiệt hóa nguồn Am-Be. Việc xác định đặc trưng trường chuẩn liều neutron này được thực hiện thông qua việc sử dụng kết hợp giữa hệ phổ kế cầu Bonner với các chương trình tách phổ MAXED và FRUIT. Sự sai khác giữa các kết quả liên quan đến trường chuẩn như thông lượng neutron trên toàn phổ, tương đương liều neutron môi trường, H*(10), thỏa mãn các điều kiện sai số chuẩn theo khuyến cáo của tiêu chuẩn ISO 12789. Việc nghiên cứu, phát triển các trường chuẩn liều neutron mô phỏng thực tế sẽ tiếp tục được thực hiện nhằm hỗ trợ các hoạt động nghiên cứu và ứng dụng liên quan.

Từ khóa: Suất thông lượng neutron, nguồn Am-Be, trường chuẩn mô phỏng.

Email: tranhoainam4@dtu.edu.vn

1. Introduction

In recent years, the increasing usage of radiation and neutron sources for researches and industrial applications demands neutron calibration fields for calibrating neutron measuring devices for the purpose of radiation protection. Recently, the Institute for Nuclear Science and Technology (INST), a sub-institute of the Vietnam Atomic Energy Institute, possesses the unique secondary standard dosimetry laboratory (SSDL) in Vietnam in ionizing radiation dosimetry and calibration which is a member in the IAEA/WHO SSDL network [1][2].

The total neutron spectrum of a neutron source measured by the devices consists of two components: a direct component of neutrons coming to the devices directly from the source and a scattered component coming to the devices after interactions with surrounding objects such as the air and concrete walls. Accurate measurement of radiation dose rate is of high importance for safety assessment and radiation worker protection. Although it is still a challenge to measure personal neutron dose equivalent, many attempts have been done to standardize neutron reference fields in dealing with source production, field characterization and calibration of neutron measuring devices. The spectra of common neutron sources such as ^{252}Cf and ^{241}Am–Be extend in the energy range of 10^{-7} MeV to 20 MeV [3][4]. However, the neutron spectra encountered in workplaces may extend in a wider energy range from 10^{-9} MeV to 20 MeV. Moreover, the neutron ambient dose equivalent rates, H*(10), measured by neutron dosemeters are significantly dependent on the incident neutron spectra. Thus, the calibration of neutron measuring devices to be used at workplaces with the ISO 8529 series reference neutron fields could be less meaningful [5][6][7]. Therefore, the simulated workplace neutron fields should be created in order to be able to calibrate neutron

dosemeters with neutron spectra similar to those appearing at real workplaces. Several simulated workplace neutron fields have been created successfully [8][9][10][11][12].

To verify the reliability of a neutron dosemeter operation in the determination of H*(10) at a workplace neutron field, two approaches are commonly used. The first one is to measure the workplace neutron spectrum, which is then accompanied with the response function of the neutron dosemeter to derive the meter's H*(10) value which is after that compared with the reference H*(10) value of the field. This approach is applicable once the intrinsic response function of the neutron dosemeter is available. The second approach is to create a simulated neutron field in the laboratory with the neutron spectra similar to that at the workplaces to calibrate the neutron measuring devices to be used in the equivalent workplaces [6][7].

In this paper, the development of a simulated workplace neutron field using the ^{241}Am-Be source moderated by a methylmethacrylate (PMMA) sphere is presented. Characterization of the simulated neutron field has been conducted using the Bonner sphere spectrometer in the combination with MAXED and FRUIT unfolding codes [13][14][15].

2. Calibration room, neutron source and instruments

The calibration room has the inner dimensions of 700 cm × 700 cm × 700 cm. An aluminum mid-floor, consisting of intermittent parallelepiped bars, with the thickness of about 0.2 cm is installed at the height of 230 cm from the floor base for the detector installation process. This aluminum mid-floor does not affect the scattering of neutron much due to its low neutron scattering cross section. In constructing the calibration room and manufacturing the experimental facilities, we followed the international standard guided in the PNNL-15870 Rev. 1 report of Pacific Northwest

National Laboratory [16]. The source is located at the center of the calibration room (120 cm higher than the aluminum mid-floor) so that the cylindrical symmetric axis is perpendicular to the floor. A radionuclide neutron ^{241}Am–Be source supplied by Hopewell Designs, Inc., USA was installed in a container at the center of the base floor. The initial source strength on January 23, 2015 is 1.299×10^7 s^{-1} with the expanded uncertainty of 2.9% (k = 2). When performing the calibration, the neutron source is pumped up to the center of the calibration room by a pneumatic system through a cylindrical aluminum pipe which has the wall thickness of 0.5 cm. Fig. 1 displays the neutron calibration room with the experimental arrangement.

The BSS system consists of a thermal neutron sensitive detector of ^{6}LiI(Eu) and a set of polyethylene moderator spheres with the diameters of 2, 3, 5, 8, 10, and 12 inches as shown in Fig. 2. The neutrons are detected by the ^{6}LiI(Eu) detector via the reaction 6Li(n,α)^{3}H (Q = 4.78 MeV). The configuration of the BSS system allows detecting neutrons from thermal energy up to 20 MeV and basically not sensitive to photons by applying a suitable discrimination level [2] [17]. In previous work, the characterization of the neutron field with the standard bare Am–Be source using the BSS system was described at the laboratory [2].

In this paper, the characterization of the simulated workplace neutron field in terms of total spectral neutron fluence rate and total neutron H*(10) was presented. More details of the characterization process can be found in the previous works [1][2].
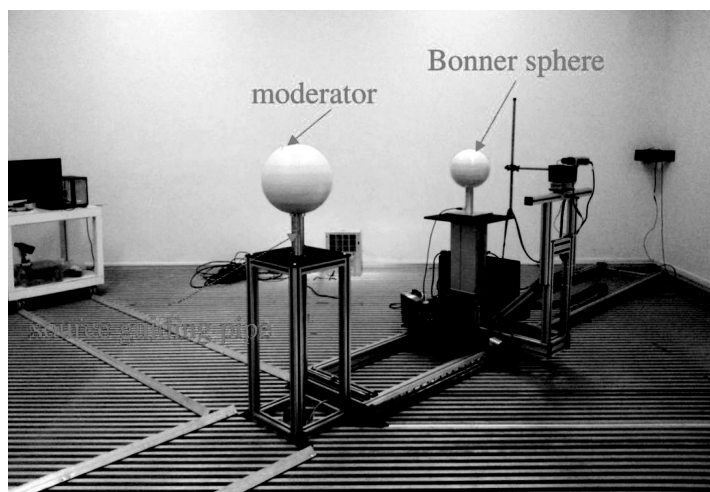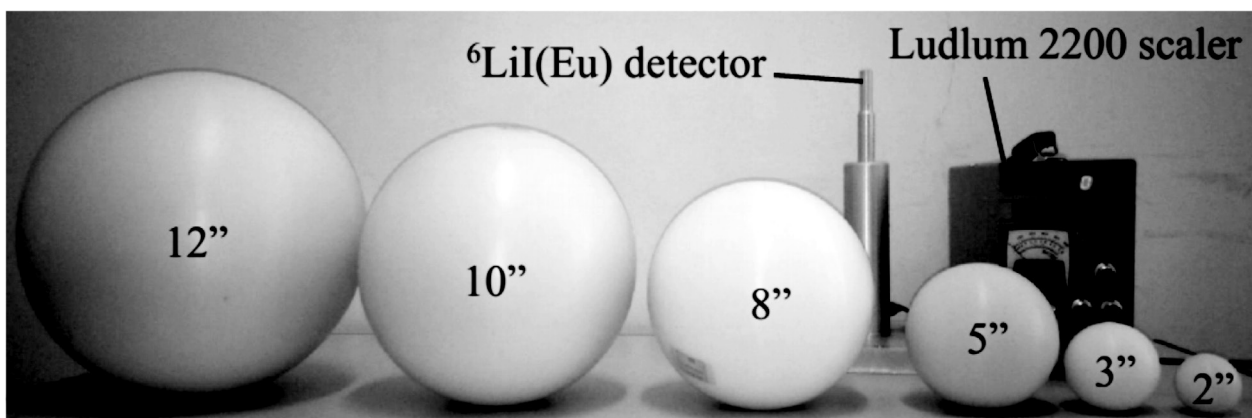

Fig. 1 Neutron calibration room

Fig. 2 Bonner sphere spectrometer system

3. Results and discussion

3.1 Neutron fluence rate spectra

Fig. 3 depicts the neutron fluence rate spectra due to the total fields moderated by the PMMA sphere as a function of the distances from the source. At low energy region, the thermal neutron peaks of the spectra appeared as the results of the thermalization process. At further distances, the high neutron energy peaks decreased rapidly due to the inverse square-distance law while the thermal neutron peaks are nearly constant caused by scattered component. Comparing the neutron fluence rate spectra obtained from the unfolding processes using MAXED and FRUIT codes, good agreements can be seen in Fig. 3. It is slightly different in the overall region of the spectra from thermal to fast energies. However, the integral neutron fluence rates and $H^*(10)$ of the total component, calculated from the neutron fluence rate spectra are expected to be in good agreements.

3.2 Neutron fluence rate and H*(10) rate

The integral neutron fluence rates were calculated based on the neutron fluence rate spectra obtained from the unfolding process. The values of integral neutron fluence rates at the distances of 80 cm and 100 cm are about 164 and 115 cm^{-2}.s^{-1}, respectively, with the use of the 15 cm-diameter PMMA moderated sphere. The neutron fluence rate at the distance of 250 cm decreases by factors of 4.04, 2.85 compared to that at 80 cm and 100 cm, respectively. This discrepancy obtained from the MAXED and FRUIT codes is less than 8%, which is satisfied with the ISO 12789-1 recommendation on the standard uncertainty of the integral neutron fluence rate [3].

Since neutron fluence dose equivalent rate, $H^*(10)$, is an important quantity to radiation safety assessment, the evaluation of $H^*(10)$ in the comparison between the two unfolding codes is necessary to qualify the field characterization. Fig. 4 depicts the total $H^*(10)$ rates as functions of the distances from the source calculated based on the neutron fluence rate spectra obtained from the two codes. The values of $H^*(10)$ are about 160 and 107 μSv/h at the distances of 80 and 100 cm from the source, respectively, with the 15 cm-diameter PMMA moderated sphere. Comparing the $H^*(10)$ rates obtained from the two codes, the discrepancy is less than 6%.

3.3 Fluence-to-dose equivalent conversion coefficients

Fig. 5 shows the values of fluence-to-dose equivalent conversion coefficients, h_Φ, obtained from the MAXED and FRUIT codes. One can see that the values of h_Φ vary in the range of 145-281 pSv.cm^2 obtained from MAXED code. The h_Φ decreases by a factor of 1.5 at the distance of 250 cm compared to that at 80 cm with the PMMA moderated sphere of 15 cm in diameter (result obtained from MAXED). Fig. 5 also depicts the ratio of h_Φ obtained from the MAXED and FRUIT codes, which varies in the range of 0.97-1.12. This means that the discrepancy of the conversion coefficients obtained from the two codes is about 12%. One can see the trend that the h_Φ values obtained from the MAXED code are greater than that obtained from the FRUIT code. The discrepancy, however, satisfies the ISO 12789-2 recommendation on the standard uncertainty of the conversion coefficient of 15% for the characterization using the BSS system [7].
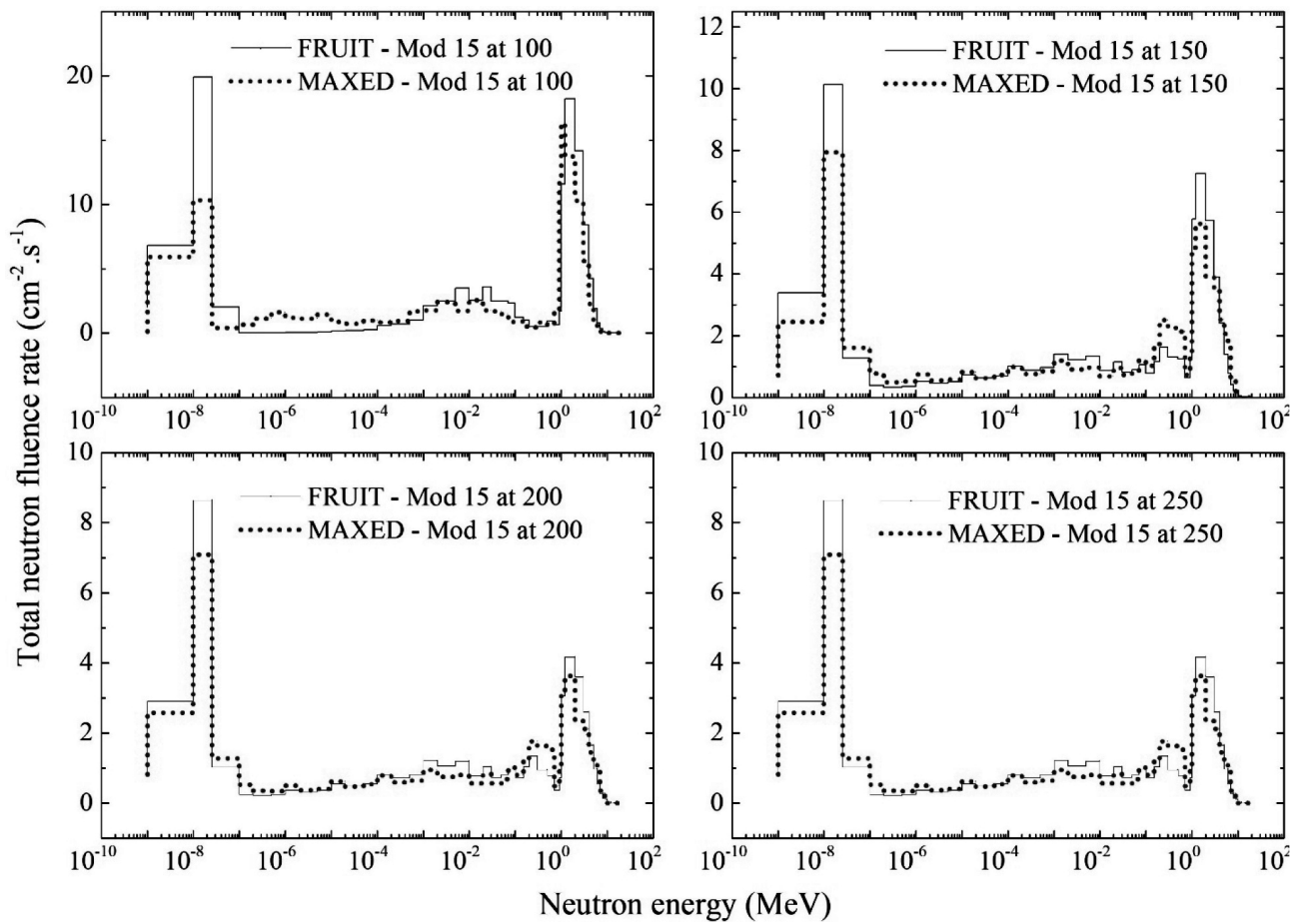
Fig. 3 Neutron fluence spectra at different distance from the moderated Am-Be source.
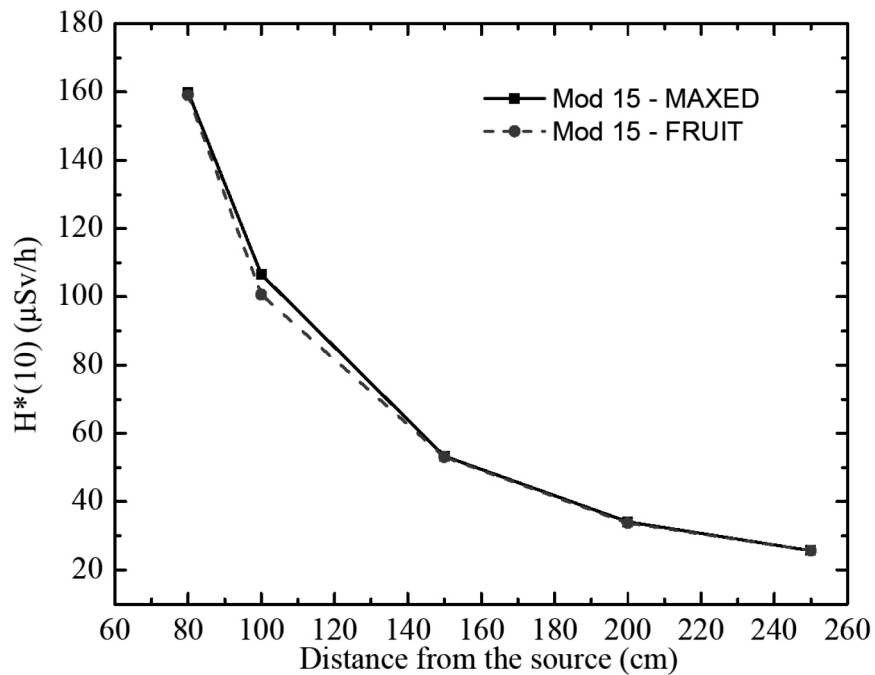

Fig. 4 Neutron fluence dose equivalent rate as a function of distance from the source.
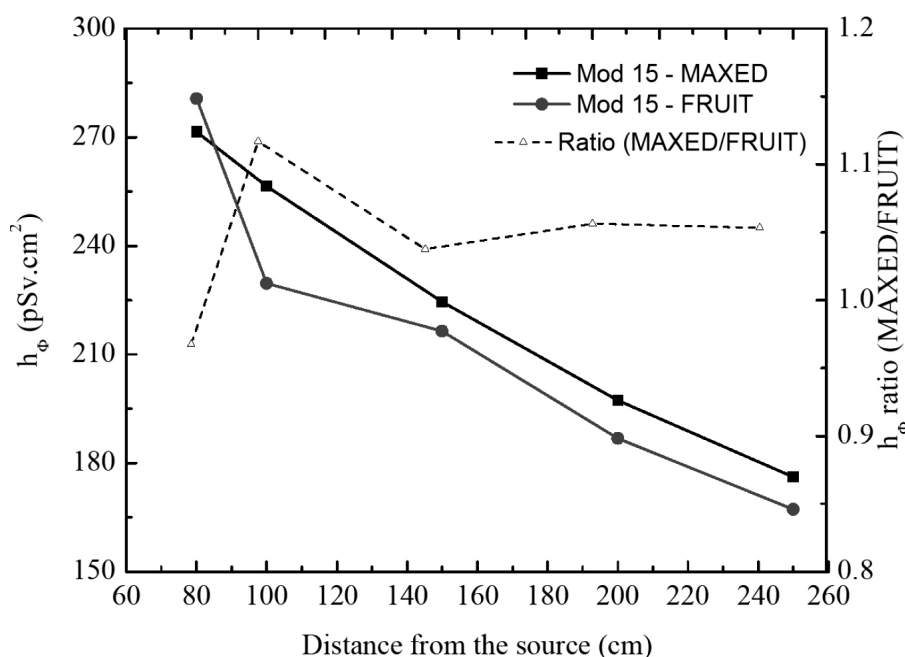
Fig. 5 Fluence-to-dose equivalent conversion coefficients

4. Conclusions

A simulated workplace neutron field of the Am-Be source moderated by the PMMA sphere has been developed and characterized using the BSS system in combination with MAXED and FRUIT unfolding codes. Neutron fluence rate spectra and the field related quantities were also calculated. The average neutron fluence-to-ambient dose equivalent conversion coefficients, h_Φ, is within 145-281 pSv.cm^2 in the distance range of 80 cm to 250 cm far from the source. Comparing the results obtained from the two codes, the discrepancies of the neutron fluence rates and the H*(10) are less than 8% and 6%, respectively. The value of h_Φ was obtained with the discrepancies of less than 12%. The discrepancies of the field related quantities satisfy the standard uncertainty criteria as recommended by ISO 12789 series.

Acknowledgements

References

[1] Le, T.N., Tran, H.N., Nguyen, K.T., Trinh, G.V., 2017. Neutron calibration field of a bare ^{252}Cf source in Vietnam. Nuclear Engineering and Technology **49**, 277-284.

[2] Le, T.N., Tran, H.N., Nguyen, Q.N., Trinh, G.V., Nguyen, K.T., 2018. Characterization of a neutron calibration field with 241Am-Be source using bonner sphere spectrometers. Applied Radiation and Isotopes **133**, 68-74.

[3] ISO 12789-1:2008(E), 2008. Reference radiation fields simulated workplace neutron fields Part 1: Characteristics and methods of production. Technical Report p.32. International Standard Organization.

[4] ISO 12789-2:2008(E), 2008. Reference radiation fields simulated workplace neutron fields Part 2: Calibration fundamentals related to the basic quantities. Technical Report p.32. International Standard Organization.

[5] ISO 8529-1:2001 (E), 2001. Reference Neutron Radiations Part 1: Characteristics and Methods of Production. Technical Report p.32. Switzerland.

[6] ISO 8529-2:2001 (E), 2000. Reference Neutron Radiations- Part 2: Calibration Fundamentals of Radiation Protection Devices Related to the Basic Quantities Characterizing the Radiation Field. Technical Report. Switzerland.

[7] ISO 8529-3:1998 (E), 1998. Reference Neutron Radiations Part 3: Calibration of Area and Personal Dosimeters and Determination of Their Response as a

Function of Neutron Energy and Angle of Incidence. Technical Report p.32. Switzerland.

[8] Chartier, J., Jansky, B., Kluge, H., Schraube, H., Wiegel, B., 1997. Recent developments in the specification and achievement of realistic neutron calibration fields. Radiation Protection Dosimetry **70**, 305-312.

[9] Lacoste, V., 2010. Review of radiation sources, calibration facilities and simulated workplace fields. Radiation Measurements **45**, 1083-1089.

[10] Rottger, S., Schler, K., Nolte, R., 2010. A new simulated neutron workplace field at PIAF. Radiation Measurements **45**, 1154-1158.

[11] Saegusa, J., Tanimura, Y., Yoshizawa, M., Yoshida, M., 2004. Conceptual design of spectrum changeable neutron calibration fields in JAERI/FRS. Radiation Protection Dosimetry **110**, 91-95.

[12] Taylor, G., Thomas, D., Bennett, A., 2007. Results of field trials using the npl simulated reactor neutron field facility. Radiation Protection Dosimetry **126**, 89-92.

[13] Reginatto, M., 2004. The "few-channel" unfolding programs in the UMG package: MXD FC33, GRV FC33 and IQU FC33. Technical Report. Physikalisch-Technische Bundesanstalt (PTB), version 3.3, p. 51.

[14] Reginatto, M., Goldhagen, P., 1998. MAXED, A computer code for the deconvolution of multisphere neutron spectrometer data using the maximum entropy method. Technical Report. Environmental Measurements Laboratory, US-DOE Report EML 595, p. 40.

[15] Bedogni, R., Domingo, C., Esposito, A., Fernndez, F., 2007. Fruit: An operational tool for multisphere neutron spectrometry in workplaces. Nuclear Instruments and Methods in Physics Research Section A: Accelerators, Spectrometers, Detectors and Associated Equipment **580**, 1301-1309.

[16] J. McConn Jr., C.J. Gesh, R.T. Pagh, R.A. Rucker, R.G. Williams III, Compendium of Material Composition Data for Radiation Transport Modeling, PNNL-15870 Rev. 1, Pacific North West National Laboratory, Washington, 2011, p. 375.

[17] Knoll, G.F., 2010. Radiation detection and measurement. 4th edition ed., Wiley.

Calculation of HPGe detector efficiencies for extended sources: Monte Carlo method

Tính hiệu suất của đầu dò siêu tinh khiết HPGe cho các nguồn thể tích bằng phương pháp Monte Carlo

Sy Minh Tuan Hoang[a,*], Thi Hong Bui[b]

Hoàng Sỹ Minh Tuấn, Bùi Thị Hồng

[a]*Institute of Fundamental and Applied Sciences, Duy Tan University, Ho Chi Minh City, Vietnam*
Viện Nghiên cứu Khoa học Cơ bản và Ứng dụng, Đại học Duy Tân, Thành phố Hồ Chí Minh, Việt Nam
[b]*Faculty of Physics, VNU University of Science, 334 Nguyen Trai, Hanoi, Vietnam*
Khoa Vật lý, Trường Đại học Khoa học Tự nhiên, 334 Nguyễn Trãi, Hà Nội, Việt Nam

Abstract

Gamma spectrometry utilizing a HPGe detector is widely used for the analysis of low concentrations of radionuclides in samples. The accurate efficiencies are always required to determine the activity of radioactive sources. However, the information provided by manufacturers for detector models is insufficient to calculate the efficiencies, value and leads to strong discrepancies between simulated and experimental efficiencies, especially for low photon energies. For this purpose, the detailed model was developed to calculate the total and full energy peak efficiency of a p-type coaxial HPGe detector using GEANT4 toolkit. In the simulation, aqueous gamma sources containing several radionuclides were used, covering the energy range from 59.50 to 1836.01 keV. In the case of extended sources, the coincidence summing correction factors for ^{60}Co and ^{88}Y were calculated from the total efficiencies obtained by GEANT4. Based on the modified model of the detector including the summing effect, the simulated efficiencies of full energy peak agreed with the experimental values within 3%, except for the high energy range which is less than 4 %, between 122 and 1836 keV for the small extended sample.

Keywords: GEANT4, HPGe, Full energy peak efficiency, Coincidence summing, Cylindrical sources.

Tóm tắt

Hệ phổ kế gamma sử dụng đầu dò siêu tinh khiết HPGe đã được ứng dụng rộng rãi trong phân tích các mẫu phóng xạ hoạt độ thấp. Đường chuẩn hiệu suất luôn đòi hỏi sự chính xác trong việc xác định hoạt độ. Tuy nhiên, những thông tin về đầu dò được cung cấp bởi nhà sản xuất dùng cho việc mô phỏng để tính hiệu suất là không đầy đủ, dẫn tới sự sai khác lớn giữa kết quả hiệu suất thu được từ tính toán và thực nghiệm. Mô hình chi tiết về đầu dò siêu tinh khiết cho việc tính toán hiệu suất đỉnh năng lượng toàn phần sử dụng chương trình GEANT4 đã được phát triển trong nghiên cứu này. Nguồn dung dịch chuẩn dùng trong mô phỏng có dải năng lượng từ 59,50 tới 1836,01 keV. Đối với các nguồn thể tích, hệ số hiệu chỉnh tổng trùng phùng cho ^{60}Co và ^{88}Y được tính dựa trên hiệu suất tổng thu được bằng mô phỏng GEANT4. Với việc tinh chỉnh lại mô hình bao gồm cả hiệu ứng tổng trùng phùng, sai khác giữa hiệu suất tính toán của đỉnh năng lượng toàn phần và thực nghiệm trong khoảng 3%, riêng đối với khoảng năng lượng từ 122 đến 1836 keV là 4% cho nguồn thể tích nhỏ.

Từ khóa: GEANT4, đầu dò HPGe, hiệu suất đỉnh năng lượng toàn phần, hiệu ứng tổng trùng phùng, nguồn trụ.

Email: hsmtuan@gmail.com

1. Introduction

High-resolution gamma-ray spectroscopy with a High Purity Germanium (HPGe) detector is often utilized for the non-destructive assay of radioactive materials. It has many applications, which include food testing, neutron activation analysis [1, 2], fundamental physics research [3, 4] and environmental analysis [5, 6]. To determine the activity of each radionuclide, it is necessary to calculate the full energy peak efficiency (ε_{cal}) at the energy of γ-ray emissions for a given measuring geometry. It is difficult to achieve the accurate efficiency of HPGe detectors due to the two major factors, the intrinsic characteristics of the detector (geometry, active volume, dead layer, and end cap thicknesses) and extended source dimension. Besides, in many cases, the efficiency calibration curve would require a large amount of counting time and sample preparation. Some theoretical approaches required approximations and simplifications in source-detector geometric calculations. For these reasons, Monte Carlo (MC) methods were adopted. The importance of such MC methods is that they enable one to quickly calculate a new efficiency value for changes in the measured conditions. Several studies in the response of the HPGe detector efficiency curve with MC methods were published. Most of the studies obtained agreement between simulated and experimental efficiency curves with discrepancy equal to 10% [7-9], and in recent years some studies used optimized detector parameters in simulation and obtained good agreement with experimental results to about less than 3% [10-13], except for the low energy range.

The major problem in the calibration of the simulation efficiency curve is the lack of accurate data regarding the details of the detector geometry which are usually not well known [14-16]. To achieve good accuracy in the simulated result, an accurate detector model should be developed. In addition, when the source is positioned close to the detector, a coincidence summing effect arises in those nuclides which emit cascade γ-rays. Many authors observed some strong deviation from experimental results without including the effect of coincidence summing in the simulation [17, 18]. For correction of such effect, the total efficiency (ε_{Tcal}) is also required with the full energy peak efficiency. Debertin and Schotzig [19] used the ratio of the total number of pulses recorded to the number of photons emitted by the source (total efficiency) and calculated coincidence summing correction factor (SCF) in measurements. Abbas and Nafee [20, 21] used the analytical approach to calculate SCF with total efficiency. Most of the authors used total efficiencies in the simulation for the calculation of SCF [22-25]. In the case of a point source or small extended sample, the variation of the efficiency over the sample volume can be neglected for the calculation of SCF [26].

A sensitivity analysis of the active volume of detector, effective thicknesses of a dead layer and end cap was performed by varying the value of each parameter in the detector model. Low energy γ-rays are more sensitive to errors in these detectors' parameters. However, photons in this energy range are very interested in environmental studies. In this study, GEANT4 electromagnetic standard physics (G4EMStandardPhysics) class was used and developed a detector model to simulate the full energy peak and total efficiencies of a p-type coaxial HPGe detector. The simplest and modest method was used in the GEANT4 toolkit to calculate the coincidence summing correction factor (SCF$_{cal}$) with the above-mentioned approach. After the adjustment of the active volume, the thicknesses of germanium dead layer and end-cap in the simulated model of detector including the summing effect, a minimum average discrepancy was obtained with the experimental results reported by Abbas et al. [27] for the small extended sample.

2. Monte Carlo Simulation

The simulations have been carried out using the GEANT4 Monte Carlo toolkit developed at CERN (version 10.5). The GEANT4 toolkit includes simulation of the electromagnetic interaction of charged particle, gamma, and optical photons. The code follows the history of each primary photon until its energy dissipated in the detector and produces secondary particles as a result of photoelectric and Compton effects, pair production, multiple scattering, bremsstrahlung, and ionization. The secondary electrons formed by photon interaction processes were also taken into consideration in the simulation. G4EMStandardPhysics class was applied for low-level γ-ray spectrometry in this simulation since the energy limit of the electromagnetic process is 10 keV to 100 TeV. Therefore, Ge X-rays of energy below 10 keV cannot be processed. GEANT4 also includes low-level electromagnetic processes that can simulate a particle down to 250 eV. The number of total histories (10^8 primary photons) was considered for the simulation to obtain a statistical uncertainty of no more than 0.1%.

Only the γ-rays, which deposit their full energy in the active volume of the detector, were considered in the evaluation of full energy peak efficiency. The simulations of full energy peak efficiencies are obtained from Eq. 1:

$$\varepsilon_{cal} = \frac{C}{N} \tag{1}$$

Where, ε_{cal} is the full energy peak efficiency. C is the number of counts that deposit their full energy in the active detector volume. N is the number of total simulated γ-rays counts for a given energy, E.

The calculated coincidence summing correction factors are defined as Eq. 2:

$$SCF_{cal}^a = \frac{1}{1 - \varepsilon_{Tcal}^b}$$
$$\tag{2}$$
$$SCF_{cal}^b = \frac{1}{1 - \frac{\gamma_1}{\gamma_2} \varepsilon_{Tcal}^a}$$

Where, SCF_{cal}^a and SCF_{cal}^b are the calculated coincidence summing correction factors. ε_{Tcal}^a and ε_{Tcal}^b are the simulated total efficiencies of 1173 and 1332 keV, respectively. It is similarly applied for [88]Y.

The true simulated full energy peak efficiency is obtained from Eq. 3:

$$\varepsilon_{cal}^* = \frac{C}{N} SCF_{cal} \tag{3}$$

The detector considered for GEANT4 simulation was a p-type coaxial HPGe detector (Canberra) with a crystal length of 89.7 mm and radius of 34.95 mm. There is no information about the diameter and length of the cavity as well as the thickness of the germanium dead layer. The active volume was also unknown. The detector has an aluminum end-cap window of 1 mm in nominal thickness, placed at a distance of 4 mm from the crystal. No information was available by the manufacturer about whether the Ge crystals had rounded edges. Sharp edges of the crystals were assumed in the simulation. A cylindrical beaker source of radius (34.8 mm) filled with gamma radionuclides aqueous solution of 10 ml in volume was used to obtain the ε_{cal} values. The multi-source used for measurements was a calibration gamma mixed solution, which contains [241]Am, [109]Ce, [85]Sr, [57]Co, ^{60}Co, [109]Cd, [88]Y, [203]Hg, [113]Sn and ^{137}Cs, covering a wide energy range from 50 keV to 2 MeV. The cylindrical beaker source was placed in contact with the detector end-cap window. The coincidence summing effect on ε_{cal} calibration was considered when simulations were performed. The coincidence correction factors of radionuclides ^{60}Co and [88]Y were taken into account in experimental full energy peak efficiency (ε_{exp}) result. A commercial program, GENIE 2000, has been used to acquire and analyze spectra for each measurement.

3. Results and Discussion

First simulation analysis was performed to evaluate the influence of the active volume on the detector efficiency with 10 ml source volume. Five

values as 79171.33, 52369.54, 31082.86, 18960.18, and 5873.68 mm³ of different active volume were considered for this simulation with the length and diameter of detector provided by the manufacturer. The dead layer and end-cap materials were not included first. Table 1 shows that each detective active volume of the simulated efficiency (ε_{cal}) is strongly dependent on high energy range. When the active volume was decreased, ε_{cal} decreased for all energies except for the low energy range (59 to 122 keV), the efficiency remained the same. In addition, for the energy range (165 and 279 keV) ε_{cal} slightly decreased when the active volume was reduced. However, it reduced more strongly at high photon energy range. A good agreement with experimental efficiency (ε_{exp}) value can be expected when reducing the active volume of the detector. The reduction of the active volume has a greater influence on the high energies of photon. For the energy range (898 to 1836 keV), the best agreement with the ε_{exp} value was achieved for

the active volume of (18960.18 mm3), but ε_{cal} value significantly decreases with the reducing of active volume.

The dead layer in germanium crystals is not useful for the detection of the counting rate, but strongly depends on the efficiency of the detector. From the reduction of the active volume, only the high energy photon efficiency agreed well with the experimental one, but large discrepancies were obtained at low energy range. The thickness of the dead layer has a large influence on the detector efficiency, especially for low energy range, where the photons with low energies are increasingly absorbed. For this purpose, the simulation was performed to observe the influence of the germanium dead layer on efficiency values and adjust the thickness of the dead layer to obtain the correct ε_{cal} values. Different dead layers were modeled by varying the thickness of the dead layer while maintaining the active volume value of 18960.18 mm³.

Table 1. Full energy peak efficiency values for different Ge active volumes

Energy (keV)	ε_{exp}	ε_{cal}				
		Active volume (mm³)				
		79171.33	52369.54	31082.86	18960.18	5873.68
59.5	0.03627	0.4155	0.4155	0.4155	0.4155	0.41552
88.02	0.1088	0.2051	0.2051	0.2051	0.20504	0.20454
122.06	0.11573	0.18643	0.18643	0.18638	0.18606	0.18508
165.85	0.11307	0.16048	0.16039	0.16019	0.1598	0.15772
279.19	0.0896	0.1066	0.10616	0.10531	0.10376	0.09945
391.69	0.0672	0.08232	0.08195	0.08053	0.07926	0.0726
513.99	0.05547	0.0665	0.06589	0.06401	0.06288	0.05569
661.66	0.04373	0.05367	0.05331	0.05271	0.05134	0.04495
898.02	0.03413	0.04791	0.04757	0.04673	0.03453	0.02351
1173.24	0.0266	0.0367	0.03664	0.035	0.0266	0.01823
1332.5	0.02453	0.03315	0.03272	0.03172	0.02461	0.0146
1836.01	0.0208	0.02635	0.02609	0.02428	0.02075	0.01431

Five values (0.5, 0.6, 0.7, 0.75, and 0.8 mm) of the thickness of the dead layer considered for the small extended source volume are shown in Table 2. First, the efficiency value for the low photon energy ranging from 59 to 661 keV was evaluated;

a good agreement with the experimental result was obtained for the dead layer thickness of 0.75 mm. Although at this value, the ε_{cal} values did not agree with the experimental one for the energy range (898 to 1836 keV). However, for the dead

layer thickness of 0.6 mm, the ε_{cal} values were much closer to the experimental one. Therefore, only the dead layer thickness of value 0.6 mm was considered for further simulation.

Additional analysis was performed on aluminum end cap thickness. For high energy range, a good agreement with the experimental efficiency was obtained using the combination of the active volume of 18960.18 mm³ and germanium dead layer thickness of 0.6 mm. In terms of low energy range, the ε_{cal} values deviated from the experimental results. Regarding the effect of aluminum material surrounding the detector, there is a probability of the attenuation of low energy photon in this region. In our model, the radiation enters only through the upper face of the crystal and therefore, the sidewall thickness has no influence on ε_{cal} value. To simulate this effect, the detector was modeled with five end cap thicknesses (0.2, 0.3, 0.4, 0.5, and 0.6 mm), but for a single dead layer thickness value (0.6 mm) and active volume (18960.18 mm³). As shown in Table 3, at low photon energy, the best agreement between simulation and experiment was an optimized end cap thickness of 0.5 mm.

Table 2. Full energy peak efficiency values for different Ge dead layer thicknesses

Energy (keV)	ε_{exp}	ε_{cal}				
		Dead layer thickness (mm)				
		0.5	0.6	0.7	0.75	0.8
59.5	0.03627	0.05215	0.0395	0.03806	0.03671	0.0309
88.02	0.1088	0.1391	0.13067	0.12522	0.1082	0.09751
122.06	0.11573	0.14413	0.13728	0.13029	0.12097	0.10831
165.85	0.11307	0.13633	0.13192	0.12824	0.12076	0.10704
279.19	0.0896	0.09616	0.09468	0.09303	0.09012	0.08893
391.69	0.0672	0.07479	0.07317	0.07235	0.06802	0.06124
513.99	0.05547	0.06039	0.06003	0.05908	0.05601	0.05417
661.66	0.04373	0.04954	0.04808	0.04663	0.04498	0.04296
898.02	0.03413	0.0325	0.03203	0.0315	0.0312	0.03086
1173.24	0.0266	0.02496	0.02467	0.02426	0.02381	0.02332
1332.5	0.02453	0.02291	0.0225	0.02224	0.0218	0.02154
1836.01	0.0208	0.0192	0.01892	0.01876	0.01849	0.01817

Table 3. Comparison of experimental and simulated full energy peak efficiency values for different aluminum end cap thicknesses

Energy (keV)	ε_{exp}	ε_{cal}				
		End-cap thickness (mm)				
		0.2	0.3	0.4	0.5	0.6
59.5	0.03627	0.03851	0.03794	0.03693	0.03634	0.03547
88.02	0.1088	0.11395	0.11216	0.11005	0.10956	0.10546
122.06	0.11573	0.13404	0.13333	0.13239	0.118	0.11751
165.85	0.11307	0.12898	0.12424	0.1206	0.115	0.11488
279.19	0.0896	0.09297	0.09219	0.09117	0.0899	0.0891
391.69	0.0672	0.07224	0.07098	0.06917	0.0678	0.06627
513.99	0.05547	0.05872	0.05854	0.05784	0.0557	0.05513
661.66	0.04373	0.04785	0.0473	0.04698	0.0443	0.04357

898.02	0.03413	0.03198	0.03165	0.03121	0.0308	0.03002
1173.24	0.0266	0.02465	0.02431	0.02407	0.0238	0.02306
1332.5	0.02453	0.02251	0.02239	0.02221	0.0219	0.02158
1836.01	0.0208	0.01899	0.01881	0.01877	0.01857	0.018

For the energy range from 59 to 661 keV, a good agreement was achieved with a modified detector model. However, for the high energy range from 898 to 1836 keV, minimum discrepancies were obtained due to the non-inclusion of SCF in ε_{cal} values. In the case of extended sources, the ε_{Tcal} needs to be taken into account to find SCF_{cal} for ^{60}Co and ^{88}Y. Table 4 shows the ε_{Tcal} values obtained by GEANT4 for the small extended sample.

Table 4. Simulated full energy peak and total efficiencies for the small extended sample

Energy (keV)	ε_{cal}	ε_{Tcal}
59.5	0.03634	0.03911
88.02	0.10956	0.11337
122.06	0.118	0.16226
165.85	0.115	0.15926
279.19	0.0899	0.15748
391.69	0.0678	0.14768
513.99	0.0557	0.14216
661.66	0.0443	0.13556
898.02	0.0308	0.13086
1173.24	0.0238	0.1218
1332.5	0.0219	0.12072
1836.01	0.01857	0.11247

The ε_{Tcal} values obtained by our simulation approach are simple and precise to be used to calculate the SCF. The values of the γ-ray emission probability (P) and the correction factor for 60 88 Co and Y are shown in Table 5 and 6. The SCF_{cal} is independent of the detector count rate, but it is strongly dependent on the full energy peak and total efficiency. By comparison,

there is an inverse relationship between ε_{Tcal} and SCF_{cal} values for nuclides ^{60}Co and ^{88}Y.

Table 5. Multi gamma ray nuclides with emission probability.

Radionuclides	Energy (keV)	P (%)
^{60}Co	1173.24	99.90
	1332.50	99.98
^{88}Y	898.00	93.70
	1836.01	99.35

Table 6. Calculated coincidence summing correction factors for ^{60}Co and ^{88}Y

Radionuclides	Energy (keV)	SCF_{cal}
^{60}Co	1173.24	1.137
	1332.50	1.138
^{88}Y	898.00	1.126
	1836.01	1.140

The true full energy peak efficiency (ε_{cal}^{*}) values were obtained by applying the SCF_{cal} in the simulation for nuclides ^{60}Co and ^{88}Y. Table 7 shows a good agreement with the experimental results, with discrepancies less than 3 % for the small extended sample.

Figure 1 shows the comparison between the ε_{cal} curves with the modified model of detector, including SCF_{cal} and the experimental ones for all energy peaks included in the calibration. The average relative deviation between the simulated and the experimental efficiency values is less than 3 % for the entire energy range. The modified detector model and its parameters are shown in Fig. 2.

Table 7. Comparison of experimental and simulated full energy peak efficiency values with SCF

Radionuclides	Energy (keV)	ε_{exp}	ε_{cal}	ε_{cal}^{*}
^{60}Co	1173.24	0.02660	0.02380	0.02700
	1332.50	0.02453	0.02190	0.02492

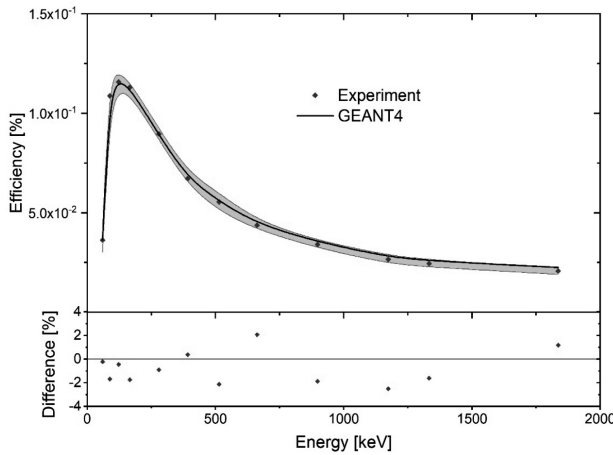|				
^{88}Y	898.00	0.03413	0.03080	0.03468
	1836.01	0.02080	0.01850	0.02109

Fig. 1. Comparison of experimental and simulated (with modified detector model including the CSFcal) full energy peak efficiency curve.
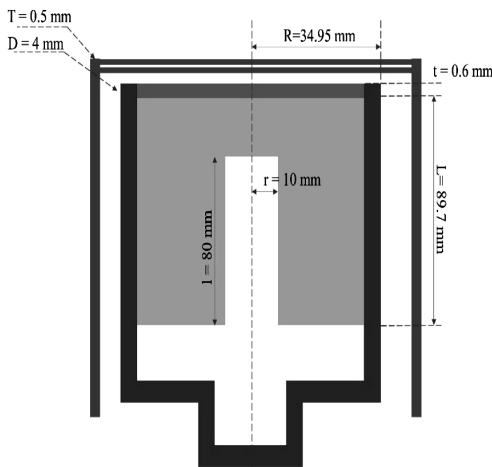

Fig. 2 Schematic of the detector. Modified detector parameters are cavity length (l), cavity radius (r), dead layer thickness (t), and end cap thickness (T).

4. Conclusions

In order to determine the active volume, dead layer, and end cap thicknesses, GEANT4 toolkit-based simulation was performed to simulate the collaboration of the coaxial HPGe detector efficiencies for the small extended sample. An accurate simulated detector model was developed to obtain minimum discrepancies with experimental results. For the high energy photon, the non-inclusion of coincidence summing correction factors produces some discrepancies in full energy peak efficiency results. A new method was used in GEANT4 to calculate the coincidence summing correction factors from total efficiencies and obtained accurate simulated results; the average discrepancies between the experimental and simulated efficiencies were found at 3 %. The proposed simulated method avoids the preparation of a great variety of radioactive samples with several isotopes and has advantages of saving time, assets and effort.

Acknowledgements

References

[1] Mauerhofer, E., U. Tharun, H. O. Denschlag, R. Schmidt, and J. V. Kratz. A Compton suppression spectrometer for neutron activation analysis. Nucl. Instr. Meth. Phys. Res. A., 371, no. 3 (1996): 465-471. DOI: https://doi.org/10.1016/0168-9002(95)01009-2

[2] Landsberger, S., S. R. Biegalski, D. J. O'kelly, and M. S. Basunia. Use of coincident and non-coincident gamma-rays in Compton suppression neutron activation analysis. J. Radioanal. Nucl. Chem. 263, no. 3 (2005): 817-821.

[3] Alharbi, T., P. H. Regan, P. J. R. Mason, N. Mărginean, Zs Podolyák, A. M. Bruce, E. C. Simpson et al. "Electromagnetic transition rates in the N= 80 nucleus 58 138 Ce." Phys. Rev. C 87, no. 1 (2013): 014323. DOI: https://doi.org/10.1103/PhysRevC.87.014323

[4] Mason, P. J. R., Zs Podolyák, N. Mărginean, P. H. Regan, P. D. Stevenson, V. Werner, T. Alexander et al. "Half-life of the yrast 2+ state in 188 W: Evolution of deformation and collectivity in neutron-rich tungsten isotopes." Phys. Rev. C 88, no. 4 (2013): 044301. DOI: https://doi.org/10.1103/PhysRevC.88.044301

[5] Kapsimalis, R., S. Landsberger, and N. Reguigui. "Measurement of uranium in small quantities in phosphates by use of γ-ray spectrometry and the 1001 keV peak of 234mPa." J. Radioanal. Nucl. Chem. 280, no. 2 (2009): 293-298.

[6] Habib, A. S., A. L. Shutt, P. H. Regan, M. C. Matthews, H. Alsulaiti, and D. A. Bradley. "Characterization of naturally occurring radioactive materials in Libyan oil pipe scale using a germanium detector

and Monte Carlo simulation." Radiat. Phys. Chem. 95 (2014): 352-355. DOI: https://doi.org/10.1016/j.radphyschem.2013.01.028

[7] J. Boson, G. Ågren, L. Johansson, A detailed investigation of HPGe detector response for improved Monte Carlo efficiency calculations, Nucl. Instr. Meth. Phys. Res. A., 587 (2008) 304-314. DOI: https://DOI. 10.1016/j.nima.2008.01.062.

[8] S. Hurtado, M. Garcıa-León, R. Garcıa-Tenorio, GEANT4 code for simulation of a germanium gamma-ray detector and its application to efficiency calibration, Nucl. Instr. Meth. Phys. Res. A., 518 (2004) 764-774. DOI: https://doi.org/10.1016/j.nima.2003.09.057.

[9] R. Helmer, N. Nica, J. Hardy et al, Precise efficiency calibration of an HPGe detector up to 3.5 MeV, with measurements and Monte Carlo calculations, Appl. Radiat. Isot., 60 (2004) 173-177. DOI: https://DOI. 10.1016/j.apradiso.2003.11.012.

[10] W. Khan, Q. Zhang, C. He et al., Monte Carlo simulation of the full energy peak efficiency of an HPGe detector, Appl. Radiat. Isot., 131 (2018) 67-70. DOI: https://doi.org/10.1016/j.apradiso.2017.11.018.

[11] D.M.M. Olivares, M.M. Guevara, F.G. Velasco, Determination of the HPGe detector efficiency in measurements of radioactivity in extended environmental samples, Appl. Radiat. Isot., 130 (2017) 34-42. DOI: https://DOI. 10.1016/j.apradiso.2017.09.017.

[12] M. García-Talavera, H. Neder, M. Daza et al., Towards a proper modeling of detector and source characteristics in Monte Carlo simulations, Appl. Radiat. Isot., 52 (2000) 777-783. DOI: https://doi.org/10.1016/S0969-8043(99)00244-4.

[13] A. Elanique, O. Marzocchi, D. Leone et al., Dead layer thickness characterization of an HPGe detector by measurements and Monte Carlo simulations, Appl. Radiat. Isot., 70 (2012) 538-542. DOI: https://doi.org/10.1016/j.apradiso.2011.11.014.

[14] J. Rodenas, A. Pascual, I. Zarza et al., Analysis of the influence of germanium dead layer on detector calibration simulation for environmental radioactive samples using the Monte Carlo method, Nucl. Instr. Meth. Phys. Res. A., 496 (2003) 390-399. DOI: https://doi.org/10.1016/S0168-9002(02)01748-5.

[15] D. Budjáš, M. Heisel, W. Maneschg et al., Optimisation of the MC-model of a p-type Gespectrometer for the purpose of efficiency determination, Appl. Radiat. Isot., 67 (2009) 706-710. DOI: https://doi.org/10.1016/j.apradiso.2009.01.015.

[16] A. Maurotto, S. Rizzo, E. Tomarchio, MCNP5 modelling of HPGe detectors for efficiency evaluation in γ-ray spectrometry, RADIAT EFF DEFECT S.164 (2009) 302-306. DOI: https://doi.

org/10.1080/10420150902809189.

[17] C. Conti, I. Salinas, H. Zylberberg, A detailed procedure to simulate an HPGe detector with MCNP5, Prog. Nucl. Energy., 66 (2013) 35-40. DOI: https://doi.org/10.1016/j.pnucene.2013.03.003.

[18] K. Debertin, U. Schötzig, Coincidence summing corrections in Ge (Li)-spectrometry at low source-to-detector distances, Nucl. Instr. Meth. Phys. Res., 158 (1979) 471-477. DOI: https://doi.org/10.1016/S0029-554X(79)94845-6.

[19] M.I. Abbas, HPGe detector photopeak efficiency calculation including self-absorption and coincidence corrections for Marinelli beaker sources using compact analytical expressions, Appl. Radiat. Isot., 54 (2001) 761-768. DOI: https://doi.org/10.1016/S0969-8043(00)00308-0.

[20] S.S. Nafee, M.S. Badawi, A.H. Ahmed, New numerical algorithm method to calibrate the HPGe cylindrical detectors using non-axial extended source geometries, Appl. Radiat. Isot., 68 (2010) 1809-1815. DOI: https://DOI. 10.1016/j.apradiso.2010.03.016.

[21] A.M. Ababneh, M.M. Eyadeh, Coincidence summing corrections in HPGe gamma-ray spectrometry for Marinelli-beakers geometry using peak to total (P/T) calibration, J Radiat Res Appl Sci.8. 8 (2015) 323-327. DOI: http://doi:org/10.1016/j.jrras.2015.05.003.

[22] Z. Wang, B. Kahn, J.D. Valentine, Efficiency calculation and coincidence summing correction for germanium detectors by Monte Carlo simulation, IEEE Trans. Nucl. Sci., 49 (2002) 1925-1931. DOI: https:// DOI. 10.1109/TNS.2002.801679.

[23] T. Vidmar, A. Likar, Calculation of total efficiencies of extended samples for HPGe detectors, Nucl. Instr. Meth. Phys. Res. A., 555 (2005) 251-254. DOI: https://doi.org/10.1016/j.nima.2005.08.101.

[24] T. Vidmar, M. Korun, B. Vodenik, A method for calculation of true coincidence summing correction factors for extended sources, Appl. Radiat. Isot., 65 (2007) 243-246. https://doi.org/10.1016/j.apradiso.2006.07.012.

[25] T.M. Semkow, G. Mehmood, P.P. Parekh et al., Coincidence summing in gamma-ray spectroscopy, Nucl. Instr. Meth. Phys. Res. A., 290 (1990) 437-444. DOI: https://doi.org/10.1016/0168-9002(90)90561-J.

[26] G. Collaboration, Geant4 user's guide for application developers. Version: geant4 9.6. 0, Publication date 30th November, (2012).

[27] M.I. Abbas, Y.S. Selim, M. Bassiouni, HPGe detector photopeak efficiency calculation including self-absorption and coincidence corrections for cylindrical sources using compact analytical expressions, Radiat. Phys. Chem., 61 (2001) 429-431. DOI: https://doi.org/10.1016/S0969-806X(01)00288-2.

Phonon sideband and Raman spectra analysis of Eu³⁺-doped Sr₂Al₂SiO₇

Phân tích phổ Phonon sideband và Raman của vật liệu Sr₂Al₂SiO₇ pha tạp Eu³⁺

Ho Van Tuyen[a,*], Le Van Khoa Bao[b], Nguyen Ha Vi[c]
Hồ Văn Tuyến, Lê Văn Khoa Bảo, Nguyễn Hạ Vi

[a]*Institute of Research and Development, Duy Tan University, 03 Quang Trung, Danang, Vietnam*
Viện Nghiên cứu và Phát triển Công nghệ cao, Đại học Duy Tân, 03 Quang Trung, Đà Nẵng, Việt Nam
[b]*Department of Scientific Research Management, Duy Tan University, 03 Quang Trung, Danang, Vietnam*
Phòng Quản lý Khoa học, Đại học Duy Tân, 03 Quang Trung, Đà Nẵng, Việt Nam
[c]*The Faculty of Natural Sciences, Duy Tan University, 03 Quang Trung, Danang, Vietnam*
Khoa Khoa học Tự nhiên, Đại học Duy Tân, 03 Quang Trung, Đà Nẵng, Việt Nam.

Abstract

In this work, vibration modes in Eu³⁺ activated in Sr₂Al₂SiO₇ phosphor were studied by a combination analysis of Raman and phonon sideband spectra. The sample was successfully synthesized by solid state reaction, and its single-phase was further confirmed by X-ray diffraction. Raman spectroscopy of the structure of Sr₂Al₂SiO₇ showed some intense vibration modes located in 100-2000 cm⁻¹ region that could be attributed to Si-O-Si network. In addition, phonon sideband analysis from photoluminescence excitation spectra displayed four phonon vibrations, in which some of vibrations coincide with to the result of Raman spectra.

Keywords: Aluminum silicate, europium, phonon sideband, Raman spectroscopy.

Tóm tắt

Trong nghiên cứu này, các dao động trong vật liệu Sr₂Al₂SiO₇ pha tạp Eu³⁺ được nghiên cứu bằng phổ tán xạ Raman kết hợp với phổ phonon sideband. Vật liệu được chế tạo thành công bằng phương pháp phản ứng pha rắn, pha cấu trúc của vật liệu được xác định bằng phép đo nhiễu xạ tia X. Phổ tán xạ Raman của Sr₂Al₂SiO₇ cho thấy các dao động mạnh trong vùng 100-2000 cm⁻¹ đặc trưng cho các liên kết Si-O-Si trong mạng tinh thể.

Bên cạnh đó, kết quả phân tích phổ phonon sideband của Eu³⁺ từ phổ kích thích phát quang của vật liệu cho thấy tồn tại bốn dải dao động phonon, trong đó một số dao động là phù hợp với kết quả quan sát được từ phổ tán xạ Raman.

Từ khóa: Aluminum silicate, europium, phonon sideband, phổ Raman.

1. Introduction

Rare earth (RE) ions doped strontium aluminum silicate (SAS) phosphors have been studied in terms of luminescent properties as well as structural characteristics in recent years. Some results on SAS system were obtained such as Eu²⁺

ion doped Sr₂Al₂SiO₇ material obtaining a green emission which had been studied by Fa-Chun Lu in 2014 [1]. This study showed that dipole-dipole interaction dominates the non-radiation energy transfer between the Eu²⁺ luminescent centers in this material. Several studies have combined Eu²⁺

Email: hovantuyen@gmail.com

ion with other RE^{3+} ions, e.g. Dy^{3+}, Ce^{3+}, Tm^{3+}co-doped into this lattice to investigate the long persistent luminescence, white light emission, and thermoluminescence property [2-4]. Besides that, energy transfer between Ce^{3+} and Dy^{3+} ions as well as the concentration quenching of Ce^{3+} in $Sr_2Al_2SiO_7$ had been investigated and reported in 2016 [5, 6]. The luminescence and thermoluminescence properties of $Sr_2Al_2SiO_7$:Eu^{3+} have also been studied [7, 8]. The fabrication methods such as sol-gel processes, combustion method and solid state reaction for $Sr_2Al_2SiO_7$ phosphor have been reported in many papers [6, 9, 10]. Other studies on the controllable photoluminescence of $Sr_2Al_2SiO_7$/$SrAl_2Si_2O_8$:Eu^{3+} or the thermal stable of $Sr_2Al_2SiO_7$:Pr^{3+} compounds have also been published [11, 12]. However, there has been no literature until now presenting the information of the vibration energy in $Sr_2Al_2SiO_7$:Eu^{3+} (0.5 mol%) material from phonon sideband (PSB) or Raman spectra. Therefore, the target of this study is to synthesize the $Sr_2Al_2SiO_7$:$Eu^{3+}$and measure the Raman and phonon sideband spectra to determine the vibrations occurring in the $Sr_2Al_2SiO_7$:Eu^{3+}phosphor.

2. Experiment

The sample $Sr_2Al_2SiO_7$:Eu^{3+} (0.5 mol%) was fabricated by solid-state reaction method at high temperature. Firstly, the raw materials, $SrCO_3$ (AR), Al_2O_3 (AR), SiO_2 (Korea) and Eu_2O_3 (Merck) were weighed according to the nominal composition, mixed homogeneously and milled thoroughly using an agate pestle and mortar to achieve a uniform mixture. A small amount of B_2O_3 was added during mixing process to serve as a flux to promote the formation of crystal structure. After that, this mixture was ground and calcined at 1250°C for 2 hours in air. The obtained product was finally ground into powder to analyze phase compositions, photoluminescence property, and Raman spectra.

Structural characteristics of the prepared sample were investigated by X-ray diffraction (XRD) patterns and Raman scattering using X-ray diffractometer D8-Advance (Bruker, Germany) and Xplora plus (Horiba Jobin-Yvon), respectively. Photoluminescence (PL) and Photoluminescence excitation (PLE) spectra were taken out by a spectrophotometer (FL3-22, Horiba Jobin-Yvon) at room temperature. Phonon sideband spectrum of the $^7F_0$-$^5D_2$ transition was also analyzed from PLE spectra of Eu^{3+} ion.

3. Results and discussion

The phase purity of $Sr_2Al_2SiO_7$:Eu^{3+} was figured out by X-ray diffraction (XRD) using Cu K-alpha (0.154 nm) radiation. Figure 1 presents the XRD pattern of the prepared sample, showing a good match with the $Sr_2Al_2SiO_7$ standard PDF card of 75-1234. No impure phases were found indicating the single phase Eu^{3+} activated $Sr_2Al_2SiO_7$ phosphor has been synthesized.

Figure 2 shows the Raman scattering spectra of $Sr_2Al_2SiO_7$:Eu^{3+} using laser 532 nm. The structure of strontium alumino-silicate material consists of silicate and aluminate network. The Raman bands locating in 300-500 cm^{-1} region are attributed to mixed stretching and bending modes of Si-O-Si units [13, 14]. The bands centered at 565 cm^{-1} and 602 cm^{-1} are assigned to the bending vibrations of the bridging oxygen bonds of SiO and Si-O-Si bending vibration, respectively [15-17]. The vibration energies at 780 and 973 cm^{-1} are due to Si-O-Si network and stretching vibration of silicon-oxygen tetrahedral [15, 18] and vibration at 1360 cm^{-1} is now unknown. All Raman peaks of the $Sr_2Al_2SiO_7$:Eu^{3+} sample are summarized in Table 1. Besides the Raman spectra, some vibration modes can be found from phonon sideband spectra of the $Sr_2Al_2SiO_7$:Eu^{3+} sample which is discussed in the next paragraph.
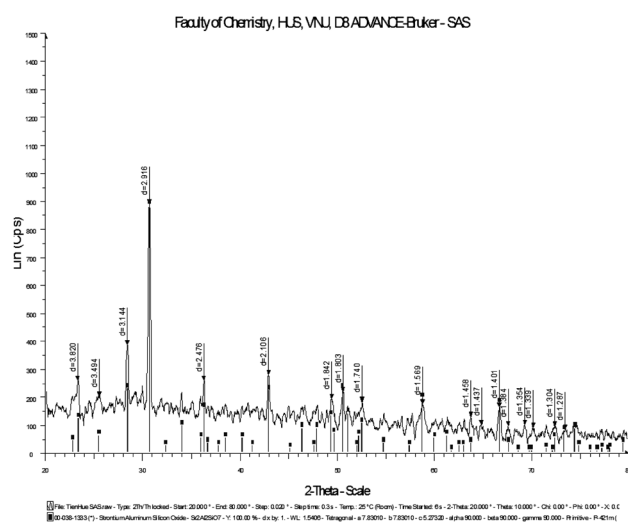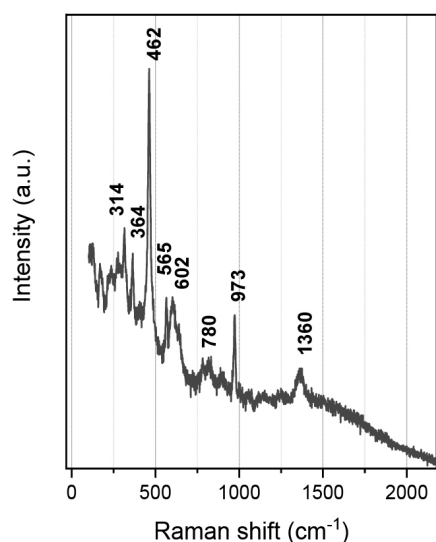
Figure 1. XRD pattern of $Sr_2Al_2SiO_7$:Eu^{3+}.

Figure 2. Raman spectrum of $Sr_2Al_2SiO_7$:Eu_{3+}.

Table 1. Assignment of Raman bands in the spectrum of strontium alumino-silicate phosphor.

Wavenumber (cm⁻¹)	Raman assignments	Reference
300-500	Mixed stretching and bending modes of Si-O-SiO units	[13, 14]
565	Bending vibrations of the bridging oxygen bonds of SiO	[15]
602	Si-O-Si bending vibration	[16, 17]
780	Si-O-Si network, AlO_4 units with three BO_s and one NBO	[15]
973	Stretching vibration of silicon-oxygen tetrahedral	[18]

The photoluminescence excitation spectrum of $Sr_2Al_2SiO_7$:Eu^{3+} monitored the $^5D_0$–$^7F_2$ emission at 617 nm is shown in Figure 3. PLE spectrum includes an intense broadband in 240-300 nm region and several sharp peaks in 350-575 nm. Among them, the broadband is ascribed to the electric charge transfer due to the ligand-to-metal charge transfer states, O^{2-}–Eu^{3+} [19, 20], meanwhile the sharp peaks are attributed by the excited transitions from ground sate $^7F_0$ to excited state of Eu^{3+} ion in $Sr_2Al_2SiO_7$ lattice. Two intense excited transitions of Eu^{3+} located at 392 and 462.5 nm are the $^7F_0$-$^5L_6$ and $^7F_0$-$^5D_2$ transitions, respectively. It is known that there is no any energy level between the excited $^5D_2$ and $^5D_3$ levels of Eu^{3+}. Therefore, if any excitation peak locates between those two levels, then it is due to the phonon energy.

In order to further investigate the phonon energy of the sample, the understanding of vibration behaviors of lattice in immediate vicinity of rare earth ions is necessary with a help of a powerful tool like PSB spectrum [19, 20]. The $^7F_0$–$^5D_2$ is a pure-electric transition (PET) and the barycenter wave number of PET is as a reference for the zero-phonon line, which can be used to calculate the phonon energy from PLE spectrum. The PSB associated with the pure electronic transition $^7F_0$–$^5D_2$ at 462.5 nm of the prepared sample are shown in Fig. 4; and their phonon energies are listed in Table 2. The PSB spectrum consists of four bands centered at 423.5 nm, 433.5 nm, 441.5 nm and 446 nm which are denoted by PSB1, PSB2, PSB3 and PSB4, respectively. The energy of PSB4 locating at 777 cm⁻¹ is closed with the vibration energy of Si-O-Si network (780 cm⁻¹) which is analyzed from Raman spectra. Meanwhile, the PSB3 with energy of 1005 cm⁻¹ may be assigned to the stretching vibrations of Si-O−Al [17], and the PSB1 at 1967 cm⁻¹ is due to the stretching and bending vibration of O–H groups [21] . However, the PSB2 energy at 1423 cm⁻¹ has not been reported in any literature.
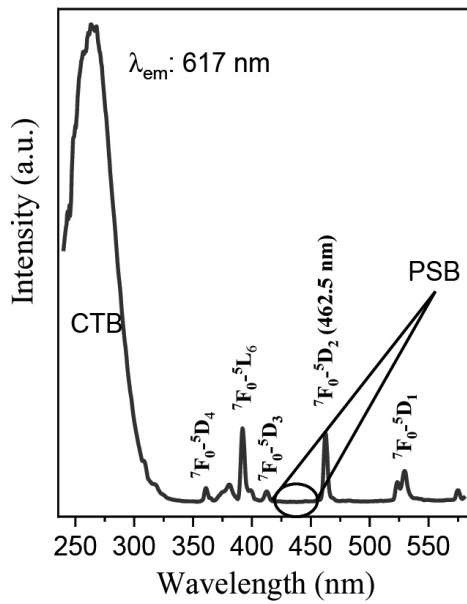
Figure 3. PLE spectrum of $Sr_2Al_2SiO_7:Eu^{3+}$.
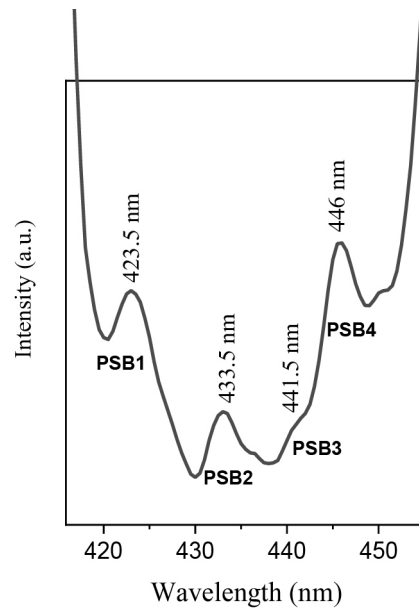
Figure 4. PSB spectrum of $Sr_2Al_2SiO_7:Eu^{3+}$.

Table 2. The energies of PET and PSBs of strontium alumino-silicate phosphor.

PET (nm)	Peak PSB1 (nm)	Peak PSB2 (nm)	Peak PSB3 (nm)	Peak PSB4 (nm)	PSB1 (cm^{-1})	PSB2 (cm^{-1})	PSB3 (cm^{-1})	PSB4 (cm^{-1})
462.5	423.5	433.5	441.5	446	1967	1423	1005	777

The PL spectrum of $Sr_2Al_2SiO_7:Eu^{3+}$ sample excited by radiation of 392 nm at room temperature is presented in Figure 5. As can be seen, the emission of Eu^{3+} ion in 550-750 nm includes five sharp peaks which belong to the $^5D_0$-^7F_J transitions (J = 0, 1, 2, 3, 4) of $4f^n$ configure. Among these, the $^5D_0$-$^7F_2$ is an electric dipole transition, which is hypersensitive to the change of Eu^{3+}- surroundings. Meanwhile, the $^5D_0$-$^7F_1$ is a magnetic dipole transition, which hardly varies with the evolution of Eu^{3+}-surrounding. Hence, the intensity ratio (R) of $^5D_0$-$^7F_2$ transition to $^5D_0$-$^7F_1$ can thus be used as a measure of coordination state and site symmetry of rare earth ions [22, 23]. The intensity ratio R is defined by the following equation:

$$R = \frac{I(^5D_0 \rightarrow {}^7F_2)}{I(^5D_0 \rightarrow {}^7F_1)} \qquad (1)$$

For $Sr_2Al_2SiO_7:Eu^{3+}$, the intensity ratio R was found to be around 2.26, a clear indicator implying that Eu^{3+} ions are not located on an inversion center [24].
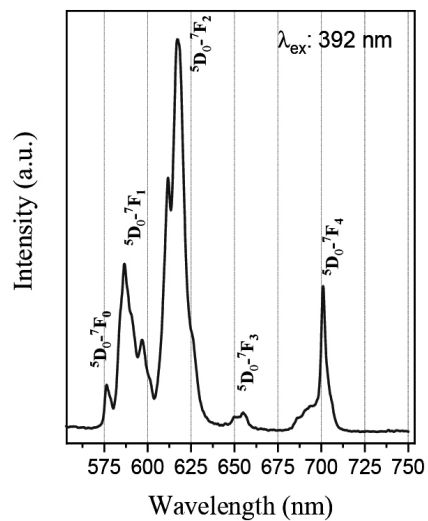
Figure 5. PL spectra of $Sr_2Al_2SiO_7:Eu^{3+}$ sample.

4. Conclusion

A single phase Eu^{3+} activated $Sr_2Al_2SiO_7$ phosphor has been synthesized successfully by using solid state reaction method at 1250°C. The vibration modes assigned to Si-O-Si network, AlO_4 units in $Sr_2Al_2SiO_7:Eu^{3+}$ have been presented via Raman spectra. By analyzing on phonon sideband spectra, it was found that the $Sr_2Al_2SiO_7$ phosphor

has vibrations that belong to Si-O-Si network, Si-O-Al bonds and O-H groups. Further studies on luminescent property suggested that Eu^{3+} ions are not located on an inversion center.

References

[1] F.C. Lu, L.J. Bai, W. Dang, Z.P. Yang, P. Lin, Structure and Photoluminescence of Eu^{2+} Doped $Sr_2Al_2SiO_7$ Cyan-Green Emitting Phosphors, ECS Journal of Solid State Science and Technology, 4 (2014) R27-R30.

[2] Y. Ding, Y. Zhang, Z. Wang, W. Li, D. Mao, H. Han, C. Chang, Photoluminescence of Eu single doped and Eu/Dy codoped $Sr_2Al_2SiO_7$ phosphors with long persistence, Journal of Luminescence, 129 (2009) 294-299.

[3] G. Li, M. Li, L. Li, H. Yu, H. Zou, L. Zou, S. Gan, X. Xu, Luminescent properties of $Sr_2Al_2SiO_7$:Ce^{3+},Eu^{2+} phosphors for near UV-excited white light-emitting diodes, Materials Letters, 65 (2011) 3418-3420.

[4] A. Jadhaw, V.D. Sonwane, A.S. Gour, P. Jha, Thermoluminescence properties of Eu-doped and Eu/Dy-codoped $Sr_2Al_2SiO_7$ phosphors, Luminescence, 32 (2017) 1349-1353.

[5] Y. Gong, Y. Wang, Y. Li, X. Xu, Ce^{3+}, Dy^{3+} Co-Doped White-Light Long-Lasting Phosphor: $Sr_2Al_2SiO_7$ Through Energy Transfer, Journal of The Electrochemical Society, 157 (2010) J208.

[6] M. Kolte, V.B. Pawade, S.J. Dhoble, Quenching and dipole–dipole interactions in $Sr_2Al_2SiO_7$:Ce^{3+} host lattice, Applied Physics A, 122 (2016).

[7] H.Y. Jiao, Y.H. Wang, Intense red phosphors for near-ultraviolet light-emitting diodes, Applied Physics B, 98 (2009) 423-427.

[8] I.P. Sahu, D.P. Bisen, N. Brahme, R.K. Tamrakar, Studies on the luminescence properties of europium doped strontium alumino-silicate phosphors by solid state reaction method, Journal of Materials Science: Materials in Electronics, 26 (2015) 10075-10086.

[9] W. Pan, G. Ning, Y. Lin, X. Yang, Sol-gel processed Ce^{3+}, Tb^{3+} codoped white emitting phosphors in $Sr_2Al_2SiO_7$, Journal of Rare Earths, 26 (2008) 207-210.

[10] W. Zhou, X. Ma, M. Zhang, Y. Luo, Z. Xia, Effect of different RE dopants on phosphorescence properties of $Sr_2Al_2SiO_7$:Eu^{2+} phosphors, Journal of Rare Earths, 33 (2015) 700-705.

[11] P. Zhang, Z. Lu, Q. Yuan, Q. Hou, T.D. Golden, X. Ren, L. Weng, H. Wang, A novel composite phosphor via one-pot synthesis: Single matrix with controllable luminescence, Materials Chemistry and Physics, 134 (2012) 1190-1196.

[12] H. Zou, D. Peng, Z. Chu, X. Wang, Y. Li, X. Yao, A highly thermal stable and waterproof red phosphor: Pr^{3+}-doped $Sr_2Al_2SiO_7$, Journal of Materials Science, 48 (2013) 7981-7985.

[13] B.G. Parkinson, D. Holland, M.E. Smith, C. Larson, J. Doerr, M. Affatigato, S.A. Feller, A.P. Howes, C.R. Scales, Quantitative measurement of Q3 species in silicate and borosilicate glasses using Raman spectroscopy, Journal of Non-Crystalline Solids, 354 (2008) 1936-1942.

[14] A.K. Yadav, P. Singh, A review of the structures of oxide glasses by Raman spectroscopy, RSC Advances, 5 (2015) 67583-67609.

[15] S. Petrescu, M. Constantinescu, E.M. Anghel, I. Atkinson, M. Olteanu, M. Zaharescu, Structural and physico-chemical characterization of some soda lime zinc alumino-silicate glasses, Journal of Non-Crystalline Solids, 358 (2012) 3280-3288.

[16] M. Wang, J. Cheng, M. Li, F. He, Raman spectra of soda–lime–silicate glass doped with rare earth, Physica B: Condensed Matter, 406 (2011) 3865-3869.

[17] K. Park, H. Kim, D.A. Hakeem, Effect of host composition and Eu^{3+} concentration on the photoluminescence of aluminosilicate $(Ca,Sr)_2Al_2SiO_7$:Eu^{3+} phosphors, Dyes and Pigments, 136 (2017) 70-77.

[18] C. Huang, E.C. Behrman, Structure and properties of calcium aluminosilicate glasses, Journal of Non-Crystalline Solids 128 (1991) 310-321.

[19] S. Arunkumar, K. Venkata Krishnaiah, K. Marimuthu, Structural and luminescence behavior of lead fluoroborate glasses containing Eu^{3+} ions, Physica B: Condensed Matter, 416 (2013) 88-100.

[20] H. Lin, H. Liang, G. Zhang, Q. Su, The luminescence of Eu^{3+} activated $Ba_2Mg(BO_3)_2$ phosphors, Applied Physics A, 105 (2011) 143-147.

[21] I.P. Sahu, D.P. Bisen, N. Brahme, R.K. Tamrakar, R. Shrivastava, Luminescence studies of dysprosium doped strontium aluminate white light emitting phosphor by combustion route, Journal of Materials Science: Materials in Electronics, 26 (2015) 8824-8839.

[22] S. Tanabe, S. Todoroki, K. Hirao, N. Soga, Phonon sideband of Eu^{3+} in sodium borate glasses, Journal of Non-Crystalline Solids, 122 (1990) 59-65.

[23] J.A. Capobianco, P.P. Proulx, M. Bettinelli, F. Negrisolo, Absorption and emission spectroscopy of Eu^{3+}in metaphosphate glasses, Physical Review B, 42 (1990) 5936-5944.

[24] Q. Yue, J. Yang, G.-H. Li, G.-D. Li, J.-S. Chen, Homochiral Porous Lanthanide Phosphonates with 1D Triple-Strand Helical Chains: Synthesis, Photoluminescence, and Adsorption Properties, Inorganic chemistry, 46 (2006) 4431-4439.

Homogenization in strain-limiting theories of elasticity

Đồng nhất hóa trong lý thuyết giới hạn biến dạng của sự đàn hồi

Tina Mai

Mai Ti Na

Institute of Research and Development, Duy Tan University, 03 Quang Trung, Danang, Vietnam
Viện Nghiên cứu và Phát triển Công nghệ cao, Đại học Duy Tân, 03 Quang Trung, Đà Nẵng, Việt Nam

Abstract

We study homogenization in a class of periodically layered composite materials consisting of two layers per base cell, in dimension one, within the setting of strain-limiting elasticity.

Keywords: Homogenization, periodically layered composite materials, nonlinear problem, strain-limiting elasticity.

Tóm tắt

Chúng tôi nghiên cứu sự đồng nhất hóa trong một tập các vật liệu tổng hợp phân lớp tuần hoàn gồm hai lớp cho mỗi khối, trong một chiều, với thiết lập đàn hồi giới hạn biến dạng.

Từ khóa: Đồng nhất hóa, vật liệu tổng hợp phân lớp tuần hoàn, bài toán phi tuyến, sự đàn hồi giới hạn biến dạng.

1. Introduction

Being a model reduction technique for handling multiscale problems, homogenization involves upscaling the media properties to represent macroscopic behaviors. Toward homogenization study of our considering strain-limiting models, we focus on a class of periodically layered composite materials consisting of two layers per base cell, in dimension one, as the simplest case. (The elastic properties of such a layered material only change in one coordinate direction.) The strain-limiting parameter here is a function depending on the position variable, which is different from the constant in [1, 2].

2. Formulation of the problem

2.1. Classical formulation

Let us consider, as in Figure 1 in the *x*-direction, the spatially periodic 1D composite rod consisting of alternating layers of nonlinear elastic materials $\Omega^{(1)}$ and $\Omega^{(2)}$. The microscopic size l corresponds to the length of a periodically repeated base cell. The macroscopic size of the whole sample $\Omega \subset \mathbb{R}$ of the rod is denoted by

Email: maitina@duytan.edu.vn
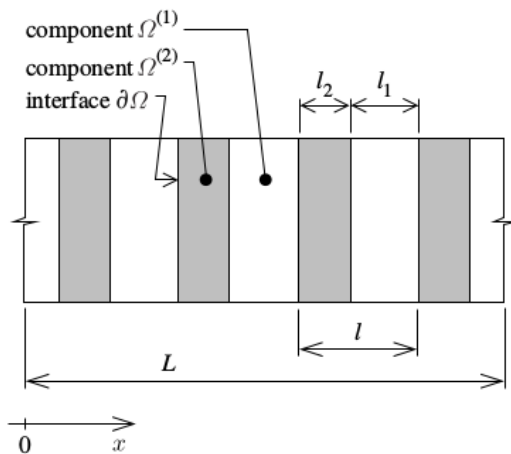
Hình 1. Layered composite structure (from [3]).

L. Without loss of generality, we take $l = \epsilon$ (the period of the structure) and choose $L = 1$ so that

$$\epsilon = \frac{l}{L} = \frac{\epsilon}{1} = \frac{k\epsilon}{k1} . \qquad (1)$$

Here, $\dfrac{x}{\epsilon}$ stands for the local position.

We assume that the rod is being at a static state after the action of body forces (along the rod) $f : \Omega \to \mathbb{R}$ and traction forces $G : \partial\Omega_T \to \mathbb{R}$. The boundary of the set Ω is denoted by $\partial\Omega$, which is Lipschitz continuous, consisting of two parts $\partial\Omega_T$ and $\partial\Omega_D$, where the displacement $u : \Omega \to \mathbb{R}$ is given on $\partial\Omega_D$. We are considering the strain-limiting model of the form (as in [1])

$$E = \frac{\sigma}{1 + \beta(x)|\sigma|} . \qquad (2)$$

Equivalently,

$$\sigma = \frac{E}{1 - \beta(x)|E|} . \qquad (3)$$

In the equations (2) and (3), $\beta(x)$ will be introduced in the next paragraph, σ denotes the Cauchy stress $\sigma : \Omega \to \mathbb{R}$; whereas, E denotes the classical linearized strain tensor

$$E := \frac{1}{2}(\nabla u + \nabla u^{\mathrm{T}}) . \qquad (4)$$

In one-dimensional setting, it becomes

$$E := u' , \qquad (5)$$

which is the spatial derivative of u. Thus, by (3),

$$\sigma = \frac{u'}{1 - \beta(x)|u'|} . \qquad (6)$$

The strain-limiting parameter function is denoted by $\beta(x)$, which depends on the position variable x, and it is constant in each layer, with $\beta_\epsilon(x) = \beta(\epsilon^{-1}x)$. We notice from (2) that

$$|E| = \frac{|\sigma|}{1 + \beta(x)|\sigma|} < \frac{1}{\beta(x)} . \qquad (7)$$

This means that $\dfrac{1}{\beta(x)}$ is the upper-bound on $|E|$ and taking large enough $\beta(x)$ raises the limiting-strain small upper-bound, as wishing. Nevertheless, we avoid too large $\beta(x)$. If $\beta(x) \to \infty$ then $|E| < \dfrac{1}{\beta(x)} \to 0$, a contradiction. Moreover, $\beta(x)$ is assumed to be smooth and have compact range $0 < m \le \beta(x) \le M$. Also, we assume that

$$\beta(x) = \begin{cases} \beta_1 & \text{if } jl < x < (j + \alpha)l \text{ for some } j \in \mathbb{N}, \\ \beta_2 & \text{otherwise} . \end{cases}$$
$$(8)$$

Here, β_1 and β_2 are chosen so that the strong ellipticity condition [1] holds. In practice, the requirement of strong point-wise ellipticity in each layer is not essential, for all the important instability phenomena occur well below the stress levels corresponding to the loss of ellipticity of the weakest layer (see [4, 5]).

2.2. Function spaces

Our considered space is $V := H_0^1(\Omega)$. However, the techniques here can be used in more general space $H_0^p(\Omega)$, where $2 \leq p < \infty$. The space $W_0^{1,2}(\Omega)$ is considered because we can characterize displacements that vanish on the boundary $\partial \Omega$ of Ω.

The dual space, which is the space of continuous linear functionals on $H_0^1(\Omega)$, is denoted by $H^{-1}(\Omega)$, and the value of a functional $b \in H^{-1}(\Omega)$ at a point $v \in H_0^1(\Omega)$ is denoted by $\langle b, v \rangle$. The Sobolev norm $\| \cdot \|_{H_0^1(\Omega)}$ is of the form

$$\|v\|_{H_0^1(\Omega)} = (\|v\|_{L^2(\Omega)}^2 + \|\nabla v\|_{L^2(\Omega)}^2)^{\frac{1}{2}} \, .$$

The dual norm to $\| \cdot \|_{H_0^1(\Omega)}$ is $\| \cdot \|_{H^{-1}(\Omega)}$.

Let Ω be a bounded, connected, open, Lipschitz domain of $\mathbb{R}$,

$$f \in H_*^1(\Omega) = \left\{ g \in H^1(\Omega) \Big| \int_\Omega g \, dx = 0 \right\} \, .$$

We consider the following problem: Find $u \in H^1(\Omega)$ and $\sigma \in L^1(\Omega)$ ([6]) such that

$$\begin{aligned}
-\text{div}(\sigma) &= f \quad \text{in } \Omega \, , \\
\sigma &= \frac{u'}{1 - \beta(x)|u'|} \quad \text{in } \Omega \, , \quad (9) \\
u &= 0 \quad \text{on } \partial \Omega_D \, , \\
\sigma &= G \quad \text{on } \partial \Omega_T \, .
\end{aligned}$$

The considered model (2) is compatible with the laws of thermodynamics [7, 8], which means that the class of materials are non-dissipative and are elastic.

For the later discussion about homogenization, we consider $u_\epsilon(x) \in W_0^{1,2}(\Omega)$. Assume that $u_\epsilon(x) = u\left(\frac{x}{\epsilon}\right)$ is a periodic function in x with period ϵ, equivalently $u(y) = u\left(\frac{x}{\epsilon}\right)$ is a periodic function in y with period 1. This means that for any integer k,

$$u_\epsilon(x) = u_\epsilon(x + \epsilon) = u_\epsilon(x + k\epsilon) \, ,$$

correspondingly,

$$u\left(\frac{x}{\epsilon}\right) = u\left(\frac{x}{\epsilon} + 1\right) = u\left(\frac{x}{\epsilon} + k1\right) = u(y + k) \, .$$

This remark supports the expressions of ϵ in (1). (Note that the spatial periodicity of the composite induces the same periodicity for u.)

For the sake of simplicity, we assume perfect bonding conditions at the interface $\partial \Omega$ between the layers, i.e., the displacement and traction are continuous across each interface for all possible deformations:

$$\begin{aligned}
(u_\epsilon)_{(1)} &= (u_\epsilon)_{(2)} \quad \text{on } \partial \Omega \, , \\
(\sigma_\epsilon)_{(1)} &= (\sigma_\epsilon)_{(2)} \quad \text{on } \partial \Omega_T \, .
\end{aligned} \quad (10)$$

We assume $\partial \Omega_T = \emptyset$. In homogenization theory, using (9), we write the considered formulation in the form of displacement problem: Find $u \in H^1(\Omega)$ such that

$$-\text{div}\left(\frac{u'_\epsilon}{1 - \beta_\epsilon(x)|u'_\epsilon|} \right) = f \quad \text{in } \Omega \, , \quad (11)$$

$$u_\epsilon = 0 \quad (u_\epsilon)_{(1)} = (u_\epsilon)_{(2)} \quad \text{on } \partial \Omega \, . \quad (12)$$

We denote

$$a_\epsilon(x, u'_\epsilon) = \frac{u'_\epsilon}{1 - \beta_\epsilon(x)|u'_\epsilon|} \, , \quad (13)$$

in which $u_\epsilon(x) \in W_0^{1,2}(\Omega)$.

3. Existence and uniqueness

The existence and uniqueness of solution to (11)-(12) is proved in [9], and thanks to the following Lemma ([10, 11, 9]).

Lemma 3.1. *Let*

$$\mathcal{Z} := \left\{ \zeta \in L^\infty(\Omega) \mid 0 \leq |\zeta| < \frac{1}{M} \right\} \, . \quad (14)$$

For any $\xi \in \mathcal{Z}$, consider the mapping

$$\xi \in \mathcal{Z} \mapsto F(\xi) := \frac{\xi}{1 - \beta_\epsilon(x)|\xi|} \in \mathbb{R} \, .$$

Then, for each $\xi_1, \xi_2 \in \mathcal{Z}$, we have

$$|F(\xi_1) - F(\xi_2)| \leq \frac{|\xi_1 - \xi_2|}{(1 - \beta_\epsilon(x)(|\xi_1| + |\xi_2|))^2} \, , \quad (15)$$

$$(F(\xi_1) - F(\xi_2))(\xi_1 - \xi_2) \geq |\xi_1 - \xi_2|^2 \, . \quad (16)$$

In our case of 1D, the solution u can be found directly from (11)-(12).

4. Homogenization

We discuss homogenization for the one-dimensional quasilinear elliptic equation (11), for $u_\epsilon \in W_0^{1,2}(\Omega)$,

$$-(a_\epsilon(x, u'_\epsilon))' = f, \qquad (17)$$

where $a_\epsilon(x, u'_\epsilon)$ was defined in (13). This form (17) is as in [12].

The homogenization of nonlinear partial differential equations has been studied previously (see, e.g., [13]). It can be shown that a sequence of solutions u_ϵ converges weakly (up to a subsequence) to u_* in an appropriate norm, where $u_* \in W_0^{1,2}(\Omega)$ is a solution of the homogenized equation

$$-(a_*(x, u'_*))' = f. \qquad (18)$$

In our present work, the homogenized coefficient a_* can be computed because the material is periodic. We thus formulate an auxiliary problem and use it in the calculation of the homogenized flux a_*. The discussion in details is as follows.

Consider the equation (11):

$$-\left(\frac{u'_\epsilon(x)}{1 - \beta_\epsilon(x)|u'_\epsilon(x)|}\right)' = f.$$

The cell problem is given by

$$-\frac{d}{dy}\left(\frac{\xi + \frac{d}{dy}N_\xi}{1 - \beta(y)\left|\xi + \frac{d}{dy}N_\xi\right|}\right) = 0, \qquad (19)$$

in Y, the unit period, and $N_\xi \in W_{\text{per}}^{1,p}(Y)$ is the solution of this equation. In which, N_ξ has periodic boundary conditions, and $W_{\text{per}}^{1,p}(Y)$ is the set of mean value zero functions.

Assume that the solution of the equation

$$\frac{\zeta}{1 - \beta(y)|\zeta|} = \alpha$$

is given by

$$\zeta = \zeta(y, \alpha) = \frac{\alpha}{1 + \alpha\beta(y)\text{sign}(\zeta)}.$$

We then have

$$\xi + \frac{d}{dy}N_\xi = \frac{c}{1 + c\beta(y)\text{sign}\left(\xi + \frac{d}{dy}N_\xi\right)}, \qquad (20)$$

where c is a constant.

From the cell problem (19), we can write

$$N_\xi = \chi \cdot \xi,$$

where $\xi \neq 0$, and χ solves

$$-\frac{d}{dy}\left(1 + \frac{d}{dy}\chi(y)\right) = 0.$$

Indeed, the cell problem is equivalent to the following problem:

$$-\frac{d}{dy}\left(\frac{\xi\left(1 + \frac{d}{dy}\chi(y)\right)}{1 - \beta(y)|\xi|\left|1 + \frac{d}{dy}\chi(y)\right|}\right) = 0$$

$$\frac{d}{dy}\left(1 + \frac{d}{dy}\chi\right) - \beta(y)|\xi|\left|1 + \frac{d}{dy}\chi\right|\frac{d}{dy}\left(1 + \frac{d}{dy}\chi\right)$$

$$+\beta(y)|\xi|\left(1 + \frac{d}{dy}\chi\right)\frac{d}{dy}\left|1 + \frac{d}{dy}\chi\right| = 0$$

$$\frac{d}{dy}\left(1 + \frac{d}{dy}\chi\right) = 0$$

$$1 + \frac{d}{dy}\chi = a$$

$$\chi = (a - 1)y + b,$$

where a, b are constants. Thus,

$$\text{sign}\left(\xi + \frac{d}{dy}N_\xi\right) = \text{sign}\left(\xi\left(1 + \frac{d}{dy}\chi\right)\right)$$

$$= \text{sign}(a\xi)$$

From (20), we obtain

$$\xi\left(1 + \frac{d}{dy}N_\xi\right) = \frac{c}{1 + c\beta(y)\text{sign}(a\xi)}.$$

Integrating over Y to find c:

$$\xi = \int_Y \frac{c}{1 + c\beta(y)\text{sign}(a\xi)}dy$$

$$= \frac{cl^{(1)}}{1 + c\beta_1\text{sign}(a\xi)} + \frac{cl^{(2)}}{1 + c\beta_2\text{sign}(a\xi)}$$

$$= \frac{cl^{(1)}(1 + c\beta_2\text{sign}(a\xi)) + cl^{(2)}(1 + c\beta_1\text{sign}(a\xi))}{(1 + c\beta_1\text{sign}(a\xi))(1 + c\beta_2\text{sign}(a\xi))}$$

Equivalently,

$$((\beta_1 l^{(2)} + \beta_2 l^{(1)})\text{sign}(a\xi) - \beta_1\beta_2\xi)c^2 \\ +(1 - (\beta_1 + \beta_2)\xi\text{sign}(a\xi))c - \xi = 0 \,. \tag{21}$$

Here, each of $l^{(1)}$, $l^{(2)}$ denotes the sum of length of layers within the material unit Y, having $\beta_\epsilon(x) = \beta_1$, $\beta_\epsilon(x) = \beta_2$, respectively; and $l^{(1)} + l^{(2)} = 1$.

With appropriate $\beta_\epsilon(x)$, solving the quadratic equation (21) for c, we obtain $c = \phi(\xi)$.

To compute the homogenized coefficient a_*, we notice that

$$\begin{aligned} a_*(\xi) &= \int_Y a(y, \xi + \nabla_y N_\xi(y))dy \\ &= \int_Y cdy = c = \phi(\xi) \,, \end{aligned} \tag{22}$$

where a_* satisfies the conditions similar to (15) and (16).

5. Conclusions

In this paper, we investigate homogenization in a class of periodically layered composite materials, whose each base cell contains two layers, in one dimensional and strain-limiting settings. By analysis, we obtained the homogenized coefficient. An open question is comparing the homogenized solution and the specific solution in each layer. Another question is taking into account the ratio of layers' thickness.

References

[1] Tina Mai and Jay R. Walton. On strong ellipticity for implicit and strain-limiting theories of elasticity. *Mathematics and Mechanics of Solids*, 20(II):121–139, 2015. DOI: 10.1177/1081286514544254.

[2] Tina Mai and Jay R. Walton. On monotonicity for strain-limiting theories of elasticity. *Journal of Elasticity*, 120(I):39–65, 2015. DOI: 10.1007/s10659-014-9503-4.

[3] Igor V Andrianov, Vladimir I Bolshakov, Vladyslav V Danishevs'kyy, and Dieter Weichert. Higher order asymptotic homogenization and wave propagation in periodic composite materials. *Proceedings of the Royal Society of London A: Mathematical, Physical and Engineering Sciences*, 464(2093):1181–1201, 2008.

[4] Giuseppe Geymonat, Stefan Müller, and Nicolas Triantafyllidis. Homogenization of nonlinearly elastic materials, microscopic bifurcation and macroscopic loss of rank-one convexity. *Archive for Rational Mechanics and Analysis*, 122(3):231–290, 1993. DOI: 10.1007/BF00380256.

[5] N. Triantafyllidis and B.N. Maker. On the comparison between microscopic and macroscopic instability mechanisms in a class of fiber-reinforced composites. *J. Appl. Mech*, 52(4):794 – 800, 1985.

[6] Lisa Beck, Miroslav Bulíček, Josef Málek, and Endre Süli. On the existence of integrable solutions to nonlinear elliptic systems and variational problems with linear growth. *Archive for Rational Mechanics and Analysis*, 225(2):717–769, Aug 2017.

[7] K. R. Rajagopal and A. R. Srinivasa. On the response of non-dissipative solids. *Proceedings of the Royal Society of London, Mathematical, Physical and Engineering Sciences*, 463(2078):357–367, 2007.

[8] K.R Rajagopal and A.R Srinivasa. On a class of non-dissipative materials that are not hyperelastic. *Proceedings of the Royal Society of London A: Mathematical, Physical and Engineering Sciences*, 465(2102):493–500, 2009.

[9] Shubin Fu, Eric Chung, and Tina Mai. Generalized multiscale finite element method for a strain-limiting nonlinear elasticity model. *Journal of Computational and Applied Mathematics*, 359:153 – 165, 2019.

[10] M. Bulíček, J. Málek, and E. Süli. Analysis and approximation of a strain-limiting nonlinear elastic model. *Mathematics and Mechanics of Solids*, 20(I):92–118, 2015. DOI: 10.1177/1081286514543601.

[11] Miroslav Bulíček, Josef Málek, K. R. Rajagopal, and Endre Süli. On elastic solids with limiting small strain: modelling and analysis. *EMS Surveys in Mathematical Sciences*, 1(2):283–332, 2014.

[12] Y. Efendiev, J. Galvis, M. Presho, and J. Zhou. A multiscale enrichment procedure for nonlinear monotone operators. *ESAIM Math. Model. Numer. Anal.*, 48(2):475–491, 2014.

[13] Alexander Pankov. *G-convergence and homogenization of nonlinear partial differential operators*, volume 422 of *Mathematics and its Applications*. Kluwer Academic Publishers, Dordrecht, 1997.

Thermal quenching and anomalous photoluminescence of Eu²⁺-doped strontium borate materials

Dập tắt nhiệt và phát quang dị thường của vật liệu Strontium Borate pha tạp Eu²⁺

Ho Van Tuyen[a,*], Nguyen Ha Vi[b], Le Van Khoa Bao[c]
Hồ Văn Tuyến, Nguyễn Hạ Vi, Lê Văn Khoa Bảo

[a]*Institute of Research and Development, Duy Tan University, Danang, Vietnam.*
Viện Nghiên cứu và Phát triển Công nghệ cao, Đại học Duy Tân, Đà Nẵng, Việt Nam.
[b]*The Faculty of Natural Sciences, Duy Tan University, Danang, Vietnam.*
Khoa Khoa học Tự nhiên, Đại học Duy Tân, Đà Nẵng, Việt Nam.
[c]*Department for Management of Scientific Research, Duy Tan University, Danang, Vietnam.*
Phòng Quản lý Khoa học, Đại học Duy Tân, Đà Nẵng, Việt Nam.

Abstract

$Sr_3B_2O_6:Eu^{2+}$ (1mol%) phosphor was fabricated by combustion method and their luminescent, thermoluminescence (TL) properties were investigated and discussed. The intense orange emission near 574 nm that originates from 5d→4f transition of $Sr_3B_2O_6:Eu^{2+}$ with the large stokes shift and the large bandwidth is an anomalous emission. The investigation of luminescence at different temperature showed the energy for the thermal quenching of 0.429 eV. Result of TL estimation from glow curve presented a trap with activation energy about 0.95 eV. The mechanism of anomalous emission is explained by the presence of trap in lattice.

Keywords: Strontium borate, Thermal quenching, Thermoluminescence, Europium.

Tóm tắt

Vật liệu phát quang $Sr_3B_2O_6:Eu^{2+}$ (1mol%) được chế tạo bằng phương pháp nổ và các đặc trưng phát quang, nhiệt phát quang (TL) của vật liệu cũng đã được nghiên cứu và thảo luận. Bức xạ phát quang màu cam cường độ mạnh ở bước sóng 574 nm bắt nguồn từ chuyển dời 5d→4f của $Sr_3B_2O_6:Eu^{2+}$ có độ dịch stokes và độ bán rộng lớn là thuộc về phát quang dị thường. Khảo sát phổ phát quang của vật liệu tại các nhiệt độ khác nhau đã chỉ ra năng lượng dập tắt nhiệt vào khoảng 0.429 eV. Kết quả phân tích từ đường cong nhiệt phát quang tích phân cho thấy sự tồn tại của bẫy ứng với năng lượng 0.95 eV. Cơ chế của phát quang dị thường được giải thích thông qua sự có mặt của bẫy trong mạng tinh thể.

Từ khóa: Strontium borate, Dập tắt nhiệt, Nhiệt phát quang, Europium.

1. Introduction

Lanthanide (Ln) ions either in their divalent or trivalent charge state form a very important class of luminescence activators in phosphors. In all phosphor applications, the emission color and thermal stability of the emission are crucially important factor and these aspects are related to the location of the lanthanide energy levels [1, 2]. After excited from the 4f ground state to the 5d level, a lanthanide ion relaxes to the lowest 5d level and then it makes 5d→4f emission as from this level to ground state. In most trivalent

Email: hovantuyen@gmail.com

lanthanide ions, 5d→4f emission is not observed because it is normally quenched by rapid multi-phonon relaxation from the lowest $4f^{n-1}5d$ states to $4f^n$ ground state. For the divalent lanthanide ion, 5d→4f emission is obtained for Sm^{2+}, Eu^{2+}, Tm^{2+} and Yb^{2+}. In the other divalent ions, the 5d→4f emission is quenched by again relaxation to $4f^n$ ground state. Among divalent ions, Eu^{2+} ion has been doped in many compounds because its 5d→4f transition has strong intensity and variant color in different materials. The Eu^{2+} emission can be normal or anomalous emission which depends on effect of host lattice on energy level position 5d of Eu^{2+} ion in the compound.

Among inorganic compounds applied for lighting and display, strontium borate materials doped Ln ion can change component to obtain a lot of luminescent phosphor as $Sr_3B_2O_6$, $Sr_2B_2O_5$ and SrB_2O_4. In which $Sr_3B_2O_6$ material has studied for past twenty years with many results which are potential for light technology [3-5]. By this time, this material is still attracting the scientists to study with many papers published in 2017 and 2018 [6-8]. However, no literature explains anomalous emission of Eu^{2+}-doped $Sr_3B_2O_6$ lattice. Therefore, the targets of this work are to synthesize $Sr_3B_2O_6$ materials and explain the anomalous emission of Eu^{2+}-doped in this lattice.

2. Experiment

Sample $Sr_3B_2O_6$ doped Eu^{2+} (1 mol%) ion in this study was fabricated by combustion method using urea (NH_4N_2O) as a combustion fuel. The raw materials are strontium nitrate $Sr(NO_3)_2$ (Merck), acid boric H_3BO_3 (AR), europium nitrate $Eu(NO_3)_3$ (Sigma). The solution of ingredients was mixed and heated at 70°C by a magnetic stirring machine to obtain a gel. Next, the gel was dried at 50°C for 2 hours using the low temperature furnace. The dry gel, in next step, was introduced into a furnace and was heated to 600°C under the CO reduced gas for the combustion occurred within 5 minutes. Finally, the sample was cooled naturally to room temperature with the furnace, obtaining the sample in terms of white powder.

Structural characteristic of the prepared sample was investigated by X-ray diffraction (XRD) patterns using a X-ray diffractometer D8-Advance (Bruker, Germany). Photoluminescence (PL) and photoluminescence excitation (PLE) spectra were taken out by a spectrophotometer (FL3-22, Horiba Jobin-Yvon). A beta-source of ^{90}Sr was used for irradiation of the samples. Thermoluminescence properties were carried out by the glow curves using Harshaw 3500 TLD reader.

3. Results and discussion

3.1 X-ray diffraction of $Sr_3B_2O_6$: Eu^{2+}.

Phase purity of the prepared samples $Sr_3B_2O_6$:Eu^{2+} (1 mol%) was figured out by X-ray diffraction (XRD) using Cu K-alpha (0.154 nm) radiation and the XRD patterns are presented in Fig. 1. The measured XRD pattern matches well with the $Sr_3B_2O_6$ standard PDF card of 31-1343. No impure phases have been found which indicated that the single phase Eu^{2+} activated $Sr_3B_2O_6$ phosphor has been successfully synthesized. The crystal system of the prepared sample was identified as a rhombohedral structure with space group R3c. The average particle size calculated using Sherrer's formula is given [9]:

$$d = \frac{0.9\lambda}{\beta.\cos\theta}, \qquad (1)$$

where λ= 0.154 nm is the X-ray wavelength, β is the full-width at haft maximum (FWHM) intensity (in radian), θ is the diffraction angle (in degrees), d is the average size of the particle. The value d of the prepared samples is around 38 nm. The lattice parameters are showed in Table 1.
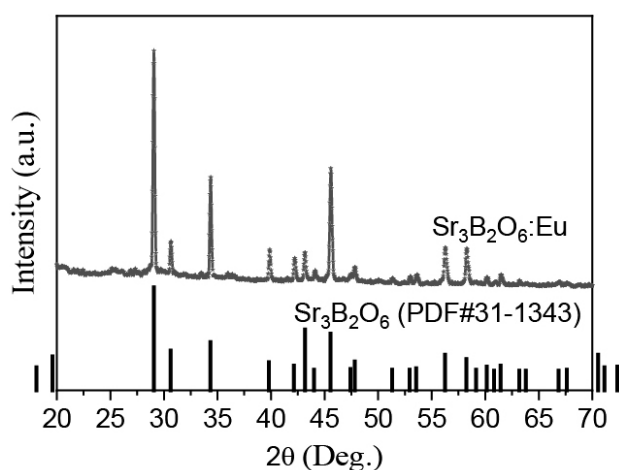
Figure 1. XRD patterns of $Sr_3B_2O_6$:Eu^{2+}.

Table 1 Structural parameters of SAS:Eu^{3+} sample.

Sample	$Sr_3B_2O_6$:Eu^{2+}
Crystal system	Rhombohedral
Space group	R3c
a	9.046 Å
b	9.046 Å
c	12.566 Å
α=β	90°
γ	120°
Crystal size	38 nm

3.2 Luminescence and thermoluminescence (TL) study of $Sr_3B_2O_6$:Eu^{2+}

The PLE and PL spectra at rom temperature of Eu^{2+} activated $Sr_3B_2O_6$ lattice are shown in Figure 2. The emission of Eu^{2+} excited by the 435 nm radiation (Fig. 2.b) is a broad band peaking at 574 nm which results from the transition from the $4f^{n-1}5d$ excited state to the $4f^n$ ground state of electron. The PLE spectrum recorded at the 574 nm emission wavelength is a broad band from 275 nm to 500 nm which is assigned to $4f^n{\rightarrow}4f^{n-1}5d$ transition of Eu^{2+} ion. The yellow emission and the broad-band excitation suggested that $Sr_3B_2O_6$:Eu^{2+} phosphor can be applied on wLED when it is pumped by blue LED or near UV-LEDs. Besides that, Fig. 2.b also showed the large bandwidth of the emission spectra of 3017 cm^{-1} which is one of the characteristic indicating the presence of anomalous emission [10, 11].
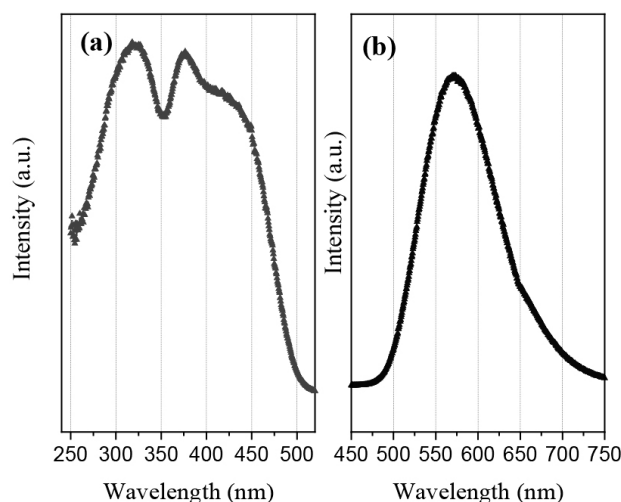
Figure 2. PLE and PL spectra of $Sr_3B_2O_6$:Eu^{2+}.

Several earlier studies showed that there is a relationship between the presence of anomalous emission and the location of the excited 5d levels of Ln^{2+} ions relative to the conduction band [10, 11]. The energy difference between the 5d levels and the conduction band of the host crystal can be calculated from the thermal quenching of emission spectra [12-14]. PL spectra of $Sr_3B_2O_6$:Eu^{2+}as a function of measurement temperature is illustrated in Fig. 3a. The emission spectra did not change the position of peak and its intensity decreased with increasing measurement temperature. The correlation between the intensity I(T) of $5d{\rightarrow}4f$ emission and temperature T is given [15, 16]:

$$I(T) = \frac{I_0}{1 + A\exp\left(\frac{-\Delta E}{kT}\right)}, \qquad (1)$$

where I_0 is the initial intensity, $I(T)$ is the intensity at a given temperature T, A is a constant, ΔE is the activation energy for thermal quenching, and k is Boltzmann's constant (8.617×10^{-5} eV K^{-1}). Based on eq.1, Fig. 3b plots ln $[(I_0/I)-1]$ variation dependency of $1/(kT)$. The fitted line gives the slope which is also ΔE of 0.429 eV. This is the energy barrier for the thermal quenching of luminescence in $Sr_3B_2O_6$:Eu^{2+}.
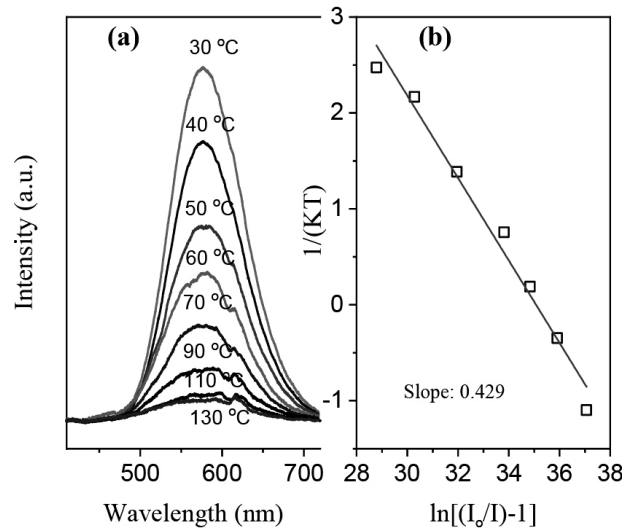
Figure 3. PL of $Sr_3B_2O_6$:Eu_{2+} sample at various temperature.

The presence of anomalous emission in some materials can be explained by the impurity-traped exciton mode [12, 17]. Hence, the TL glow curve of $Sr_3B_2O_6$:Eu^{2+} sample was investigated to determine the presence of traps in host lattice. Sample irradiated by a beta-source of ^{90}Sr with the dose of 3 Gy. TL glow curve of sample which was recorded by using Harshaw 3500 TLD reader with linear heating rate of 2 ^{0}Cs^{-1} is shown in Fig.4. The TL glow curve includes a single peak at 160°C

and the activation energy E_a is calculated by the initial-rise method. In this method, the initial rise part of a glow curve depends exponentially on temperature according to

$$I(t) = const.\exp(-E_a / kT). \qquad (2)$$

When a plot of $\ln(I)$ versus $1/T$ is made over this initial rise region, then a straight line with slope $-E_a$/k is obtained, so the activation energy E_a is found. The activation energy from the glow curve of $Sr_3B_2O_6$:Eu^{2+} is around 0.95 eV.
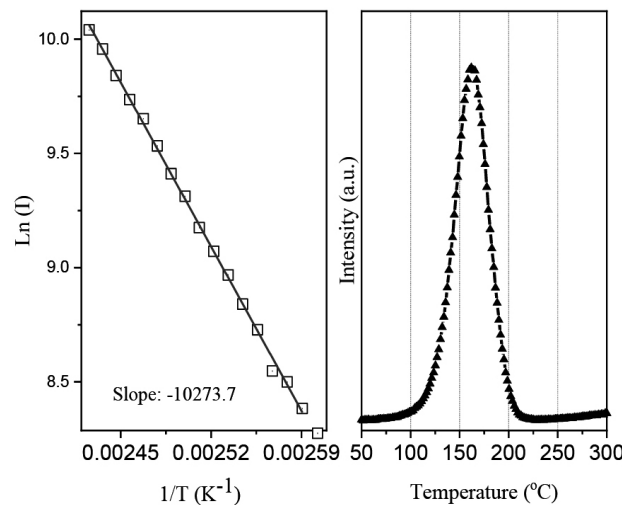
Figure 4. TL glowcurve (a) and the initial rise method to calculate the activation energy (b) of $Sr_3B_2O_6$:Eu^{2+}.

3.3 Anomalous photoluminescence in $Sr_3B_2O_6$:Eu^{2+}

It is known that europium ions doped materials are in trivalent or divalent states

depend the prepared condition. Luminescence of the trivalent state is from the 4f→4f transitions and it has the red light with a number of narrow lines. While the luminescence of the divalent

state is a broad-band emission which is due to the 5d→4f transitions and its color depends on the crystal field. Dorenbos distinguishes two types of broadband emission: "normal" and "anomalous" emission. In the case of the normal emission, the 5d→4femission has the common Stokes shift (ΔS) and the bandwidth (Γ) about 1350 and 1600 cm^{-1}, respectively [18]. While anomalous emissions characterized by a much larger Stokes shift ($\Delta S(2+, X)> 4000$ cm^{-1}), a much larger bandwidth ($\Gamma>3000$ cm^{-1}), deviant temperature quenching and decay profile [10, 11]. For $Sr_3B_2O_6$:Eu^{2+}, the Stokes shift and the bandwidth of the emission spectra are 5567 cm^{-1} and 3017 cm^{-1}, respectively. Therefore, from the viewpoint of the large Stokes shift, the large emission bandwidth and the temperature quenching profile, the observed emission of $Sr_3B_2O_6$:Eu^{2+} is anomalous.

According to the studies of anomalous emission, the location of 5d levels relative to the conduction band and the phenomenon of "anomalous" emission are relative to each other. This is explained by the impurity-traped exciton model [12, 17] in Fig. 5. For normal emission, Eu^{2+} excited level located well below the conduction band edge and there is no low-energy crossing possible between the Eu^{2+} excited level and the conduction band. Whereas, in the anomalous emission, upon excitation of Eu^{2+} ion [transition (1)], it becomes autoionized and an impurity-traped exciton is created [transitions (2) and (3)]. The above result of TL study showed the presence of the traps near the conduction band with the activation energy of 0.95 eV. When the localized levels of the impurity ion are excited, the excitation leads either to radiationor to nonradiation decay into the lower energy levels. Generally, when an electron from the lowest excited state makes a transition into ground state the emission is observed. On the other hand, when the excited level locates above the exciton energy

then it may first decay upto the exciton level and then it makes an emission from this level to the ground state [transition (4)]. This makes the large redshift in the emission spectra.
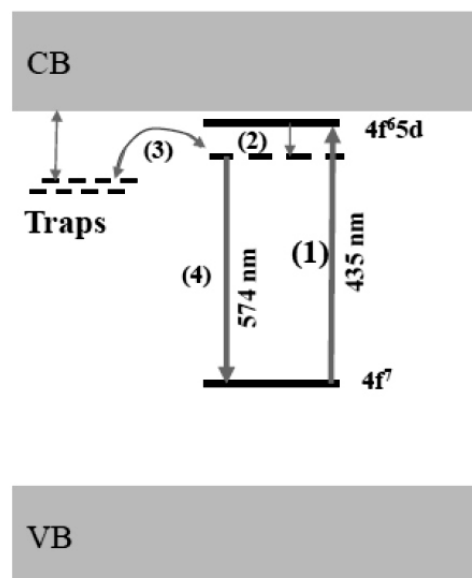
Figure 5. Energy- level scheme for anomalous emission in $Sr_3B_2O_6$:Eu_{2+}.

4. Conclusion

$Sr_3B_2O_6$:Eu^{2+} phosphor was successful synthesized by combution method and it's yellow emission is a broad band peaking at 574 nm. The Stokes shift and the bandwidth of the emission spectra are 5567 cm^{-1} and 3017 cm^{-1}. The results of luminescence and glow curve indicated the luminescence of Eu^{2+}-doped $Sr_3B_2O_6$ was anomalous emission and this emission was relative to the presence of the traps in this host lattice.

References

[1] T. Shalapska, P. Dorenbos, A. Gektin, G. Stryganyuk, A. Voloshinovskii, Luminescence spectroscopy and energy level location of lanthanide ions doped in La(PO$_3$)$_3$, Journal of Luminescence, 155 (2014) 95-100.

[2] P. Dorenbos, Thermal quenching of Eu^{2+} 5d–4f luminescence in inorganic compounds, Journal of Physics: Condensed Matter, 17 (2005) 8103-8111.

[3] W.-S. Song, Y.-S. Kim, H. Yang, Yellow-emitting phosphor of Sr$_3$B$_2$O$_6$:Eu^{2+} for application to white light-emitting diodes, Materials Chemistry and Physics, 117 (2009) 500-503.

[4] C.-K. Chang, T.-M. Chen, Sr$_3$B$_2$O$_6$:Ce^{3+},Eu^{2+}:

A potential single-phased white-emitting borate phosphor for ultraviolet light-emitting diodes, Applied Physics Letters, 91 (2007) 081902.

[5] S. Hoon Jung, D. Seok Kang, D. Young Jeon, Effect of substitution of nitrogen ions to red-emitting $Sr_3B_2O_{6-3/2x}N_x:Eu^{2+}$ oxy-nitride phosphor for the application to white LED, Journal of Crystal Growth, 326 (2011) 116-119.

[6] H. Liu, Z. Guo, Ce^{3+} and Dy^{3+} doped $Sr_3B_2O_6$: Solid state synthesis and tunable luminescence, Journal of Luminescence, 187 (2017) 181-185.

[7] S. Khursheed, V. Kumar, V.K. Singh, J. Sharma, H.C. Swart, Optical properties of $Sr_3B_2O_6:Dy^{3+}$ /PMMA polymer nanocomposites, Physica B: Condensed Matter, 535 (2017) 184-188.

[8] K.-W. Chae, T.-R. Park, C. Cheon, II, J.S. Kim, Persistent luminescence of RE^{3+} co-doped $Sr_3B_2O_6:Eu^{2+}$ yellow phosphors (RE = Nd, Gd, Dy), Journal of Luminescence, 194 (2018) 649-655.

[9] S. Som, M. Chowdhury, S.K. Sharma, Band gap and trapping parameters of color tunable Yb^{3+}/Er^{3+} codoped Y_2O_3 upconversion phosphor synthesized by combustion route, Journal of Materials Science, 49 (2013) 858-867.

[10] P. Dorenbos, Anomalous luminescence of Eu^{2+} and Yb^{2+} in inorganic compounds, Journal of Physics: Condensed matter, 15 (2003) 2645-2665.

[11] B.P. Kore, N.S. Dhoble, S.J. Dhoble, Study of anomalous emission and irradiation effect on the thermoluminescence properties of barium aluminate, Journal of Luminescence, 150 (2014) 59-67.

[12] P.F. Smet, J.E. Van Haecke, F. Loncke, H. Vrielinck, F. Callens, D. Poelman, Anomalous photoluminescence inBaS:Eu, Physical Review B, 74 (2006).

[13] X. Qin, X. Liu, W. Huang, M. Bettinelli, X. Liu, Lanthanide-Activated Phosphors Based on 4f-5d Optical Transitions: Theoretical and Experimental Aspects, Chemical reviews, 117 (2017) 4488-4527.

[14] C.W.E.v. Eijk, Novel γ-ray and thermal-neutron scintillators search for high-light yield and fast-response materials, IOS Press, Amsterdam, The Netherlands, 2007.

[15] F.C. Lu, L.J. Bai, W. Dang, Z.P. Yang, P. Lin, Structure and Photoluminescence of Eu^{2+} Doped $Sr_2Al_2SiO_7$ Cyan-Green Emitting Phosphors, ECS Journal of Solid State Science and Technology, 4 (2014) R27-R30.

[16] J.Y. Han, W.B. Im, G.-y. Lee, D.Y. Jeon, Near UV-pumped yellow-emitting Eu^{2+}-doped $Na3K(Si_{1-x}Al_x)_8O_{16\pm\delta}$ phosphor for white-emitting LEDs, Journal of Materials Chemistry, 22 (2012) 8793.

[17] V. Bachmann, T. Jüstel, A. Meijerink, C. Ronda, P.J. Schmidt, Luminescence properties of $SrSi_2O_2N_2$ doped with divalent rare earth ions, Journal of Luminescence, 121 (2006) 441-449.

[18] P. Dorenbos, Energy of the first $4f^7$-$4f^65d$ transition of Eu^{2+} in inorganic compounds, journal of Luminescence, 104 (2003) 239-260.

Newton-PGMRES Method for Integrated Hydrologic Models

Phương pháp Newton-PGMRES cho các mô phỏng thủy lợi kết hợp

Thai An Nguyen, Trung Hieu Nguyen*, Quoc Hung Phan
Nguyễn Thái An, Nguyễn Trung Hiếu, Phan Quốc Hưng

Institute of Research and Development, Duy Tan University, 03 Quang Trung, Danang, Vietnam
Viện Nghiên cứu và Phát triển Công nghệ cao, Đại học Duy Tân, 03 Quang Trung, Đà Nẵng, Việt Nam

Abstract

We investigate the use of the Newton-PGMRES method for solving nonlinear systems arising from integrated hydrologic models. We propose a new termination scheme based directly on the PGMRES residual norm. The effectiveness of the resulting modified Newton-PGMRES method is demonstrated by solving nonlinear systems of equations arising from transient simulations of the Integrated Water Flow Model (IWFM), a water resources management and planning model developed by California Department of Water Resources. For two real-world IWFM simulations, the proposed modified Newton-PGMRES method reduces the number of outer Newton iterations by up to 20% and consequently reduces the total simulation time by up to 10%.

Keywords: Newton-PGMRES, Newton method, GMRES, IWFM.

Tóm tắt

Trong bài báo này, chúng tôi nghiên cứu các phương pháp Newton-PGMRES để giải phương trình phi tuyến xuất hiện trong các mô phỏng thủy lợi dạng kết hợp. Một cách tiếp cận mới trong việc xây dựng điều kiện dừng của phương pháp PGMRES được đề xuất. Tính hiệu quả của cải tiến này được thể hiện qua việc giải các phương trình phi tuyến trong IWFM, một gói phần mềm quản lý và lên kế hoạch trong việc sử dụng tài nguyên nước được phát triển bởi phòng Tài nguyên nước bang California. Trong hai mô phỏng thực tế bằng IWFM, phương pháp cải tiến giúp giảm 20% số bước lặp Newton và 10% thời gian mô phỏng.

Từ khóa: Newton-PGMRES, phương pháp Newton, GMRES, IWFM.

1. Introduction

In integrated hydrologic models, the following systems of nonlinear equations need to be solved:

$$F(x) = 0, \qquad (1)$$

where $F : \mathbb{R}^n \to \mathbb{R}^n$ is a nonlinear function. Newton-type or gradient-based methods are generally regarded as being very efficient for solving this type of system [13] when F is continuously differentiable everywhere in $\mathbb{R}^n$. When applied to (1) with the initial guess x_0, the Newton method iteratively builds a sequence of approximate so-

Email: nguyentrunghieu14@dtu.edu.vn

lutions $\{x_k\}$. Specifically, the approximate solution x_{k+1} at $(k+1)$ iteration is generated by

$$x_{k+1} = x_k + s_k, \qquad (2)$$

where the update direction s_k is the solution of the system of linear equations

$$J(x_k)s_k = -F(x_k), \qquad (3)$$

and $J(x_k)$ is the Jacobian of F at x_k. The Newton method converges locally with quadratic rate of convergence, provided the Jacobian is Lipschitz continous at the solution. Comprehensive studies of the Newton method can be found, for example, in [15, 10, 9].

In practice, solving (3) to a high accuracy in every Newton iteration might be computationally expensive and unnecessary, especially in the early iterations. In [6], an inexact Newton method is proposed to solve the linear system (3) up to an accuracy controlled by the so-called *forcing term* η_k, i.e., finding s_k such that

$$\|r_k\| = \|F(x_k) + J(x_k)s_k\| \le \eta_k \|F(x_k)\| \equiv \tau_k, \quad (4)$$

where the vector $r_k = F(x_k) + J(x_k)s_k$ is the residual of (3), as well as a local linear model of F evaluated at x_k. The forcing term η_k sets the accuracy of the update direction s_k. It is proven that the inexact Newton method converges locally and superlinearly under the proper choice of η_k [6].

For solving the linear systems (3), Krylov subspace projection methods have a distinct advantage over direct methods for large-dimension problems because they use less numerical computation and require little matrix storage [4, 5]. When the linear system (3) is non-symmetric, the Generalized Minimum Residual algorithm with Preconditioning (PGMRES) is commonly used. The combined scheme is called a Newton-PGMRES method [16, 4, 1]. In this case, the update direction s_k is a solution of the preconditioned linear system

$$M_k^L J(x_k) M_k^R (M_k^R)^{-1} s_k = -M_k^L F(x_k), \qquad (5)$$

where M_k^L and M_k^R are the left- and right-preconditioners, respectively. A survey of the Newton-PGMRES method and other Newton-Krylov methods can be found in [11].

When the Newton-PGMRES method uses only right-preconditioning (i.e., $M_k^L = I$), the residual norm of an approximate solution s_k is unchanged. The termination criterion (4) is still applicable. However, when a left-preconditioner is used, the residual norm with respect to the original system (3) is no longer available directly. Consequently, the criterion (4) is not immediately applicable. In order to use (4), additional computation is necessary to explicitly formulate the approximate solution s_k and compute the corresponding residual norm of the original system (3). To the best of the authors' knowledge, it is still an open problem to derive a proper termination criterion for the PGMRES solver with left preconditioning such that the resulting inexact Newton-PGMRES method is provable to converge locally.

The contributions of this paper is as follows. For the inner PGMRES iteration, we propose an efficient termination scheme that is applicable to the left preconditioned systems. We formulate a stopping tolerance τ_k^P to directly control the preconditioned residual norm:

$$\|M_k [F(x_k) + J(x_k)s_k]\| \le \tau_k^P. \qquad (6)$$

This termination scheme is computationally inexpensive as the left-hand side of (6) is immediately available from PGMRES. In addition, under a mild assumption, we show that the resulting modified Newton-PGMRES method converges locally and superlinearly. The proposed stopping tolerance τ_k^P also reduces the number of outer Newton iterations significantly.

We have tested the proposed new schemes in the simulations of IWFM, a water resources management and planing application developed by the California Department of Water Resources [8]. IWFM is an integrated hydrologic model that simulates groundwater flow, surface water flow and groundwater-surface water interactions as well as other components of the hydrologic system. In IWFM, the discretized groundwater flow equation, stream flow equation and lake storage equation are implicitly coupled to form a system

of nonlinear equations. This nonlinear system is solved at each time step of an IWFM simulation. Solving the nonlinear systems is the most time-consuming components of IWFM, and accounts for about 80% of the total time in a typical IWFM simulation. Numerical experiments for two real-world simulations demonstrate that the new modified Newton-PGMRES method reduces the number of Newton iterations by up to 20% and the simulation time by up to 10%.

2. Newton-PGMRES method

At the kth Newton iteration, when the PGMRES algorithm [16] is applied to the left preconditioned linear system of equations

$$M_k J(x_k) s_k = -M_k F(x_k), \qquad (7)$$

it first builds an orthonormal matrix $V_{j+1} = [v_1 \, v_2 \, \ldots \, v_j \, v_{j+1}]$ whose column vectors form a basis for the Krylov subspace $\mathscr{K}_j$ generated by the matrix $M_k J(x_k)$ and the residual vector $r_0 = -M_k(F(x_k) + J(x_k)s_k^{(0)})$, where $s_k^{(0)}$ is an initial guess of s_k. This phase is referred to as the Arnoldi procedure. In matrix notation, the Arnoldi procedure can be expressed as

$$M_k J(x_k) V_j = V_{j+1} \bar{H}_j,$$

where $\bar{H}_j = \{h_{i,l}\}$ is a $(j+1) \times j$ upper Hessenberg matrix, and $V_{j+1} = [V_j \, v_{j+1}]$. Then the jth PGMRES approximation $s_k^{(j)}$ is

$$s_k^{(j)} = s_k^{(0)} + V_j y_*,$$

where $y_* \in \mathbb{R}^j$ is the solution of the least squares problem:

$$y_* = \underset{y \in \mathbb{R}^j}{\mathrm{argmin}} \| \beta e_1 - \bar{H}_j y \|, \qquad (8)$$

with $\beta = \|r_0\|$ and $e_1 = [1 \, 0 \, \ldots \, 0]^T$.

Combining the inexact Newton method with PGMRES leads to the Newton-PGMRES algorithm (Algorithm 1) for solving the nonlinear system of equations (1), where for the simplicity of exposition, PGMRES is presented without restarting.

Algorithm 1 Newton-PGMRES algorithm

1: Let x_0, $0 < \theta_{min} < \theta_{\max} < 1$ and $t \in (0, 1)$ be given
2: NEWTON_CONV = `false`
3: **for** $k = 0, 1, \ldots$ **until** NEWTON_CONV **do**
4:     Compute $\eta_k \in (0, 1)$ and set $\tau_k = \eta_k \|F(x_k)\|$
5:     Set $s_k^{(0)} = \vec{0}$
6:     $v_1 = r_0/\beta$, where $r_0 = -M_k(F(x_k) + J(x_k)s_k^{(0)})$ and $\beta = \|r_0\|$.
7:     PGMRES_CONV = `false`
8:     **for** $j = 1, 2, \ldots$ **until** PGMRES_CONV **do**
9:         $w = M_k J(x_k) v_j$
10:         **for** $i = 1, 2, \ldots$ **to** j **do**
11:             $w = w - h_{i,j} v_i$, where $h_{i,j} = (w, v_i)$
12:         **end for**
13:         $h_{j+1,i} = \|w\|$ and $v_{j+1} = w/h_{j+1,i}$
14:         Solve the least squares problem (8) for y_*
15:         Compute $s_k^{(j)} = s_k^{(0)} + V_j y_*$
16:         Compute $\|r_k\| = \|J(x_k)s_k^{(j)} + F(x_k)\|$
17:         **if** $\|r_k\| \le \tau_k$ **then**
18:             PGMRES_CONV = `true`
19:         **end if**
20:     **end for**
21:     $s_k = s_k^{(j)}$
22:     **while** $\|F(x_k + s_k)\| > [1 - t(1 - \eta_k)]\|F(x_k)\|$ **do**
23:         Choose $\theta \in [\theta_{\min}, \theta_{\max}]$
24:         Update $s_k \leftarrow \theta s_k$ and $\eta_k \leftarrow (1 - \theta(1 - \eta_k))$
25:     **end while**
26:     Update $x_{k+1} = x_k + s_k$
27:     **if** $\|F(x_{k+1})\|/\|F(x_0)\| \le \tau_1^N$ or $\|x_{k+1} - x_k\| \le \tau_2^N$, **then**
28:         NEWTON_CONV = `true`
29:     **end if**
30: **end for**

Algorithm 1 has several drawbacks. First, the termination criterion (4) is not appropriate for multiscale simulations. It is imposed on the original system which has variables spanning a

wide range of magnitudes. It is more sensitive to changes in the variables of large scale, which can cause premature termination before the variables of small scales are solved up to the desired accuracy. Furthermore, the tolerance τ_k is formulated to protect against over-solving the inner linear systems. It can be so loose that there are only two or three PGMRES iterations per Newton iteration. This is inefficient for applications where the exclusive cost of an outer iteration is comparable or even higher than that of an inner PGMRES iteration.

Second, when the PGMRES algorithm with left preconditioning is used, the residual norm of the approximation $s_k^{(j)}$ is given by the residual norm of the least squares problem:

$$\|r_k^P\| = \|M_k(J(x_k)s_k^{(j)} + F(x_k))\| = \|\beta e_1 - \bar{H}_j y_*\|, \tag{9}$$

which is readily available at every PGMRES iteration. However, since the termination criterion (4) only requires the residual norm $\|r_k\|$ of the original system, $\|r_k^P\|$ is not used. In addition, it is expensive to compute the residual norm $\|r_k\|$ as the corresponding approximate solution s_k need to be formed explicitly in every PGMRES iteration.

3. Modified Newton-PGMRES method

To address the drawbacks of Algorithm 1 we propose a modified Newton-PGMRES algorithm (Algorithm 2). The most notable features of the modified algorithm is a redesigned termination criterion for the inner PGMRES iteration.

Let us first discuss the formulation of the stopping tolerance τ_k^P for the inner iteration (line 14 of Algorithm 2):

$$\|r_k^P\| \leq \tau_k^P. \tag{10}$$

Note that the residual r_k of the original system and the residual r_k^P of the preconditioned system is related by

$$r_k = M_k^{-1} r_k^P.$$

By taking the norm and applying (10), we have

$$\|r_k\| \leq \|M_k^{-1}\| \|r_k^P\| \leq \|M_k^{-1}\| \tau_k^P \equiv \eta_k^M \|F(x_k)\|, \tag{11}$$

where the forcing term is

$$\eta_k^M = \frac{\|M_k^{-1}\| \tau_k^P}{\|F(x_k)\|}. \tag{12}$$

Therefore, to guarantee the local convergence of Algorithm 2, τ_k^P should be chosen so that $\eta_k^M \leq \eta_{\max}^M < 1$ for all k.

Algorithm 2 Modified Newton-PGMRES algorithm

1: Let x_0 be given
2: NEWTON_CONV = false
3: **for** $k = 0, 1, \ldots$ **until** NEWTON_CONV **do**
4:     Compute τ_k^P
5:     Set $s_k^{(0)} = \vec{0}$
6:     $v_1 = r_0/\beta$, where $r_0 = -M_k(F(x_k) + J(x_k)s_k^{(0)})$ and $\beta = \|r_0\|$.
7:     PGMRES_CONV = false
8:     **for** $j = 1, 2, \ldots$ **until** PGMRES_CONV **do**
9:         $w = M_k J(x_k) v_j$
10:         $h_{i,j} = (w, v_i), \ i = 1, 2, \cdots, j$
11:         $\hat{v}_{j+1} = w - \sum_{i=1}^{j} h_{i,j} v_i$
12:         $h_{j+1,i} = \|\hat{v}_{j+1}\|$ and $v_{j+1} = \hat{v}_{j+1}/h_{j+1,i}$
13:         Solve the least squares problem (8) for y_* and obtain the residual norm $\|r_k^P\|$
14:         **if** $\|r_k^P\| \leq \tau_k^P$ **then**
15:             PGMRES_CONV = true
16:         **end if**
17:     **end for**
18:     Compute $s_k^{(j)} \equiv s_k^{(0)} + V_j y_*$
19:     $s_k = s_k^{(j)}$
20:     Compute damping factor θ_k
21:     Update $x_{k+1} = x_k + \theta_k s_k$
22:     **if** $((\|F(x_{k+1})\|/\|F(x_0)\| \leq \tau_1^N)$ or $(\|x_{k+1} - x_k\| \leq \tau_2^N))$ **then**
23:         NEWTON_CONV = true
24:     **end if**
25: **end for**

To this end, we propose the following formulation for the stopping tolerance

$$\tau_k^P = \gamma_M \xi_k^M \frac{\|F(x_k)\|}{\|F(x_0)\|} \text{ for } k \geq 0, \tag{13}$$

where γ_M is defined as

$$\gamma_M = \min_{k \geq 0} \left\{ \frac{\|F(x_0)\|}{\|M_k^{-1}\|} \right\}. \quad (14)$$

In the formulation of τ_k^P in (13), ξ_k^M plays the role of the forcing term, adjusting τ_k^P adaptively based on the current progress towards a solution. The factor $\|F(x_k)\|/\|F(x_0)\|$ is the relative reduction ratio of the function F. It defines the asymptotically behavior of τ_k^P.

From (13) and (14), we have

$$\begin{aligned}
\tau_k^P &\leq \frac{\|F(x_0)\|}{\|M_k^{-1}\|} \xi_k^M \frac{\|F(x_k)\|}{\|F(x_0)\|} \\
&= \xi_k^M \frac{\|F(x_k)\|}{\|M_k^{-1}\|} \\
&\leq \xi_k^M \frac{\|M_k^{-1}\| \|M_k F(x_k)\|}{\|M_k^{-1}\|} \\
&= \xi_k^M \|M_k F(x_k)\|. \quad (15)
\end{aligned}$$

Note that the quantity $\|M_k F(x_k)\|$ is the residual norm corresponding to the GMRES initial guess $s_k^{(0)} = \vec{0}$, i.e.,

$$\|r_k^P(s_k^{(0)})\| = \|M_k(J(x_k)\vec{0} + F(x_k))\| = \|M_k F(x_k)\|. \quad (16)$$

Hence, if $\sigma < 1$, then at least a few GMRES iterations are performed at each Newton iteration.

By (12), (13) and (14), the forcing term η_k^M satisfies:

$$\begin{aligned}
\eta_k^M &\leq \frac{\|M_k^{-1}\|}{\|F(x_k)\|} \frac{\|F(x_0)\|}{\|M_k^{-1}\|} \xi_k^M \frac{\|F(x_k)\|}{\|F(x_0)\|} \\
&= \xi_k^M. \quad (17)
\end{aligned}$$

In general, ξ_k^M should be chosen to be uniformly bounded by 1: $\xi_k^M \leq \xi_{\max} < 1$. This guarantees that Algorithm 2 converges locally and superlinearly since $\eta_k^M \leq \eta_{\max} = \xi_{\max} < 1$. However, to avoid the over-solving, σ should not be chosen too small. The choice with $\sigma = 10^{-2}$ was found to be very competitive in our experiments.

In practice, it is sufficient to find an estimate for the formulation of γ_M in (14). If M_k is an incomplete LU (ILU) preconditioner, it is easy to obtain an estimate of $\|M_k^{-1}\|$ [17, 12]. As k varies

the change in the condition number of ILU preconditioner M_k can be controlled by adaptively adjusting the process of dropping small entries [2, 3]. If the change in $\|M_k^{-1}\|$ is not significant, we can effectively use the minimization in (14) over only first few values of k to calculate γ_M. This approach is shown to be efficient in our numerical experiments.

Since there might be temporary increases in $\|F(\cdot)\|$ that make it exceed $\|F(x_0)\|$, i.e., $\|F(x_{k-1})\| > \|F(x_0)\|$, or τ_k^P becomes too small, a safeguarding stopping tolerance τ_k^P for the inner PGMRES loop is given by

$$\tau_k^P = \max \left\{ \tau_{\min}, \frac{\sigma \gamma_M \|F(x_k)\|}{(1+k)^\rho \max\{\|F(x_0)\|, \|F(x_{k-1})\|\}} \right\}, \quad (18)$$

where $\tau_{\min}$ sets the smallest tolerance. The default is $\tau_{\min} = 10^{-6}$.

4. Numerical experiments

In this section, we illustrate the effectiveness of the modified Newton-PGMRES method (Algorithm 2) for solving nonlinear systems of equations arising from IWFM simulations (version 3.02). In IWFM, the conservation equation for a multi-layer aquifer system is discretized by the finite element method [8]. IWFM preserves the nonlinear aspects of the surface and subsurface flow processes, and must therefore solve a system of nonlinear equations at every time step. Two real-world simulations C2V and Walla are used for numerical experiments. C2V is a simulation for the Central Valley of California, while Walla is a simulation for the Walla Walla basin in Oregon. More details can be found in [8, 7, 14].

Table 1 shows the total numbers of outer Newton iterations and inner PGMRES iterations and CPU elapsed time for three algorithms for solving sequences of nonlinear systems. The CPU elapsed time is for the entire simulation, including initialization and data I/O. From Table 1, we observe that the modified Newton-PGMRES algorithm uses about 50% more inner PGMRES iterations but about 20% fewer outer Newton iterations than the Newton-PGMRES algorithm does. The overall IWFM simulations with the

		NP τ_k	MNP τ_k^P
C2V	Time steps	372	372
	Newton iters.	8042	6457
	GMRES iters.	22308	32687
	Time(sec.)	126	113
Walla	Time steps	1096	1096
	Newton iters.	33836	27556
	GMRES iters.	72813	117148
	Time (sec.)	6283	5569

Bảng 1. Performance of Newton-PGMRES (NP) and modified Newton-PGMRES (MNP)

modified Newton-PGMRES algorithm perform better for both examples and reduce the total simulation time by about 10%.

5. Concluding remarks

In this paper, we studied the use of the double-loop Newton-PGMRES method. We proposed a new termination scheme for the inner PGMRES loop that is applicable for the left-preconditioned linear systems. The modified Newton-PGMRES method resolves important numerical constraints and has reduced the computational time for the IWFM simulation of realistic integrated hydrologic systems. Therefore, the proposed modified Newton-PGMRES method is a good alternative in solving nonlinear systems arising from integrated hydrologic models.

References

[1] Stefania Bellavia and Benedetta Morini. A globally convergent Newton-GMRES subspace method for systems of nonlinear equations. *SIAM J. Sci. Comput.*, 23(3):940–960, 2001.

[2] M. Bollhofer. A robust ILU with pivoting based on monitoring the growth of the inverse factors. *Linear Algebra and its Applications*, 338(1-3):201–218, 2001.

[3] M. Bollhofer and Y. Saad. Multilevel preconditioners constructed from inverse-based ILUs. *SIAM Journal on Scientific Computing*, 27(5):1627–1650, 2006.

[4] Peter N. Brown and Youcef Saad. Hybrid Krylov methods for nonlinear systems of equations. *SIAM J. Sci. Statist. Comput.*, 11(3):450–481, 1990.

[5] Peter N. Brown and Youcef Saad. Convergence theory of nonlinear Newton-Krylov algorithms. *SIAM J. Optim.*, 4(2):297–330, 1994.

[6] Ron S. Dembo, Stanley C. Eisenstat, and Trond Steihaug. Inexact Newton methods. *SIAM J. Numer. Anal.*, 19(2):400–408, 1982.

[7] Matthew F. Dixon, Zhaojun Bai, Charles F. Brush, Francis I. Chung, Emin C. Dogrul, and Tariq N. Kadir. Error control of iterative linear solvers for integrated groundwater models. *Ground Water*, 49(6):859–865, November/December 2011.

[8] Emin C. Dogrul and Tariq N. Kadir. Integrated Water Flow Model (IWFM v3.02) – Theoretical documentation. Technical report, Integrated Hydrological Models Development Unit, Modeling Support Branch, Bay-Delta Office, California State Department of Water Resources, 2011.

[9] C. T. Kelley. *Iterative methods for linear and nonlinear equations*, volume 16 of *Frontiers in Applied Mathematics*. SIAM, Philadelphia, PA, 1995.

[10] C. T. Kelley. *Solving nonlinear equations with Newton's method*. Fundamentals of Algorithms. SIAM, Philadelphia, PA, 2003.

[11] D. A. Knoll and D. E. Keyes. Jacobian-free Newton-Krylov methods: a survey of approaches and applications. *J. Comput. Phys.*, 193(2):357–397, 2004.

[12] X.S. Li and M. Shao. A supernodal approach to incomplete LU factorization with partial pivoting. *ACM Transactions on Mathematical Software (TOMS)*, 37(4):43:1–20, 2011.

[13] Steffen Mehl. Use of Picard and Newton iteration for solving nonlinear ground water flow equations. *Ground Water*, 44(4):583–594, 2006.

[14] Hieu Nguyen, Zhaojun Bai, Charles F. Brush, Francis I. Chung, Emin C. Dogrul, and Tariq N. Kadir. Adaptive accuracy control of nonlinear newton-krylov methods for multiscale integrated hydrologic models. In *XIX International Conference on Computational Methods in Water Resources*, pages 1–8, Illinois, USA, 2012. Submitted.

[15] J. M. Ortega and W. C. Rheinboldt. *Iterative solu-*

tion of nonlinear equations in several variables, volume 30 of *Classics in Applied Mathematics*. SIAM, Philadelphia, PA, 2000. (Reprint of the 1970 original).

[16] Youcef Saad and Martin H. Schultz. GMRES: a generalized minimal residual algorithm for solving non-symmetric linear systems. *SIAM J. Sci. Statist. Comput.*, 7(3):856–869, 1986.

[17] Yousef Saad. ILUT: a dual threshold incomplete *LU* factorization. *Numer. Linear Algebra Appl.*, 1(4):387–402, 1994.

Enhancement of CO_2 capture by using nitric acid treated pine cone biomass

Tăng cường khả năng loại bỏ CO_2 bằng cách sử dụng axit nitric hoạt hóa sinh khối quả thông

Pham Thi Huong[a,*], JiTae Kim[a], Nguyen Minh Viet[b]
Phạm Thị Hường, JiTae Kim, Nguyễn Minh Việt

[a]Center for advanced Chemistry, Insitute of Reseach and Development, Duy Tan University, Danang, Vietnam
Trung tâm Hóa tiên tiến, Viện Nghiên cứu và Phát triển, Trường Đại học Duy Tân, Đà Nẵng, Việt Nam
[b]VNU Key Laboratory of Advanced Materials for Green Growth, University of Science, Hanoi National University, Hanoi, Vietnam
Phòng Thí nghiệm trọng điểm Vật liệu tiên tiến ứng dụng trong phát triển xanh, Trường Đại học Khoa học Tự nhiên, Đại học Quốc gia Hà Nội, Hà Nội, Việt Nam

Abstract

This study investigated the potential application of nitric acid treated pine cone biomass (HNO_3-PC) for capturing CO_2 in the air. The basics physical-chemical properties of PC and HNO_3-PC were determined by surface morphology (SEM), Surface functional group (FTIR), Surface area (BET) and elemental analysis (EA). The CO_2 capture process was done by mixtures containing 20% by volume CO_2 and 80% by volume N_2 in a temperature range of 20-60°C along with pressure 0.1-1.5 atm. The adsorption capacity of CO_2 on HNO_3-PC was 3.9 mmol/g which is much higher than that of untreated pine cone (1.6 mmol/g). Based on these findings, HNO_3-PC could be utilized as promising low-cost adsorbent for CO_2 capturing in the air.

Keywords: pine cone biomass, Nitric acid treated, CO_2 capture, adsorption cost.

Tóm tắt

Nghiên cứu này nhằm mục đích đánh giá tiềm năng ứng dụng của quả thông sau khi được xử lý bằng axit nitric (HNO_3-PC) để loại bỏ khí CO_2 trong không khí. Các tính chất hóa lý cơ bản của PC và HNO_3-PC được kiểm tra thông qua các phương pháp đo: SEM, FTIR, BET và EA. Quá trình hấp thu CO_2 được thực hiện thông qua việc trộn hỗn hợp khí 20% CO_2 và 80% N_2 theo thể tích, trong điều kiện nhiệt độ từ 20-60°C cùng với áp suất 0,1-1,5 atm. Khả năng hấp phụ của CO_2 trên HNO_3-PC thu được là 3,9 mmol/g, kết quả này cao hơn nhiều so với sinh khối thông chưa được hoạt hóa (1,6 mmol/g). Dựa trên những kết quả nghiên cứu trên đây, HNO3-PC có tiềm năng để được sử dụng như một chất hấp phụ với chi phí thấp để loại bỏ CO_2 trong không khí.

Từ khóa: Sinh khối quả thông, Hoạt hóa bởi acid nitric, Hấp thu CO_2, Giá thành hấp phụ.

1. Introduction

The CO_2 emissions are responsible for almost 60 % of global warming and it is considered to be the paramount contributor to global warming and climate change [1-2]. According to the new annual data of the National Oceanic and Atmospheric Administration-Earth System Research Laboratory in the United States, the

Email: phamthihuong4@dtu.edu.vn

CO_2 level in the atmosphere has increased at 2.1 ppm per year over the past decade (2005-2014) and 1.9 ppm per year in the prior decade (1995-2004). The total CO_2 concentration in the atmosphere has been rapidly increasing from 280 (in 1995) to 398.55 ppm (in 2015) [3-5]. Such a rapid increase in CO_2 is also the driving force responsible for major climate change such as the increase in the average surface temperature of the earth [6]. Therefore, it is very important that proper mitigation measures are found to counteract CO_2 emissions through effective CO_2 capture.

Activated carbon is considered to be a promising adsorbent for capturing of CO_2 because of its characteristics such as high surface areas, porous structure, high stability and widely available source [7-8]. Forestry waste materials usually employed as adsorbent may have potential marketing advantage for adsorption process over other adsorbent types because they are of low cost, environmentally friendly, naturally available and efficient. Korea produces large amounts of pine cone biomass based on the high area of pine forestry (2.68 mil ha). Therefore, pine cone biomass have potential as low-cost adsorbent which can be applied in adsorption process (such as water treatment and air pollution control) by their natural or chemically modified forms.

The main aim of this study was to investigate potential application of pine cones biomass and HNO_3 treated pine cones for capturing of CO_2 from the air. The basic physical-chemicals properties of materials were identified by SEM, FTIR, BET and EA analysis. Also, the CO_2 adsorption capacity and selectively were determined.

2. Material and methods

2.1. Materials

All of the chemicals used in this study were of analytical reagent grade (obtained from Daejung Chemical and Metals Co. LTD., South Korea) and used as received without further purification.

Aqueous solutions of HNO_3 were prepared by dissolving HNO_3 in deionized distilled water.

PCs biomass were collected from mountainous area located 500 m from the University of Ulsan in Nam-gu, Ulsan, South Korea. After that, the PCs were washed with deionized water to remove impurities such as dirt, sand, and leaves then dried at 50°C for 24 h. The dried PCs were sieved using mesh (DA-354) to obtain a uniform particle size range between 50 and 100 μm. The sieved PCs were stored in an airtight plastic container until they were used for experiments.

50g of PC were mixed with 200 ml of 0.1M HNO_3 at room temperature for 3h. The HNO_3-PC was then filtered and repeatedly washed with distilled water. The resulting washed HNO_3-PC was dried 24 h in an oven at 30°C and used for characterization and CO_2 capture experiments.

2.2. Methods

Scanning electron micrographs were taken for the surface morphology analysis of PC and HNO_3-PC (SEM Hitachi 4700 microscope). Infrared spectra (Perkin – Elmer infrared spectrophotometer) were obtained using a Nicolet Nexus 470 FTIR spectrometer in the 4000–500 cm^{-1} region in transmission mode and IR samples were prepared in the form of pellets with KBr at ambient conditions. The specific surface area and porosity measurements of the PC and HNO_3-PC were carried out using adsorption isotherms obtained from the Micromeritics BET ASTP 2010 surface area and a porosity analyzer 27 at 77±0.5K under gas nitrogen atmosphere as well as by using the BET equation. The elemental analysis was performed using an elementary analyzer (Elementar Analysensysteme GmbH, Germany), and provided composition information of the PC and HNO_3-PC in terms of the weight fraction (wt %) of contained elements including carbon (C), hydrogen (H), oxygen (O), and nitrogen (N).

2.3. Design system for CO_2 adsorption experiments

Fig. 1 shows the CO_2 adsorption experimental setup. The system consisted of three parts: an adiabatic sorption column, a gaseous mixture system for controlling the composition and temperature of gaseous mixture, and a CO_2 analyzer. The temperature of the adsorption column could be adjusted and maintained at a constant value with an accuracy of ±0.05°C. In the adsorption experiments, 0.5 g of adsorbent was packed in the adsorption column (inner diameter (I.D) 2cm * length (L) 25cm). The composition of the gaseous mixture was adjusted

and controlled by a mass flow controller (MFC) which simultaneously controlled the flowrates of the two gases in the mixing chamber: CO_2 and N_2.

The PC and HNO_3-PC were first dried at 100°C in pure N_2 for 120 min to remove moisture and/ or other gases and then cooled down to the room temperature (20±1°C). After the temperature was stabilized, a mixture of CO_2 and N_2 was introduced into the sample chamber by using the MFC and the sample weight was recorded in order to calculate the CO_2 uptake. The CO_2 concentrations before and after passing the adsorption bed were monitored by an on-line CO_2 analyzer (Alpha Omega Instrument series 9610).
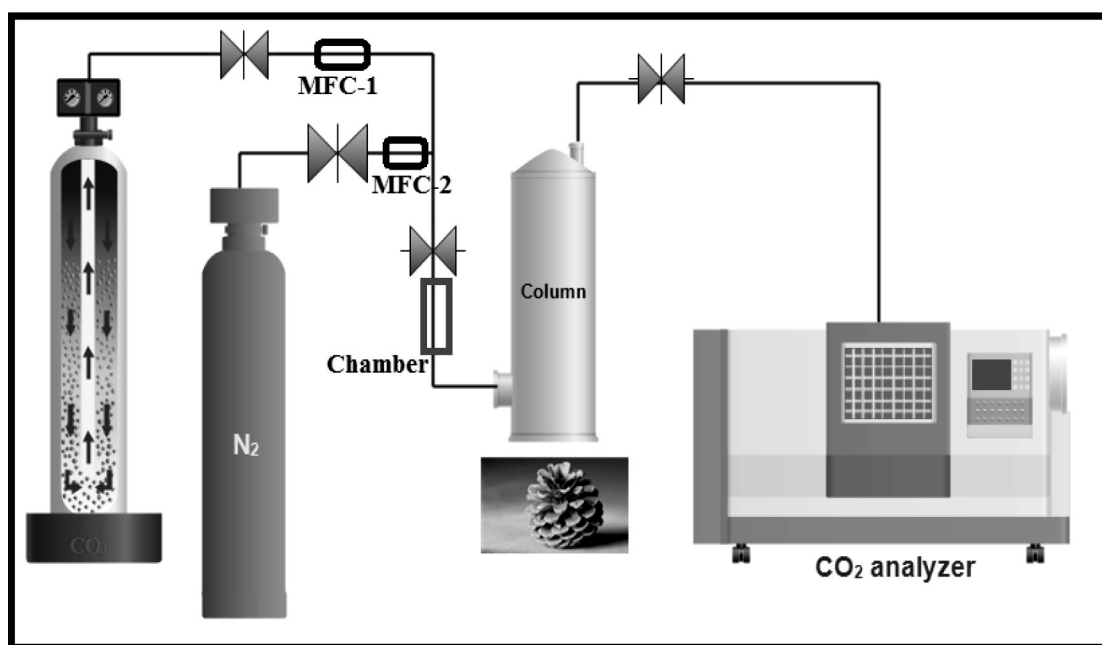
Fig. 1. Designing system for CO_2 adsorption process

3. Results and Discussion

3. 1. Scanning Electron Microscopy (SEM)

Fig. 2a & 2b showed the SEM images of the PC and HNO_3-PC in this study. It can be observed that the surface morphology of PC biomass is so different as compared to the HNO_3-PC. The surface

morphology of PC (Fig. 2a) was smooth with regular edges. However, the surface morphology of HNO_3-PC appeared with number of pores (Fig. 2b). The increasing in the number of pores in the HNO_3-PC will potentially increase the specific surface area and pore volume of PC [9-11].
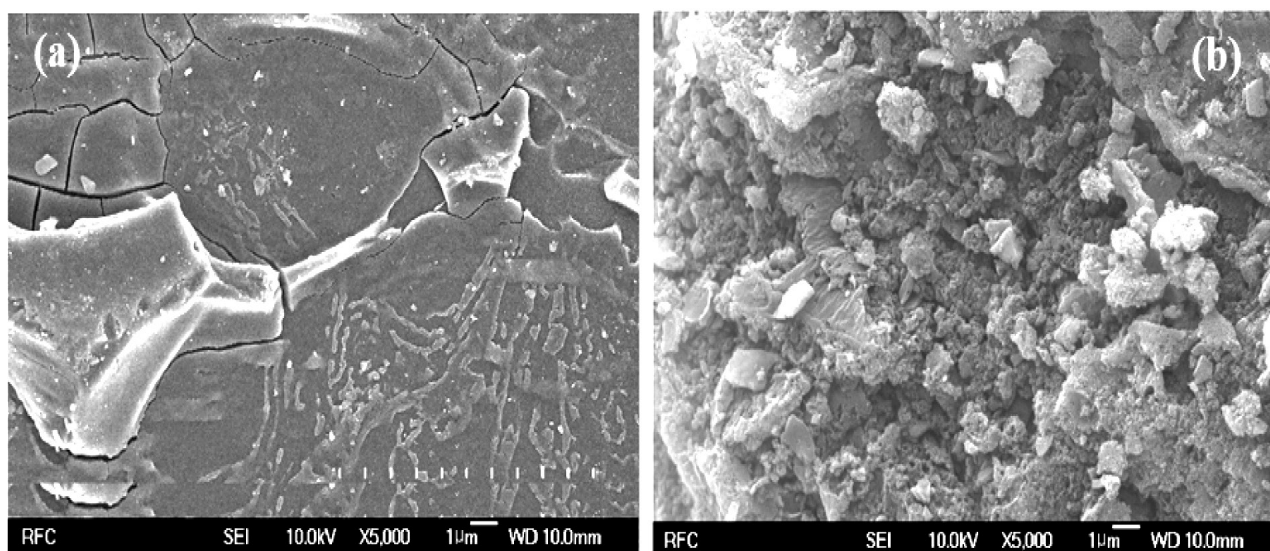
Fig. 2.SEM analysis of (a): PC; (b): HNO$_3$-PC

3.2. Fourier-Transformed Infrared (FTIR) Spectroscopy analysis

The FTIR analysis used to determine the functional groups which presented in the PC and HNO$_3$-PC. **Fig. 3a & 3b** showed the result of FITR spectra of the PC and HNO$_3$-PC in the range of 500-400 cm^{-1}. A wide band located in the range of 3200-3450 cm^{-1} was identified and taken to represent the stretch peak of hydroxyl groups associated with hydrogen bonding. The band at 1700-1650 cm^{-1} was indicative of a stretching vibration of C=O bonds associated with carboxylic acids or esters present in the PC biomass. A band at approximately 2900 cm^{-1} corresponded to a C–H vibration. The infrared spectra of the HNO$_3$-PC showed similar characteristics to PC. However, there was a substantial increase in peak intensity of C=O peak absorbance and shrinking of the hydroxyl group absorbance in the HNO$_3$-PC. The HNO$_3$-PC appeared a strong adsorption band at 700 cm^{-1}, which can be assigned by stretching of polar nitro functional groups (NO$_2$).

In general, the surface chemistry and pore structure of adsorbents had highly effect on the adsorption process. The surface chemistry of adsorbents, particularly surface oxygen complexes, is a very important factor that affects their applications as adsorbent supports for

CO$_2$ capture [12]. The surface oxygen complexes of porous PC and HNO$_3$-PC effectively provide electron-rich properties, which can enhance the interaction between the surface of absorbents and CO$_2$ due to the introduction of various polar groups, such as hydroxyl (OH), nitrogen (NO$_2$) and carboxyl (COOH) groups. Therefore, the increasing in polar functional groups including COOH and NO$_2$ can be effective in improvement of CO$_2$ adsorption capacity using HNO$_3$-PC.
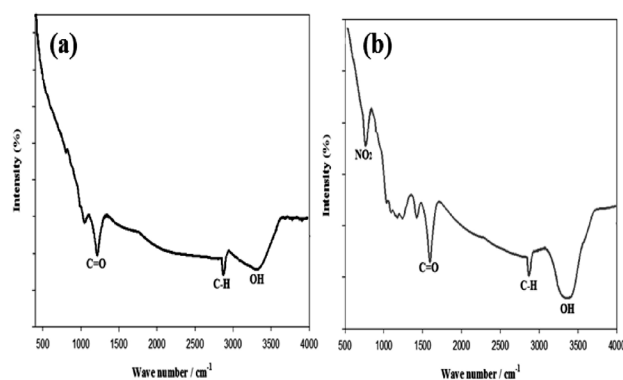
Fig. 3. FTIR analysis (a): PC; (b): HNO$_3$-PC

3.3. Specific surface area analysis

Table 1 showed the surface area and elemental composition analysis of the PC and HNO$_3$-PC. It was observed that the specific surface area and total pore volume of HNO$_3$-PC (180.85 m^2/g and 0.48 cm^3/g, respectively) greatly increased as compare to PC (51.24 m^2/g and 0.16 cm^3/g, respectively). This may be due to the effect of

the enlargement of small pores and the resulting collapse of partial porous structure, which offsets the contribution of the creation of new pores. In adsorption process, the increase in specific surface area of HNO_3-PC leads to increase adsorption performance of CO_2.

The elemental analysis showed that besides the dominant carbon, the PC also contain oxygen (48.19%), hydrogen (6.78%) and nitrogen (0.97%). The contents of these elements represented in the PC were changed after modified with HNO_3. The oxygen and nitrogen contents much increased at 50.47 and 5.2%, respectively. The result indicated that more fractions of oxygenated functional groups such as carboxylic and NO_2 were developed on the HNO_3-PC and which would be contributed to increasing CO_2 adsorption capacity.

Table 1. Chemical composition and specific surface area of PC and HNO_3-PC

Adsorbent	S_{BET} (m²/g)	V_t pores (cm³/g)	Elemental composition			
			C	**H**	**O**	**N**
PC	51.24	0.16	44.06	6.78	48.19	0.97
HNO_3-PC	180.85	0.48	38.12	6.21	50.47	5.2

3.4. CO_2 adsorption experiments

Adsorption capacity and selectivity on the PC and HNO_3-PC

In order to evaluate adsorbents (PC and HNO_3-PC), CO_2 adsorption isotherm and selectivity over N_2 were conducted. Fig. 4a & 4b presented the adsorption isotherms of CO_2 at 20, 40 and 60°C on PC and HNO_3-PC.

The HNO_3-PC exhibits a much more curved isotherm than the PC. The highest CO_2 uptake capacity at 1 atm and 20°C on PC was 1.6 mmol/g, while the corresponding for HNO_3-PC is 3.92 mmol/g at 60°C. This high CO_2 adsorption by HNO_3-PC is explained based on the introduction of polar functional groups onto the surface of HNO_3-PC, leading to more ease to interact with CO_2.
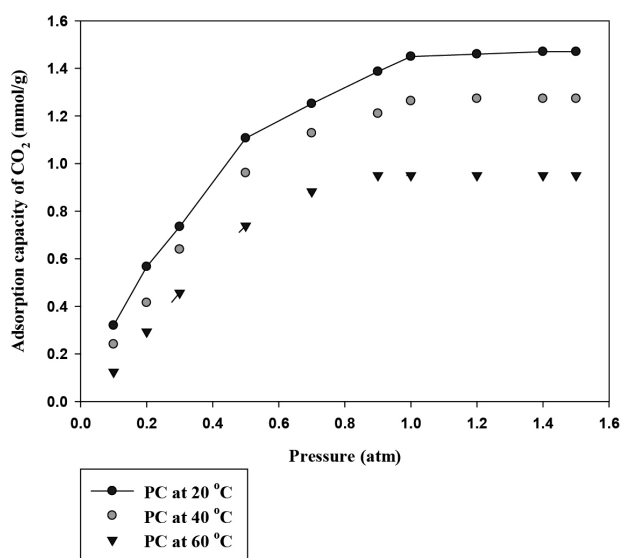
Fig. 4 a. Adsorption isotherm of CO_2 on PC
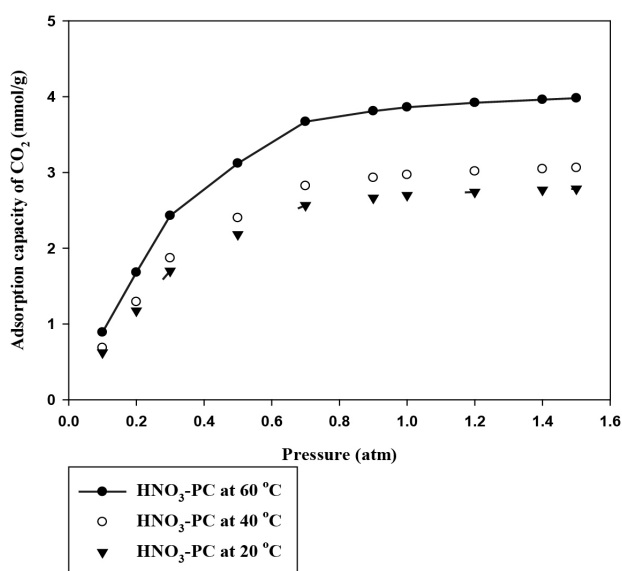
Fig. 4 b. Adsorption isotherm of CO_2 on HNO_3-PC

CO_2 adsorption selectivity

The CO_2 and N_2 are the two main components of flue gas and there are commonly used to investigate the adsorption selectivity of adsorbent [25-30].

The adsorption selectivity of CO_2 versus N_2 gas is defined as shown in the equation (2):

$$\text{Selectivity} = (\frac{q_1}{q_2}/\frac{p_1}{p_2}) \quad (2)$$

where q_i is the uptake and p_i is the partial pressure of component i.

The equilibrium selectivity of CO_2 over N_2 by PC and HNO_3-PC were calculated and presented in Table 2. The adsorption selectivity of CO_2 over N_2 by HNO_3-PC increased (18.8-36.8) as the temperature was increased from 20 to 60°C. It would be explained based on the interaction between CO_2 and HNO_3-PC was mostly followed by chemisorption, leading to increased adsorption selectivity with increasing the temperature. However, the adsorption selectivity of CO_2/N_2 by PC decreased from 14.7 to 9.2 as temperature increased up to 60°C. The interaction of CO_2 and PC was mainly followed by physisorption, thus decreased adsorption selectivity with increasing temperature.

Table 2. Adsorption selectivity of CO_2 over N_2 by PC and HNO_3-PC

Adsorbent	Selectivity CO_2/N_2		
	20°C	40°C	60°C
PC	14.7	11.5	9.2
HNO_3-PC	1.9	29.1	36.8

4. Conclusion

This study investigated the potential application of PC biomass and HNO_3-PC as an adsorbent for capturing CO_2 in the air. The adsorption capacity of CO_2 using PC was 1.6 mmol/g while the HNO_3-PC exhibits the CO_2 adsorption capacity of 3.9 mmol/g, respectively. The high adsorption capacity of CO_2 by using HNO_3-PC attributed to both high surface area and polar functional groups. Based on these findings, the available PC biomass in Korea, as well as HNO_3-PC could be utilized as promising low-cost adsorbent for capturing of CO_2 in the air.

References

[1] Aminu M.D., Nabavi S.A., Rochelle C.A., Manovic V.A. review of developments in carbon dioxide storage. Applied Energy, 208 (2017), pp. 1389-1419

[2] Godec M., Koperna G., Petrusak R., Oudinot A. Potential for enhanced gas recovery and CO2 storage in the Marcellus Shale in the Eastern United States. International Journal of Coal Geology, 118 (2013), pp. 95-104

[3] Li X., Elsworth D. Geomechanics of CO_2 enhanced shale gas recovery. Journal of Natural Gas Science and Engineering, 26 (2015), pp. 1607-1619

[4] S. Choi, J.H. Drese, C.W. JonesAdsorbent materials for carbon dioxide capture from large anthropogenic point sources. ChemSusChem, 2 (2009), pp. 796-854

[5] G. Yin, Z. Liu, Q. Liu, W. WuThe role of different properties of activated carbon in CO_2 adsorption. Chem. Eng. J., 230 (2013), pp. 133-140

[6] V. Presser, J. McDonough, S.-H. Yeon, Y. Gogotsi. Effect of pore size on carbon dioxide sorption by carbide derived carbon. Energy Environ. Sci., 4 (2011), pp. 3059-3066

[7] P.I. Ravikovitch, A. Vishnyakov, A.V. Neimark. Density functional theories and molecular simulations of adsorption and phase transitions in nanopores. Phys. Rev. E, 64 (2001), Article 011602

[8] P.I. Ravikovitch, A. Vishnyakov, R. Russo, A.V. Neimark. Unified approach to pore size characterization of microporous carbonaceous materials from N_2, Ar, and CO_2 adsorption isotherms. Langmuir, 16 (2000), pp. 2311-2320

[9] Y.H. Abdelmoaty, T.D. Tessema, N. Norouzi, O.M. El-Kadri, J.B.M. Turner, H.M. E-Kaderi. Effective approach for increasing the heteroatom doping levels of porous carbons for superior CO_2 capture and separation performance. ACS Appl Mater Interfaces, 9 (41) (2017), pp. 35802-35810

[10] S.Y. Lee, S.J. Park. A review on solid adsorbents for carbon dioxide capture. J Ind Eng Chem, 23 (2015), pp. 1-11

[11] J. Yang, L.M. Yue, B.B. Lin, L.L. Wang, Y.L. Zhao, Y. Lin. CO_2 Adsorption of nitrogen-doped carbons prepared from nitric acid preoxidized petroleum coke. Energy Fuels, 31 (10) (2017), pp. 11060-11068

[12] Y.K. Kim, G.M. Kim, J.W. Lee. Highly porous N-doped carbons impregnated with sodium for efficient CO_2 capture. J Mater Chem A, 3 (20) (2015), pp. 10919-10927.

Mosquito larvicidal activity of the essential oil of *Centratherum punctatum* Cass. species growing wild in Da Nang

Hoạt tính tiêu diệt bọ gậy muỗi *Aedes albopictus* và *Culex quinquefasciatus* của tinh dầu từ loài cúc sợi tím (*Centratherum punctatum* Cass.) mọc hoang tại Đà Nẵng

Do Thi Lai[a], Ta Thi Thanh[a], Phan Thi Kim Thoa[a], Huynh Thi My Dung[a], Ho Thi Nhi[a], Nguyen Phan Hoai Linh[a], Nguyen Thi Quynh Trang[a], Thieu Anh Tai[a], Nguyen Huy Hung[b,*]

Đỗ Thị Lài, Tạ Thị Thanh, Phan Thị Kim Thoa, Huỳnh Thị Mỹ Dung, Hồ Thị Nhị, Nguyễn Phan Hoài Linh, Nguyễn Thị Quỳnh Trang, Thiều Anh Tài, Nguyễn Huy Hùng

[a]*Department of Pharmacy, Duy Tan University, Danang, Vietnam*
Khoa Dược, Đại học Duy Tân, Đà Nẵng, Việt Nam
[b]*Center for Advanced Chemistry, Institute of Research and Development, Duy Tan University, Danang, Vietnam*
Trung tâm Hóa tiên tiến, Viện Nghiên cứu và Phát triển, Đại học Duy Tân, Đà Nẵng, Việt Nam

Abstract

The essential oils from the aerial parts, leaves, flowers, and stems of *Centratherum punctatum* growing wild in Da Nang, Vietnam, were obtained by hydrodistillation and analyzed by gas chromatography – mass spectrometry. The essential oils were dominated by sesquiterpene hydrocarbons (86.1-92.7%), including β-caryophyllene (25.4-28.3%), cyclosativene (3.6-4.6%), α-copaene (5.5-6.8%), *trans*-α-bergamotene (4.6-5.6%), (Z)-β-farnesene (6.8-8.4%), α-humulene (6.2-6.9%), germacrene D (5.8-9.7%), bicyclogermacrene (2.2-4.2%), and δ-cadinene (3.3-7.0%). The essential oil from aerial parts have been screened for mosquito larvicidal activity against *Aedes albopictus* and *Culex quinquefasciatus*. The essential oil showed strong larvicidal activity against *Ae. albopictus* (24-h LC_{50} 21.9) and *Cx. quinquefasciatus* (24-h LC_{50} = 61.135 µg/mL).

Keywords: Centratherum intermedium, essential oil, *Aedes albopictus*, *Culex quinquefasciatus*.

Tóm tắt

Tinh dầu từ các bộ phận trên mặt đất, lá, hoa và thân của loài cúc sợi tím (*Centratherum punctatum)* mọc hoang tại Đà Nẵng thu được bằng phương pháp chưng cất lôi cuốn hơi nước và phân tích thành phần hóa học bằng phương pháp sắc ký khí ghép khối phổ (GC-MS). Thành phần tinh dầu chiếm chủ yếu là các sesquiterpene hydrocarbon (86.1-92.7%), gồm β-caryophyllene (25.4-28.3%), cyclosativene (3.6-4.6%), α-copaene (5.5-6.8%), *trans*-α-bergamotene (4.6-5.6%), (Z)-β-farnesene (6.8-8.4%), α-humulene (6.2-6.9%), germacrene D (5.8-9.7%), bicyclogermacrene (2.2-4.2%), và δ-cadinene (3.3-7.0%). Tinh dầu thu được từ các phần trên mặt đất đã được thử nghiệm hoạt tính độc cấp tính chống lại bọ gậy của hai loài muỗi *Aedes albopictus* và *Culex quinquefasciatus*. Tinh dầu đã thể hiện hoạt tính diệt bọ gậy mạnh mẽ chống lại *Ae. albopictus* (24-h LC_{50} 21,9) và *Cx. quinquefasciatus* (24-h LC_{50} = 61,135 µg/mL).

Từ khóa: Centratherum intermedium, tinh dầu, *Aedes albopictus*, *Culex quinquefasciatus*.

1. Introduction

Aedes albopictus (Skuse) (Diptera: Culicidae) are important vectors of arboviral infections, including yellow fever, dengue, Zika, and chikungunya [1–3]. Vietnam is classified as a hyperendemic dengue country, with all four

Email: huyhung2602@gmail.com

dengue serotypes present throughout the year [4]. In the last half century, dengue fever epidemics have increased in frequency, corresponding to a median annual incidence of 232 cases per 100,000 people [4]. Furthermore, chikungunya is expected to become a major health threat in Vietnam in the near future [4,5]. *Culex quinquefasciatus* Say (Diptera: Culicidae), the southern house mosquito, is a vector of lymphatic filariasis [6] as well as several arboviruses such as West Nile virus and St. Louis encephalitis virus [7] and possibly Zika virus [8].

Vector control is one of the primary approaches to reduce the spread of arboviral infections. However, current methods for controlling *Aedes* mosquitoes have been largely ineffective [9]. Botanical insecticides in general [7,8] and essential oils in particular [9,10] have emerged as promising, environmentally friendly alternatives to synthetic pesticides for mosquito control.

Centratherum punctatum Cass. (syn. C. intermedium (Link) Less.) is native to the Neotropics, from Mexico [11] through Paraguay [12] and northern Argentina [13]. The plant has been introduced as an ornamental to topical regions worldwide but has escaped cultivation and is considered an invasive pest in Hawaii [14], the Galápagos [15], Australia [16], and Vietnam [17]. In Vietnam, *C. punctatum* is found throughout the country, from urban to mountainous areas, for example, Nui Coc Lake (Thai Nguyen province), and Bach Ma National Park (Thua Thien-Hue province) [18]. This species is also found in Thailand and Indonesia. A bath prepared from a decoction of *C. punctatum* is used to bathe women after childbirth.

2. Materials and Methods

2.1. Plant material

Aerial parts of *C. punctatum* were collected from plants growing in Hoa Vang district, Da Nang city (16°01'0.6" N, 108°4'25.6" E) in April 2018. These plants were identified by Dr. Do Ngoc

Dai, and voucher specimens (LTH129) have been deposited in School of Natural Sciences Education, Vinh University. Fresh plant materials (leaves, stems, and flowers) were kept at room temperature (≈25°C), and 2 kg samples of each of the plant materials were shredded and hydrodistilled for 4 hours using a Clevenger type apparatus.

2.2. Gas chromatographic-Mass spectral analysis

Each of the *C. punctatum* essential oils was analyzed by gas chromatography–mass spectrometry (GC-MS) using a Shimadzu GCMS-QP2010 Ultra operated in the electron impact (EI) mode (electron energy = 70 eV), scan range = 40–400 atomic mass units, scan rate = 3.0 scans/s, and GC–MS solution software. The GC column was a ZB-5 fused silica capillary column with a (5% phenyl)-polymethylsiloxane stationary phase and a film thickness of 0.25 μm. The carrier gas was helium with a column head pressure of 552 kPa and flow rate of 1.37mL/min. The inject or temperature was 250 °C and the ion source temperature was 200 °C. The GC oven temperature program was programmed to have an initial temperature of 50 °C, and the temperature increased at a rate of 2 °C/min to 260 °C. A 5% *w/v* solution of the sample in CH_2Cl_2 was prepared, and 0.1 μL was injected with a splitting mode (30:1). Identification of the oil components was based on their retention indices determined by reference to a homologous series of *n*-alkanes, and by comparison of their mass spectral fragmentation patterns with those reported in the literature [19] and stored in-house Sat-Set library [20].

2.3. Mosquito larvicidal assay

Wild larvae of *Ae. albopictus* and *Culex quinquefasciatus* (Say) were collected from Hoa Khanh Nam district (16°3'14.9" N, 108°9'31.2" E). For the assay, aliquots of the aerial parts (leaves and stems) and essential oils

of *C. punctatum* dissolved in dimethylsulfoxide (DMSO) (1% stock solution of essential oil in DMSO) were placed in 500 mL beakers and added to water that contained 25 larvae (fourth instar). With each experiment, a set of controls using DMSO was also run for comparison. Mortality was recorded after 24 hours and again after 48 hours of exposure, during which no nutritional supplement was added. The experiments were carried out at 25 ± 2 °C. Each test was conducted with four replicates with six concentrations (150, 100, 50, 25, 12.5 μg/mL). Permethrin was used as a positive control.

2.4. Data analysis

It was shown through experimental testing that over 20% of the controlled mortality was discharged and repeated. When the level of controlled mortality was at 1–20%, the observed mortality was corrected by Abbott's formula (Abbott, 1925). Using probity analysis, the LC_{50} and LC_{90} regression equations, as well as a 95% confidence limits, were then calculated [21].

3. Results and discussion

The essential oils, obtained as colorless, with mild pleasant aromas, were obtained in yields of 0.43% (v/w; aerial parts); 0.52% (v/w; leaves), 0.17% (v/w; stems), and 0.23% (v/w; flowers), calculated on a dry weight basis.

3.1. Essential oil compositions

The chemical compositions from the aerial parts, leaves, flowers, and stems of *C. punctatum* are compiled in Table 1. A total of 115 compounds were identified in the essential oils accounting for 99.8, 99.7, 98.7, and 98.7% of the compositions, respectively. Sesquiterpene hydrocarbons dominated all essential oil samples from this plant species. The most abundant component was β-caryophyllene (25.4-28.3%), but cyclosativene (3.6-4.6%), α-copaene (5.5-6.8%), trans-α-bergamotene (4.6-5.6%), (Z)-β-farnesene (6.8-8.4%), α-humulene (6.2-6.9%), germacrene D (5.8-9.7%), bicyclogermacrene (2.2-4.2%), and δ-cadinene (3.3-7.0%), were also abundant.

Table 1: Chemical compositions of essential oils from Centratherum punctatum growing wild in Da Nang

RI	Compound	aerial parts	leaves	Flowers	stems
931	α-Pinene	0.1	0.1	-	---
970	Sabinene	0.1	0.1	-	tr[b]
976	β-Pinene	0.1	0.1	-	tr
987	Myrcene	0.1	0.1	-	---
1023	*p*-Cymene	-	tr	-	---
1028	Limonene	-	-	-	tr
1044	(*E*)-β-Ocimene	0.2	0.2	-	tr
1098	Isopentyl 2-methyl butanoate	tr	tr	-	tr
1103	Nonanal	-	---	tr	---
1205	Decanal	-	---	tr	---
1229	(3*Z*)-Hexenyl 2-methylbutanoate	tr	0.1	tr	tr
1234	(3*Z*)-Hexenyl 3-methylbutanoate	-	tr	---	---
1287	Dihydroedulan IA	---	---	tr	---
1330	Bicycloelemene	0.2	0.3	0.2	0.1
1333	Silphiperfol-5-ene	---	---	0.1	0.1
1334	δ-Elemene	0.2	0.2	---	---
1342	7-*epi*-Silphiperfol-5-ene	---	tr	tr	---
1345	α-Cubebene	0.1	0.1	0.1	0.1

1369	Cyclosativene	4.5	4.5	3.6	4.6
1375	α-Copaene	6.7	6.8	5.5	6.7
1382	β-Bourbonene	1.0	0.7	0.6	0.7
1386	7-*epi*-Sesquithujene	0.5	0.5	0.4	0.5
1388	β-Elemene	0.8	0.8	0.7	0.7
1391	Sativene	0.1	0.1	---	0.1
1401	Cyperene	0.1	---	tr	---
1401	Sesquithujene	---	tr	---	tr
1404	Ylanga-2,4(15)-diene	0.1	0.1	0.1	0.1
1405	β-Maaliene	0.8	0.9	0.6	0.7
1410	α-Gurjunene	tr	tr	---	---
1411	*cis*-α-Bergamotene	0.1	0.1	0.1	0.1
1419	β-Caryophyllene	25.0	25.6	25.4	28.3
1429	β-Gurjunene	0.9	0.8	0.7	0.7
1432	*trans*-α-Bergamotene	4.6	5.2	4.6	5.6
1434	α-Guaiene	0.4	0.4	0.4	0.5
1437	Aromadendrene	0.1	0.2	0.1	---
1440	(*Z*)-β-Farnesene	6.9	8.1	6.8	8.4
1443	*cis*-Muurola-3,5-dine	0.1	---	0.1	---
1444	Myltayl-4(12)-ene + Isopentyl octanoate	tr	0.1	0.2	0.2
1448	*trans*-Muurola-3,5-diene	0.2	0.2	0.2	0.2
1451	(*E*)-β-Farnesene	1.5	2.0	0.7	1.5
1451	Sesquisabinene	---	---	0.7	---
1454	α-Humulene	6.8	6.8	6.2	6.9
1459	Alloaromadendrene	0.6	0.5	0.7	0.4
1461	*cis*-Cadina-1(6),4-diene	0.1	0.1	0.1	tr
1467	9-*epi*-(*E*)-Caryophyllene	0.1	---	---	---
1471	Dauca-5,8-diene	0.3	0.2	---	---
1471	γ-Gurjunene	---	---	0.2	0.2
1474	*trans*-Cadina-1(6),4-diene	0.7	0.6	0.7	0.6
1476	γ-Curcumene	0.4	0.4	0.3	0.2
1481	Germacrene D	8.6	9.7	6.4	5.8
1483	(*Z,Z*)-α-Farnesene	2.7	2.8	2.9	3.1
1485	δ-Selinene	0.1	0.1	0.1	---
1488	β-Selinene	1.8	1.5	1.8	1.6
1490	α-Selinene	---	0.3	---	0.2
1491	*trans*-Muurola-4(14),5-diene	0.8	0.5	0.6	0.3
1494	Bicyclogermacrene	3.9	4.2	3.0	2.2
1497	α-Muurolene	1.3	1.1	1.2	1.0
1500	α-Bulnesene	0.2	0.2	0.3	0.1
1505	β-Bisabolene	0.1	0.1	0.2	0.1
1507	β-Curcumene	0.6	0.5	0.3	0.2
1511	δ-Amorphene	0.6	0.4	0.6	0.5
1513	Cubebol	0.1	0.1	0.1	0.1

1517	δ-Cadinene	5.6	4.0	7.0	3.3
1520	*trans*-Calamenene	0.2	0.2	0.3	0.3
1522	β-Sesquiphellandrene	0.5	0.4	0.5	0.4
1525	*(E)-γ*-Bisabolene	tr	tr	---	---
1531	*trans*-Cadina-1,4-diene	0.1	0.1	0.1	---
1535	α-Cadinene	0.1	0.1	0.1	0.1
1539	α-Calacorene	0.3	0.2	0.4	0.3
1541	*cis*-Sesquisabinene-hydrate	0.2	0.2	0.3	0.2
1546	Elemol	tr	tr	---	---
1549	Isocaryophyllene oxide	---	---	0.1	0.2
1553	Humulene epoxide I	0.1	---	---	---
1557	Germacrene B	tr	---	---	---
1559	*(E)*-Nerolidol	tr	0.2	0.2	0.2
1560	β-Calcorene	0.1	0.1	0.2	0.3
1566	1,5- Epoxysalvial-4(14)-ene	---	---	---	0.1
1568	Caryophyllenol	---	---	0.1	0.1
1569	Palustrol	tr	tr	---	---
1571	Sesquirosefuran	0.1	---	0.1	---
1575	Spathulenol	0.7	0.6	0.9	1.2
1577	*trans*-Sesquisabinene hydrate	0.1	0.1	---	---
1581	Caryophyllene oxide	2.0	1.4	3.1	3.3
1584	Globulol	0.1	0.4	0.4	0.4
1592	Viridiflorol	1.3	1.2	1.9	1.2
1594	Guaiol	0.1	---	0.1	---
1594	Cubeban-11-ol	---	---	---	0.1
1597	*cis*-Bisabol-11-ol	tr	---	---	---
1602	Ledol	0.3	0.2	0.4	0.3
1605	5-*epi*-7-*epi*-α-Eudesmol + β-Oplopenone	tr	tr	0.1	0.1
1608	Humulene epoxide II	0.3	0.2	0.4	0.4
1611	5-*epi*-7-*epi*-β-Eudesmol	0.1	0.1	0.2	0.1
1613	1,10-di-epi-Cubenol	0.1	---	---	---
1624	Muurola-4,10(14)-dien-1β-ol	0.2	0.1	0.3	0.1
1626	1-epi-Cubenol	0.2	0.2	0.2	0.2
1630	*iso*-Spathulenol	0.3	0.2	0.4	0.3
1635	Caryophylla-4(12),8(13)-dien-5β-ol	0.3	0.2	0.4	0.2
1640	*epi*-α-Cadinol	0.1	0.1	0.2	0.1
1642	*epi*-α-Muurolol	0.1	0.1	0.2	0.1
1644	δ-Cadinol	0.1	0.1	0.2	0.2
1653	α-Cadinol	0.4	0.3	0.6	0.5
1656	Pogostol	0.1	0.1	0.2	0.2
1663	*cis*-Calamenen-10-ol	---	---	tr	---
1663	Selin-11-en-4β-ol	tr	tr	tr	---
1668	14-Hydroxy-9-epi-(E)-caryophyllene	---	---	0.5	0.2
1669	*epi*-β-Bisabolol	0.3	0.3	---	---

1683	α-Bisabolol	0.1	0.1	0.1	0.1
1688	Eudesma-4(15),7-dien-1β-ol	tr	---	---	---
1713	Pentadecanal	0.1	---	0.2	---
1739	Aromadendrane-4,10-diol	---	tr	0.1	0.2
1822	Methandrostenolone	---	tr	0.1	0.2
1838	Phytone	---	---	0.2	---
1838	α-Chenopodiol	---	---	---	0.1
1859	Platambin	---	tr	0.1	0.2
2104	Phytol	---	tr	0.1	---
	Monoterpene hydrocarbons	0.6	0.7	0.0	0.0
	Oxygenated monoterpenoids	0.0	0.0	0.0	0.0
	Sesquiterpene hydrocarbons	91.3	92.7	86.1	87.9
	Oxygenated sesquiterpenoids	7.9	6.3	12.2	10.4
	Others	0.1	0.1	0.6	0.4
	Total identified	99.8	99.7	98.7	98.7

The high concentration of sesquiterpene hydrocarbons is consistent with previously published reports from Brazil and from Nigeria. The essential oil from the flowering parts of *C. punctatum* from Fortaleza, Ceará, northeastern Brazil, was composed largely of sesquiterpenes, including δ-cadinene (17.9%), β-caryophyllene (11.1%), γ-cadinene (8.6%), germacrene D (5.7%), and α-copaene (5.6%), in addition to the monoterpene β-pinene (9.1%) [22]. A sesquiterpene-rich essential oil from the leaves and flowering tops of *C. punctatum* from Araraquara, São Paulo, Brazil, has also been reported [23], but unfortunately, too few components were identified for useful comparison. The major components in the leaf essential oil of *C. punctatum* growing in Nigeria were β-caryophyllene (16.6%), globulol (5.7%), germacrene D (6.4%), α-copaene (5.3%), (*Z*)-β-farnesene (reported as sesquisabinene, but the RI is more consistent with (*Z*)-β- farnesene), δ-cadinene (4.7%), and α-humulene (4.1%) [24]. In another report, the essential oil from the aerial parts (herb) of *C. punctatum* from Nigeria was also dominated by sesquiterpene hydrocarbons, β-caryophyllene (27.4%), α- humulene (7.0%), δ-cadinene (6.6%), germacrene D (5.9%), and α-copaene (5.0%) [25].

3.2. Mosquito larvicidal activities

The essential oils from the aerial parts of *C. punctatum* collected from Da Nang were screened for mosquito larvicidal activity (see Tables 2).

Table 2. Mosquito larvicidal activity of Centratherum punctatum aerial parts (leaves and stems) essential oil.

Mosquitoes	Percentage of mortality	Observed Responses	Number of exposed larva	Concentration (μg/mL)	LC$_{50}$ (μg/mL)[a]	LC$_{90}$ (μg/mL)[a]	χ^2
Cx. quinquefasciatus	5	4	80	12.5	60.135 (50.392 – 74.985)	250.434 (171.422 – 455.647)	0.932
	20	16	80	25			
	33.75	27	80	50			
	53.75	43	80	100			
	100	80	80	150			
	0	0	80	0			

Ae. albopictus	20	16	80	12.5	21.90 (18.929 – 25.070)	58.584 (47.047 – 82.524)	0.795
	42.5	34	80	25			
	70	56	80	50			
	100	80	80	100			
	100	80	80	150			
	0	0	80	0			

[a] 95% Confidence interval

Table 3. Mosquito larvicidal activity of permethrin

Mosquitoes	Treatment Time	LC_{50}, µg/mL [b] (Fiducial Limits)	LC_{90}, µg/mL [b] (Fiducial Limits)	Regression Equation	χ^2	*p*
Ae. Albopictus	24 h	0.0023 (0.0021– 0.0026)	0.0042 (0.0038– 0.0049)	y = -1.628 + 686.9x	4.73	0.03
Cx. Quinquefasciatus	24 h	0.0167 (0.0152– 0.0183)	0.0294 (0.0270– 0.0326)	y = -2.292 + 121.6x	26.62	< 0.001

[b] There was no mortality in the DMSO controls.

The essential oils from the aerial parts of *Centratherum punctatum* showed strong larvicidal activity against *Ae. albopictus*. The 24 h LC_{50} value was 21.90 µg/mL, which compared very favorably with other essential oils reported in the literature against this species [26–28].

The major components of *C. punctatum* aerial parts essential oil, β-caryophyllene, α-copaene, and α-humulene, germacrene D, have all shown good mosquito larvicidal activity (see Table 4). The LC_{50} values for β-caryophyllene average around 38.6 and 44.7 µg/mL against *Ae. aegypti* and *Ae. albopictus*, respectively, but is higher (95 µg/mL) against *Cx. quinquefasciatus* [29]. β-Caryophyllene has shown LC_{50} of 38.6 and 39.5 µg/mL against *Ae. aegypti* and *Ae. albopictus*, respectively [30].

Table 4. Mosquito Larvicidal activities (24-h LC_{50}) of essential oil components against various mosquito species.

Compounds	Mosquito species	LC_{50} (µg/mL)	Ref.
β-caryophyllene	*Ae. albopictus*	44.77	[31]
	Ae. albopictus	39.52	[30]
	A. aegypti	88.3	[32]
	A. aegypti	38.58	[30]
	Culex tritaeniorhynchus	48.17	[31]
	Culex pipiens pallens	93.65	[32]
	Culex pipiens pallens	47.79	[30]
α-Copaene; β-caryophyllene	*A. aegypti*	24	[33]
δ-cadinene	*An. gambiae*	34	[34]
δ-Cadinene; (*E*)-caryophyllen	*A. aegypti*	63	[35]
β-Caryophyllene; α-humulene	*A. aegypti*	18	[36]
Germacrene D; β-caryophyllene	*A. aegypti*	28	[37]

The larvicidal activities of *C. punctatum* essential oil can be attributed to the high concentrations of β-caryophyllene. However, synergy between essential oil components may also be important [38,39]. Scalerandi and coworkers have demonstrated that *Musca domestica* preferentially metabolizes the major components in an essential oil while leaving the components of lower concentrations to act as toxicants [40].

4. Conclusions

Mosquito larvicidal screening of *Centratherum punctatum* indicates good larvicidal activity, which can be attributed to their major components. Thus, this work provides evidence that otherwise noxious introduced weeds might provide low-cost vector control agents to prevent the spread of arboviral infections in Vietnam.

References

[1] Tilak, R., Ray, S., Tilak, V. W., & Mukherji, S. (2016). Dengue, chikungunya… and the missing entity–Zika fever: A new emerging threat. *Medical journal armed forces india*, *72*(2), 157-163.

[2] Mayer, S. V., Tesh, R. B., & Vasilakis, N. (2017). The emergence of arthropod-borne viral diseases: A global prospective on dengue, chikungunya and zika fevers. *Acta tropica*, *166*, 155-163.

[3] Wilder-Smith, A., Gubler, D. J., Weaver, S. C., Monath, T. P., Heymann, D. L., & Scott, T. W. (2017). Epidemic arboviral diseases: priorities for research and public health. *The Lancet infectious diseases*, *17*(3), e101-e106.

[4] Kim Lien, P. T., Briant, L., Tang, T. B., Trang, B. M., Gavotte, L., & Cornillot, E. Surveillance of dengue and chikungunya infection in Dong Thap, Vietnam: A 13-month study. *Asian Pac J Trop Med. 2016 Jan; 9* (1): 39–43.

[5] Thi, K. L. P., Briant, L., Gavotte, L., Labbe, P., Perriat-Sanguinet, M., Cornillot, E., ... & Afelt, A. (2017). Incidence of dengue and chikungunya viruses in mosquitoes and human patients in border provinces of Vietnam. *Parasites & vectors*, *10*(1), 556.

[6] Bowman, L. R., Donegan, S., & McCall, P. J. (2016). Is dengue vector control deficient in effectiveness or evidence?: Systematic review and meta-analysis. *PLoS neglected tropical diseases*, *10*(3), e0004551.

[7] Benelli, G. (2015). Research in mosquito control: current challenges for a brighter future. *Parasitology research*, *114*(8), 2801-2805.

[8] Benelli, G. (2015). Plant-borne ovicides in the fight against mosquito vectors of medical and veterinary importance: a systematic review. *Parasitology research*, *114*(9), 3201-3212.

[9] Masetti, A. (2016). The potential use of essential oils against mosquito larvae: a short review. *Bull Insectology*, *69*, 307-10.

[10] Pavela, R., & Benelli, G. (2016). Essential oils as ecofriendly biopesticides? Challenges and constraints. *Trends in plant science*, *21*(12), 1000-1007.

[11] Redonda-Martínez, R. (2017). Diversidad y distribución de la tribu Vernonieae (Asteraceae) en México. *Acta botánica mexicana*, (119), 115-138.

[12] De Egea, J., Pena-Chocarro, M., Espada, C., & Knapp, S. (2012). Checklist of vascular plants of the Department of Ñeembucú, Paraguay. *PhytoKeys*, (9), 15.

[13] Missouri Botanical Garden Tropicos. org www. tropicos.org (accessed Dec 29, 2017).

[14] PIER PIE at R. Centratherum punctatum http://www.hear.org/pier/species/centratherum_punctatu m.htm (accessed Dec 29, 2017).

[15] Guerrero, A. M., Pozo, P., Chamorro, S., Guezou, A., & Buddenhagen, C. E. (2008). Baseline data for identifying potentially invasive plants in Puerto Ayora, Santa Cruz Island, Galapagos. *Pacific Conservation Biology*, *14*(2), 93-107.

[16] Groves, R. H. C., Hosking, J. R., Batianoff, G. N., Cooke, D. A., Cowie, I. D., Johnson, R. W., ... & Randall, R. P. (2003). Weed categories for natural and agricultural ecosystem management. *Bureau of Rural Sciences, Canberra*.

[17] Tan, D. T., Thu, P. Q., & Dell, B. (2012). Invasive plant species in the national parks of Vietnam. *Forests*, *3*(4), 997-1016.

[18] Biên LK. Thực vật chí Việt Nam - Flora of Vietnam, Vol. 7. Science and Technics Publishing House, Hanoi, Vietnam, 2007.

[19] Adams, R. P., & Sparkman, O. D. (2007). Review of Identification of Essential Oil Components by Gas Chromatography/Mass Spectrometry. *J Am Soc Mass Spectrom*, *18*, 803-806.

[20] Satyal, P. (2015). *Development of GC-MS Database of Essential Oil Components by the Analysis of Natural Essential Oils and Synthetic Compounds and Discovery of Biologically Active Novel Chemotypes in Essential Oils: A*

Dissertation(Doctoral dissertation, University of Alabama in Huntsville).

[21] Finney, D. J., & Tattersfield, F. (1952). *Probit analysis*. Cambridge University Press; Cambridge.

[22] Craveiro, A. A., Andrade, C. H. S., Matos, F. J. A., Alencar, J. W., & Machado, M. I. L. (1984). Essential oils of Brazilian Northeastern plants: *Centratherum punctatum*. *Journal of Natural Products*, *47*(4), 743-743.

[23] Mancini B, Bernardi AC, Neto JJ. Óleo essencial de *Centratherum punctatum* Cass., Compositae: Análise cromatográfica e espectrofotométrica. Rev. Ciências Farm. 1983; 5:1-4.

[24] Ogunwande, I. A., Olawore, N. O., & Usman, L. (2005). Composition of the leaf oil of Centratherum punctatum Cass. growing in Nigeria. *Journal of Essential Oil Research*, *17*(5), 496-498.

[25] Gbolade, A. A., Dzamic, A. M., Ristic, M. S., & Marin, P. D. (2009). Essential oil composition of Centratherum punctatum from Nigeria. *Chemistry of natural compounds*, *45*(1), 118-119.

[26] Dias, C.N. and Moraes, D.F.C., 2014. Essential oils and their compounds as Aedes aegypti L.(Diptera: Culicidae) larvicides. *Parasitology research, 113*(2), pp.565-592.

[27] Pavela, R., 2015. Essential oils for the development of eco-friendly mosquito larvicides: a review. *Industrial crops and products*, *76*, pp.174-187.

[28] Amer, A. and Mehlhorn, H., 2006. Larvicidal effects of various essential oils against Aedes, Anopheles, and Culex larvae (Diptera, Culicidae). *Parasitology Research, 99*(4), pp.466-472.

[29] Pavela, R., 2015. Acute toxicity and synergistic and antagonistic effects of the aromatic compounds of some essential oils against *Culex quinquefasciatus* Say larvae. *Parasitology research*, *114*(10), pp.3835-3853.

[30] Lee, D. and Ahn, Y.J., 2013. Laboratory and simulated field bioassays to evaluate larvicidal activity of Pinus densiflora hydrodistillate, its constituents and structurally related compounds against *Aedes albopictus, Aedes aegypti* and *Culex pipiens pallens* in relation to their inhibitory effects on acetylcholinesterase activity. *Insects*, *4*(2), pp.217-229.

[31] Govindarajan, M., Rajeswary, M., Hoti, S.L., Bhattacharyya, A. and Benelli, G., 2016. Eugenol, α-pinene and β-caryophyllene from Plectranthus barbatus essential oil as eco-friendly larvicides against malaria, dengue and Japanese encephalitis mosquito vectors. *Parasitology research*, *115*(2), pp.807-815.

[32] Perumalsamy, H., Kim, N.J. and Ahn, Y.J., 2009. Larvicidal activity of compounds isolated from Asarum heterotropoides against Culex pipiens pallens, Aedes aegypti, and Ochlerotatus togoi (Diptera: Culicidae). *Journal of Medical Entomology*, *46*(6), pp.1420-1423.

[33] Chung, I.M. and Moon, H.I., 2011. RETRACTED: Composition and immunotoxicity activity of essential oils from Lindera obtusiloba Blume against Aedes aegypti L. *Immunopharmacology and immunotoxicology*, *33*(1), pp.146-149.

[34] Matasyoh, J.C., Wathuta, E.M., Kariuki, S.T. and Chepkorir, R., 2011. Chemical composition and larvicidal activity of Piper capense essential oil against the malaria vector, Anopheles gambiae. *Journal of Asia-Pacific Entomology*, *14*(1), pp.26-28.

[35] Santos, R.P., Nunes, E.P., Nascimento, R.F., Santiago, G.M.P., Menezes, G.H.A., Silveira, E.R. and Pessoa, O.D.L., 2006. Chemical composition and larvicidal activity of the essential oils of Cordia leucomalloides and Cordia curassavica from the northeast of Brazil. *Journal of the Brazilian Chemical Society*, *17*(5), pp.1027-1030.

[36] Trindade, F.T.T., Stabeli, R.G., Pereira, A.A., Facundo, V.A. and de Almeida, A., 2013. Copaifera multijuga ethanolic extracts, oilresin, and its derivatives display larvicidal activity against Anopheles darlingi and Aedes aegypti (Diptera: Culicidae). *Revista Brasileira de farmacognosia*, *23*(3), pp.464-470.

[37] Aguiar, J.C., Santiago, G.M., Lavor, P.L., Veras, H.N., Ferreira, Y.S., Lima, M.A., Arriaga, A.M., Lemos, T.L., Lima, J.Q., Alves, P.B. and Braz-Filho, R., 2010. Chemical constituents and larvicidal activity of Hymenaea courbaril fruit peel. *Natural product communications*, *5*(12), pp.1977-1980.

[38] Pavela, R., 2015. Acute toxicity and synergistic and antagonistic effects of the aromatic compounds of some essential oils against Culex quinquefasciatus Say larvae. *Parasitology research*, *114*(10), pp.3835-3853.

[39] Tak, J.H. and Isman, M.B., 2017. Penetration-enhancement underlies synergy of plant essential oil terpenoids as insecticides in the cabbage looper, Trichoplusia ni. *Scientific reports*, *7*, p.42432.

[40] Scalerandi, E., Flores, G.A., Palacio, M., Defagó, M.T., Carpinella, M.C., Valladares, G., Bertoni, A. and Palacios, S.M., 2018. Understanding synergistic toxicity of terpenes as insecticides: contribution of metabolic detoxification in Musca domestica. *Frontiers in plant science*, *9*.

Hetero-cycloaddition reactions of azoalkenes

Phản ứng cộng đóng vòng dị nguyên tử của các azoalkene

Thien Trong Nguyen

Nguyễn Trọng Thiện

Institute of Research and Development, Duy Tan University, Danang, Vietnam
Viện Nghiên cứu và Phát triển Công nghệ cao, Đại học Duy Tân, Đà Nẵng, Việt Nam

Abstract

Azoalkenes are useful intermediates in the preparation of numerous azo-heterocyclic systems through cycloaddition reactions. This mini review discusses a few examples of azoalkens in hetero-cycloaddition, focusing on the chemical reactivity that can be utilized for versatile building blocks in organic synthesis. These species have been used for the assembly of various heterocyclic systems, spanning from five- to seven-membered heterocycles.

Keywords: Azoalkene, cycloaddition, heterocycles.

Tóm tắt

Các azoalkene là những chất trung gian chìa khóa trong phản ứng điều chế các hệ thống dị vòng nitơ thông qua các phản ứng đóng vòng. Bài tổng quan này thảo luận một vài ví dụ của các phản ứng đóng vòng này, nhấn mạnh hoạt tính hóa học của azoalkene trong việc tạo ra các cấu trúc với nhiều ứng dụng trong tổng hợp hữu cơ. Các azoalkene đã được sử dụng để hình thành nên nhiều hệ thống dị vòng bao gồm các vòng 5, 6, và 7.

Từ khóa: Azoalkene, đóng vòng, dị vòng.

1. Introduction

Azoalkenes have received much interest in recent decades since they are useful intermediates in the preparation of numerous aza-heterocyclic systems through hetero-cycloaddition reactions [1-7]. The strong electrophilic property of these species is resulted from N=N moiety. The cyclo-adducts are very useful for pharmacological studies and organic synthesis [8]. The physical properties and stabilities of azoalkene species are largely determined by the electron-withdrawing or –donating character of the substituents. Electron-deficient azoalkenes are typically unstable and are generated in situ, whereas the electron-sufficient ones can be isolated and characterized. The most common method for the preparation of azoalkenes is dehydrohalogenation of α-hydrazones with TEMPO, I_2, or HgO [9-11]. Being inspired by recently excellent review [12,13], this mini review briefly describes the preparation of azoalkene species and their reactivity toward various cycloaddition reactions including [4+2], [4+1], [4+3], and [3+2] cycloadditions.

Email: nguyentrongthien@duytan.edu.vn

2. Preparation of azoalkene species

Azoalkenes are typically reactive species. Therefore, their isolation is usually difficult. They can be generated *in situ* from dehalogenation of α-halo hydrazones or α-haloazo compounds (**1** → **3** and **2** → **3**). Another way to prepare

azoalkenes is by the deprotonation of α,β-epoxyhydrazones followed by ring opening of the epoxide (**4** → **5**). This gives rise to an intermediate that is susceptible to Eschenmoser-Tanabe fragmentation producing aldehyde **6** and alkyne moiety **7** [14,15].
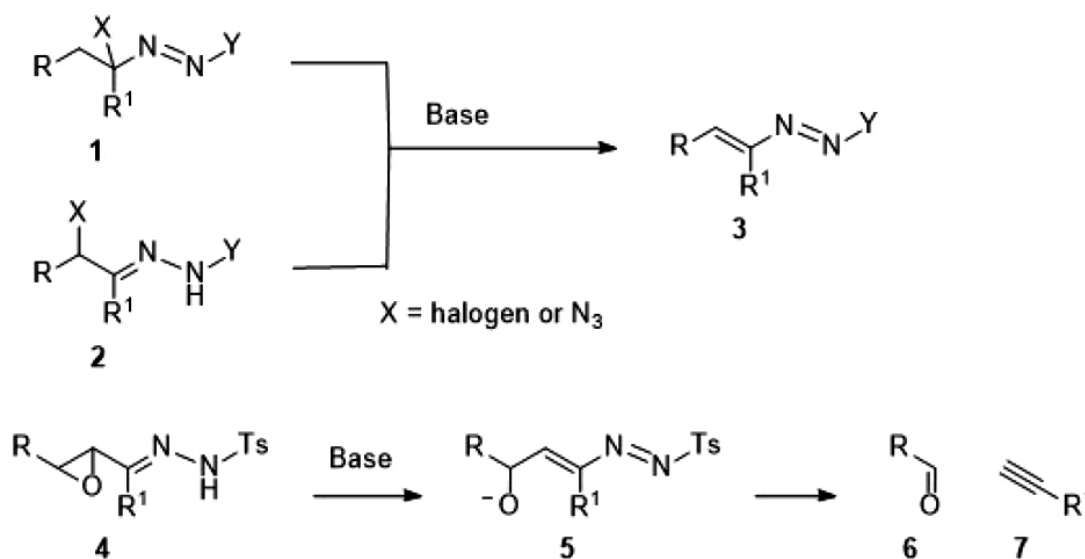
Scheme 1. Preparation of azoalkenes

3. [4+2] Cycloaddition

The α-alkylation of ketones via azoalkenes is also well-established in the context of cycloaddition. One of the first [4+2] cycloadditions of an electron-

deficient azoalkene and electron-rich alkenes was reported in the late 1970s by Sommer [16]. The cyclo-adducts (1,4,5,6-tetrahydropyridazine, **9**) was synthesized in good yield.

R = OC$_2$H$_5$: **9a**, 70%
R = 4-OCH$_3$C$_6$H$_4$: **9b**, 72%
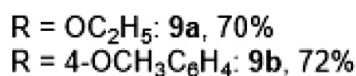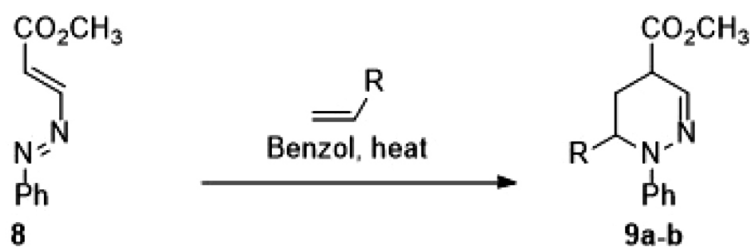
Scheme 2. [4+2] cycloaddition of an electron-deficient azoalkene and electron-rich alkenes

In 1979 Gilchrist *et al*. reported another cycloadditon of azoalkene species (**10**), generated *in situ* from α-chloroacetophenone hydrazones, with cyclopentadiene and furan [17]. Azoalkenes bearing electron-withdrawing group on the azo group or electron-rich dienes facilitated the

cycloaddition and generated the pyridazine derivatives (**11**) in good yields. In 1991, Roberts *et al*. reported a similar cycloaddition of *in situ* generated azoalkenes with alkenes and heterocycles in the presence of sodium carbonate (**12** → **13**) [18].

R = 2,4-(NO$_2$)$_2$C$_6$H$_3$, Y = CH$_2$: **11a**, 96%
R = Ts, Y = CH$_2$: **11b**, 72%
R = COOEt, Y = CH$_2$: **11c**, 96%
R = 2,4-(NO$_2$)$_2$C$_6$H$_3$, Y = O: **11d**, 89%
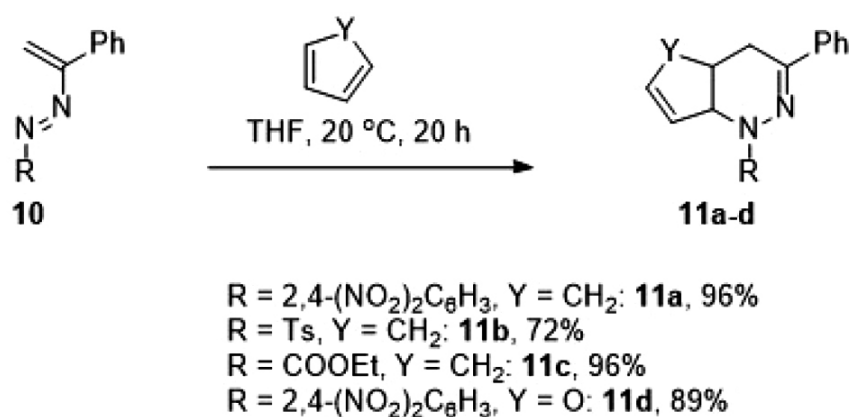
Scheme 3. [4+2] cycloaddition of electron-deficient azoalkenes and electron-rich alkenes by Gilchrist *et al.*
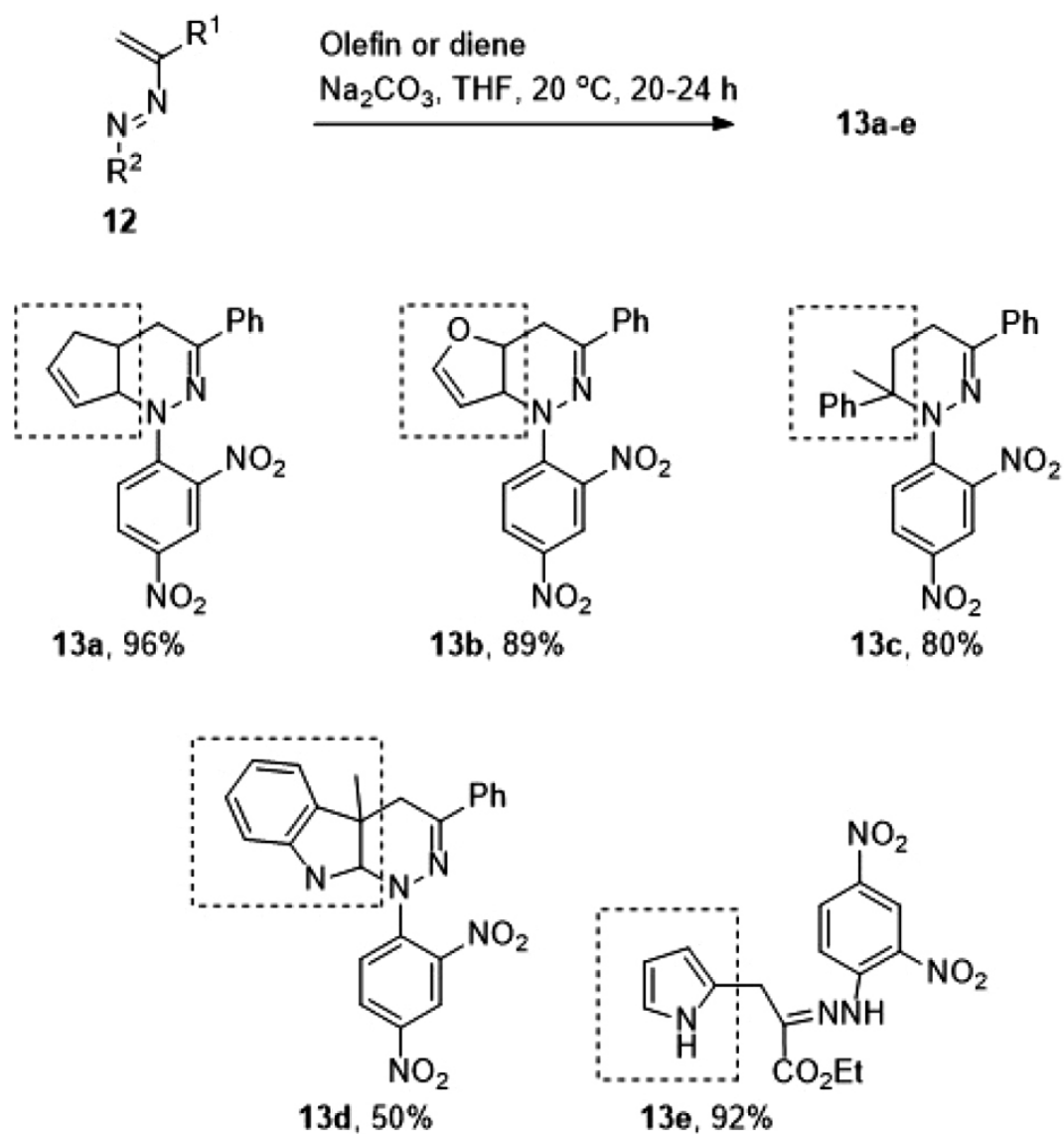
Scheme 4. [4+2] cycloaddition of electron-deficient azoalkenes and electron-rich alkenes

Azoalkenes (**16**), generated *in situ* from α-choloroazo compounds (**15**), underwent reaction with olefins to form adducts (**17**) in good yield [19]. In this process, the phenyl hydrazones of ketones were treated with chloramine-T in ethanol and formed α-choloroazo compounds (**14 → 15**), followed by dehydrohalogenation to form azoalkenes (**15 → 16**). Cycloaddition of the azoalkenes with olefins produced tetrahydropyridazines (**16 → 17**).

R¹ = Ph, R² = H, R³ = Ph: **17a**, 74%
R¹ = *p*-NO₂C₆H₄, R² = H, R³ = Ph: **17b**, 70%
R¹ = Et, R² = H, R³ = Ph: **17c**, 69%
R¹ = Ph, R² = Me, R³ = CN: **17d**, 65%
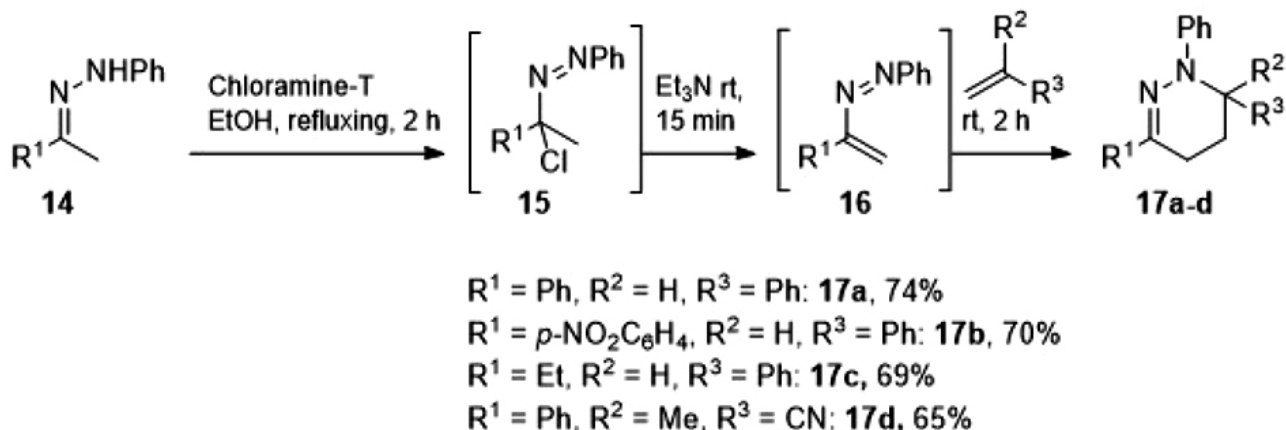
Scheme 5. [4+2] cycloaddition of electron-deficient azoalkenes and electron-rich alkenes

In 2014 Wang *et al*. reported the copper-catalyzed asymmetric aza-Diels-Alder reactions of an *in situ* generated azoalkene (**18**) and indoles (**19**) to generate tetrahydropyridazine derivatives (**20**) [20]. Using a chiral nonracemic ligand and copper (I) as a chelating metal to the azoalkene, the cycloaddtion of this azoalkene with indoles generated adducts with excellent yields and high levels of enantioselectivity.

R¹ = H, R² = Me, R³ = Me: **20a**, 95%, 97% *ee*
R¹ = 4-Br, R² = Me, R³ = Me: **20b**, 85%, 97% *ee*
R¹ = 7-OMe, R² = Me, R³ = Me: **20c**, 91%, 96% *ee*
R¹ = H, R² = Me, R³ = Bn: **20d**, 87%, 94% *ee*
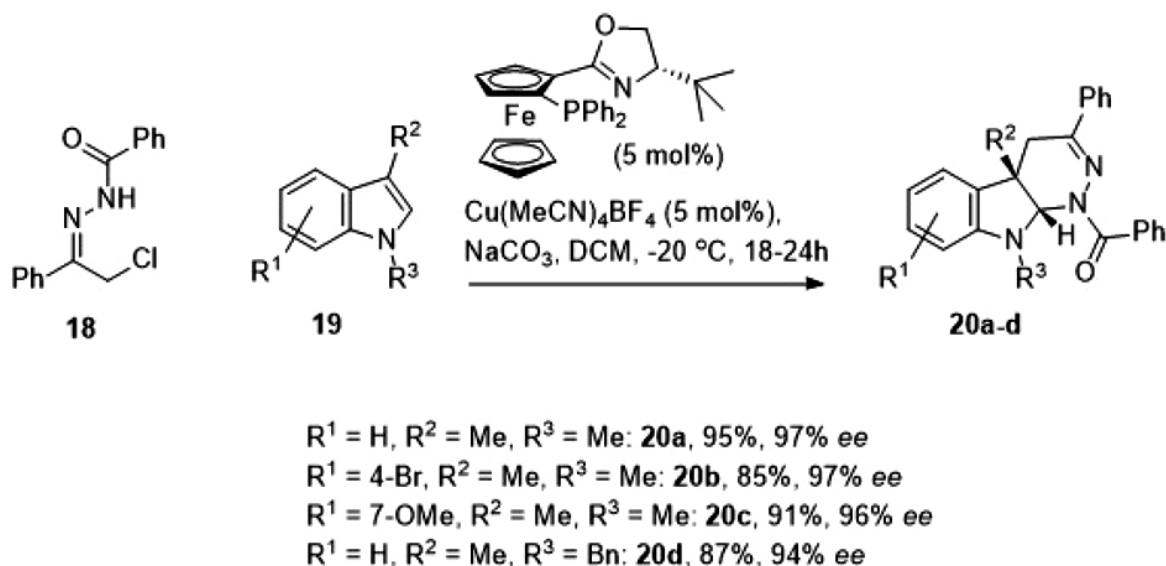
Scheme 6. Catalytic asymmetric aza-Diels-Alder reactions of an azoalkene with indoles

4. [4+1], [4+3], and [3+2] Cycloaddition

The copper-catalyzed asymmetric [4+1] cycloaddition of *in situ* generated azoalkenes with sulfur ylides to produce dihydropyrazole derivatives was reported in 2012 by Bolm *et al*. (**21 → 22**) [21].

In the presence of base (Na₂CO₃), α-halo hydrazones (**21**) underwent a dehydrohalogenation to form azoalkenes, which was presumably activated by Cu(OTf)₂ complexed to the chiral nonracemic Tol-BINAP ligand (**L**). The cycloaddition of the activated

azoalkenes with ylides produced synthetically and biologically important dihydropyrazoles (**22**) in

good yields (83-97%) with high enantioselectivitives (up to 97:3 *er*).

R¹ = H, R² = Ph: **22a**, 89%, 91:9 *er*
R¹ = H, R² = 4-ClC₆H₄: **22b**, 85%, 90:10 *er*
R¹ = H, R² = 4-OMeC₆H₄: **22c**, 95%, 90:10 *er*

R¹ = OMe, R² = Ph: **22d**, 84%, 97:3 *er*
R¹ = OMe, R² = 4-ClC₆H₄: **22e**, 93%, 96:4 *er*
R¹ = OMe, R² = 4-OMeC₆H₄: **22f**, 95%, 92:8 *er*
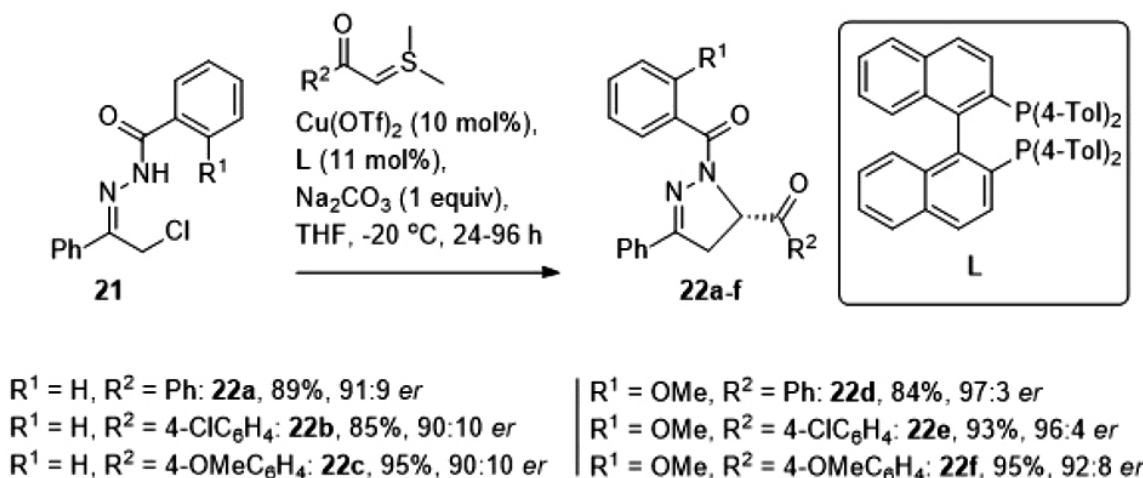
Scheme 7. Asymmetric [4+1] cycloaddition of *in situ*-derived azoalkenes with sulfur ylides

The enantioselective [4+3] annulation reactions between enals and *in situ* formed azoalkenes was reported in 2014 by Glorius *et al* (**23 → 24**) [22]. This organocatalysis process,

catalyzed by an *N*-heterocyclic carbene generated from **Precatalyst** (Scheme 8), produced a diverse set of 1,2-diazepine derivatives (**24**) in good yields with excellent enantioselectivities.

R¹ = Ph, R² = H: **24a**, 70%, 99% *ee*
R¹ = Ph, R² = F: **24b**, 60%, 99% *ee*
R¹ = Ph, R² = Me: **24c**, 63%, 99% *ee*

R¹ = 4-OMeC₆H₄, R² = Ph: **24d**, 68%, 99% *ee*
R¹ = 4-FC₆H₄, R² = Ph: **24e**, 58%, 98% *ee*
R¹ = 4-CF₃C₆H₄, R² = Ph: **24f**, 61%, 99% *ee*
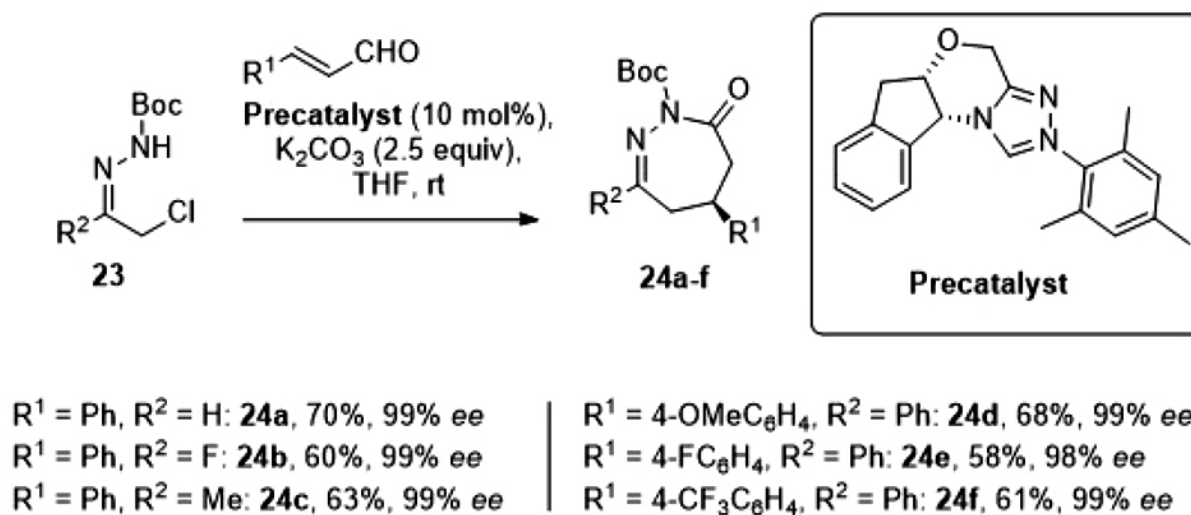
Scheme 8. Asymmetric [4+3] cycloaddition of *in situ*-derived azoalkenes with enals

In 1982 Attanassi *et al*. reported [3+2] cycloadditions of azoalkenes and methylene activated compounds (e.g. β-ketoamide, β-nitrilamide), generating pyrrole derivatives (**25 → 27**) [23]. In this process, treatment of acyclic or cylic azoalkenes (**25**) with β-ketoamides in

the present of CuCl₂ produced the 1,4-adducts (**26**), which underwent the intramolecular condensation to form pyrrole derivatives (**27**). A similar process using the cyclic system was reported by the same group in 2009 (**28 → 30**) [24].
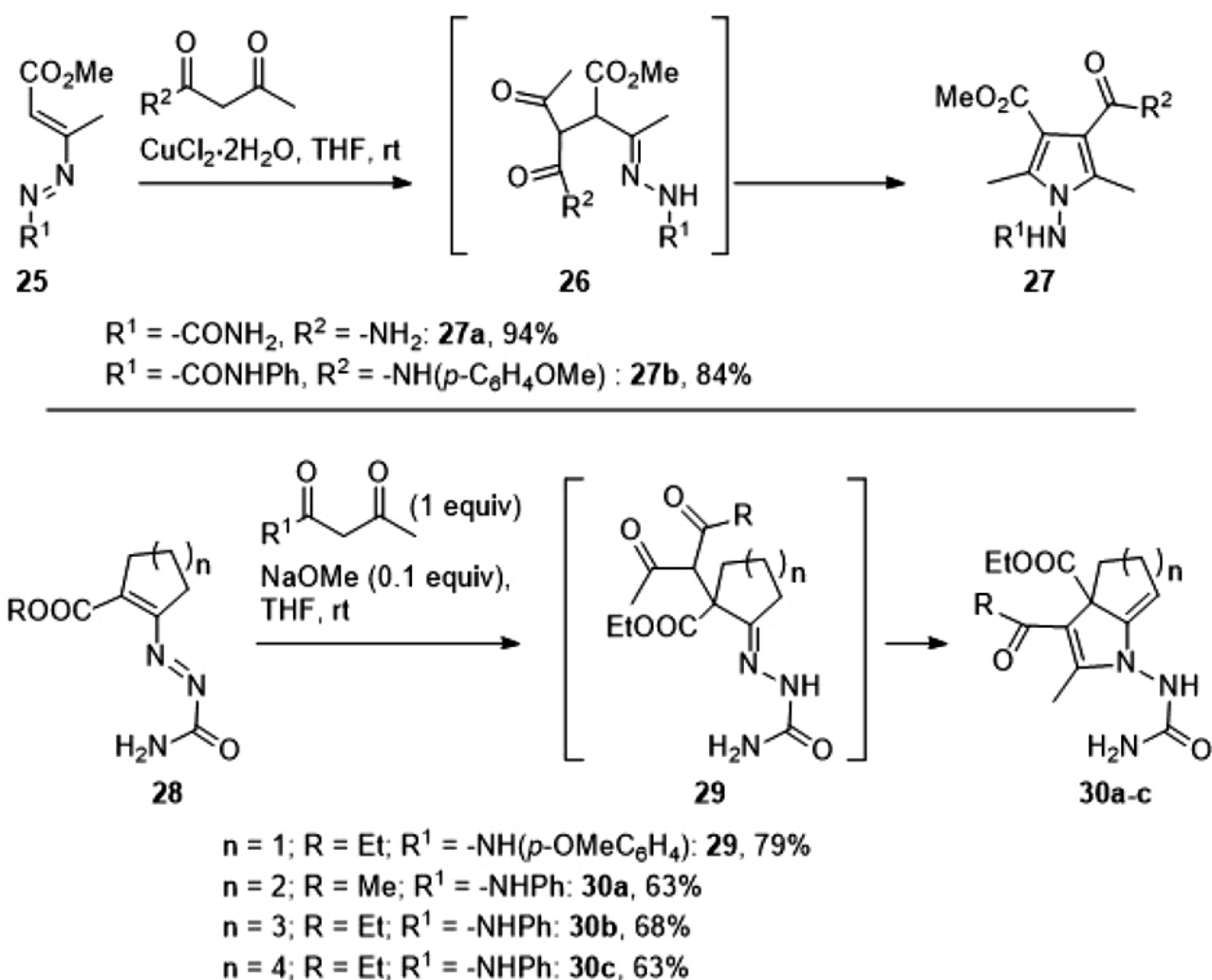
Scheme 9. [3+2] cycloaddition of azoalkenes and activated methylene compounds

5. Conclusion

This mini review has described the chemistry of azoalkenes as valuable scaffolds in hetero-cycloaddition reactions. The reactions that were presented illustrate the versatility of these building blocks for the synthesis and functionalization of a wide range of invaluable heterocycles, including those with chiral derivatives. It should be noted that only a few examples of asymmetric hetero-cycloaddition have been reported in the literature. Given the significance of generating useful heterocycles which can be used for the synthesis of biologically active molecules, this is an area that should be received more attention.

References

[1] Blond, G.; Gulea, M.; Mamane, V. "Recent Contributions to Hetero Diels-Alder Reactions." Curr. Org. Chem. 2016, 20, 2161- 2210.

[2] Attanasi, O. A.; De Crescentini, L.; Favi, G.; Filippone, P.; Mantellini, F.; Perrulli, F. R.; Santeusanio, S. "Cultivating the Passion to Build Heterocycles from 1,2-Diaza-1,3-dienes: the Force of Imagination." Eur. J. Org. Chem. 2009, 3109-3127.

[3] Attanasi, O. A.; De Crescentini, L.; Filippone, P.; Mantellini, F.; Santeusanio, S. "1,2-Diaza-1,3-butadienes: Just a Nice Class of Compounds, or Powerful Tools in Organic Chemistry? Reviewing an Experience." Arkivoc 2002, 11, 274-292.

[4] Attanasi, O. A.; Filippone, P. "Working Twenty Years on Conjugated Azo-alkenes (and environs) to find New Entries in Organic Synthesis." Synlett 1997, 1128-1140.

[5] Lemos, A. Cycloaddition Reactions of Conjugated Azoalkenes. In Targets in Heterocyclic Systems: Chemistry and Properties; Attanasi, O. A., Spinelli, D., Eds.; Soc Chimica Italiana: Rome 2010, 14,

pp 1-18.

[6] Brachet, E.; Belmont, P. "Inverse Electron Demand Diels-Alder (IEDDA) Reactions: Synthesis of Heterocycles and Natural Products Along with Bioorthogonal and Material Sciences Applications." Curr. Org. Chem. 2016, 20, 2136-2160.

[7] Belskaya, N. P.; Eliseeva, A. I.; Bakulev, V. A. "Hydrazones as Substrates for Cycloaddition Reactions." Russ. Chem. Rev. 2015, 84, 1226-1257.

[8] Lange, J. H. M.; den Hartog, A. P.; van der Neut, M. A. W.; van Vliet, B. J.; Kruse, C. G. "Synthesis and SAR of 1,4,5,6-Tetrahydropyridazines as Potent Cannabinoid CB1 Receptor Antagonists." Bioorg. Med. Chem. Lett. 2009, 19, 5675-5678.

[9] Yang, X. L.; Peng, X. X.; Chen, F.; Han, B. "TEMPO-Mediated Aza-Diels-Alder Reaction: Synthesis of Tetrahydropyridazines Using Ketohydrazones and Olefins." Org. Lett. 2016, 18, 2070-2073.

[10] Schantl, J. "2-Phenylazo-1-alkenes." Monatsh. Chem. 1972, 103, 1705-1717.

[11] Lopes, S. M. M.; Cardoso, A. L.; Lemos, A.; Pinho e Melo, T. M. V. D. "Recent Advances in the Chemistry of Conjugated Nitrosoalkenes and Azoalkenes" Chem. Rev. 2018, 118, 11324-11352.

[12] Wei, L.; Shen, C.; Hu, Y.; Tao, H.; Wang, C. "Enantioselective synthesis of multi-nitrogen-containing heterocycles using azoalkens as key intermediates" Chem. Com. 2019, 55, 6672-6684.

[13] Schantl, J. "CIS-α,β-Dialkylated and TRANS-α,β-Dialkylated Phenylazo-alkenes." Monatsh. Chem. 1972, 103, 1718-1729.

[14] Eschenmoser, A.; Felix, D.; Ohloff, G. "New fragmentation reaction of α,β-unsaterated carbonyls. Synthesis of exaltone and rac-muscane from cyclododecanone" Helv. Chim. Acta 1967, 50, 708-713.

[15] Tanabe, M.; Crowe, D. F.; Dehn, R. L. "Novel fragmentation reaction of α,β-unsaterated carbonyls. Synthesis of acetylenic ketones" Tetrahedron Lett. 1967, 3943-3946.

[16] Sommer, S. "[4+2]-Cycloadditionen of azoalkenen with electron-rich alkene" Chemistry Lett. 1977, 6, 583-586.

[17] Faragher, R.; Gilchrist, T. L. "Cycloadition reactions of nitrosoaslkenes and azoalkenes with cyclopentadiene and other dienes" J. Am. Chem. Soc., Perkin Trans.1. 1979, 249-257.

[18] Clarke, S. J.; Gilchist, T. L.; Lemos, A.; Roberts, T. G. "Reactions of azoalkenes derived from hydrazones of ethyl bromopyruvate with electron rich alkenes and heterocycles" Tetrahedron 1991, 47, 5615-5624.

[19] Gaonkar, S. L.; Lokanatha Rai, K. M. "A New method for the generation of azoalkenes from ketohydrazones and its application to the synthesis of tetrahydropyridazine derivatives" Tetrahedron Lett. 2005, 46, 5969-5970.

[20] Wei, L.; Wang, C. "The Catalytic asymmetric synthesis of tetrahydropyridazines via inverse electron-demand aza-diels-alder reaction of enol ethers with azoalkenes" Chem. Comm. 2015, 51, 15374-15377.

[21] Chen, J.; Dong, W.; Candy, M.; Pan, F.; Jorres, M.; Bolm, C. "Enantioselective synthesis of dihydropyrazoles by formal [4+1] cycloaddition of in situ-derived azoalkenes and sulfur ylides" J. Am. Chem. Soc. 2012, 134, 6924-6927.

[22] Guo, C.; Sahoo, B.; Daniliuc, C. G.; Glorius, F. "N-Heterocyclic carbene catalyzed switchable reactions of enals with azoalkenes: formal [4+3] and [4+1] annulations for the synthesis of 1,2-diazepines and pyrazoles" J. Am. Chem. Soc. 2014, 136, 17402-17405.

[23] Attanasi, O. A.; Bonifazi, P.; Foresti, E.; Pradella, G. "Effect of metal ions in organic synthesis. Part 10. Synthesis and X-ray crystal structure of some 1-(arylamino)pyrrole derivatives by reaction of (arylazo)alkenes and β-dicarbonyl compounds in the presence of copper(II) chloride: J. Org. Chem. 1982, 47, 684-687.

[24] Attanasi, O. A.; Berretta, S.; Crescentini, L. D.; Favi, G.; Golobic, A.; Mantellini, F. "Synthesis of new cycloalkenyliden-pyrroles by domino reaction" Tetrahedron 2009, 65, 2290-2297.

Paragraph writing ability of second year English-majored students, Duy Tan University

Khả năng viết đoạn của sinh viên chuyên ngữ năm thứ hai, Đại học Duy Tân

Tho Thi Tran
Trần Thị Thơ

Foreign Languages Department, Duy Tan University, Danang, Vietnam
Khoa Ngoại ngữ, Đại học Duy Tân, Đà Nẵng, Việt Nam

Abstract

In order to gain a clear picture on the writing abilities of Duy Tan University's English-majored students in paragraph composing, and thus, give proper solutions to the problems, this paper will focus on two main issues (1) to identify and study the reality of students' learning in paragraph writing, and (2) to suggest some solutions to improving the teaching methods of writing 3, and composing skills in general for teachers of English.

Keywords: writing/composing, paragraph, skills, English-majored.

Tóm tắt

Để có cái nhìn rõ ràng về khả năng viết của sinh viên chuyên ngữ Đại học Duy Tân trong lĩnh vực soạn thảo đoạn văn và nhờ đó, có thể đưa ra được những giải pháp thích hợp cho vấn đề này; bài báo sẽ tập trung vào hai nội dung chính: (1) Xác định và nghiên cứu thực trạng khả năng học của sinh viên trong lĩnh vực viết đoạn văn, (2) Đưa ra giải pháp cải thiện phương pháp giảng dạy môn viết 3 nói riêng và kỹ năng viết nói chung cho giảng viên chuyên ngữ Anh.

Từ khóa: viết/soạn thảo, đoạn văn, kỹ năng, chuyên ngữ Anh.

1. Introduction

Nowadays, being good at four communicative skills is a must for all language learners in general and for those specializing in English in specific. However, according to the common fact, writing skills seem always an obstacle for most of them, as they cannot do it well, be good at it and get confident in it.

It is a fact that students have had a lot of problems in learning this subject. Besides, their writing abilities are of different levels, depending on their knowledge - both in English and in cultural-social understanding, and personal interests. As a result, the problems they encounter and the challenges they face up are various, which makes a big obstacle for teachers of this skill in dealing with such a multi-level class.

Similarly, students at the department of Foreign Languages, Duy Tan University also have different and uneven abilities and skills in writing. In fact, they cannot grasp the technique of writing paragraphs, and make a lot of mistakes in every

---

Email: tranthitho97@gmail.com

aspect. For these reasons, this paper, "*Paragraph Writing Ability of Second Year English-Majored Students, Duy Tan University*", will aim at getting a better and more proper method for the teaching and learning of writing skills at Department of Foreign Languages, Duy Tan University.

2. Paragraph Writing Ability of Second Year English-Majored Students, Duy Tan University

2.1. Methods of the Study

To implement this analysis properly, the author has applied the three methods of quantitative, qualitative and descriptive, which will be orderly described as follows:

2.1.1 The quantitative method

An investigation of the writing skills and abilities of second year students of English majored at DFL will be carried at first. At this stage, the number of various kinds of paragraph mistakes would be counted first. After that, all these faults should be classified into categories and estimated.

2.1.2 The qualitative and descriptive methods

Based on the quantitative data gotten from (1), the study will be carried out. Both the qualitative and descriptive methods will be applied to analyze the faults in writing of second year students at Duy Tan University.

This method will be dealt with in different aspects. The theoretical background of writing, and English paragraphs as well as paragraph writing will be considered first. Some examples will be taken to illustrate this point. Then come the hypothesis, data interpretation and analysis. To make a thorough view, other examples will be analyzed to show up the causes and solutions for each kind of mistakes.

2.2. Paragraph writing ability of second year English-majored students at Duy Tan university

2.2.1. An overview from academic results

Since the first academic year of DFL, English - majored students at DTU have been taught with

paragraph writing skills, as the course of writing 3 has long been adopted to the requirements of the field and students' abilities in English communication. From the general syllabus, the book "Wring Academic English" by A. Oshima was chosen as the course book, along with other referential materials for writing skills.

To get a thorough view of students' recorded performance in this subject, the author believes that the academic results should be the first thing to be shown and analyzed. For this aim, the final marks of students in five successive years, from 2013 to 2017 (accordingly, from K18 to K22) were searched thoroughly. In the first year of 2013, K18 had 4 classes, including about 100 students. The next year, around 80 students of K19 were chosen. In the following year, there were 4 classes of K20 with roughly 95 students to be taken into account; in 2016, K21 of DFL had 8 classes and around 220 students, and lately, K22 of 2017 gathered 210 students in 8 classes. The results are illustrated in the following chart:
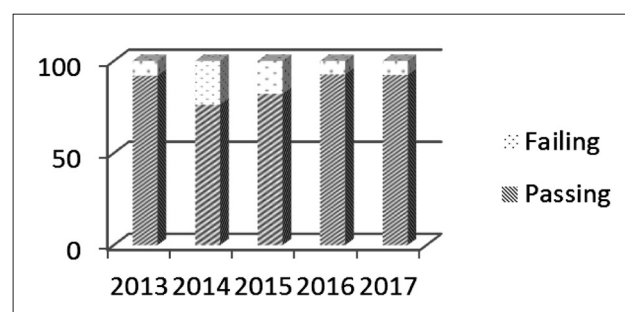
Chart 1.: Academic results of first year students in writing 3 (2013-2017)

As clearly shown in chart 1, it is obvious that in 2013, students' performance was rather good. The final result points out that only 92 students out of 100 passed this course, accounting for 92.00%. However, the next two years witnessed a decrease in students' performance when only 61 students of K19 and 78 students of K20 had acceptable marks in this subject, accounting for 76.25% and 82.11%, respectively.

Nonetheless, things went much better in the fourth year, when 92.72% of the total 220

students scored 4.0 or above. 2017 witnessed a slight fall in the number of successful students, with 92.38% students (194) passing this subject.

2.2.2. Students' attitudes toward writing 3

A small survey among second – year students of English major at DFL, DTU about their attitudes in the class of writing 3 was carried out. The 500 subjects of this survey, who were randomly chosen in 5 successive years from 2013 to 2017, were asked to fill in a questionnaire for their thinking and feelings of the courses, the book, the teachers, as well as their likes and dislikes about the field, and so on.

For the general opinions about the subject, the teachers and the course book, as well as other materials in use in Writing 3, the results are summarized in chart 2:
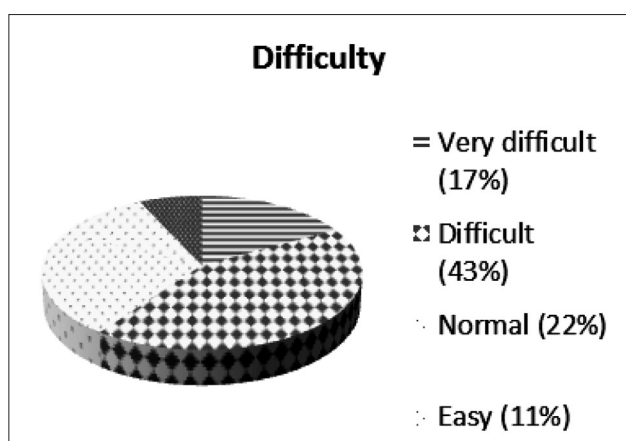
Chart 2.: The level of difficulty of the subject

On the whole, not many students dared to think that this subject was simple, only 7% and 11% of them considered this to be very easy and easy, respectively. Surprisingly, this rate is nearly the same with those who found it very difficult (17%). The majority told that this subject was difficult (43%), or just normal (22%).

More detailedly, students were also required to give their ideas on their involvement in class' activities, as can be seen through Chart 3:
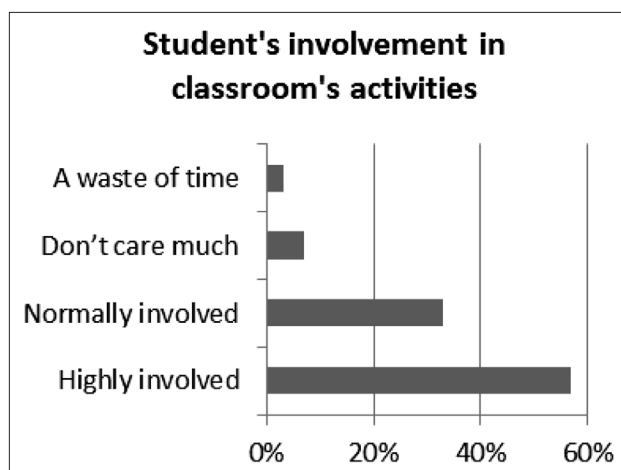
Chart 3.: Second year student's involvement in writing class' activities

Commonly, second-year students of English major are judged by many teachers as fairly motivated learners in every class, which can be illustrated in Chart 3. Most of them felt very interested in the lessons and appeared extremely likely in every class, writing included. In fact, 57% of the subjects said "highly involved" and another 33% chose "normally", which means that the activities of Writing 3 made them feel happy and attracted enough to acquire the knowledge, along with doing the exercises related.

2.2.3. Analysis of paragraph written by second year English - majored students at Duy Tan University

As required by the syllabus, second year students of English major at DFL, DTU are taught to get familiar, and then write – step by step - three major parts of a paragraph, as well as 5 kinds of paragraph composing, in any topics as pre-demanded.

When asked about the levels of challenges in each of the parts above, the majority of students ranked the last aspect (relating to idea developing for different kinds of paragraph) to be very difficult (87% said this), while the first two, namely writing topic and concluding sentence, undoubtedly, were

of "easy" (91% agreement). Surprisingly, none of the session was considered as "very easy", as this option was chosen by no one.

For better illustration, 200 samples of students' writing of paragraph composing in English were collected throughout 5 academic years to analyze and criticize. The pieces of writing are carefully studied in the following aspects:

(1) A good topic sentence

(2) A suitable and sound concluding sentence

(3) The coherence of sentence and ideas

(4) The unity - no irrelevant sentences found

(5) Idea development for each kind of paragraph

(6) Good vocabulary and structure in use

The figures for this are clearly shown in the graph below:
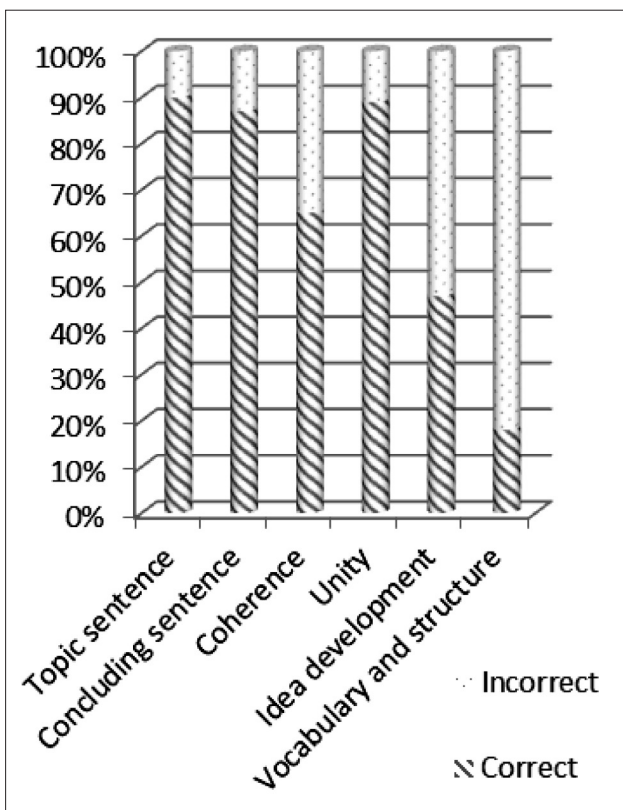
Chart 4: Percentage of correct parts in paragraph writing of second year students - English major at DTU

The incorrect parts will then be further analyzed for their problems. For better treatment and solutions, the flaws will then be categorized into different kinds for each part. Besides, two related charts will be shown first, one is for students' ideas on their own faults, and the other represents the percentage of students' real writing in this subject.

In order to get students' opinion on their own obstacles in writing, 7 different factors have been pointed out, they are: *Difficulties in inventing and arranging the ideas, Challenges in writing topic and concluding sentences, A lack of vocabulary, Insufficient knowledge in English grammar and/or structure, Connecting ideas, Avoiding irrelevant sentence(s), and Limited amount of time*. And here are the results:
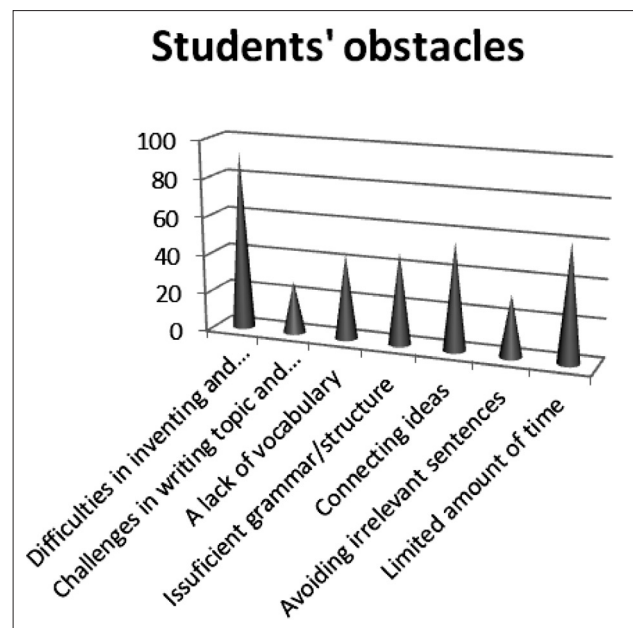
Chart 5: Second-year Students' obstacles in Writing 3

As can be seen from Chart 5, the most difficult thing for students is obviously the step of *inventing ideas*, which causes nearly 90% learners find it challenging when writing a paragraph, then come the limitation in time, idea connection and English structures. Surprisingly, writing topic and concluding sentences are not very hard for them, as only 20% found this impossible in some ways.

In addition, the collected samples of students' writing give out an almost similar explanations on the following issues:

(i) Incorrect topic sentence

Among the various types of mistakes made by those second year, English - majored learners

at DFL, writing faulty topic sentences is not commonly found in all the kinds of paragraphs. In fact, this only appears in 24% of the sentences collected. The following example can illustrate this point:

Example 1: (*Topic: Smoking*)

→ (1) Today, many people smoke everywhere.

→ (2) Science proves that smoking may cause lung cancer, which is a very serious disease.

→ (3) Smoking has many disadvantages but it hasn't any advantages.

For the topic of *smoking*, all these topic sentences are problematic:

- The first one, "*Today, many people smoke everywhere*", is too general, as it contains no specific controlling ideas for further development.

- The second one, "*Science proves that smoking may cause lung cancer, which is a very serious disease.*" is, in contrary, too narrow. There is just one piece of information presented in this one, and thus, the body cannot be developed.

- The third one, "*Smoking has many disadvantages but it hasn't any advantages*" has the two necessary parts – the topic "*smoking*" and the controlling ideas "*many disadvantages – no advantages*"; however, it is grammatically incorrect and clumsy, as the verb *to have* and the conjunction *but* are incorrectly used in this case.

Obviously, three most common mistakes of the topic sentence should be (i) it is too general, (ii) it is, on the other hand, too narrow, and (iii) it is grammatically wrong. All these problems make the topic sentence a bad one and cannot be used to start a paragraph.

(ii) Unsuitable concluding sentence

This kind of mistake takes only 18% in total, the smallest portion of all. Errors in concluding sentences fall into two types (i) it doesn't

match with the topic sentence and/or the whole paragraph, and (ii) it has grammar/ vocabulary mistakes, as in example 2:

Example 2: (topic: people's life quality today)

→ *Topic sentence*: Nowadays, there're a lot of high - class services to satisfy demands of people, so their life quality is improved.

→ *Concluding sentence*:

- (1) In conclusion, people can live longer and wants to live longer because of life's development.

- (2) In short, life quality's people is gooder because of there are many new conveniences in life.

From these two concluding sentences, it can be seen that the first one does not match with the topic sentence since it discusses another idea - *people can live longer*. Besides, the second one has three grammar mistakes in *life quality's people*, *gooder* and *because of*.

(iii) No coherence

Nearly a half of the paragraphs collected (47%) have this kind of mistakes. When some or all of the sentences are not connected by linkers (namely conjunctions or conjunctive adverbs/ phrases), and/or a consistent use of pronoun throughout the composition, the paragraph is incoherent.

(iv) A lack of unity

Totally, there is about one-fourth of the samples fall into this flaw. In their writing, sometimes students insert one or two irrelevant sentences which discuss another idea, and the unity of the paragraph is broken.

(v) Faulty use of vocabulary and structures

Out of common belief, students of English major, in their second year, still encounter so many mistakes in vocabulary and grammatical structures. As pointed out in chart 3.10, 42% of the writings have this kind of problem.

(vi) Poor, non-creative ideas

It's surprising that as many as 61% students questioned in this survey said that it's too hard for them to think about *what to write*, especially in *a limited amount of time* like in a mid-term or final test (the same number of students felt stressful and couldn't do well under this pressure of time). Homework seems to be easier due to the fact that they have more time to look on the Internet or other materials for *ideas*. The thing that makes everyone startle is that the topics given in writing are not too complex or academic, as students are required to write about such normal fields as *education, entertainment, family, sport, health, travelling,* and so on.

2.3 Solutions to improving second year students' writing ability in paragraph composing

With the help of the facts, strong and weak points of students' writing ability as analyzed and discussed above, the solutions can be given to help not only learners in their learning Writing 3, but also teachers in their lessons of this subject.

There are so many things to do to improve students' writing ability from this very academic step. Their vocabulary must be upgraded; their knowledge of English grammar and structures needs to be arranged and made it more practical. Moreover, they also need more practice in paragraph composing process and ideas inventing. For more specific treatment, some solutions are given as follows:

2.3.1 Extra exercises and activities to upgrade students' vocabulary stock

The ways of learning every single word seem to be outdated when students enter college. The thing they need now is a logical arrangement of words, phrases and expressions, as well as their special uses in situations. Therefore, writing teachers, besides the main lessons, can use some extra exercises or activities to widen learners' vocabulary stock and make it their own "treasure" for present and later use, not only in Writing 3 but also other subjects

2.3.2 A review of useful structures and/or grammatical points for every lesson

At the beginning of the term, it is suggested that teachers should let students do a quick test of grammar to check their level in this. Then, during every class, a little reminding of related grammar rules is advisable. Students need to have good awareness of the close connection between grammar and writing, so that they can avoid silly mistakes.

In addition, in every lesson, there should be a corner for language revision. For example, when learning about process describing, students ought to be reviewed with passive structures and words/ phrases for chronological order. Likewise, in the part of writing concluding sentence, the technique of paraphrasing should be revised first hand, and so on.

For students' writing, a lot of teachers still have the habit of correcting all their mistakes; however, experienced lecturers don't do so. Detailed correction is done for some of the first tasks for illustration, then incorrect parts will be underlined/ highlighted and students are asked to edit themselves. Otherwise, for a more objective way, some teachers require students to exchange their writing in groups and peer - editing is also of good support. A good and easy way to do this is to tell students that this is just a grammar task, and all they need to do is simply correct the grammatical errors underlined in the sentences.

2.3.3 "Practice makes perfect" in English paragraph writing

Despite the fact that English paragraph composing is complicated, there are still many ways for students to overcome this challenge, with the support of their teachers.

- A logical understanding of the 3 parts in English paragraph is the first need for students. They must be aware of the topic sentence, the body and the concluding sentence, as well as the close relationship among them. Only by doing

so can students' confusion be reduced and thus, they can be more confident in writing their own paragraph.

- The practice exercises in the course book are very helpful for class activities. There are different kinds of tasks, ranging from simple to difficult, for students to first get familiar with the theory and then practice writing, either under control or on their own.

However, for students' work at home, the exercises in this course book seem to be not enough. It is said that "practice makes perfect", therefore, more tasks should be created by teachers for learners' homework. After finishing controlled writing tasks in class, students can deal with freer activities in a variety of topics after that as further practice. This is the only way for their improvement in Writing 3.

- Peer editing and group work in class and at home can be very effective for students: in class, under the supervision of teachers, students can work together in small groups, exchange experience and help each other for self - correction. Besides, after finishing writing, they can share their work among group members for critics and improvement. This also can be done after class, but it requires students' self - awareness and motivation, since there's no teacher in the library or at home to control their chit-chats.

- Finally, students, consulted by their teachers, can themselves find referential materials on English paragraph composing in the library or on the Internet, and making themselves having more knowledge about that through reading and do more practice in that source of information.

2.3.4 Knowledge upgrading in social and cultural topics

The weak point of lacking general knowledge seems to be the hardest to overcome. Vocabulary can be upgraded, grammar knowledge can be improved and made more practical, and writing the whole paragraph can be practiced to get more

familiar; and many students can do that well. However, gaining sufficient general knowledge for writing is still a big challenge for them, as knowledge cannot be widened in one day or one month or even one year, and the habit of "asking Mr. Google for everything" is in their blood!

Unfortunately, even experienced teachers cannot help much in this field. Lecturers can only suggest materials and books to read, correct the errors, and students have to manage everything themselves, depending on their effort and intelligence to enlarge their own mind in every field.

The study would like to suggest some possible ways to widen students' knowledge, in order to help them gain more ideas for their own writing:

- Read more: with the boom of technology nowadays, within a click of the mouse, or a visit to a bookstore nearby, a huge store of information appears in front of students. They can easily find books, newspapers, magazines, etc. everywhere, which can help them update their knowledge and widen their understanding about almost all general things on earth.

- Learn more: the things they read will easily be dropped out if learners fail to "learn" from that. Every piece of information is a lesson that can be useful at present or in the future. Read and memorize them all, turn them into ideas in writing paragraphs!

- Build up the good habit of reading and being curious about new things: for long term effect, students must build up the habit and interest in reading and learning, however difficult or time-consuming it is. College study requires learners to be as knowledgeable as possible, and for Writing 3, simple ideas cannot make good paragraphs!

3. Conclusion

With a brief view on students' academic results and detailed analysis of their real performance

in writing 3, the study has clearly shown the writing ability of second year students of English major at DTU. A survey has been carried out to get students' self - evaluation and opinion in the subject, so that a more objective point of view can be gained for a thorough research of the matter.

In addition, their strong and weak points are also discussed, together with some possible solutions to improving all the problems. Like a two-sided coin, second year students' writing ability in this very challenging subject of their students' life contains both advantages and disadvantages. Being young and new, they are gifted with the love for knowledge, the energetic interest in the lesson and the wish to learn more. Still, being so young and inexperienced, their mistakes in every corner, from vocabulary to grammar, from headachy new structures to idea inventing, are inevitable and, to some extent, should be tolerated. The role of teachers in this beginning year is, therefore, vitally needed, to support and supervise. All blocked gates have their own keys, and so does this issue. Undoubtedly, students' writing ability in sentence building will sooner or later be improved.

References

[1] Canale, M. and M. Swain (1980). *Theoretical Bases of Communicative Approaches to Second Language Teaching and Testing*. Longman Publisher.

[2] Cook, V.(2001). *Second Language Learning and Language Teaching*. London: Hodder Arnold.

[3] Ellis, R. (1997). *Second Language Acquisition*. Oxford University Press.

[4] Jacob, Roderick (1999). *English Syntax*. Cambridge University Press.

[5] Mile, Robert, Marc Bertonasco, and William Karns. (1991) *Prose Style: A contemporary Guide*, Second edition. Englewood Cliffs, New Jersey: Prentice Hall.

[6] Oshima, Alice and Hogue, Ann, (2003) *Writing Academic English, Third edition.* Nxb Trẻ.

[7] *Oxford Advanced Learner's Dictionary* (1997), Oxford University Press.

[8] *Oxford Advanced Learner's Encyclopedia Dictionary* (1997)

[9] Rei RNoguchi, (1991) *Grammar and the Teaching of Writing*.

[10] *Webster's Third New International Dictionary* (1993), Merriam-Webster Inc

[11] Weinreich, U. (1953). *Languages in Contact*. NewYork Linguistic Circle.

[12] William, Joseph. (2010) *"Cohesion and Coherence" Style: Ten Lessons in Clarity and Grace*, 10th edition. Boston: Longman.

Characteristics of the Historic Urban Cities of Viet Nam in comparative study with the others in Asian countries

Đặc trưng của đô thị lịch sử Việt Nam trong nghiên cứu đối sánh với các nước châu Á

Le Vinh An[a], Nguyen Thi Kim Nhung[b]
Lê Vĩnh An, Nguyễn Thị Kim Nhung

[a]*Faculty of Architecture and Fine Art, Duy Tan University, Danang, Vietnam*
Khoa Kiến trúc, Đại học Duy Tân, Đà Nẵng, Việt Nam
[b]*Faculty of Tourism, Duy Tan University, Danang, Vietnam*
Khoa Du lịch, Đại học Duy Tân, Đà Nẵng, Việt Nam

Abstract

This paper presents an overview of the formation process and typical features of the ancient urban cities of Vietnamese from the 3rd BC to 19th century by combining a series of research methodology such as: historical documents study, measurement investigation on sites by using the optimal machine, analyzing of the architectural measurement data, mapping study on the ancient urban cities to extract the rules and typical characteristics of ancient urban of Vietnamese. Additionally, the paper presents the features of the Hue's UNESCO World Cultural Heritage site as the case study in this paper.

In addition, the paper also conducted a comparative study between the characteristics of ancient urban cities of Vietnam with other ancient urban cities of Asia countries in the regional relationship to find out the similarities and common denominator among them, approximate the origins of these in Asia.

Keywords: Vietnam, Historic urban, Comparative study, Asia countries.

Tóm tắt

Bài báo này trình bày tổng quan về quá trình hình thành và những đặc trưng tiêu biểu của các đô thị lịch sử Việt Nam từ thế kỷ thứ 3 đến thế kỷ 19 bằng cách kết hợp một loạt phương pháp nghiên cứu: Nghiên cứu tài liệu lịch sử, đo đạc thực địa bằng máy toàn đạc quang tuyến, phân tích dữ liệu bản vẽ kiến trúc, nghiên cứu tư liệu bản đồ cổ để rút ra những quy tắc và đặc trưng tiêu biểu của các đô thị lịch sử của Việt Nam. Thêm vào đó, bài báo trình bày về những đặc trưng của đô thị Huế - Di sản Văn hóa Thế giới UNESCO như là trường hợp nghiên cứu điển hình.

Ngoài ra, bài báo cũng đã tiến hành nghiên cứu đối sánh giữa các đô thị lịch sử của Việt Nam và các đô thị lịch sử của các nước châu Á trong mối quan hệ vùng để tìm ra những điểm tương đồng và mẫu số chung giữa chúng, từ đó xác định nguồn gốc của các đô thị lịch sử châu Á.

Từ khóa: Việt Nam, Đô thị lịch sử, Nghiên cứu đối sánh, Châu Á.

1. Introduction

Architecture and Urban are indispensable places to give the people a comfortable life, an biological environment of thinking, researching and healthy way of their cultural development. Since primary, the ancient Vietnamese have a

Email: levinhan@dtu.edu.vn

knowhow of chosen the good lands to settle, set up their villages, organize production, improvement and development of their used land. The traditional villages of the Vietnamese or the ancient capital city of the feudal dynasties of Vietnam are mainly based on the natural feature of the land characteristized by the bigest rivers (water factor) and the higest mountain (landmark factor) from which appeared the concept of "Giang/River-Son/ Moutain" (江山) refered to the concept of Country which has been common used up to nowaday.

Historically, every movement of each capital city caused by changing of hydrological geography is associated with a new occupied land that directly or indirectly affect the prosperity or decline of the feudal dynasties. In fact, from the "Co Loa" ancient capital city (Dong Anh district, Ha Noi) of An Duong Vuong king (257-208 BC) to the "Hoa Lu" capital city (Ninh Binh province) of Dinh Bo Linh king (968-1009), the "Thang Long" capital city (Ha Noi) of Ly Thai To king (1010-1788), the "Tay Do" capital city (Thanh Hoa province) of Thanh Nguyen king (1400-1407)[1], the "Phu Xuan" capital city (Thua Thien Hue province) of Quang Trung king (1788-1802), the "Gia Dinh" citadel (Sai Gon) of Nguyen Phuoc Anh landlord (1836-1859)[2] to the Hue capital city of Gia Long king (1802-1945)[3].

2. Characteristics of the Historic Urban Cities of Viet Nam

2.1. Urban of "Rectangle of water"

Co Loa citadel, the capital of Au Lac country during the An Duong Vuong period was built around 3rd century BC, then later became the capital of other feudal state during Ngo Quyen period in early 10th century[4]. Co Loa citadel located at the top of the Hong/Red river delta where plays an important role of waterways and roads exchange, on a hill in the left bank-side of the Hoang Giang river (now deposited by alluvial deposits into a small canal) connecting with the Hong river and the Cau river. In terms of waterway traffic, Co Loa has an ideal geographic location than anywhere else in the

Northern delta of Viet Nam at that time built on a rectangle of water formed by three rivers: the Hong river in South side, Cau river in North side and Hoang river in East side.

Thang Long citadel, the capital of Dai Viet country during the Ly dynasty (1010-1225) until the end of the Le Trung Hung dynasty (1533-1789), was built on the old site of Dai La citadel during the An Nam Do Ho Phu (安南都護府) period (679-886)[5]. Thang Long citadel is also built on a rectangle of water formed by three rivers: the Hong river in East side, the To Lich river in North side and the Kim Nguu river in South side. In the early 11th century, Ly Thai To king moved the capital from Hoa Lu (Ninh Binh province) to this land, expanded to build a new one and renamed by Thang Long citadel (fig.1).
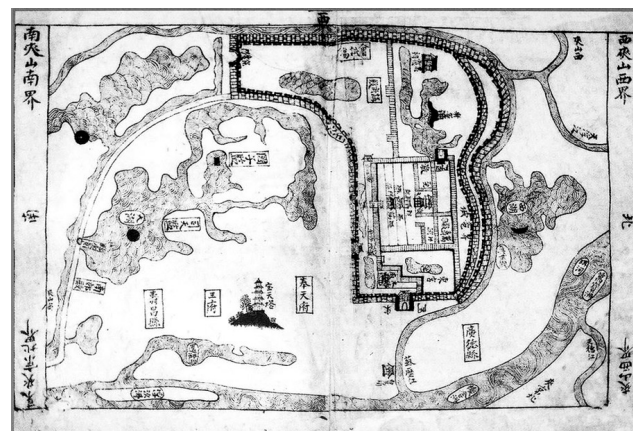
Fig 1. Site map of the Thang Long citadel

Tay Do citadel, the capital of Dai Ngu country, built by Thanh Nguyen king (Ho Quy Ly) in 1397[6], is also located on a rectangle of water formed by two rivers: the Ma river in West side and the Buoi river in East side wind their way through the capital those connected together at the South side, Northern side of the capital obstructed by the Tho Tuong mountain. This land, however, wasn't the ideal land that Thanh Nguyen king would like to choose, but due to the urgent circumstances of the historical context before the threat of invasion by the Ming (China), the priority for military defense is paramount,

so the chosen land must have a lot of military advantage and good navigation on waterways and roads.

Hoi An ancient town (15-19 centuries) was formerly a large port of Champa country, well known as Dai Chiem port, also played an important role of international trading port of Viet Nam during the Nguyen dynasty[7], located at the intersection of the Hoai river (a tributary of the Thu Bon river) and the Co Co river (through the Tourane bay) open up a wide stretch of water ahead of them to the Dai Chiem beach.

Hue citadel, the capital city of Viet Nam country during the Nguyen dynasty (1802-1945) was built by Gia Long king in 1805, basically completed in 1832 under Minh Mang king[8]. The land chosen to build the capital is also located on a rectangle of water formed by three rivers: the Huong Giang river (front river side) in South side, the Kim Long river (central river) and the Bach Yen river (back river side) in North side. Huong Giang river and Bach Yen River are closed in the East and the West side to form a middle ground that called "Vuong Dao" (land of kingdom) by the Nguyen dynasty. This is an ideal land for a traditional capital city oriented by the theory of "Feng Shui", which was the place where there were two dynasties met each other: the Phu Xuan capital city of Quang Trung king and the Hue capital city of Gia Long king are preserved upto present (fig.2).
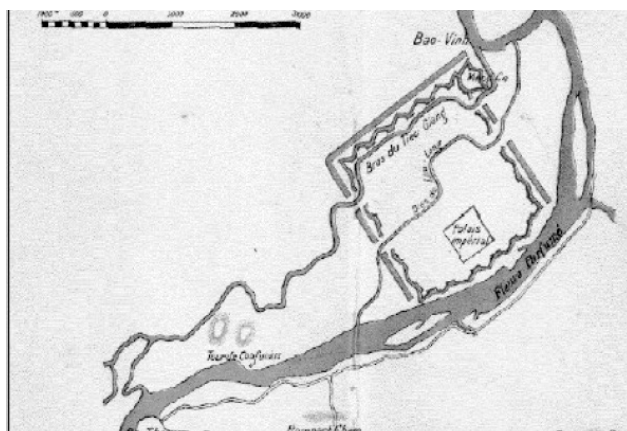
Fig 2. Site map of the Hue citadel

Gia Dinh citadel (formerly known as Phien An Gia Dinh citadel (formerly known as Phien An bastion or Bat Quai bastion) was a base of Nguyen family during the warring time[9]. On the same land that once existed two citadels were built and destroyed (1790-1859). The land chosen to build the Gia Dinh citadel is also located on a rectangle of water bounded by three rivers: the Saigon river in East side, the Thi Nghe river in North side and the Ben Nghe river in South side. After captured of the Gia Dinh citadel and destroyed it, the French shifted their urban center 1 km forward to the South and formed the administrative, economic, port and military center of the District 1, Ho Chi Minh city nowaday (fig.3).

Bản đồ Gia Định năm 1985 do Trần Văn Học vẽ
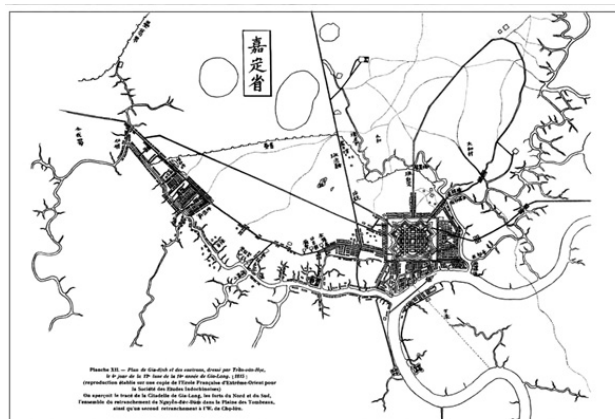
Fig 3. Site map of the Gia Dinh citadel

Thus, it can be said that the mind of "Water" in the traditional urban planning is shaped very early time and have persistence vitality. The chosen lands have eloquently demonstrated their role through the development history of the Vietnamese nation.

2.2 Urban of "Mountain and River"

Mountain and River are usually the basic geographical factors for a settlement of ancient Vietnamese in particular and of ancient Asia people in general (fig.4). The concept of "Non-Nuoc" (峯/Mountain-水/Water factor) is distinguished from the "Phong-Thuy" (Feng-shui/風水) concept which originally came from ancient China civilization.
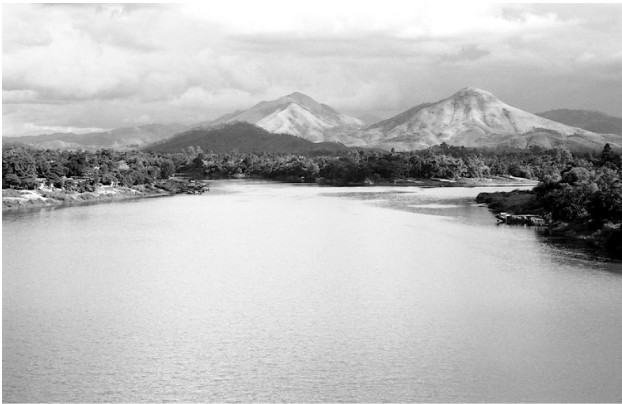
Fig 4. Mountain and River of the Hue urban

Indeed, if the "Water" to be an essential factor for the life, then the "Mountain" to be a necessary landmark factor to find the place of residence. Really, a pair of Mountain and River are common over the country such as: Hong river and Tan Vien mountain (Ha Noi - Trang An region), Lam river and Hong Linh mountain (Thanh Hoa - Nghe An region), Huong Giang river and Kim Phung mountain (Hue region), Thu Bon river and Nui Chua mountain (Quang Nam region), Saigon river and Ba Den mountain (Saigon - Gia Dinh region), Dong Nai river and Chua Chan mountain (Bien Hoa - Dong Nai region) etc. Most of the Vietnamese historic urban cities are based on those two factors .

2.3 Urban of "Spiral shape"

The earliest ancient carpital city of Viet Nam has been recognized is Co Loa citadel (3rd BC). The name "Co Loa" comes from the shape looked like trumpet spiralling from bottom to top which including three layers of soild-walls and bamboo. According to the dicsription in historic documents and archaeological ecavation results, date and scale of the citadel have been definded attaching with amount of tagible evidents which have been continuoslly conserved at the site. This type of citadel is unique in Vietnam.

2.4 Urban of "Magic square"

In the early periods, the place of residence of Vietnamese had been formed along river bank-sides of the big rivers. Accordingtly, the shape

of ancient capital cities and its citadel was also formed basing on the shape of natural geographic, such as Hoa Lu citadel and Thang Long citadel.

Since the Ho dynasty (1400-1407), the citadel has changed into quadrilateral shape absoluted symmetry over the central axis. By the Nguyen dynasty, the magic square in urban planning has been characterized by the "Tinh Dien" principle dating from the Zhou dynasty (1123-323 BC). Regardingly, each land is divided into 9 equal squares, the square in the middle used for public (public rice field), other 8 rounded square used for private (private rice field). Accordingly, the land plots, transport axes and architectural residences are arranged in a grid pattern matching the axes. This magic square in urban planning is typical of the countries influenced by ancient Chinese civilizations (fig. 5).
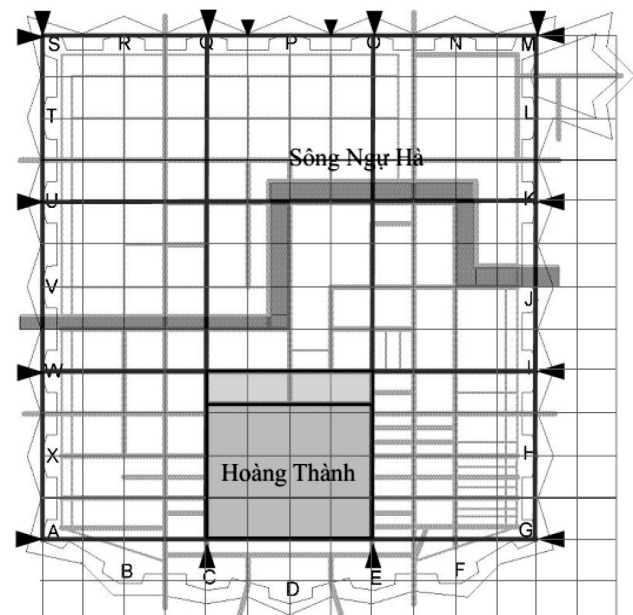
Fig 5. Site planning of the Hue citadel

3. Characteristics layouts of the Hue ecological urban city

3.1 Natural features of the Hue area

The Hue capital city is the great assembly of the typical historic architectures of the one history stage in Vietnam from early 19th century to middle of 20th century, which is including the citadel planned at the central, imperial palaces

located inside the citadel, imperial mausoleums planned at the West-South direction of the urban city, temples, shrine, pagodas, esplanade, royal arena and mandarins residence planned surrounding the citadel.

It can be said that the Hue area located in a dreamlike beauty of natural landscapes along with full-factor of the native oriental geomancy idea marked by the Kim Phung Son (highest mountain) and Huong Giang (bigest river), which composed the pair of „Mountain and River" to form whole natural feature of the Hue capital city which has been whole conserved continuously till nowadays.

3.2 "Fengshui" concept of the Hue capital city

Historically, the land-cote of the Hue capital city is lower than the present around 1.2m, thus, the Nguyen dynasty had to gather clean-land from over country to filling up the area for construction[10]. In 1805, Minh Mang emperor gave a decision to fix main axis of the Citadel faces to East-South direction (slanting 25 degree from North-South direction) based on the theory of Fengshui[11]. It is an ideal direction for the Emperors govern a state (fig.6) and the physical conditions of architectural construction.
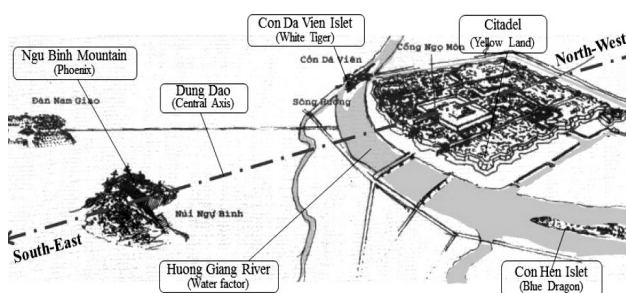
Fig 6. Fengshui concept of the Hue urban city

The architects of Nguyen Court were very skillful to engage the Capital city into great beauty natural landscape with full natural factor of ancient Fengshui theory: The Ngu Binh mountain placed on the central axis, in front of the Citadel, plays a role of Tien An/Phoenix; the Hen island placed on the left hand-side of the Citadel, plays a role of Thanh Long/Blue Dragon; the Da Vien island placed on the right hand-side of the Citadel, plays a role of Bach Ho/White Tiger; the Truong Son mountain placed on back side of the Citadel, plays a role of Huyen Vu/Black Turtle; the Citadel placed at central, plays a role of the Huynh Tho/Yellow Earth, and Huong Giang river winds through front-base of the Citadel, plays a role of Minh Duong/Water as a salient factor of substantial environment for whole city, winds its way through front-base of the Citadel to shape "Z" feature of river brings prosperous for the Capital city.

3.3 Magic square and Vauban defensive system of the Hue citadel

The Citadel of Hue is a combination between the construction ideas of ancient Chinese's capital city which including three wall-layers (Citadel - Imperial city - Forbidden city) and the concept of defensive system of Vauban style which was popular in Europe in 17th century (fig.7).

Site plan of the Citadel was divided into 9 equal parts as "Tinh Dien" (井田) principle. The central part is originally used for Imperial City was a little bit moved to South side, its area equal 1/9 of the Citadel, then area of the Forbidden city equal 1/3 Imperial city.

Basing on historical documents study and the analyzing results of the site investigation by using optimal measurement machine[12] could bring the understanding that: small units (u) used for architectural design called "Thuoc" (1u = 426mm), the large unit (U) used to plan the axis of the Citadel called "Truong" (1U = 4260mm), the small unit (s) used to determine the grid called "Luoi Truong" (1s = 4260 x 4260mm = 18.15m2), and the large unit (S) used to classify its ground-lot called "Phuong" (1S = 45s x 45s = 36,754m²). Total area of Hue citadel = 12s x 12s = 5,292,000m² (equivalent to 529.2 ha = 5,292 km²)

In a word, Hue capital city is the resonance

of urban of "Rectangle of water" – urban of "Mountain and River" – urban of "Fengshui" and urban of "Magic square" combinated with defensive system of Vauban.

Fig 7. Aerial photo and Magic square of the Hue citadel

4. Similar between those and the others in Asia countries

It is possible to recognize the similarity of the location of ancient urban of Asian countries in many cases, although the geographic distance between these urban is quite far, varies in terms of time and the civilization. Hereafter are some case of comparative studies could be mentioned.

4.1 Similar in "Rectangle of water"

There are 9 of 15 historic urbans listed in Table 1[(13)] (accounting for 60%) were formed on the lands located at the intersection of rivers which forming a "Rectangle of water" bounded the ancient towns. These urban belonging to the countries influenced from both China and India civilization, dating very early (Jinan/China, 722 BCE) to late (Hue/Vietnam, 19th AD). Formation of urban which based on the naturally "Rectangle of water" express the way of agricultural production and waterway tranpostation from the earliest stages of Asian history (fig.8, 9).
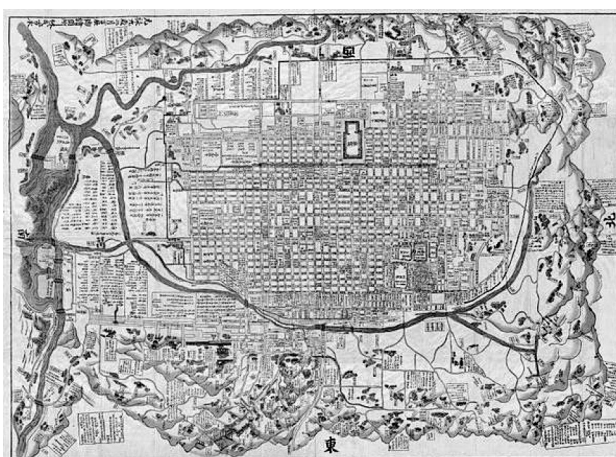
Fig 8. "Rectangle of water" of Kyoto, Japan
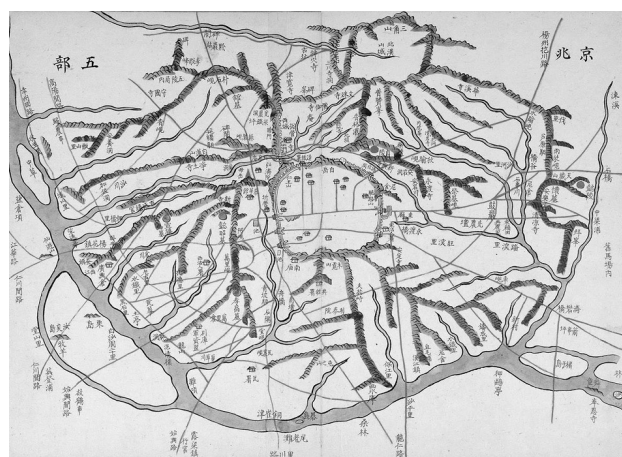
Fig 9. "Rectangle of water" of Hanyang/Seoul, Korea

4.2 Similar in "Mountain and River"

Similarly, there are 9 of 15 historic urbans (accounting for 60%) formed based on the geographic typicalized by higest mountain in pair with bigest river, this feature may including or excluding of the "Rectangle of water" mentioned above. All of these are belonging to the countries influenced from both China and India civilization. This form of urbanization is very common in the island and peninsula countries in Asia (refer to 2.2).

4.3 Similar in "Magic square"

There are 6 of 15 historic urban (accounting for 40%) are planned according to the principle of "Magic square" (fig.10) dating from the 7th to the 19th century. These urban are mostly of

China or belonging to the countries influenced from China civilization, such as Vietnam, Japan and Myanmar. However, the case of South Korea and North Korea are directly affected by Chinese civilization, but there isn't any manifesting of this urban style. "Magic square" of urbanization began to emerge in the Asia region when Chinese civilization began to expand its influence to the surrounding areas.
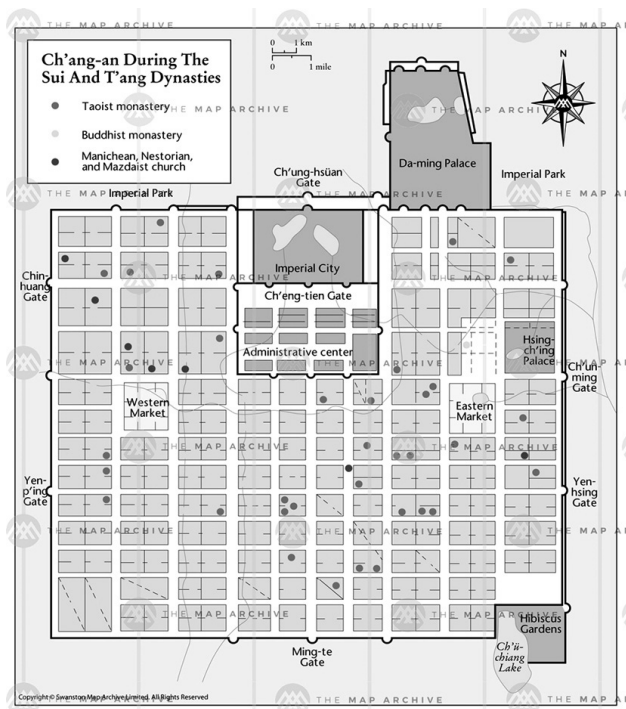
Fig 10. "Magic square" of Ch'ang-an, China

4.4 Similar in "Fengshui"

Similar to the case of urban "Magic square", there are 7 of 15 ancient urban (accounting for 46,6%) are planned based on the ancient Chinese Feng Shui theory represented with five elements (refer to 3.2) dating from the 7th to the 19th centuries. These urban type are in Asian countries such as China, Korea, Japan and Vietnam.

4.5 Similar in "Spiral shape" and "Vauban"

The lowest ratio (accounting for 13.3%) of the 15 historic urban are "Spiral shaped" and "Vauban system", appearing in Vietnam (3rd BC, 19th AD) and Japan (17th, 19th AD). The appearance of this urban type in two Asian countries and varies in term of times separated from 200 years up to 2000 years is a very special phenomenon and unintelligible.

5. Common denominator

The results in Table 1 show that the urban type of "Rectangle of water" and "Mountain and river" among the countries is highest ratio (60%). Its dating was also very early (from 722 BCE until 19th century) and appeared in almost country influenced from both China and India civilization. This allows us to speculate that: The "Rectangle of water" and "Mountain and river" urban type are cornerstone of Asia countries, and may have existed before these countries took effect from civilizations. Other urban features are the layers added later by acculturation through history.

The similarities of urban type of "Magic Square" and "Fengshui" took the ratio from 40% to 46,6%, also appeared very early and began to flourish from the 7th to the 19th centuries. These type of urban are typicalize for the countries influenced by Chinese civilization such as China, Japan, South Korea and Vietnam.

Urban features of "Spiral shape" and "Vauban system" are special phenomena, occurring only at very low ratio (13,3%) and there are no rules for these. It can be said that this type of urban features can only appear in special circumstances

Tab 1. Statistical charts of historic urban cities in Asia countries

Stt	Urban/Country	Date	Rectangle of water (1)	Mountain and river (2)	Magic square (3)	Fengshui (4)	Spiral shape (5)	Vauban system (6)
1	Co Loa/Vietnam	3rd BC	X	X			X	
2	Hue/Vietnam	19th AD	X	X	X	X		X
3	Nara/Japan	8th AD	X	X	X	X		
4	Kyoto/Japan	17th AD	X	X	X	X		
5	Hakodate/Japan	19th AD						X
6	Edo (Tokyo) /Japan	17th AD					X	
7	Ayutthaya/Thailand	14th AD	X					
8	Bangkok/Thailand	18th AD	X					
9	Watphou/Laos	5th AD		X				
10	Hanyang/S. Korea	14th AD	X	X		X		
11	Pyongyang/N. Korea	2nd BC	X	X				
12	Mandalay/Myanmar	19th AD		X	X			
13	Jinan/China	722 BCE	X	X		X		
14	Chang'an/ China	7th AD			X	X		
15	Beijing/China	14th AD			X	X		
	Ratio		60%	60%	40%	46,6%	13,3%	13,3%

of history once that country was in danger of facing an invasion war from foreign.

6. As a conclusion

The past exists or does not exist directly affect to the present space and time of human. Urban development, if not based on traditional inheritance, that denies the results of the natural selection process. Respect for history in this case is to respect the hydrological conditions of each selected land through history. Understanding the causes and mechanisms of traditional urban formation will be appropriate to ensure sustainable development of that urban cities.

References

[1] Ngo Si Lien, Dai Viet Su Ky Toan Thu (大越史記全書), 1697.
[2] Cao Xuan Duc, Quoc Trieu Chanh Bien Toat Yeu, 1908.
[3] Nguyen dynasty, Kham Dinh Dai Nam Hoi Dien Sự Le, Cong Bo (欽定大南會典事例).
[4] Vien Su Hoc, Lich Su Viet Nam, Tap 1, NXB Dai Học và Giao Dục Chuyen Nghiep, 1991.
[5] Ngo Si Lien, Dai Viet Su Ky Toan Thu, NXB Van Hoc ISBN 0032891, Ha Noi 1989.
[6] https://vi.wikipedia.org/wiki/Thanh_nha_Ho
[7] https://vi.wikipedia.org/wiki/Hoi_An
[8] Nguyen dynasty, Kham Dinh Dai Nam Hoi Dien Sự Le, Cong Bo (欽定大南會典事例); Dai Nam Nhat Thong Chi, Kinh Su.
[9] Trinh Hoai Duc, Gia Dinh Thanh Thong Chi (嘉定城通志), 1830.
[10] According to the results of excavation carried out by the Hue Monuments Conservation Center in September, 2008,
[11] Nguyen dynasty, Kham Dinh Dai Nam Hoi Dien Sự Le, Cong Bo (欽定大南會典事例)
[12] Investigation result of the UNESCO World Heritage Institute, Waseda University, Japan 2007.
[13] Mapping study results based on old map of the sites and Wikipedia digital dictionary.

An investigation into pragmatic failure in English utterances made by third-year English majors at Duy Tan University

Tìm hiểu thất bại ngữ dụng học trong phát ngôn tiếng Anh của sinh viên năm thứ ba chuyên ngữ tại Đại học Duy Tân

Huu Phuoc Duong

Dương Hữu Phước

Faculty of Foreign Languages, Duy Tan University, Danang, Vietnam
Khoa Ngoại ngữ, Trường Đại học Duy Tân, Đà Nẵng, Việt Nam

Abstract

This article investigates pragmatic failure in English utterances made by third-year English majors at Duy Tan University (DTU) in producing the speech acts of refusal and apology. Based on the obtained results, it puts forward a number of suggestions about English learning and teaching with a view to assisting the students in avoiding this failure and enhancing their ability to communicate with native speakers.

Keywords: pragmatic failure, speech act, refusal, apology, utterance.

Tóm tắt

Bài báo tìm hiểu thất bại ngữ dụng học trong phát ngôn tiếng Anh của sinh viên năm thứ ba chuyên ngữ tại Đại học Duy Tân khi đưa ra lời từ chối và xin lỗi. Từ kết quả khảo sát, bài báo đưa ra một số đề xuất về việc dạy và học tiếng Anh với hy vọng giúp cho người học khắc phục sự thất bại này và nâng cao hiệu quả giao tiếp với người bản ngữ.

Từ khóa: thất bại ngữ dụng, diễn ngôn, lời từ chối, lời xin lỗi, phát ngôn.

I. Introduction

Successful communication in the target language requires not only a knowledge of grammar and vocabulary but also pragmatic competence and knowledge about the culture of target language (Rezvani & Ozdemir, 2010) [16]. As Eslami-Rasekh (2004) [10] puts it, the development of pragmatic and sociolinguistic rules of language use is important for language learners. If learners are unaware of this issue, pragmatic failure is inevitable.

As a teacher of English, I find that most of the students majoring in English at DTU have difficulty communicating with English native speakers in spite of having a good grasp of vocabulary and grammar. They are inclined to transfer sociolinguistic rules of speaking from their mother tongue to the target language. Improper performance of utterances might result in serious consequences, including misunderstanding, embarrassment, and even rudeness.

Email: huuphuoc101981@gmail.com

With a view to helping the students at DTU in particular and students in Vietnam in general get over this failure, I would like to conduct an investigation into pragmatic failure encountered by third-year English majors at DTU.

This study aimed to examine students' regularities of language use in the speech acts of refusal and apology. Based on the research findings resulted from an analysis and evaluation of the students' responses, constructive suggestions are provided to help them produce appropriate utterances in those speech acts. In addition, some recommendations in terms of the learning and teaching approaches are offered in the research to enable learners to avoid this failure.

II. Content

1. Definition of "Pragmatic Failure"

Pragmatic failure was firstly coined by Jenny Thomas in her article Cross-cultural Pragmatic Failure in 1983. She defined and classified pragmatic failure in the essay and set a theoretical foundation for the analysis of pragmatic failure in cross-cultural communication. Since then, pragmatic failure has been a focus of cross-cultural pragmatics. Riley (1984) [18] explained pragmatic failure as follows:

Pragmatic failure occurs when we fail in some way to understand a speaker's full intention in saying something. For some reason, we do not go successfully from what is said to what is meant. It is, therefore an umbrella term covering a wide variety of communicative problems which prevent the successful grasping of the contextual meaning of an utterance.

Qian Guanlian (2002) [17] points out that "Pragmatic failure is committed when the speaker uses grammatically correct sentences, but unconsciously violates the interpersonal relationship rules, social conventions, or takes little notice of time, space and addressee."

From my perspective, pragmatic failure is regarded as a communicative failure committed in the process of interpreting or expressing utterances due to a lack of the capability of accurate interpretation or of appropriate use of language in different contexts.

2. Speech act theory

Speech act theory has aroused the widest interest of all the issues in general theory of language usage (Levinson, 1983) [14]. It plays a core role in the field of pragmatics. Philosophers, such as Wittgenstein, Austin and Searle, proposed the foundation of speech act theory. Wittgenstein(1953, cited in Bach, 2004) [25] made a significant contribution to the field of pragmatics by stating that language was a social activity and "the meaning of a word is its use in language" (Bach, 2004, p.463) [3]. Austin was the father of pragmatics (Mott, 2003) [15] and founded the speech act theory (Austin, 1962, 1975) [2].

Austin (1962) [1] introduced the concept of the speech act, and his speech act theory was built on the basis of his belief that speakers do not use language to say things, but to do things. Therefore, utterances are regarded as speech acts. Austin developed a system to distinguish three components of speech act, which was regarded as seminal work:

(a) the locutionary act: the utterance of a sentence with determinate sense and reference

(b) the illocutionary act: the making of a statement, offer, promise, etc. In uttering a sentence, by virtue of the conventional force associated with it or with its explicit performative paraphrase

(c) the perlocutionary act: the bringing about of effects on the audience by means of uttering the sentence, such effects being special to the circumstances of utterance

Searle (1976) [21] advanced Austin's notion of speech acts and classified five categories of illocutionary force:

(a) representatives, which commit the speaker to the truth of the expressed proposition (paradigm cases: asserting, concluding, etc.)

(b) directives, which are attempts by the speaker to get the addressee to do something (paradigm cases: requesting, questioning).

(c) commissives, which commit the speaker to some future course of action (paradigm cases: promising, threating, offering).

(d) expressives, which express a psychological state (paradigm cases: thanking, apologizing, welcoming, congratulating).

(e) declarations, which effect immediate changes in the institutional state of affairs and which tend to rely on elaborate extra-linguistic institutions (paradigm cases: excommunicating, declaring war, christening, firing from employment).

2.1. Speech act of refusal

Refusals are face-threating acts (Brown & Levinson, 1987) [7] and only occur when a speaker directly or indirectly says no to a request or an invitation. Refusals belong to the classification of commissives, for they commit speakers to future action (Searle,1977) [22]. Chen (1996) [9] indicated that refusals are opposite to the interlocutor's expectation, and they are often achieved through indirect strategies. Refusals are important as they are sensitive social variables, such as gender, age, education level, power and social distance (Brown & Levinson, 1987) [7]

2.2. Speech act of apology

Olshtain (1989) proposed that an apology was "a speech act which is intended to provide support for the hearer who are actually or potentially malaffected by a violation" (pp. 156-157). When a person apologizes, he or she shows a willingness to disgrace himself or herself to the person/s being apologized to. Apologizing is face-saving act for the hearer and face-threating act for the speaker (Bataineh, 2006) [4].

Gooder and Jacobs (2000) [12] pointed out that "the features of the proper apology are the admission of trespass, the implied acknowledgment of responsibility, an expression of regret, and a promise of a future in which injury will not recur" (p.214).

Brown and Attardo (2000) [6] proposed five components of an apology as follows:

(a) an expression of apology, in which the wrongdoer repeats the feelings of an regret

(b) an explanation of the situation, whereby the wrongdoer tries to reconstruct the incident to see that he/she deserve forgiveness.

(c) an acknowledgment of responsibility, in which the wrongdoer states his/her responsibility for what has happened as a part of the apology.

(d) an offer of repair whereby the wrongdoer tries to offer a way to compensate for the harm.

(e) a promise of non-recurrence, in which the wrongdoer promises not to repeat the offense.

3. Research Methods

3.1. Research Approach

Both quantitative and qualitative methods were applied in this study. The data were collected and analyzed with quantitative techniques embedded into a primarily qualitative research framework. It was believed that a combined quantitative and qualitative method was better than only one approach in discovering DTU students' pragmatic failure and pragmatic competence.

3.2. Respondents

There were approximately four hundred third-year English majors in the academic years from 2014 to 2017 at DTU. Among these, a hundred students were invited to complete the questionnaire and discourse completion test voluntarily. They were fully informed of the aims and significance of the study by the researcher prior to the beginning of the study, and made their decisions independently as to whether to join or not.

3.3. Research Instruments

3.3.1. Questionnaire

The questionnaire designed for this study included six open-ended questions. Each provided a real-life communicative context (see Appendix A). The 100 respondents were required to write down appropriate utterances according to their own understanding and they were allowed to look up unfamiliar words in the dictionary. By using open questions instead of multiple choice questions, the researcher intended to prevent the respondents from using elimination skills in answering these questions so as to guarantee the validity of the research feedback.

3.3.2. Discourse completion test

This research used a discourse completion test (DCT) including five situations (see Appendix B), which required students to read a description of each situation and then asked them to write down what they would say in that situation. The use of DCT aimed to collect data about students' pragmatic knowledge and to examine whether their utterances are appropriate in given situations or not. Failure to use language properly is referred to as pragmatic failure.

4. Research results

4.1. Findings from the questionnaire

In this section, there were six situations designed to examine how participants make apologies. Based on Brown and Attardo's (2000) [6] five components of an apology, this study applied three R's- namely regret, responsibility, and remedy (Bataineh & Bataineh, 2006) [6] to analyze the apologies provided by respondents in the questionnaire.

Table 1 shows the percentage of participants' use of components when making an apology.

Table 1: Frequency of components used in apologies

Components	Situation1	Situation2	Situation3	Situation4	Situation5	Situation6
Regret	100%	100%	100%	100%	100%	100%
Responsibility	98%	99%	98%	97%	98%	97%
Remedy	75%	76%	87%	79%	85%	73%

As can be seen from the table, virtually all apologies offered by students contained a regret for the offense, e.g. "Sorry, I am sorry/very sorry." and a statement of responsibility, e.g. "I have an important interview". About thirty per cent of the apologies provided a remedy and a promise for committing the offense "I will be more careful", "I won't make the same mistake again".

The findings showed that about seventy five per cent of participants were able to recognize the apology situation and apply proper expressions of apology. Many provided an apology including an indication of taking responsibility and a promise to rectify the situation so as to win forgiveness from the recipient. Remedies offered by students showed their willingness to make up for the mistake. This kind of appropriate social behavior in such a social interaction helps to avoid pragmatic failures in communication (Rose & Kasper, 2001) [19]. However, there were a small number of students who did not offer a remedy for their offense. They did not understand how to give appropriate apologies. That is to say, they lacked appropriate pragmatic knowledge in social communication.

4.2. Findings from discourse completion test

In the DCT, there were five situations designed to examine learners' speech acts of refusal. Their inappropriate responses were considered as pragmatic failure. Refusal strategies or

semantic formulas were analyzed based on the classification adapted from Beebe et al. (1990) [5], including direct and indirect refusals.

Table 2 summarizes the frequency of participants' use of components in the semantic formula.

Table 2: Semantic formula for responses to a refusal

Semantic Formula	Components	Situation 1	Situation 2	Situation 3	Situation 4	Situation 5
Direct strategies	No	0%	5%	2%	6%	4%
	Negative ability	98%	99%	98%	99%	97%
Indirect strategies	Regret	100%	95%	98%	94%	96%
	Positive opinion	2%	3%	6%	6%	1%
	Excuse, Reason, Explanation	75%	85%	90%	85%	87%
	Alternative	0%	0%	0%	7%	0%

In this study, most of research subjects rarely employed 'no', especially to a person of a higher status. The percentage of respondents using 'no' was very low, except in situations in which interlocutors were of equal status, such as a friend's invitation and request. However, some of them responded by using 'no'. That is to say, this word was inappropriate in certain situations involving interaction with people of higher statuses.

As regards 'explanation', respondents frequently used it in almost all situations. However, unlike native speakers, respondents in this study gave vague and dishonest explanations. For example, 'I am sorry, I am busy' in most situations. This seems to show that cultural background affects the selection of utterances. In Vietnam, indirectness is highly valued. In cross-cultural communication, native speakers may feel embarrassed by such explanations.

In terms of 'gratitude', it was realized that a small number of students did not express thanks when refusing invitations and offers. They were unaware of politeness when using English. This revealed that learners had not had adequate pragmatic knowledge to respond appropriately in social communication.

In the present study, it was found that most participants were more likely to use 'regret' in response to invitations and offers than English native speakers. For instance, native speakers frequently employed 'positive feeling' when responding to invitations and offers such as 'I'd love to, but...'. In order to use language function effectively, language learners need to acquire these expressions.

The findings in relation to giving refusals highlighted that many English majors at DTU had known how to respond properly to the speech act of refusal. But not all participants were able to make effective applications in all situations. A small number of participants showed a low level of pragmatic competence. Their responses were unclear and unspecific. The inappropriate utterances led to pragmatic failure in cross-cultural interaction.

The obtained data from both the DCT and the questionnaire indicated that many English majors at DTU lacked pragmatic competence, which is an important component that facilitates successful cross-cultural communication. In many cases, they were unable to produce proper utterances to speech acts of refusal and apology. It follows that students need to have more

practice in speech acts, strategies in using speech acts and mastering pragmatic information in their language learning process to further develop their pragmatic competence. It is inevitable that learners' improper regularities of language use result in pragmatic failure.

5. Recommendations for English learning and teaching

5.1. Recommendations for students and teachers

5.1.1. For students

It should be noted that learners should not assume that English language learning is merely aimed at exam tests. That is to say, they need to grasp both linguistic competence and pragmatic competence to communicate effectively in cross-cultural contexts because the main target of leaning a language is to interact with people in that language.

In addition to knowledge instruction from teachers, learners should make good use of different learning strategies in order to gain required goals, especially pragmatic knowledge used in intercultural communication. Moreover, learners should have a good mastery of cultural knowledge of the target language to the greatest possible.

5.1.2. For teachers

Teachers are responsible for imparting linguistic and cultural knowledge of the target language to the learners. Thus it is absolutely essential that English teachers meet the needs of their students. To develop their language and teaching competence, they should be encouraged and required by the university authorities to attend professional training programs, where they can update their knowledge about English and learn new teaching techniques. In addition, they have to broaden their linguistic and cultural knowledge about the target language through self-study and make good use of all the available resources, which include all kinds of academic journals and books published

in Vietnam and abroad, academic conferences, research projects, and short-term courses abroad and thus improve their language proficiency. In terms of teaching approaches, teachers should avoid introducing pragmatic knowledge in a fixed way. Instead, they should teach students to interpret the meaning of utterances from both linguistic and pragmatic perspectives so as to obtain correct understanding. In fact, EFL learners are inclined to adhere to linguistic patterns they have learned in class and they may not be able to make adjustment in different contexts. For instance, most of the Vietnamese learners may respond to the greeting 'How are you?' by saying 'Fine, thanks. And you?'. This response can cause misunderstanding to English native speakers because it is merely a greeting for them like 'Hello'.

5.2. Recommendations for English course design

English teaching at colleges by teachers still puts an emphasis on the development of learners' linguistic competence while communicative competence is neglected. It is crucial to realize that a college English course is not only a language course offering basic linguistic knowledge as well as pragmatic knowledge, but also a communicative skill development course that assists learners in learning about the culture of the target language.

In designing English courses, it is essential to consider the development of learners' linguistic and pragmatic capacity as well as cultural capacity, which can help them use English effectively.

In order to integrate the culture into English teaching, specific requirements about the contents and methods of culture teaching should be added to the syllabus.

III. Conclusion

Based on the empirical data from the discourse completion test and questionnaire, the researcher has realized that about forty per cent of the

100 respondents could not produce utterances which conform to the rules of target language speech. The article also offers some useful recommendations to help leaners communicate effectively with native speakers as well as proposes some changes in English learning and teaching aimed at overcoming this pragmatic failure.

Appendix A

Questionnaire

__Instructions__: As part of a research project on pragmatic failure investigation, I would like you to help me complete the questionnaire by writing your answers in the space provided to the following situations according to your own understanding. The answers to the questions will ensure the accuracy of the data. Thank you very much for your cooperation!

1. You borrowed a magazine from your best friend, and you ripped the cover page by accident. You are giving the magazine to your friend and say:

....

2. In a cafeteria, you accidentally bump into an older person. The coffee spills all over that person. You might say:

....

3. The librarian lent you several books. Today is the deadline for returning them to the library but you left them at home. As you meet him/her, you might say:

....

4. You are having an important interview at a company. You got up late this morning and hurried to the company. When you got there, you slammed against a secretary and dropped her files. You might say:

....

5. You came to class late today and your teacher complained to you about this, you might say:

....

6. Your manager asked you to complete the report today, but something came up and you couldn't finish it, you might say:

....

Appendix B

Discourse Completion Test (DCT)

Name: …………………   **Age:** ………………….

Native Language: ………

Directions: *Please read the following five situations. After each situation, you are asked to write a response in the blank after "you." Respond as you would talk to the person in English in real life conversation. Please respond as naturally as possible and do not worry about your grammar. You have thirty minutes to finish the following task.*

__Situation 1:__ You are at the office in a meeting with your boss. It's closing to the end of the day and

you want to leave the office because you also have an appointment this evening.

Boss: If you don't mind, I'd like you to spend an extra hour or two tonight so that we can finish up with this work.

You:..

Boss: That's too bad. I was hoping you could stay.

Situation 2: You are a junior in college. You attend classes regularly and take good notes. Your friend often misses a class and asks you for the lecture notes.

Classmate: Oh God! We have an exam tomorrow but I don't have notes from last week. I'm sorry to ask you about this, but could you please lend me your notes once again?

You:..

Classmate: OK, then I guess I'll have to ask somebody else.

Situation 3: You are the owner of a language institute. A teacher asks to speak to you privately.

Teacher: As you know, I have been here just over a year now, and I know you have been pleased with my work here, but to be honest, I really need an increase in pay.

You:..

Teacher: Then, I guess I'll have to look for another institute.

*Situation 4***:** You are walking on campus. A friend of yours invites you to have lunch. In fact, You also want but you do not have enough money.

Friend: Hi, Would you like to have lunch with me?

You:..

Situation 5: You teach English at a university. It is just in the middle of the first term. One of your students comes to speak to you.

Student: Excuse me, professor. Could you give us an extension for the team presentation.

You:..

References

[1] Austin, J.L. (1962). *How to Do Things with Words*. Oxford: Oxford University Press.

[2] Austin, J.L. (1975). *How to Do Things with Words*. Cambridge, MA: Harvard University Press.

[3] Bach, K. (2004). Pragmatics and the philosophy of language. In L. Horn & G. Ward (Eds.), *The Handbook of Pragmatics* (pp.463-487). Oxford: Blackwell.

[4] Bataineh, R. F., & Bataineh, R.F. (2006). Apology strategies of Jordanian EFL university students. *Journal Pragmatics*, 38(11), 1901-1927.

[5] Beebe, L. M., Takahashi, T, & Uliss-Weltz, R. (1990). Pragmatic transfer in ESL refusals. In R. Scarcella, E. Andersen, S. D. Krashen (Eds.), On the Development of Communicative Competence in a Second Language (pp. 55-73). New York: Newbury House.

[6] Brown, S., & Attardo, S. (2000). *Understanding language structure, interaction and variation: An instruction to applied linguistics and sociolinguistics for nonspecialists*. Michigan: Michigan University Press.

[7] Brown, P., & Levinson, S.C. (1978). 'Universals in Language Usage: Politeness Phenomena', in E.N. Goody (ed.), *Questions and Politeness: Strategies in Social Interaction*. Cambridge: Cambridge University Press: 56-289.

[8] Brown, P., & Levinson, S.C. (1987). Politeness. *Some universals in language usage*. Cambridge: Cambridge University Press.

[9] Chen, H. J. (1996). *Cross-cultural comparison of English and Chinese metapragmatics in refusals*. Indiana University. (ERIC Document Reproduction Service No. ED 408 860).

[10] Eslami-Rasekh, Z., (2004). Learning the Pragmatic Awareness of Language Learners. ELT Journal.

59(3). 199 -208. http://dx.doi.org/10.1093/elt/cci039.

[11] Fraser, B. (1990). Perspectives on politeness. *Journal of Pragmatics,* 14, 219-236.

[12] Gooder, H., & Jacobs, J. (2000). On the border of the unsayable: The apology in post-colonizing Australia. *Interventions*, 2, 229-247.

[13] Herbert, R. (1986). Say "thank-you" or something. *American Speech,* 61(1), 76-88.

[14] Levinson, S. (1983). *Pragmatics.* Cambridge: Cambridge University Press.

[15] Mott, B. L. (2003). *Introductory semantics and pragmatics for Spanish learners of English*. Barcelona: Edicions Universitat Barcelona.

[16] Ozdemir, C., & Rezvani. S. A. (2010). Interlanguage Pragmatics in Action: Use of Expressions of Gratitude. *Procedia Social and Behavioral Sciences*. 3. 194-202.

[17] Qian Guanlian (2002). *Pragmatics in Chinese Culture*. Beijing: Tsinghua University Press.

[18] Riley, P. (1984) 'Understanding Misunderstandings: *Cross-cultural Failure in the Language Classroom' in Journal of Teacher Education*,Volume 7/2, pp.127-144.

[19] Rose, K.R and G. Kasper. (2001). *Pragmatics in Language Teaching* pp.1-9 in Rose, K.R. and G. Kasper (eds). Pragmatics in Language Teaching. New York: Cambridge University Press.

[20] Shaul, D. L., & Furbee, N. L. (1998). *Language and Culture*. Illinois: Waweland.

[21] Searle, J. L. (1976). The classification of illocutionary acts. *Language in Society*, 5, 1-24.

[22] Searle, J. L. (1977). A classification of illocutionary acts. In A. Rogers, B. Wall, & J. Murphy (Eds.), *Proceedings of the Texas Conference on Performatives, Presupposition, and Implicatures* (pp.27-45). Washington DC: Center for Applied Linguistics.

[23] Smith, C. (1998). Can adults 'Just Say No?': *How gender, status and social goals affect refusals. Unpublished doctoral dissertation.* University of South Florida.

[24] Thomas, J. (1983). Cross-cultural pragmatic failure. *Applied Linguistics*, 4, 20-39.

[25] Wittgenstein, L. (1953). *Philosophical investigations*. Oxford: Wode, Henning.

The sharing economy and collaborative finance:
A case of p2p lending in Vietnam

Tài chính hợp tác và chia sẻ:
Nghiên cứu trường hợp cho vay ngang hàng trực tuyến tại Việt Nam

Dinh Uyen Tran
Trần Đình Uyên

International School, Duy Tan University, Danang, Vietnam
Khoa Đào tạo Quốc tế, Đại học Duy Tân, Đà Nẵng, Việt Nam

Abstract

Peer-to-peer Online Lending (P2PO) has received increasing attention over the last years, not only because of its disruptive nature and its disintermediation of nearly all major banking functions, but also because of its rapid growth and expanding breadth of services. This model offers a new way of investing in addition to investing in traditional channels such as banking or financial company. The transaction process is done online, the personal information and terms of mobilization are completely transparent and secure in the best way. The strong development of P2PO also raises a number of issues that require careful attention in order to promote positive aspects and to limit negative ones. The research aims to highlight particular aspects of this new business model and to analyze the opportunities and risks for lenders and borrowers in Viet Nam.

Keywords: Sharing economy, P2P lending, Financial innovation, Disintermediation, Fintech.

Tóm tắt

Cho vay ngang hàng trực tuyến (Peer-to-peer Online Lending - P2PO) đã nhận được sự chú ý ngày càng tăng trong những năm qua, không chỉ vì tính đổi mới và việc loại bỏ các chức năng trung gian của các ngân hàng mà còn bởi sự tăng trưởng nhanh chóng và mở rộng phạm vi dịch vụ của nó. Mô hình này đưa ra một cách đầu tư mới, bổ sung vào các kênh truyền thống như ngân hàng hay công ty tài chính. Quá trình giao dịch được thực hiện trực tuyến, thông tin cá nhân và các điều khoản huy động được minh bạch và an toàn một cách tốt nhất. Sự phát triển mạnh mẽ của P2PO cũng nêu lên một số vấn đề cần chú ý thận trọng để thúc đẩy tính tích cực và hạn chế các khía cạnh tiêu cực của nó. Nghiên cứu này nhằm nhấn mạnh các khía cạnh cụ thể của mô hình kinh doanh mới này và phân tích cơ hội và rủi ro đối với người cho vay và người đi vay ở Việt Nam.

Từ khóa: Nền kinh tế chia sẻ, cho vay ngang hàng, đổi mới tài chính, không trung gian, tài chính công nghệ.

1. Introduction

The development of information technology is fundamentally changing many traditional business models. The advent of the internet and the consequently facilitated opportunities for entrepreneurial activities have given a rise in an enormous number of new non-traditional businesses and business models that encompass the so-called "Sharing Economy". The business models of the Sharing Economy are usually

Email: trandinhuyen@duytan.edu.vn

platform-based to match demand and supply. The increasing use of the internet and its possibilities enable online platforms that are easy and cheap to access. Independent of the rest of the design of these non-traditional businesses, the Sharing Economy companies usually provide these platforms. These, in turn, attract demand, often on a very large scale, since they are accessible world-wide.

Known under different names such as "Collaborative Consumption", "peer-to-peer exchange", "on-demand economy", this model is expected to achieve sales of 335 billion dollars in 2025 [1], equivalent to revenue of Traditional rental sector.

The model "sharing economy" has been bringing benefits such as cost savings, environmental protection, increased economic efficiency, reduced social waste and excess capacity of service, products. These are the factors that make the sharing economy model have more potential for growth in the future Time magazine refers to the sharing economy as one of ten ideas which will change the world [2].

The online peer to peer (P2PO) lending model is one part of the Sharing Economy. With the upcoming popularity of online communities, a new way of loan origination has entered the credit market. It transfers the old idea of personal credits into the World Wide Web. In this kind of lending model the mediation of financial institutions is not required [3]. The decision process of loan origination is given into the hand of private lenders and borrowers, and the website like huydong.com offers them a platform to engage with each other. Borrowers and lenders are connected to each other more easily. Moreover, the growing demand for consumer loans has brought many advantages to promote this model [4]

The asymmetry between the benefits of the shared economy model and the P2PO platform with the reality in Vietnam in this sector has prompted a closer study of P2PO knowledge and awareness, which until now, no detailed research has been done yet, to make recommendations to promote P2PO platform development in Vietnam.

However, the researches on Sharing Economy in general and P2PO Lending are very limited. So this paper aim to collect and analyze the opinion of the financial community about the potential development of the P2PO platform in Vietnam and thereby try to give several policy recommendations for its development.

2. Research method

The paper combines qualitative analysis and data survey to serve descriptive statistics. Firstly, the authors study the published works related to Sharing economy and P2PO in the world, combining with the reality in Vietnam to build a specific research structure and questionnaire survey. The questionnaire which was modified after testing surveys will be used in the official survey. The results will eliminate invalid answers, and in total we had 347 valid responses for the next analysis.

The questionnaire is designed for the following three directions:

• Firstly, 9 questions related to the situation of P2PO lending are designed to collect personal background information and historical data from borrowing and lending.

• Secondly, 11 questions concerning the prospect of the new P2PO model and the development dynamics of this model as well as barriers.

• Finally, 5 questions designed to examine the reaction of Vietnamese regulators to this model, which could be used to support or restrict this new model in Vietnam.

The final data will serve as descriptive statistics to answer the research questions. The method in our opinion is reasonable because this study is one of the first scientific research

on P2PO lending in Vietnam in general and Da Nang in particular. Therefore, the results of this study will greatly contribute to the foundation of further qualitative and quantitative research in the future.

3. Papers review on

- The Sharing Economy

The Sharing Economy in recent times has emerged as a global phenomenon. Companies that are emerging in this new paradigm as a David are relying on internet technology to compete face-to-face with the Goliath giants. These new companies are actually Web platforms or Mobile application that brings together individuals who have underutilized assets with people who would like to rent those assets short-term. This model has many economic benefits such as having a positive impact on economic growth and welfare, stimulating new consumption, raising productivity, and catalyzing individual innovation and entrepreneurship [5].

Sharing Economy companies have significantly increased competition in most markets they are active in. Even in markets that are already competitive, the entry of a Sharing Economy company causes an increase in a competition that is mostly unparalleled when compared to traditional business models. The main reason for this is that Sharing Economy companies often do not apply the framework and regulation of the respective market to their activities while traditional companies do. The motivation for this behavior is that they believe that existing, pre-Sharing Economy regulation is inapplicable to Sharing Economy companies, especially P2P models. The argument being made is that the supplier is in fact an individual, not a company. In consequence, it is reasoned that a framework of a market geared to companies could not be applied. Not surprisingly, traditional companies disagree and strive to apply framework and regulation to all companies (and in case

of Sharing Economy businesses to individual suppliers) in a market in the same way [6].

Sharing Economy companies work hard to establish trust since it is a prerequisite for conducting business in this environment. The most common avenue of creating trust is a rating system where consumers and suppliers rate each other after each transaction [7]. What separates peer-to-peer networks from electronic markets is that the main aim is sharing and borrowing, not buying [8].

- Drivers of Sharing Economy

- Technology is the main driver of the Sharing Economy. It makes economic activities easier and cheaper by reducing transaction costs. Moreover, the customer's networking is connected easily and conveniently by social network and digital market.

- The advent of the Sharing Economy coincides with the global financial crisis. Research conducted by an expert team working for the European Commission shows that the loss of trust in traditional companies during the financial crisis was a major enabler for the feasibility of many business models of the Sharing Economy

- While technology is the main driver of the Sharing Economy, at the same time, an aversion to web-based applications in general or insufficient knowledge about their possibilities and limitations are obstacles to trust in Sharing Economy businesses [9].

- About peer-to-peer online lending (P2PO)

A category of Sharing Economy that requires a different economic impact and regulatory discussion is P2PO lending.

"Peer-to-peer finance will challenge the nation's major financial institutions… mono-banking culture is on its way out" - Andrew Haldane (Bank of England)

"This would mean revolution, fundamentally re-shaping the financial system" - (Bank of England Governor, Mark Carney)

Peer-to-peer (P2P) lending platforms are online platforms where borrowers place requests for loans online and private lenders bid to fund these in an auction-like process. Such platforms became available in 2005 and have increasingly been used ever since. Nowadays, they are available in a wide range of countries, such as the United Kingdom (ZOPA), Germany (SMAVA), the United States (PROSPER) or Viet Nam (HUYDONG)

Unlike a commercial bank, the platform does not take risks through its own contractual positions. Whereas banks accumulate risks by taking positions on their balance sheet, platforms decentralize the risks by spreading them to their users.

The concept of private loans is not a new business model and rather the traditional way for private persons to borrow money without any mediation [10]. What makes online P2P lending a young phenomenon is the transfer into the internet using online P2P lending platforms.

- **The motivation of this model**: behind building such platforms was to circumvent banks as intermediaries, which may have the following advantages:

- An expensive middleman is replaced by a more cost-effective online platform, thus reducing transaction costs

- Borrowers are given the chance to present their loan case in much detailed, provide information to lenders that banks with their standardized decision processes usually do not take into consideration

- The loan generation process is transparent and creates a feeling of fairness (all bids are visible and traceable online)

- Loans on peer-to-peer lending platforms are said to generate higher returns for investors (compared to traditional bank savings) and to be cheaper for borrowers [11].

Lending process

Online P2P lending platforms differ in the way the borrower's interest rate is set. Sites, like prosper.com use an auction process [3] where borrowers are able to set a maximum interest rate they are willing to pay.

If the lending process leads to a fully funded loan-request, some platforms like prosper.com have implemented another verification of the borrower's ability to pay, including the verification of a steady income. The loan is then granted to the borrower, who will eventually start the repayment process [12].

The platform conducts its own assessment of the underlying credit risk. If the credit risk is acceptable and fits the platform's risk categories, the platform sets a risk-appropriate interest rate.

If the borrower agrees with the platform's pricing, the platform publishes the offer to its users for a predefined period, typically two or four weeks. Requests for consumer loans are published anonymously, while those for business loans are normally published with the name of the potential borrower. Lenders have this period to place their offers to provide small portions of the required financing amount.

The intermediating online P2P lending platforms generate their revenue via service fees, which they collect from borrowers as well as lenders [11]. Many collect a closing fee of a certain percentage of the funded loan from the borrowers, as well as fees for late or failed payments. Lenders often have to pay a service fee based on the amount they have funded to borrowers.

The platform then services the loan, collecting and distributing interest and redemption payments until the loan matures. Normally P2P-loans are structured as monthly annuity loans. If the borrower defaults, the platform is obliged to arrange the collection of payments on behalf of crowd lenders although the platform itself is not liable for losses, which are borne by lenders/

investors. Some platforms arrange a sale of non-performing loans on behalf of lenders to a debt collection agent for a fixed price to recover a mini-mum amount (for example, 15% to 30%) of the credit claim. Others have developed automated litigation and recovery processes for the time when loans default. Here, the recovery rates are higher.

In a research about Peer-to-peer lending and financial innovation in the UK, the authors found that generally, loans run between 12 and 60 months, though loan agreements often can be sold before maturity in secondary markets operated by platforms. The platforms typically make their profits by charging various transaction fees at origination [13].

4. Results and discussion

Current situation in Viet Nam

Data analysis results indicated that nearly 90% of respondents have been involved in lending or borrowing directly without financial intermediaries such as banks. We observed a remarkable point that more than 70% have never loaned any unacquainted person. It is also interesting to note that, according to the analysis above, the important feature of online P2P lending is the openness of the data disclosure of participants in the system and the assessments, the comments of the borrowers or the lenders, so we can provide credit to people who we have never known based on the assessment. Therefore we see that the opportunities for P2PO are huge with market gaps that traditional financial institutions have not met yet.

When participating in the P2PO system, profits from lending activities will be taxed according to the law and according to the group of authors, this can be an obstacle to this activity. However, as a result of the statistics obtained, more than 70% of respondents are willing to pay taxes to be safer in direct borrowing and lending.

Willingness to participate

In particular, nearly 90% (figure 1) of respondents chose to participate in the P2PO system in order to make the borrowing process become more convenient and more secure. This can be explained by the advantages of this model over that of traditional banks. In practice, banking regulations and procedures are relatively complex, and consumer finance companies use simpler procedures with very high interest rates ranging from 40% to 60% and the operation of these companies also puts a lot of questions about management. Therefore, 90% of respondents claim to participate in the P2PO lending system, which demonstrates a legitimate expectation of consumers about a more appropriate financial option for them. The demand for having a system that helps people who need a loan directly connect people who have unused funds and want to earn higher interest rates than traditional banks is actually a reality in Vietnam.
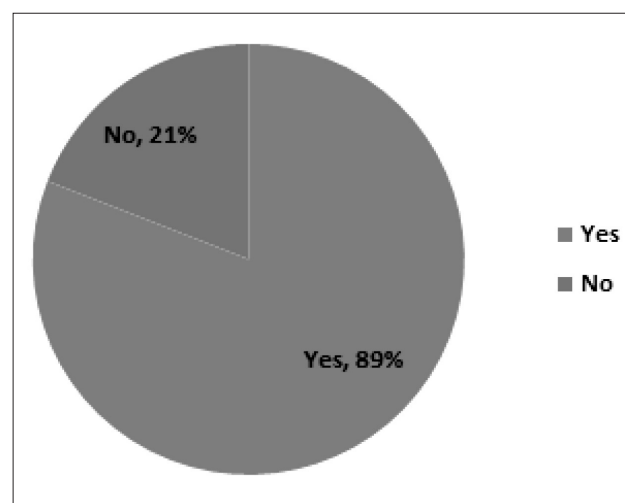

Figure 1: Rate of participation in P2PO model

Motivations

This research also explores the motivations for interviewees to participate in the P2PO lending system. We found that two factors, which are "Know the information of lenders, borrowers as well as transaction history,

evaluation (eg in Uber, Grab is 4 stars, 5 stars)" with more than 62.6% (figure 2) selected, and "when lending in the platform of new system, interest rates will be higher than bank deposits" with 51% of respondents choosing. This result is also consistent with many studies in the world, for example, the loan generation process is transparent and creates a feeling of fairness and loans on peer-to-peer lending platforms are said to generate higher returns for investors (compared to traditional bank savings) and to be cheaper for borrowers [11]
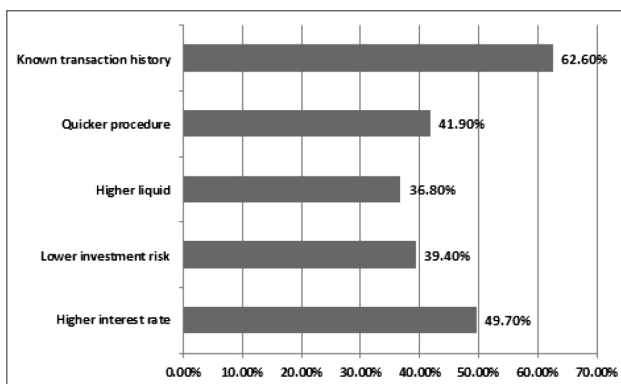

Figure 2: Motivation to participate in P2PO model

Barriers

Among the barriers to be investigated, two factors were specially paid attention by the investigators: "There is no insurance against the lender" and "Not yet aware of the law" (figure 3). These two factors are in line with the authors' prediction as these are the two most differentiating factors from traditional bank deposits. First, with the bank, when opening an account and depositing savings, according to the law, depositors are insured deposits up to 50 million. However, when lent to an online peer-to-peer loan system, the loan amount is not, or, more accurately, uninsured. Thus, the risk to lenders is higher if the borrower deliberately or unwillingly does not pay the loan.
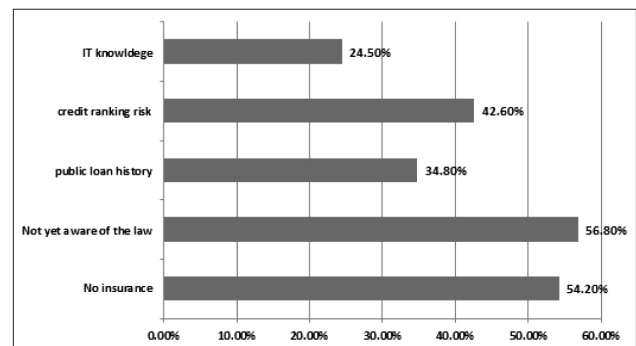

Figure 3: Barries to joining the P2PO model

Provisions of laws

Indeed, provisions of the law with regard to sharing economy in general and lending system online, a component of the sharing economy system, in particular, has not kept pace with the rapid development of this model economy. This fact is not only in Vietnam but also in many countries in the world, including in developed countries. We can find that many cases in which the law are applicable to the model of new economy are not consistent even within a country, such as Uber and Grab can operate in Hanoi and Ho Chi Minh City, while in Da Nang, there have been cases where Uber and Grab drivers were subjected to be fined by traffic inspections with a fine of 2.5 million VND, close to one month of minimum Vietnamese income.

Opportunity or risk?

Another interesting point from this research is that when asked whether P2PO lending is an opportunity for traditional banking, 51% (figure 4) of respondents agreed with the above, while only 11.6% did not agree. In another view, 25.8% of respondents said that P2PO lending would be a threat to the old model, while the opposite is nearly double, 41.5%. From the above data, we can draw many implications. It is clear that since the emergence of a new paradigm - the sharing economy in general and P2PO lending in particular, competition has increased dramatically in the sectors which has the presence of this new model.
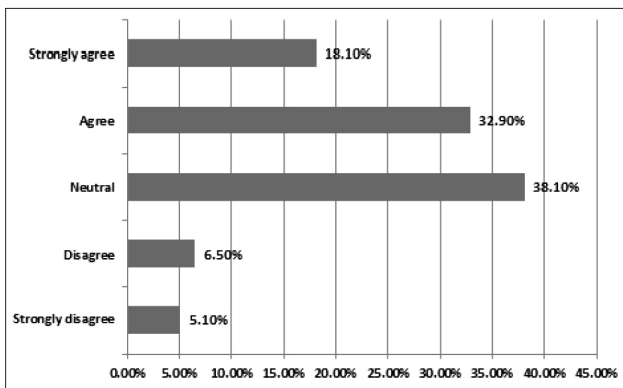
Figure 4: P2PO is an opportunity for the banking
and finance industry

If traditional banks could have a respect for this new model and combined with the P2PO lending companies, leveraging the strengths of both, at that time, the rights of customers would get more care and then served more fully. This new paradigm with advantages of technology and innovation, once combine with the old paradigm - with the strength of credibility, government assurance and a new paradigm will bring benefits for both in the spirit of win-win. This argument is more relevant when, in the next question of the study, 47% of respondents believe that the traditional banking market experience can be applied to the P2PO lending market compared to 15% who do not agree.

Competition

Returning to the topic of competition, from the survey results, the authors found that the field will be "the main battlefield" between traditional banking and the new model is the field of consumer loans with 65.3% selected, and unsecured loans with 51% of the respondents (differ with consumer loans in which this type of loan does not have collateral). This finding corresponds to several studies that have been conducted which confirmed that the consumer credit market is one of the largest, most important credit markets, with outstanding credit of $3.5 trillion in 2015 [14].

On the other hand, with P2PO lending, loan screening is primarily based on algorithms, and

the process can also be flexibly adapted to suit the time. In addition, the authors agree on the "knowledge used to manage and assess risk" as one of the fundamental differences between the two models. In the traditional model, bankers are generally well-educated, so the knowledge that is used to manage and assess risk can outperform the new paradigm when lenders, who may not have a strong financial background, play an important role in deciding whether to lend or not to lend their own money. That is one of the things to keep in mind while doing further research.

The researcher looked at what factors motivated the P2PO platform to develop, and it is interesting to note that the survey results show that the first and second factors are: High demand for customer loans and ability to meet high demand based on technology, at 64.5% and 47.4% (figure 5) respectively. High demand for consumer loans motivates borrowers to seek cheaper financing, more favorable loan conditions, and a P2P platform that meets this requirement. Besides, to satisfy this need, the connection between the borrower and the lender can only be based on the new technology that can be realized as perceived by the P2PO platform. This result is also consistent with the results of the study of data on the prosper.com platform in the US market [15], and the research results in the Chinese market which are booming P2PO model [16].
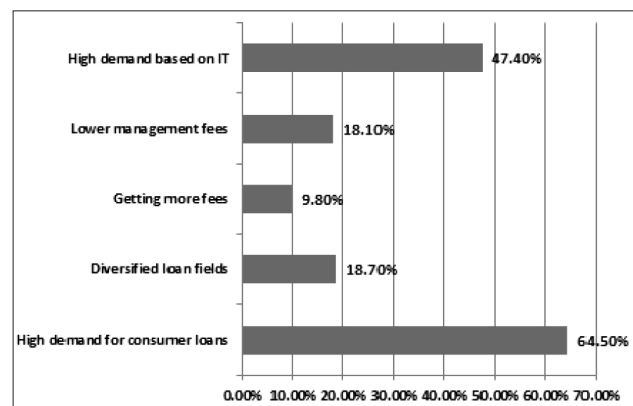

Figure 5: Factors driving P2PO model to develop

Governance

The survey also showed that the number of people who believed that the government would support and would not support was similar, at 28.8% and 27.4% (figure 6), respectively. While most, 44.1%, survey participants did not identify the attitude of the Government to the P2PO platform. This reflects the Government's unclear behavior on the model and platform that reflects on the perceptions of the people. This situation is also consistent with what has taken place in the real that has been reflected in the problem space of the paper, as the same type of business, but the activity is licensed and activities are not granted. And even if it is allowed by the Government, the local government still bans.
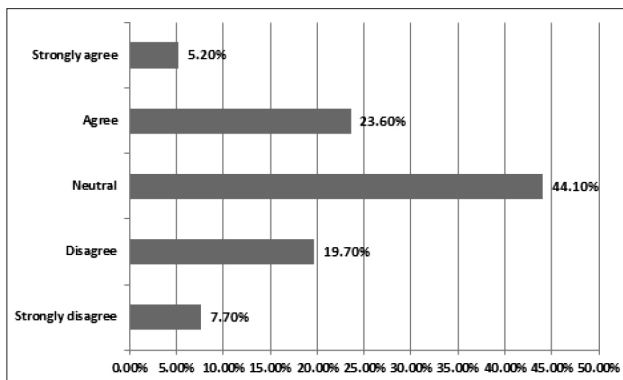

Figure 6: The level of support of the government for the P2PO model

The reason which accounts for the highest proportion, 50.7%, for that the government would supports this model is that it will promotes competition, strengthens the lending market and, in particular, consumer loans, thereby providing additional benefits to the participants. Secondly, 46.7% (figure 7), said that the government supported the model for growth, contributing to the mobilization of idle capital in the population and increasing the borrowing capacity of the people, thereby stimulating production and business development. These choices are consistent with the review because the lending market is being priced by intermediary financial institutions. As well as willingness to participate in this model, 88.8%, is a motivation for government support.
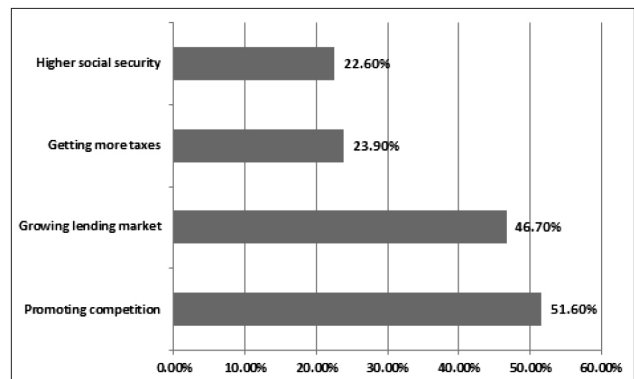

Figure 7: Benefits of the P2PO model

The survey results also show that improving the legal system must be in top priority, at 52.6% (figure 8), which is appropriate, since this platform has innovated the traditional lending model with intermediary financial institutions, so it is necessary to regulate, protect and promote it [17]. Moreover, this model is in need of government development support, at 42.6%, because of its novelty over traditional lending models such as direct versus indirect and technology-based interaction instead of through intermediary financial institution. In the process of development, each economic model must go through periods from young to maturity stage. And in the initial stage, government support is needed [14].
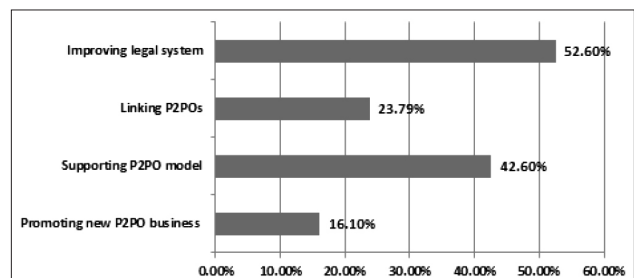
Figure 8: Issues that need the government improvement

In contrast to the above, the percentage of respondents who said that the government would not support, with the first reason, made up 57.2%, which was the group interest from the traditional Bank. This is a fact in general and Vietnam in particular. It is not just financial circles that connect with the politics that make up the plutocrat, as often happens, but also the drafter of

financial legislation in Vietnam, so protecting their own interests, traditional Bank, is sure. Therefore, instead of researching new policy proposals to meet development needs, they are willing to rely on the fact that there is no legal basis to delay the implementation of the legislation; resulting in up to 48% respondents said that the government did not support the P2PO model, due to unconfirmed legal bases, as appropriate.

The survey results showed finally that the first tool the Government will take, at 56.6% that is to restrict credit limit. This is in line with the economic reality, as any model when applied requires small-scale trials before mass deployment and larger scale. And also in line with the nature of P2PO is the unsecured microloans [18]. The next tool of choice, at 47.7%, is that the Government will heavily tax the P2PO model. Tax instruments are always a powerful and legitimate tool to regulate economic activities. Therefore, when the government has not wanted to develop the P2PO model, this option is appropriate. This result is also consistent with research in the United States [19].

5. Conclusion and limitations

Theoretical contributions

This study has shown three new points in research on particular peer lending and financing in general.

Firstly, in Vietnam in general and Da Nang in particular, the potential of online peer lending is enormous because of the need and the support of consumers when they have more choices besides banking and traditional financial service.

Secondly, P2PO is both an opportunity and a threat to the traditional banking industry. However, opportunities remain more than threatening. Once the traditional model recognizes the advantages of this new paradigm and joins together to serve the neglected segments of the market, the benefits of both and the interests of consumers are guaranteed.

Thirdly, the views of the respondents on the support of regulatory authorities show that there is almost a similarity in the proportion of respondents who believe that the government will support and vice versa, saying that regulators will restrict the Sharing economy model in general and P2PO lending in particular. This reflects the reality in Vietnam and is a useful basis for further research.

Administrative implications

This study may indicate a number of recommendations for the leaders of the traditional banks as well as the macro-level management.

P2PO not only put pressure on the traditional banks, but regulators are also under pressure to reform existing regulations in order to better manage the competition and ensure harmony of interests, and do not hold back the development of models that benefit consumers.

Traditional banks should not consider P2PO as a threat and use their impacts to influence regulators in favor of their industry. This will sometimes be counter-productive as consumers may favor stronger new models. Choosing the strengths of the new model and finding a direction to combine with the ultimate goal of better serving customers would be a solution. Because the positive aspects of peer-to-peer lending, in addition to economic efficiency, are helping to connect better the financial world and the real economy, avoiding manipulated credit in areas such as real estate, highly risky speculation. As a result, the benefits of the economy as a whole, the new and old models as well as the interests of consumers would be ensured.

Limitations and further research directions

The main drawback of this study is that the sampling is based on the online survey tool, and the sampling technique is convenient. Further studies may test generalizability with other sampling methods as well as examine the surveyed subjects from a variety of sources. At the same time, new factors could be added to this new paradigm in research.

References

[1] Pricewaterhouse Coopers (2015) Sharing or paring? Growth of the sharing economy, p.5

[2] Walsh, B. (2011). "Today's smart choice: Don't own. Share." Time International: 49-49.

[3] Galloway, I. (2009). "Peer-to-peer lending and community development finance." Community Investments 21(3): 19-23.

[4] Lenz, R. (2016). "Peer-to-Peer Lending: Opportunities and Risks." European Journal of Risk Regulation 7(4): 688-700.

[5] Sundararajan, A. (2014). "Peer-to-peer businesses and the sharing (collaborative) economy: Overview, economic effects and regulatory issues." Written testimony for the hearing titled The Power of Connection: Peer to Peer Businesses, January.

[6] Demary, V. (2015). Competition in the sharing economy, IW policy paper.

[7] Finley, K. (2013). "Trust in the sharing economy: An exploratory study." Centre for Cultural Policy Studies, University of Warwick. Online verfügbar unter http://www2. warwick. ac. uk/fac/arts/th eatre_s/cp/research/publications/madiss/ccps_a4_ma_gmc_kf_3.   pdf, zuletzt geprüft am 2: 2015.

[8] Gansky, L. (2010). The mesh: Why the future of business is sharing, Penguin.

[9] Dervojeda, K., et al. (2013). "The sharing economy: accessibility based business models for peer-to-peer markets." European Commission Business Innovation Observatory," September.

[10] Herrero-Lopez, S. (2009). Social interactions in P2P lending. Proceedings of the 3rd Workshop on Social Network Mining and Analysis, ACM.

[11] Klafft, M. (2008). "Online peer-to-peer lending: a lenders' perspective."

[12] Garman, S. R., et al. (2008). "Person-to-person lending: The pursuit of (more) competitive credit markets." ICIS 2008 Proceedings: 160.

[13] Atz, U. and D. Bholat (2016). Peer-to-peer lending and financial innovation in the United Kingdom-Ulrich Atz and David Bholat, Bank of England.

[14] Balyuk, T. (2016). "Financial Innovation and Borrowers: Evidence from Peer-to-Peer Lending."

[15] Funk, B., et al. (2015). "Online Peer-to-Peer Lending â A Literature Review." The Journal of Internet Banking and Commerce 2011.

[16] Feng, X. and J. Qin (2016). Online P2P Lending: Factors, Behaviors, and Mechanisms. Encyclopedia of E-Commerce Development, Implementation, and Management, IGI Global: 1693-1705.

[17] Bruton, G., et al. (2015). "New financial alternatives in seeding entrepreneurship: Microfinance, crowdfunding, and peer-to-peer innovations." Entrepreneurship Theory and Practice 39(1): 9-26.

[18] Lin, M., et al. (2013). "Judging borrowers by the company they keep: friendship networks and information asymmetry in online peer-to-peer lending." Management Science 59(1): 17-35.

[19] Chaffee, E. C. and G. C. Rapp (2012). "Regulating Online Peer-to-Peer Lending in the Aftermath of Dodd-Frank: In search of an evolving regulatory regime for an evolving industry." Wash. & Lee L. Rev. 69: 485.

Empathizing with animals in contemporary Vietnamese fiction

Thấu cảm với loài vật trong văn xuôi hư cấu Việt Nam đương đại

Le Thi Luu Oanh[a], Tran Thi Anh Nguyet[b,*]
Lê Thị Lưu Oanh, Trần Thị Ánh Nguyệt

[a]*Faculty of Language and Literature, Ha Noi National University of Education, Hanoi, Vietnam*
Khoa Ngữ văn, Đại học Sư phạm Hà Nội, Hà Nội, Việt Nam
[b]*Department of Humannities and Social Sciences, Duy Tan University, Danang, Vietnam*
Khoa Xã hội và Nhân văn, Đại học Duy Tân, Đà Nẵng, Việt Nam

Abstract

Before the pressure of the global environmental crisis, ecocriticism appeared in the 1970s has met requirements of the era, to become a dynamic research movement in the world today. It traced ecological risks that humans now face, thereby making feasible recommendations from humane sociologist to change the environmental discourses. Humans re-confirm the relationship with animals, not the attitude of mastering but a symbiotic relationship. The new sense of ecological ethnics in XXI century has formed new personality patterns. This study will investigate the relationship of humans and animals in contemporary Vietnamese fiction with main focus: speaking the language of animals, sharing animals' pain, comparing the writing during Renovation stage with the previous writing about animals. Since then, the study shows ecocriticism changes the discourses about the environment, gives the warnings and creates new viewpoints of humanism, not only to honor humans as lord of all things but humanize humans by sympathetic attitude to animals, empathy with damaged animals' density, protect animals and love creatures.

Keywords: ecological humanism, ecocriticism,Vietnamese fiction, animal, empathy.

Tóm tắt

Trước áp lực của khủng hoảng môi trường, phê bình sinh thái (nghiên cứu về mối quan hệ giữa con người và môi trường tự nhiên) ra đời vào khoảng những năm bảy mươi của thế kỉ XX, đã đáp ứng được yêu cầu thời đại, trở thành một phong trào năng động trên thế giới hiện nay. Lí thuyết sinh thái tôn trọng sự tồn tại bình đẳng của tạo vật, coi mọi sinh vật không có loài nào ở thế ưu trội. Con người xác nhận lại mối quan hệ với động vật, không phải thái độ làm chủ mà là mối quan hệ cộng sinh. Từ tư tưởng mang tính cách tân này, chúng tôi soi chiếu vào hình tượng loài vật trong văn xuôi hư cấu Việt Nam sau những năm Đổi mới 1986, chúng tôi nhận thấy, nhân vật loài vật không phải là cách viết theo kiểu truyện đồng thoại như trước đây, mà mỗi loài vật có một sinh mệnh độc lập, với tâm hồn, cá tính riêng. Trong văn xuôi hư cấu giai đoạn này, xuất hiện những nhân vật lắng nghe ngôn ngữ của loài vật, chia sẻ cảm giác bị đau với muôn loài. Từ đó, bài viết này chỉ ra chủ nghĩa nhân văn sinh thái đã đổi thay các diễn ngôn về môi trường, đưa ra những cảnh báo và thay đổi nội hàm của chủ nghĩa nhân văn, không phải coi con người là chúa tể muôn loài mà con người biết lắng nghe tiếng nói từ tự nhiên, cúi xuống những loài vật bị thương tổn, bảo vệ và thương yêu mọi sinh vật.

Từ khóa: chủ nghĩa nhân văn sinh thái, phê bình sinh thái, văn học hư cấu Việt Nam, loài vật, thấu cảm.

Email: trananhnguyet5@yahoo.com

1. Introduction

XXI century is the century that many researchers have believed that humans must face the most ecological risks. In modern society, with the urbanization rate and the dependence on science and technology, humans are increasingly turning back to nature, overexploiting, making nature increasingly disappear from life. The nature revenges humans not only by catastrophes, natural disasters but more frightening by the disappearance of itself. The "miracle chain of life" of nature is increasingly being destroyed. Ecocriticism has emerged as issues of climate change, environmental degradation are no longer issues of every country and nation, it affects the life that literature is interested in so its turning point ultimately relates to the essence of literature.

In the world, originating from Britain - America, ecocriticism is being a dynamic movement with studies of Chellry Glotfelty (1996), *The Ecocriticism Reader: Landmarks in Literary Ecology* edited by Cheryll Glotfelty and Harold Fromm, 1996) [10]; Gifford Terry (*Pastoral*, 1999) [9], Jonathan Bate (*The Song of the Earth*, 2000) [3]; Peter Barry (*Beginning Theory: An Introduction to Literary and Cultural Theory,* 2002) [1], Grey Garrard (*Ecocriticism (The New Critical Idiom, 2005*) [8]; Lawrence Buell *(The Future of Environmental Criticism: Environmental Crisis and Literary Imagination,* 2005) [5] ; Karen Thronber (*Ecoambiguity: Environmental Crises and East Asian Literatures*, 2012) [14]...

Since its innovation in 1986, Vietnam is a country strongly influenced by the state of climate change and sea level rise. Living in areas sensitive to environmental changes, certainly will reflect on the works, especially with sentimental, compassionate and more concerned writers with their homeland. Vietnam has accelerated market economy, industrialization, and modernization, which result in changes in the environment. The natural environment is being threatened by

the rapid growth, which means that the natural environment has to face with so many problems of the negative side of urban civilization with chaos, sprawls, and damages such as greenhouse effect, industrial waste, hydroelectric overuse without considerable environmental impacts of destruction from overfishing and deforestation... As a result, forests are being destroyed, rivers are being forced to die, animals are crying for help. In 2010, the last rhinoceros were killed. Elephants in the Central Highlands which have no forest habitats have destroyed fields. Sarus Cranes have left the West of Vietnam. A large amount of fish has died in the Center of Vietnam... Changes in climate, the crisis of ecological environment and global issues have become heavy pressures that Vietnamese literature cannot ignore.

This paper mainly focuses on the sympathy with animals in contemporary Vietnamese fictions. This sympathy is reflected through the following aspects: people speaking the language of animals and sharing animals' pain. The paper also compares the writing during this stage with the previous writing about animals.

2. Research Method

Applying "Looking back sense" of ecocriticism as a premise to realize the relationship between humans and surrounding nature as an entity of the whole ecosystem. Besides, we used interdisciplinary method: combining literature with science, analyzing literary works to show the environmental warnings. The study has applied the knowledge of scientific disciplines (ecology, ethnology, history, philosophy, politics, ethics, etc) to understand and explain some viewpoints of the works. In this study, we have discussed the relationship between humans and animals to show those who sympathize with harmed creatures, share feelings of pain with animals, listen to their voices and respect natural world. Those personality patterns are not formed by centered rational person patterns but through the

voices of lonely and idiotic characters, sideline and vulnerable individuals such as women, the elderly, children, those with the loss of wisdom, goofy, deformity, and defect in *A Wolf's Revenge* (*Sói trả thù,* 1992), *The Salt of the Jungle (Muối của rừng,* 1992), *The largest beast (Con thú lớn nhất,* 1992) by Nguyễn Huy Thiệp*; The Endless Field* (*Cánh* đồng *bất tận,* 2006), *Single Wind* (*Gió lẻ,* 2008), *Anxious Look* (*Cái nhìn khắc khoải, 2008*)… by Nguyễn Ngọc Tư, *A Person Who Speaks the Language of Doves* (*Người nói tiếng chim bồ câu,* 2010) by Mạc Can, *The dog and the divorce* (*Con chó và vụ li hôn,* 1992) by Dạ Ngân, wrote *Ants and Human (Kiến và người,* 1990*), Termites and Human (Mối và người,* 1992*),* Trần Duy Phiên...

3. Finding and Discussion

3.1. A different animal's image before 1986

Nature in Vietnamese literature before 1986 basically appeared in 2 formats. First of all, nature was personalized. For example, fairy tales about animals explained natural features of animals (such as turtles' carapaces in *A good lesson* (*Bài học tốt*) by Võ Quảng), or folk tales: with animal characters, animals gave a philosophic lessons with educational content (such as *The second trip* (*Chuyến* đi *thứ hai*) by Võ Quảng, *Tet of a kitty* (*Cái Tết của mèo con*) by Nguyễn Đình Thi, *The Adventure of Sir Dusk* (*Cuộc phiêu lưu của Văn Ngan tướng công*) by Vũ Tú Nam, *The adventure of a cricket* (*Dế mèn phiêu lưu kí*) by Tô Hoài,...). They are all children stories. In general, in this kind of format, the nature is personalized ("The mother asked Ko-nia tree/ Where its roots take water?/ It said: "from the North of Viet Nam", *The shade of Ko-nia tree* by Ngoc Anh). Nature was in the harmony with humans ("Xa nu forest protected the villagers", *Xa Nu forest*- Nguyễn Trung Thành).

Secondly, nature appeared as a means of expressing personalities and the soul of humans ("When a person is sad, things around him look sad too"– *Kiều Story*, Nguyễn Du), the ability to conquer nature, by catching crocodiles, snakes, or honey bees, killing boars and tigers, building dams to prevent rivers, or controlling the sea... in such works as *The scent of the Ca Mau forest* (*Hương rừng Cà Mau*) by Sơn Nam, *Southern forest land* (*Đất rừng phương Nam*) by Đoàn Giỏi. Despite authors' different ways to express their viewpoints, literature during this time writing about nature was actually about human beings, and was human-centered to describe, express and evaluate the nature.

3.2. Speaking animal's language

The nature in literature since 1986 has had a new inspiration: "it had real life". They had fates, personalities, souls... As Mac Ngon, a notable writer said, "I suddenly found grasses around me, and even cows and goats which could talk to people, they had not only their lives, but also their emotions" ("Literature had to make people trust each other more and more*" (Conversation between Oe Kenzaboko and Mac Ngon) [15]. When comparing animals to humans, authors upset the conventional belief that humans are superior to animals with their unique properties: feelings, languages, and cultures. In literary works, animals have their own languages. Human cannot recognize such languages, but they do exist. People are always proud of their languages because they have mental ability thanks to their languages. Therefore, we tend to deny languages of animals and plants. Ecologists assert that, "we think that the animals do not have languages, because we do not understand their languages" (Fontenay E., 2013).

Actually, animals communicate with each other by their own languages. Some literary characters can understand their talks and can use their languages. Mr. Su Da climbed capulin trees, listened and talked with doves when he was a little boy. He said, "Honestly, speaking doves' language is not difficult, it is much easier than

English... "coo" is a sound which means different things in different circumstances, It's a sound with various meanings" (*A Person Who Speaks the Language of Doves,* Mạc Can).

That a person can understand an animal' language did appeared in Oriental folk stories and this ability was actually a gift for kind people. In legendary stories, in order to communicate with people, animals usually "disguised themselves as people". Nowadays, listening to animals' talks, people can realize defects, imperfection, and loneliness. This is quite different from medieval literature, where people found peace in communication with animals. This ability indicates the loneliness in human life. Due to the life's imperfection, people have to endure psychological instability, the inability to communicate with each other and this is why they have to come to the world of animals. It is current tragedy of losing human words. Doan in *The dog and the divorce* by Dạ Ngân was patiently silent to endure injustices, patriarchal behavior, selfishness of her husband and even said nothing at the court facing the suspicious judge and her husband's rage. However, it was the husband's merciless treatment to her pet dog that she finally came to the decision about the divorce.

According to authors of this stage, the world of animals is more truthful, more peaceful, more tolerant, and freer than that of humans. People treat each other rationally rather than emotionally and they get falsehood to hide the clarity of languages. A girl in *Single Wind* by Nguyễn Ngọc Tư wondered that "whether in this world, there is any bird that wants to die because of the twitter of other birds? There is any dog suddenly hitting its head against a stone to death because other dog's barking? There is any cow jumping into the river to commit suicide because of the moo of another cow?". Nương in *The endless field* by Nguyễn Ngọc Tư said "We learn to love ducks (hopefully, she will not suffer as she used to when loving a

person in the past)". Communicating with people made her sad, so she has begun talking with ducks. She recognized that "The world of ducks is open – with no jealousy or anger, may be their small head is just enough for love". Mr. SuDa in *A Person Who Speaks the Language of Doves* by Mạc Can asserted : "Surprisingly, pigeons rarely have conflicts. Unlike humans, pigeons mean what they "speak".

Many characters refused to communicate with people. Nương and Điền in *The endless field* by Nguyễn Ngọc Tư spoke duck language to forget "the sorrow of the human world". That is even the self-defense of two lonely kids thirsty for love: "we do not speak human language", "amorously with a new language, we accept to let people see us like crazy (as long as contemporarily forget human realm)". A girl in the work *Single Wind* written by Nguyễn Ngọc Tư witnessed the tragedy of her own family when her father scolded her mother, which made her mother commit the suicide. Afterward, her father calmly told a lie about her mother's death. Being in this situation, she realized that human speech contained a lot of false, heartless, ruthless contents. Therefore, she refused human language but speak birds' language because "Animals do not hurt each other using their languages"... Indeed, refusing human language to come to animal language demonstrates that humans are so lonely in this world. Understanding animal languages was one of the motifs in Vietnamese fictions before 1986, since then human have not only been able to understand but also can speak animal languages.

3.3. Sharing the pain of animals

Through their writing on the massacres of animals, authors express their anxiety about man's humanity: thoughtlessly killing animals and being apathetic to creatures will lead to apathy toward humans. When humans do not feel the pain of animals, they will not feel the pain of their fellow human beings. When humans killing

animals without limitation, it will push them to a killing instinct. Humans realize the most inhuman actions which is killing animals**.**

A Wolf's Revenge by Nguyễn Huy Thiệp, Hoàng Văn Nhân was an excellent shot. Before him, his father, his grandfather, and his great- grandfather had all been the same. So, his son, Hoàng Văn San, followed him into the forest from the age of five. Mr Nhan was determined to train San to become a good hunter. He decided the time had come to teach his child to hunt wild animals, he took his twelve – years - old child to hunt wolves. By the end of the hunting day, the wolf pack had been nearly destroyed by the hunters. The hunters cornered the leader wolf in her deep cave. She bit her baby wolf and lelf a mark on its forehead just before she was shot dead. San carried the pup home. The pup grew up among domesticated dogs. Time went by, and San was thirteen. Nhan held a birthday party for his son and planned to kill the baby wolf which was grown up now on the occasion. But unluckily, San got caught on the stairs and mouth bled. The blood awakened something within the hazy subconsciousness of the beast. Baring its sharp white fangs it sprang forward, and it snapped at San's neck. But, Instead of killing the wolf, Mr Nhan swung the axe down onto the metal chain to release it. The wolf howled and ran towards the forest. When he fell to his knees by the corpse of his only child, Nhan felt the pain of wolf pack which he had killed years ago. He, at that time, understood the warning from the elderty in the village: "You must teach your son to fear the forest!". The story reminds us to be reverent to the natural life, otherwise humans will only get the loss.

So, loving animals is the way to nurture humanity. Old Dieu in *The Salt of the Jungle* by Nguyễn Huy Thiệp went hunting but he felt "the stillness and tranquility of the forest penetrated him thoroughly". When he caused the disaster for a family of monkey, he was regretful "the chaos in the pack made Old Dieu tremble with fright. He had just done something evil". He shot the leader monkey and it was injured. He felt the pain of the monkey, so he was very uncomfortable and "tried to avoid looking into it". Then, "he had no choice but to take off his briefs, using them to bandage the monkey's wound".

During his trip back home from the mountain, a female monkey followed him all the way. Because of the perseverance of the female monkey, Old Dieu found that "It turned out that in life the responsibilities weighing down on the backs of each living thing were truly heavy". Finally, he decided "Well, I think I will just release you". On the way coming back his home, he lost all things: a double-barreled rifle, clothes, food… but he accepted a special present from the forest "Old Dieu paused. This species of flower blossomed only once every thirty years and it was said that whoever saw Tu Huyen flowers would meet with a lot of luck. The flowers were white, salty-tasting, and as tiny as the heads of toothpicks. People called them "the salt of the jungle". So, he felt happy and peaceful "He kept on walking, naked and lonely".

Thus, there are changes in the plot motif. The plot of animal conquest is broken and replaced by another plot structure: Hunting is no longer the ability to conquer animals and character's image has changed from giant conqueror to destroyer, victim, and defeated. The characters begin to sympathize with the pain of all creatures and to be tolerant to animals to nurture their human souls. Civilized men should be more sympathetic to the nature. This is the reason for the establishments of the organizations which protect animals. They have criticized the violations of animal rights such as killlling rhinos for their horns, bears for their bile, and elephants for their tusks… Why saving wild animals is important? sselement for the sustainable development of humankind. When humans do not feel the pain of animals, they will not feel the pain of their fellow human

beings. From human rights to the animal rights is a big step toward on the path of humanism.

4. Conclusions and Suggestions

Considering the relationship between humans and animals, Vietnamese ecological fiction changed, from the conception of "centered-ecology", the authors realized that the animals have life, soul and personality with its self-perpetuating life. When the viewpoint of changes, the plot motif immediately changes from story structure of animal exploitation into a multi-plot structure (Revenge of animals, Infertility, Loss of Shelter…); character image from arrogant human to conquer and exploit nature into "crime" human, victim of the animals and human became depraved and insecure. In this table, we have compared the relationship between humans and animals.

Table 1: Comparison of the relationship
of humans and animals between the period before and after Renovation 1986.

Criteria	Fiction before 1986	Fiction after 1986
Point of view	Human-centred	Earth-centred
The conception of Animal	+ Animal and humans have the same voice + Nature is the background	+ Animals are independent beings, existing outside the human consciousness. + Animals have feelings, languages.
Content	+ Animals usually "disguised as people" (in legendary stories) + Animals expressing human personalities and souls.	+ with characters who can understand animal's language + Characters able to speak animal's language
Character's image	+ Conqueror + Hunter	+ Victim, Defeater, destroyer + Sympathetic people

From this perspective, comparing with plants and animals, ecocriticism has "upset" the default perspectives of what is still considered as exclusive of humans to "stand higher than the nature": emotion, language, culture. Actually, the world of all life is calmer, more sincere, tolerant and liberal than that of humans. Humans bring reasons into all types of emotion, taking lies to hide the clarity of the language… Facing with animals, humans find themselves become defective, incomplete and lonely. So, returning to nature is to learn how to respect all life, respect nature and adjust the attitude and behavior of humans towards a sustainable, peaceful and happy life

Characters who share feelings of pain with animals, sympathize with harmed creatures are gentle, rustic and filled with love. Ethnics of Ecological Humanism does not recommend praising humans as lord conquering nature, as the "style of all life" but a living attitude where humans know to be humble, respect nature and adjust the attitude and behavior of humans for a sustainable, peaceful and happy life. Therefore, new sense of ecological ethnics in XXI century has formed new personality patterns, those who sympathize with harmed creatures, share feelings of pain with all things, listen to the voices of all things and respect natural world. However, we are concerned about our existence and our comfort, the place we live on is the earth and we have to be in a certain relationships with animals and plants. But, the earth is in danger, animals are becoming distinct and people become insecure in the age of civilization and technology. Therefore, literature, whose function is to criticize the old-fashioned thinking needs to reflect the truth of a situation. As such, Vietnamese literature is accessible to the contemporary urgent issues in the age where ecological crisis has become a serious global

issue. Because even if we bother to anything of the human life, we are still on the earth; in every relationship, we are still in contact with animals, plants, however the earth is in danger, the animals are gradually absent in life, people become insecure in the age of civilization and technology. Therefore, literature, where began the criticisms with the trails of thinking needs to speak out the reflection of the truth of a situation.

References

[1] Barry P. (2002), "Ecocriticism", *Beginning Theory: An Introduction to Literary and Cultural Theory*, Manchester University press, p 248 - 279.

[2] Bate J. (1991), *Romantic Ecology: Wordsworth and the Environmental Tradition,* Routledge.

[3] Bate J.(2000), *The Song of the Earth*, Massachusetts: Harvard University Press.

[4] Bruke K. (2013), Coupe Laurence, "Green Theory", *The Routledge Companion to Critical and Cutural Theory*, Edit by Simon Malpas and Paul Wake, Routledge.

[5] Buell L. (2005), *The Future of Environmental Criticism: Environmental Crisis and Literary Imagination*, Black Well.

[6] Coupe L. (2000), *The Green Studies Reader: From Romanticism to Ecocriticism*, Routledge

[7] Coupe Laurence (2013), *Green Theory*, The Routlege Companion to Critical and Cultural Theory, Edited by Simon Malpas and Paul Wake, Routledge.

[8] Garrard G. (2004), *Ecocriticism (The New Critical Idiom),* Massachusetts, Routledge.

[9] Gifford T. (1999), *Pastoral* , Routledge, the Critical Idiom series.

[10] Glotfelty C. (1996)*,* "Introduction: Literary Studies in an Age of Enviromental Crisis", *The Ecocriticism Reader: Landmarks in Literary Ecology* edited by Cheryll Glotfelty and Harold Fromm*,* University of Georgia Press p xv - xxxvi.

[11] Kroeber K. (1994), *Ecological literary criticism; romantic imagining and the Biology of mind,* Columbia University Press.

[12] Leopold A. (1966), *A sand country almanac*, Oxford University press.

[13] Manes C. (1996), "Nature and Silence", *The Ecocriticism Reader: Landmarks in Literary Ecology* edited by Cheryll Glotfelty and Harold Fromm*,* University of Georgia Press, p 15- 30.

[14] Thornber K.(2011), *Ecocriticism and Japanese Literature of the Avant-Garde,* http://interlitq.org/issue8/karen_thornber/job.php

[15] *Van Nghe* newspapers, "Literature had to make people trust each other more and more*"* (Conversation between Oe Kenzaboko and Mac Ngon), Number 12 (23/03/2002).

THỂ LỆ VIẾT VÀ GỬI BÀI

1. Bài nhận đăng là các công trình mới có ý nghĩa khoa học và thực tiễn trong các lĩnh vực khoa học và công nghệ, chưa công bố ở bất kỳ tạp chí nào.

2. Một số lưu ý về hình thức và bố cục của bài báo

2.1. Hình thức của bài báo

- Bài viết được soạn thảo bằng các phần mềm soạn thảo văn bản MS Word, không quá 10 trang giấy khổ A4. Hình ảnh trong bài viết rõ ràng, theo định dạng PNG, JPG hoặc WMF. Tên hình vẽ đặt ở phía dưới, tên bảng biểu đặt ở phía trên, hình và bảng được đánh số thứ tự.

2.2. Bố cục của bài báo

- Phần tiêu đề: chứa các thông tin sau:

• Tiêu đề bài báo: bằng tiếng Việt và tiếng Anh, súc tích, đầy đủ thông tin.

• Tên các tác giả: ghi đầy đủ theo thứ tự họ, chữ lót và tên. Phía trên tên tác giả liên lạc (corresponding author) được đánh dấu *.

• Cơ quan công tác: cung cấp địa chỉ thuận lợi cho việc liên hệ.

• Địa chỉ e-mail: địa chỉ e-mail (nếu có) của các tác giả có tên trong bài báo.

- Phần tóm tắt: bằng tiếng Việt và tiếng Anh giới thiệu một cách ngắn gọn về mục đích nghiên cứu và kết quả đạt được của bài báo.

- Phần nội dung: đầy đủ các mục: a. Đặt vấn đề (nêu rõ mục đích, đối tượng nghiên cứu, tính thời sự của vấn đề); b. Giải quyết vấn đề (phương pháp nghiên cứu, phương tiện sử dụng khi nghiên cứu, nội dung nghiên cứu đã thực hiện); c. Kết quả nghiên cứu và thảo luận; d. Kết luận.

- Phần tài liệu tham khảo: chỉ nêu các tài liệu trích dẫn đã được liệt kê, sắp thứ tự bằng số chứa trong các ngoặc vuông, định dạng như sau:

• Đối với sách, luận án, báo cáo: số thứ tự, họ và tên tác giả hoặc tên cơ quan ban hành, tên sách (luận án, báo cáo), nhà xuất bản, nơi xuất bản, năm xuất bản.

• Đối với bài báo: số thứ tự, họ và tên tác giả, tên bài báo, tên tạp chí, tập, số, năm xuất bản, số trang.

3. Địa chỉ gửi bài: Tạp chí Khoa học và Công nghệ Đại học Duy Tân, 03 Quang Trung, Đà Nẵng; ĐT: 0236.3827111- 413; Email: tapchikhcn@duytan.edu.vn.

Lưu ý:

- Ban biên tập chỉ nhận những bài đã được chuẩn bị theo đúng các qui định trên. Nếu bài không được đăng, tòa soạn sẽ không trả lại bản thảo.